ACYCLIC CHELATING LIGANDS FOR RADIOMETALS

by

CATERINA FORTUNATA RAMOGIDA

B.Sc. (Hons.), Simon Fraser University, 2010

A THESIS SUBMITTED IN PARTIAL FULFILLMENT OF

THE REQUIREMENTS FOR THE DEGREE OF

DOCTOR OF PHILOSOPHY

in

The Faculty of Graduate and Postdoctoral Studies

(Chemistry)

THE UNIVERSITY OF BRITISH COLUMBIA

(Vancouver)

July 2015

Abstract

This thesis presents studies on a class of acyclic (open chain) chelating ligands based on the picolinic acid moiety. Our recent reports of the promising hexadentate chelator H_2dedpa and octadentate analogue H_4octapa for Ga(III) and In(III)/Lu(III) complexation, respectively, have spurred our interest in further developing this class of chelators, which have subsequently been dubbed the "pa" family of ligands. These ligands possess the potential to bind a variety of clinically relevant radiometal ions, such as ^{68}Ga, ^{64}Cu, ^{111}In, ^{177}Lu, or $^{86/90}$Y. When harnessed properly, the radiative emissions of these radiometals can be utilised in radiopharmaceuticals for imaging (via γ-rays for single photon emission computed tomography (SPECT) or β^+ particles for positron emission tomography (PET)) or therapy (via highly ionizing radiation from α, β^-, or Auger electron emission). A key component of these radiometal-based radiopharmaceuticals is the chelating ligand, used to securely bind the radiometal which ensures proper delivery the radioactive dose to the area of interest *in vivo*. This work focuses on further exploiting the H_2dedpa (N_4O_2) and H_4octapa (N_4O_4) scaffolds that possess ideal properties for $^{67/68}$Ga and ^{111}In radiopharmaceuticals, respectively – such as mild room temperature radiolabeling in 10 min, and the ability to form kinetically inert complexes – rare manifestations for acyclic ligands. Herein, efforts were made to incorporate dedpa^{2-} into a small molecule imaging agent for ^{68}Ga PET. A variety of dedpa^{2-} (and one octapa^{4-}) analogues were synthesized, characterized, and evaluated through thermodynamic stability, *in vitro* kinetic inertness, and radiolabeling studies to assess their "usefulness" as ligands in radiopharmaceutical design. The chiral ligands H_2*CHX*dedpa and H_4*CHX*octapa are highlights of this work; [Ga(*CHX*dedpa)]$^+$ and [In(*CHX*octapa)]$^-$ were found to be more, or equally, stable versus their achiral counterparts H_2dedpa and H_4octapa. Nitroimidazole-containing H_2dedpa and H_2*CHX*dedpa derivatives were also studied as potential ^{68}Ga PET imaging agents of tumour hypoxia. The radio-tracers showed exceptional *in vitro* stability (86 to >99% intact), and promising preferential uptake in hypoxic cell lines suggesting these ligands would be ideal candidates for further testing *in vivo*.

Preface

Chapter 1 is an adaptation of published work, and is reproduced in part, with permission from Ramogida, C. F.; Orvig, C., Tumour Targeting with Radiometals for Diagnosis and Therapy. *Chem. Commun.* **2013**, *49*(42), 4720-4739, Copyright 2013 The Royal Society of Chemistry. This review article was written by Caterina Ramogida, with input and editing from Dr. Chris Orvig.

Chapter 2 is an adaptation of published work, and is reproduced in part, with permission from Ramogida, C. F.; Cawthray, J. F.; Boros, E.; Ferreira, C. L.; Patrick, B.O.; Adam, M. J.; Orvig, C., H_2*CHX*dedpa and H_4*CHX*octapa – Chiral Acyclic Chelating Ligands for $^{67/68}$Ga and ^{111}In Radiopharmaceuticals. *Inorg. Chem.* **2015**, *54*(4), 2017-2031, Copyright 2015 American Chemical Society. Caterina Ramogida performed the synthesis, with initial assistance from Eszter Boros. X-ray crystallography was solved by Dr. Brian O. Patrick. Radiochemistry was performed by Caterina Ramogida at TRIUMF/Nordion with some assistance from Dr. Cara L. Ferreira. Potentiometric titrations and data fitting were performed by both Caterina Ramogida and Dr. Jacqueline Cawthray. DFT calculations were performed by Dr. Jacqueline Cawthray. This project was supervised by Dr. Michael J. Adam and Dr. Chris Orvig. The manuscript was written by Caterina Ramogida.

Chapter 3 is an adaptation of published work, and is reproduced in part, with permission from Ramogida, C. F.; Pan, J.; Ferreira, C. L.; Patrick, B. O.; Rebullar, K.; Yapp, D. T. T.; Lin, K.-S.; Adam, M. J.; Orvig, C., Nitroimidazole-containing H_2dedpa and H_2*CHX*dedpa derivatives as potential PET imaging agents of hypoxia with ^{68}Ga. *Inorg. Chem*. **2015**, *54* (10), 4953-4965, Copyright 2015 American Chemical Society. Synthesis was performed by Caterina Ramogida, with some assistance from Karla Rebullar during her summer NSERC USRA term. X-ray crystallography experiments were solved by Dr. Brian O. Patrick. Radiochemistry was

performed by Caterina Ramogida at TRIUMF/Nordion with some assistance from Dr. Cara L. Ferreira, or by Dr. Jinhe Pan (under supervision of Dr. Kuo-Shyan Lin) at the BC Cancer Agency. Guidance and advice for *in vitro* cell experiments was provided by Dr. Donald T. T. Yapp and were performed by Caterina Ramogida at the BC Cancer Agency. All animal experiments were performed at the BC Cancer Agency, and the protocol used was approved by the Institutional Animal Care Committee (IACC) of the University of British Columbia (protocol # A11-0060) and was performed in accordance with the Canadian Council on Animal Care Guidelines. This project was supervised by Dr. Michael J. Adam and Dr. Chris Orvig. The manuscript was written by Caterina Ramogida.

All synthesis and experimentation in **Chapter 4** was performed by Caterina Ramogida. X-ray crystallography experiments were solved by Dr. Brian O. Patrick.

Chapter 5 is an adaptation of a manuscript in preparation, Ramogida, C. F.; Murphy, L.; Cawthray, J. F.; Ross, J. D.; Adam, M. J.; Orvig, C., Novel "Bi-modal" H_2dedpa Derivatives for Radio- and Fluorescence Imaging. Expected submission date May-June 2015. The synthesis was performed by Caterina Ramogida, with significant contribution to synthetic protocol of certain precursors by Dr. Lisa Murphy with assistance from James D. Ross. Radiochemistry was performed by Caterina Ramogida at TRIUMF. 3D spheroid *in vitro* cell assays and confocal microscopy imaging were performed by Dr. Jacqueline Cawthray with assistance from Caterina Ramogida. This project was supervised by Dr. Michael J. Adam and Dr. Chris Orvig. The manuscript draft was written by Caterina Ramogida.

Chapter 6 is an adaptation of a manuscript in preparation, Ramogida, C. F.; Schneider, C.; Schindler, D.; Tan, K. Y. L.; Huh, S.; Adam, M. J.; Orvig, C., Lipophilic Cationic Ga(III) Complexes Based on H_2*CHX*dedpa for Myocardial Perfusion Imaging with ^{68}Ga PET. Expected submission date June 2015. Caterina Ramogida designed the ligands and synthetic protocols and performed

the majority of the synthesis. Dr. Kelvin Y. L. Tan, Christina Schneider, Dorothee Schindler, and Sean Huh each synthesized one ligand. Dr. Kelvin Y. L Tan was a visiting scholar who visited the Orvig lab for 6 weeks and worked with Caterina Ramogida. Christina Schneider and Dorothee Schindler were exchange students from Unversität Heidelberg and Sean Huh was an NSERC USRA summer undergraduate student, all students worked under the supervision of Caterina Ramogida in the Orvig Lab. Radiochemistry was performed by Caterina Ramogida at TRIUMF. This project was supervised by Dr. Michael J. Adam and Dr. Chris Orvig. The manuscript draft was written by Caterina Ramogida.

Chapter 7 is an adaptation of a manuscript in preparation, Ramogida, C. F.; Cawthray, J. F.; Weekes, D. M.; Patrick, B. O.; Adam, M. J.; Orvig, C.; Acyclic Hexadentate Ligand H_3dpaa for Ga(III) Radiopharmaceuticals. Expected submission date June 2015. Synthesis and radiochemistry was performed by Caterina Ramogida at University of British Columbia or TRIUMF, respectively. X-ray crystallography was solved by Dr. Brian O. Patrick. Potentiometric titrations and data fitting were performed by Caterina Ramogida with data fitting assistance from Dr. Jacqueline Cawthray. This project was supervised by Dr. Michael J. Adam and Dr. Chris Orvig. The manuscript draft was written by Caterina Ramogida.

Table of Contents

List of Tables

List of Figures

List of Schemes

List of Symbols and Abbreviations

%ID/g	percentage of injected radioactive dose per gram of tissue
2D	two dimensional
3D	three dimensional
α	alpha particle or alpha position on molecule
α-MSH	α-Melanocyte stimulating hormone peptide
Å	angstrom, $1 \cdot 10^{-10}$ m
β^-	beta particle
β^+	positron
γ	gamma ray
δ	delta of chemical shift in parts per million (NMR)
Δ	heat or reflux
λ	wavelength in nm
μ	micro (10^{-6})
μM	micromolar (10^{-6} M)
AAS	atomic absorption standard
Ab	antibody
Ac	acetate
ATSM	diacetyl-bis(N^4-methylthiosemicarbazone)
BBN	bombesin peptide
BFC	bifunctional chelate, or bifunctional ligand
Bn	benzyl
br	broad (NMR), e.g. br s (broad singlet)
°C	degrees Celsius
calcd.	calculated
CB-TE2A	4,11-bis(carboxymethyl)-1,4,8,11-tetraazabicyclo-[6.6.2]-hexadecane
CCK2	cholecysktokinin 2
CHX	cyclohexane/cyclohexyl
CHX-A"-DTPA	cyclohexyldiethylenetriaminepentaacetic acid
Ci	Curie
CN	coordination number
COSY	correlation spectroscopy (^{1}H-^{1}H NMR)
CT	computed tomography
CV	cyclic voltammetry
d	day(s) or doublet (NMR)
D	distribution coefficient (octanol/aqueous at specified pH)
Da	dalton
DCM	dichloromethane
DFT	density functional theory (*in silico* calculations)
DFO	desferrioxamine B
DIPEA	diisopropylethylamine

DMF	dimethylformamide
DMSO	dimethylsulfoxide
DOTA	1,4,7,10-tetraazacyclododecane-*N,N',N'',N'''*-tetraacetic acid
DTPA	diethylenetetraaminepentaacetic acid
E	reduction or oxidation or half potential (for electrochemistry)
EA	elemental analysis
EDTA	ethylenediaminetetraacetic acid
EF5	etanidazole pentafluoride
EGF	epidermal Growth Factor
en	ethylenediamine
EPR	enhanced permeability and retention
equiv	equivalent(s)
ESI-MS	electrospray ionization mass spectrometry
EtOAc	ethyl acetate
EtOH	ethanol
eV	electronvolt(s)
F-MISO	fluoromisonidazole
FAZA	fluoroazomycin arabinofuranoside
FDA	Food and Drug Administration (USA)
FDG	2-deoxy-2-[^{18}F]fluoro-D-glucose
FITC	fluorescein isothiocyanate
g	gram
GRP	gastrin-releasing peptide
h	hour(s)
H_2*CHX*dedpa	cyclohexyl-H_2dedpa
H_2dedpa	1,2-[[6-carboxy-pyridin-2-yl]-methylamino]ethane
H_4*CHX*octapa	cyclohexyl-H_4octapa
H_4octapa	*N,N'*-bis(6-carboxy-2-pyridylmethyl)-ethylenediamine-*N,N'*-diacetic acid
HEHA	1,4,7,10,13,16-hexaazacyclohexadecane-1,4,7,10,13,16-hexaacetic acid
HPLC	high performance liquid chromatography
HR	high resolution
HSQC	heteronuclear single bond correlation/coherence (^{1}H-^{13}C NMR)
Hz	Hertz
Ig	immunoglobulin
J	coupling constant (NMR)
k	kilo
K_{ML}	thermodynamic complex stability constant
L	litre or ligand
LET	linear energy transfer
m	milli- or multiplet (NMR)
mAb	monoclonal antibody
M	molar (moles/litre) or mega (10^6) or metal

MC1	melanocortin 1
MeCN	acetonitrile
MeOH	methanol
MEP	molecular electrostatic potential
METRO	metronidazole, 2-(2-methyl-5-nitro-1*H*-imidazol-1-yl)ethanol
min	minute(s)
mol	mole
MRI	magnetic resonance imaging
MS	mass spectrometry
m/z	mass per unit charge
n	nano (10^{-9}) or number of unit or neutron
NBS	*N*-bromosuccinimide
NHE	normal hydrogen electrode
NHL	non-Hodgkin's lymphoma
NHS	*N*-hydroxysuccinimide
NI	nitroimidazole
NMR	nuclear magnetic resonance
nM	nanomolar (10^{-9} M)
Nosyl	2-nitrobenzenesulfonamide (protecting group)
NOTA	1,4,7-triazayclononane-1,4,7-triacetic acid
NRU	National Research Universal (reactor)
OC	octreotide peptide
ORTEP	Oak Ridge Thermal Ellipsoid Plot Program
P	partition coefficient (octanol/water)
p	proton
p	para substituent
p.i.	post injection
PBS	phosphate buffered saline
PCTA	3,6,9,15-tetraazabicyclo[9.3.1]pentadeca-1(15),11,13-triene-3,6,9-triacetic acid
Pd/C	palladium on carbon (10% by weight)
PET	positron emission tomography
pH	$-\log[H_3O^+]$
pK_a	protonation constant
pm	picometer (10^{-12} m)
pM	-log[free metal], or picomolar (10^{-12} M)
ppm	parts per million
pyr	pyridyl/pyridine
q	quartet (NMR)
®	trademark
RCY	radiochemical yield
RGD	Arg-Gly-Asp cyclic peptide

RIT	radioimmunotherapy
RP	reverse phase (column chromatography)
rpm	rotations per minute
RT	room temperature
s	singlet (NMR) or second(s)
S.A.	specific activity (radioactivity per unit mass)
Sar	sarcophagine
SPECT	single photon emission computed tomography
SST	somatostatin
t	triplet (NMR) or time
t_R	retention time (HPLC)
$t_{1/2}$	half-life
TAC	time-activity curve
TATE	Octreotate peptide
TBAP	tetrabutylammonium perchlorate
TCMC	1,4,7,10-tetraaza-1,4,7,10-tetra-(2-carbamoyl methyl)-cyclododecane
TETA	1,4,8,11-tetraazacyclotetradecane-1,4,8,11-tetraacetic acid
TFA	trifluoroacetic acid
THF	tetrahydrofuran
TLC	thin layer chromatography
TM	Trade Market
TOF	time-of-flight
TRAP	1,4,7-triazacyclononane-1,4,7-tris[methyl(2-carboxyethyl)phosphinic acid
trastuzumab	HER2/*neu* targeting antibody
V	volt
VEGF	Vascular Endothelial Growth Factor
VT-NMR	variable temperature NMR
y	year

Acknowledgements

I must first acknowledge my supervisors Professor Chris Orvig and Dr. Mike Adam for their guidance and continuous support throughout the course of my PhD. They allowed me the freedom to explore my scientific interests, encouraged me, and funded my attendance at numerous international conferences.

I would also like to thank all of the wonderful people I had the pleasure to work with in the Orvig group over the past ~5 years with whom I shared the many trials, tribulations, and triumphs of graduate school. In particular, I'd like to thank Eszter B. for welcoming me to the group and the 'dedpa' project and providing scientific guidance during my first year making my transition into grad school easier; Maria T. for being a pleasure to work with and attend conferences with; Jacquie C. for the tremendous amount of work and contribution she made to my thesis as well for being a great yoga and stairs partner; Karen A. and Madeleine I. for their positive energies and for keeping me fit and active; undergrads Sean H., Karla R., Christina S., and Dorothee S. and visiting scholar Kelvin T. for their hard work and eagerness to learn. The phenomenal shops and services at UBC Chemistry are greatly appreciated – Brian P. for his amazing crystallography skills, Paul X. and Maria E. for countless discussions on NMR data, Marshall L. and the MS labs, electronic shop, mechanical shop, and bio-services. To my collaborators at the BC Cancer Agency: Don Y. for graciously letting me invade his lab and for his guidance; Nadine C. and Joseph L. for assistance with *in vivo* studies; Jinhe P. for all of his radiolabeling help. The friendly and extremely helpful staff and researchers at TRIUMF are also acknowledged and thanked. I would also like to thank Dennis W. and Cara F. for their support and mentorship. Nordion is acknowledged for isotope support. Thank you to UBC for 4YF and NSERC for CGS-M and CGS-D funding. Thank you to my PhD committee members Drs. L. Schafer, P. Kennepohl, and G. Dake for taking time out of their schedules to read my thesis and/or attend my committee meetings.

Certainly, the infinite support and love of my parents Roberto and Francesca R., brothers Bruno and Roberto R., sister-in-law Josie R., extended family and friends have been crucial and have helped me to keep my focus and achieve my goals. Finally, I must thank my husband, Adam F., whose understanding, support, and love has made this process possible.

To my family…

Chapter 1: Introduction

1.1 Background

The use of radiometals in nuclear oncology is a rapidly growing field and encompasses a broad spectrum of radiotracers for imaging *via* PET (positron emission tomography) or SPECT (single-photon emission computed tomography) and therapy *via* α, β^-, or Auger electron emission. This introduction opens with a brief overview of the imaging and therapy modalities exploited in nuclear medicine, followed by a discussion of the multi-component strategy used in radiometal based radiopharmaceutical development, known as the bifunctional chelate (BFC) method. The modular assembly is dissected into its individual components and each is discussed separately. At the heart of the BFC method is the chelating ligand, used to tightly bind a radiometal ion. These chelating ligands must possess several stringent properties (outlined in this introduction) which will make them suitable for use in a radiopharmaceutical.

The concepts and knowledge unique to metal-based designs have been outlined here, to give insight into how these radiopharmaceuticals are evaluated for use *in vivo*. Imaging nuclides ^{64}Cu, ^{68}Ga, ^{86}Y, ^{89}Zr, and ^{111}In, and therapeutic nuclides ^{90}Y, ^{177}Lu, ^{225}Ac, ^{213}Bi, $^{186/188}$Re, and ^{212}Pb are discussed herein, and relevant examples have been extracted from the literature to give the reader a sense of breadth of the field.

Given the array of radiometals that show potential for radiopharmaceutical elaboration, an equally broad spectrum of chelating ligands has been developed that possess properties of varying virtue for different metals. Some of these established ligands applied in clinical and research settings are used with essentially all radiometals, despite fundamental differences in coordination chemistry between metals; as a consequence their use comes with limitations. The specific aims of this work are to investigate new chelating ligands for radiometals which exhibit enhanced properties compared to the current industry "gold standards".

1.2 Nuclear Medicine

Cancer is the leading cause of death worldwide, accounting for 7.6 million deaths in 2008, and an estimated 13.1 million deaths in 2030.[1] The burden of cancer can be reduced by early detection and early treatment management of patients, and in this regard nuclear imaging and therapy have made great advancements in clinical medicine. Nuclear medicine is a powerful tool with the ability to both image disease non-invasively and subsequently treat the diseased state without harming surrounding healthy tissue by injecting a radioactive isotope fused to a designer molecule that has the ability to transport the radionuclide specifically to the diseased tissue. Traditionally, 'organic' isotopes, such as ^{18}F, ^{15}O, ^{13}N, ^{11}C, and ^{131}I have been incorporated into nuclear medicine agents;[2] however, these radiotracers were limited in availability and widespread use since these radioisotopes must be incorporated through covalent bond linkages into small drug mimics which often require lengthy and complex radiosyntheses taking valuable time whilst sacrificing many short half-lives of radioactivity in the process. To overcome these shortcomings, much effort has been made towards the development of metallic radionuclides with varying production methods, radioactive decay schemes, and half-lives that make them attractive for incorporation into a radiopharmaceutical.

As of 2014, of the 47 FDA-approved radiopharmaceuticals on the market, 16 employ non-metallic isotopes (^{18}F, ^{11}C, ^{14}C, ^{123}I, ^{125}I, ^{131}I, ^{13}N, ^{133}Xe) and the remainder rely on the use of metallic isotopes for their source of radiation (Table 1.1).[3] The most prevalent metal used in nuclear medicine, ^{99m}Tc, is a γ emitter used extensively in single-photon emission computed tomography (SPECT). ^{99m}Tc is incorporated into 17 FDA-approved radiopharmaceuticals, and has been widely discussed and reviewed in the literature.[4,5] The recent global supply shortage of ^{99}Mo, the parent isotope of ^{99m}Tc, due to the imminent shut down of the National Research Universal reactor in Chalk River Laboratory in Ontario, Canada, has fostered an increased interest in exploring radiopharmaceuticals using other radiometals.

Table 1.1 Selected FDA-approved radiopharmaceuticals containing radiometals (excluding ^{99m}Tc).

Radiopharmaceutical	Trade Name	Indications
^{67}Ga citrate		SPECT – demonstrates presence of Hodgkin's disease, lymphoma, bronchogenic carcinoma, acute inflammatory lesions
^{111}In capromab pendetide	ProstaScint®	SPECT - diagnostic imaging of prostate cancer
^{111}In pentetreotide	Octreoscan™	SPECT - imaging of neuroendocrine tumours bearing somatostatin receptors
^{111}In oxyquinoline		SPECT – radiolabeling autologous leukocytes to detect inflammation
^{82}Rb chloride	Cardiogen-82®	PET –myocardial perfusion imaging
^{201}Tl chloride		SPECT – myocardial perfusion imaging for diagnosis of myocardial infarction
^{223}Ra dichloride	Xofigo®	α THERAPY – treatment of castration-resistant prostate cancer, symptomatic bone metastases
^{153}Sm lexidronam	Quadramet®	β^- THERAPY - bone pain relief in patients with osteoblastic metastatic bone lesions
^{89}Sr chloride	Metastron™	β^- THERAPY – bone pain relief in patients with skeletal metastases
^{90}Y ibritumomab tiuxetan	Zevalin®	β^- THERAPY - treatment of B-cell non-Hodgkin's lymphoma (NHL)

1.2.1 Nuclear Imaging

The ability to image cancers and monitor the progression of the disease non-invasively has become common practice in clinical medicine, proving vital to patient survival. Two imaging modalities are used extensively in nuclear medicine: single-photon emission computed tomography (SPECT) and positron emission tomography (PET). Both modalities require the introduction of a radioactive nuclide into the patient; the radioactivity is attached to a targeting moiety that delivers the radionuclide to the tumour site. The photons/particles emitted are detected by cameras and ultimately converted into a 3D image visualising the accumulation of radioactivity in the body, coinciding with the localization of the tumour. The use of SPECT and PET in the clinic depends on a variety of factors such as cost, sensitivity and resolution of the technique, and availability of an appropriate radionuclide. Some important properties of each imaging modality are discussed below.

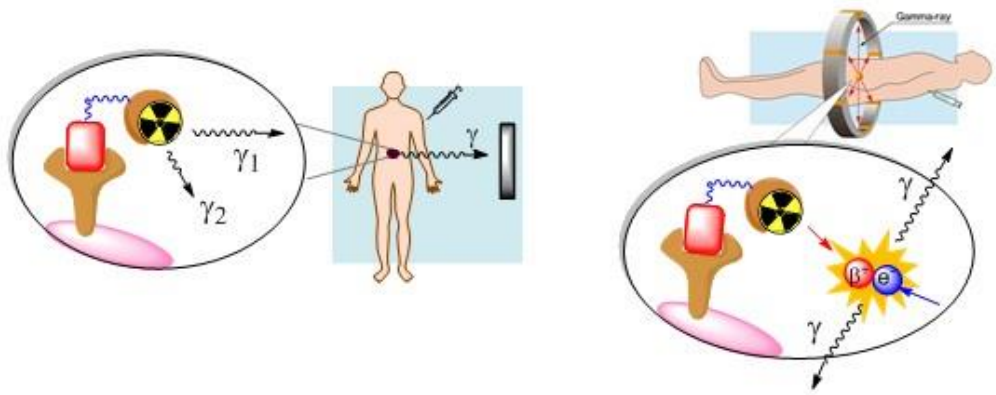

Figure 1.1 Depiction of SPECT imaging (left) and PET imaging (right).

1.2.1.1 Single-Photon Emission Computed Tomography (SPECT)

The oldest of the two techniques, SPECT requires a γ-emitting radionuclide whose emissions are recorded by detector cameras (Figure 1.1). The discovery of the γ-emitter ^{99m}Tc (in 1937) and introduction of the ^{99}Mo/^{99m}Tc generator system used in the production of the

isotope in the 1960's led to widespread use of ^{99m}Tc-labelled agents in clinical SPECT imaging, and today this generator and radionuclide are still the workhorses of medical imaging, used in about 70-80% of all radio-diagnostic scans.[6,7] There have been many extensive reviews on ^{99m}Tc.[4,5]

Industrially, γ camera/detectors are designed for specific energy windows (generally 100-250 keV),[8] and γ rays with energies outside this range will produce poor image quality. As a consequence, SPECT radionuclides should have a γ decay energy within this range to be clinically useful. Typically, SPECT systems can detect radiotracers within the body at concentrations of about 10^{-6} M;[9] however, more modern SPECT instruments have shown sensitivity down to nanomolar and even picomolar levels.[10]

1.2.1.2 Positron-Emission Tomography (PET)

As implied by its name, PET requires a β^+-emitting radionuclide. As the nuclide decays it ejects a β^+ from its nucleus; the β^+ will travel a short distance before it collides with an electron, and the two annihilate to release two 180° opposed 511 keV γ rays (Figure 1.1). The γ rays will travel in this direction until they strike the PET scanner coincidence detectors (arranged in a circular array); the output is generated only when two coincidence detectors are triggered simultaneously (the coincidence time window is approximately 5 – 15 ns).[11]

The first industrial positron emission tomograph arrived in 1975,[12] and for many years PET imaging agents were dominated by short half-life isotopes ^{18}F, ^{15}O, ^{13}N, and ^{11}C, whose production relied upon an on-site cyclotron. Not only did the need for an on-site cyclotron make PET an expensive imaging modality, but the short half-lives of the organic nuclides (122 s to 109 min) limited the use of PET for imaging biological processes that occurred over a short

time scale. Today, ^{18}F ($t_{1/2}$ = 109 min) dominates the field of PET imaging, and is readily available daily from commercial sources obviating the need for an on-site cyclotron. Nonetheless, tremendous effort has been made towards the production of β^+ emitting radioisotopes of metals such as Ga, Y, Zr and Cu,[8,13] that have varying half-lives and can circumvent some of the synthetic limitations still associated with incorporating organic β^+ emitting nuclides into small drug mimics. Despite these efforts, there is currently no FDA-approved metal-based PET imaging agent (with the exception of rubidium-82 chloride); however, many are in early to late stage clinical trials.

Compared to its single-photon analogue, PET exhibits higher resolution (2 – 4 mm or lower compared to 6 – 8 mm for SPECT) and higher sensitivities (up to ~10^{-12} M, compared to 10^{-6} M for SPECT).[13] The resolution and sensitivity of PET are tied to the intrinsic properties of β^+ emission. Firstly, the resolution depends on the initial distance the β^+ travels before annihilation; this distance is dependent on the energy of decay. Hence, lower energy β^+ emission is more desirable in PET in order to give better resolution images. Secondly, high sensitivity is a result of the coincidence detection of two γ-rays. Despite the advantages of PET imaging, SPECT is more widely used in the clinic, perhaps only because it is a more established technique.

1.2.2 Radiotherapy

Radioactivity used to target and kill cancer cells is often termed radiotherapy, and when conjugated to a large monoclonal antibody is called radioimmunotherapy (RIT). These therapeutic radiopharmaceuticals are similar in construction to their nuclear imaging analogues. An unstable radionuclide which decays via emission of high-energy ionizing radiation is attached to a targeting moiety that will deliver the radiation dose specifically to the

cancer cells; from here the emission deposits its energy in the surrounding tissue, causing cell death. In order to kill the cell, the ionization must cause DNA double-strand helix breaks that are non-repairable.[14]

Emissions of therapeutic nuclides should contain mainly non-penetrating radiation so that a damaging and highly-localised dose can be delivered to the diseased tissue without causing harm to surrounding healthy tissue.[6] Emitters of beta particles (β^-), alpha particles (α), and Auger electrons may be used for radiotherapy. Varying physical properties and effects on tissue are associated with each type of radiation, and must be matched appropriately with their intended biological target. The linear energy transfer (LET) value is used to quantify the amount of energy that is transferred from ionizing radiation to soft tissue, typically expressed in kiloelectron volts per micrometer of track length in tissue (keV/μm). Emissions of high LET will dissipate their energy in tissue close to where the nuclide is deposited (shorter 'effective range'), making them effective for treating small tumours and micrometastases. Conversely, emissions of low LET will deposit their energy through a larger range in tissue suggesting cell damage can occur many cell lengths away from where the nuclide is deposited; these emissions are more appropriately matched for treating larger or poorly vascularized tumours[15,16] (Table 1.2). It is also worth noting that β^+ emission is capable of being used therapeutically if given at an appropriate therapeutic dose.

Table 1.2 Radiative emissions used for radiotherapy with corresponding path length and decay energy.

Radiation	Typical range in biological tissue[a]	Typical energy of decay
Auger electrons	1 – 20 μm (< 1 cell diameter)	~1 – 10 keV
α particles	40 – 100 μm (< 10 cell diameters)	5 – 8 MeV
β- particles	0.5 – 10 mm (50 - 1000 cell diameters)	0.1 – 2.2 MeV

[a]Based on 10 μm average cell diameter.

1.2.2.1 Beta-Particles (β^-)

Traditionally, β^- particle emitters have most commonly been exploited for radiotherapy. β^- particles have a low LET (0.2 keV/μm) allowing the particles to reach spans of approximately 50 cell diameters[15] which makes β^- emitting nuclides appropriate for treating larger or poorly vascularized tumours. Conversely, using a β^- emitter to treat small tumours may cause damage to neighbouring healthy cells, a potential disadvantage.[15]

1.2.2.2 Alpha-Particles (α)

Alpha particles have high energies (MeV) which deposit over a very short path length (<100 μm) corresponding to a very high LET (typically about 100 keV/μm),[16] the short range and high LET of α particles renders their emitters ideal for treating small tumours since they are only effective over a few cell diameters. In addition, the short range in biological tissue offers less radiotoxicity and more favourable dosimetry profiles for surrounding healthy tissues.[6]

1.2.2.3 Auger Electrons

Most Auger electron emitters have low energies (< 500 eV) and the smallest range (several nanometers) in biological tissue of all the other ionizing radiations discussed.[17] This makes them effective only when the radionuclide is localised in the cell nucleus. With a highly-localised energy deposition, Auger electron emissions have the potential to provide an effective cell-killing dose to the target site with minimal chance of damage to surrounding cells.[18]

1.3 Construction and Evaluation of Metalloradiopharmaceuticals

1.3.1 Bifunctional Chelate (BFC) Method

The nature of radiometals in radiopharmaceuticals lends itself to an interdisciplinary approach requiring knowledge of coordination chemistry, thermodynamics and kinetics, synthetic chemistry, radiochemistry, and biology/physiology. The basis for a good inorganic radiopharmaceutical is a bifunctional chelate (BFC). The BFC has the dual function of binding a radiometal and incorporating a point of derivatisation for attachment of a biomolecule/targeting vector (the moiety that will introduce site-specific delivery). In general, a fully functional metal-based radiopharmaceutical will contain four components: 1) targeting vector, 2) radiometal (imaging handle or therapeutic effect), 3) chelate (required to bind and fully sequester the radiometal), and 4) linker (connects the chelate to the biomolecule)**.** The targeting vector is generally a biomolecule of interest (e.g. peptide, antibody, antibody fragment) that exhibits strong binding affinity for over-expressed tumour surface receptors; these are the vehicles that transport the radioactivity specifically to the tumour. The appropriate radiometal is chosen based on the radiopharmaceutical's intended purpose; γ- or β^+-emitting radionuclides for imaging, α-, β^--, or Auger electron emitters for therapy. Choice of an appropriate BFC is based on the best-fit of the radiometal governed by preferences in

coordination chemistry and donor-ability of the ligand in order to form a stable and inert metal-chelate complex. Finally, the linker is used to connect the chelate to the targeting vector. The linker should be stable under physiological conditions and must not significantly compromise the binding affinity or specificity of the biovector or the metal-complexation performance of the chelator. The BFC method is particularly attractive because all steps of the long synthetic manipulation of the chelate, linker, and biomolecule is executed before the radionuclide is added in the last step (Figure 1.2), saving many half-lives of radioactivity.

Components must be carefully chosen when designing a successful radiopharmaceutical so as to mutually complement each other in order to work as a unified agent. For example, matching the biological half-life of the biomolecule with the radioactive half-life of the nuclide is crucial. In general, radiometals with long half-lives are best matched to biomolecules with long biological half-lives (such as antibodies) that may take hours or days to circulate the blood and accumulate at the tumour site, and short half-life isotopes are best matched with biomolecules that have short biological half-lives (such as small molecules or peptides) that rapidly circulate in the blood and accumulate at the tumour site in a time frame that is comparable with the short radiological half-life of the nuclide.

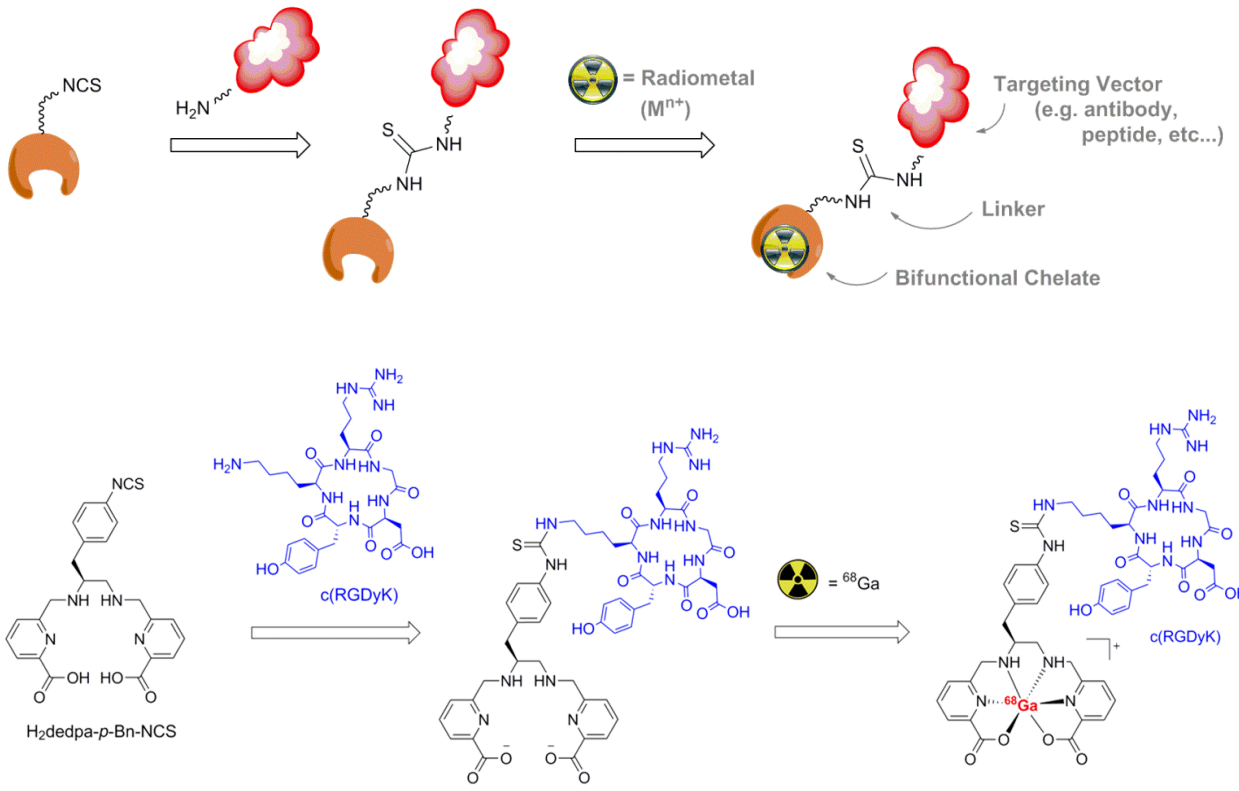

Figure 1.2 (Top) Cartoon depiction of the bifunctional chelate (BFC) strategy employed in metal-based radiopharmaceuticals; (Bottom) "Real-life" example of the BFC method previously reported by our group employing H_2dedpa-*p*-Bn-NCS as the BFC, peptide c(RGDyK) as the targeting vector, and ^{68}Ga as the radiometal.[19]

Exceptions to the BFC method, such as the 'integrated approach', are also used extensively in radiopharmaceutical design and have been discussed elsewhere.[20] The metal-chelate complex Cu(II)-ATSM (Cu(II)-diacetyl-bis(N^4-methylthiosemicarbazone) (Figure 1.3)[21] is an archetypal example of an exception to the BFC method. ATSM and its analogues have been labelled with several copper isotopes, and show a striking ability to treat or image hypoxic cancer tissue. The ability to specifically target and become entrapped in hypoxic cells is rooted in the complex's biochemical interaction with cells, and redox chemistry,[21,22] and is not dependent on a biomolecule as a means of tumour-specific transportation.

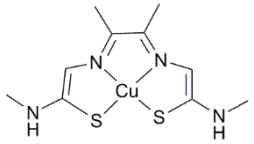

Figure 1.3 Cu(II)-ATSM.

1.3.2 Properties of a Good Radiopharmaceutical – Methods for Evaluation of a Radiopharmaceutical

Due to the 'multi-component' nature of metal-based radiopharmaceuticals, there are many properties that must be evaluated when assessing the potential of a radiopharmaceutical. Some important considerations are outlined below.

First and foremost, the metal-chelate complex must be kinetically inert and thermodynamically stable. The chelator must be a 'good fit' for the metal of choice; there are many commonly used and emerging chelates that have been used for a variety of radiometals with varying degrees of success (*vide infra*). Typically, the thermodynamic stability of the metal-chelate complex is measured *via* potentiometric titration or UV-Vis spectroscopy to calculate values of log K_{ML} and pM which are used to quantify the binding affinity of a particular metal-chelator pair, where a higher value signifies a stronger affinity between metal and chelate. More important than thermodynamic stability is the kinetic inertness of the metal-ligand complex *in vivo*.[8] There are many endogenous metal binding proteins in plasma that can compete with the chelate for the metal, thus the metal must be bound sufficiently tightly to inhibit transchelation of the metal to these proteins. Specifically, superoxide dismutase has a strong affinity for copper, and the iron binding protein transferrin has high binding affinity for both Ga(III) and In(III). In addition, highly charged ions such as Y(III) and Zr(IV) tend to

accumulate in the bone.[23,24] Kinetic inertness of the metal-ligand complex is often estimated experimentally by *in vitro* competition or challenge assays against excess metal-free protein, or blood serum. Caution must be taken when interpreting *in vitro* stability data, as *in vitro* studies rarely accurately predict *in vivo* stability of the radiopharmaceutical.

In addition to a thermodynamically stable and kinetically inert metal-chelate complex, appropriate complexation kinetics of the radioisotope are required under radiochemical conditions such as low concentrations, mild temperatures, and minimal time. The goal is to introduce as much radioactivity into the chelate-bioconjugate as possible, while protecting the integrity of the biomolecule and preserving the radioactivity of the nuclide which decays over time. These characteristics are expressed in radiochemical yield (% RCY), the percent of nuclide which is bound to the chelate, and specific activity (mCi/mg or mCi/mol), the amount of activity introduced per mass unit of compound.

Ultimately, the usefulness of any radiopharmaceutical is governed by the distribution of the agent in the body, i.e. biodistribution. Ideally, the agent will circulate in the blood and accumulate only in the tumour tissue that is meant to be imaged or given a therapeutic dose of radiation. Excess radiopharmaceutical that has not accumulated in the tumour tissue should be excreted to eliminate a background signal (for imaging), and reduce damage to surrounding healthy tissue (for therapy). This target accumulation and nonspecific clearance should occur at a time-scale which is matched with the half-life of the isotope. Biodistribution studies are done to determine the quantity and dose of radioactivity delivered to different organs in small animal models. Data are collected at different time points post-injection, and units are typically expressed in percent injected dose per gram of tissue (%ID/g); a high %ID/g value should be observed for the tumour, and low doses in all other tissues.

1.4 Radiometals

Dozens of radiometals have been considered for use in nuclear imaging or therapy, here we will focus on the radioisotopes that have garnered the most attention and have the greatest potential. The coordination and aqueous chemistry of the metal ion(s) should be well-known in order to choose the appropriate chelate to form a stable, kinetically inert radiometal complex. In addition, the radionuclide should be produced in high chemical purity with high specific activity and should be readily available to hospitals and research institutions.[7,25] Finally, the radiometal should have favourable decay characteristics: the desired decay emission should have a high branching ratio, appropriate energy of decay, and half-life to fit its intended purpose. Also, when choosing a radiometal for therapeutic purposes it is often favourable for the nuclide to have an imageable decay radiation (such as γ or β^+) in addition to the therapeutic emission, so there is means to determine the distribution of the radiopharmaceutical non-invasively for dosimetry studies. Discrepancies in physical decay data of relevant radiometals can be found throughout the literature and have been recently documented[26] and data provided herein (Tables 1.3 and 1.4) should be taken as approximate.

1.4.1 Radiometals for PET and SPECT

1.4.1.1 Copper-64 (PET)

^{64}Cu ($t_{1/2}$ = 12.7 h) decays *via* β^+ emission (18%) with a maximum β^+ energy of 653 keV, the remainder decays via electron capture (43%) and β^- emission (39%).[8,9] Despite its relatively low β^+ yield, ^{64}Cu is a popular isotope used in development of PET imaging agents, and has been proposed as a dual imaging/therapy agent because of its accompanying β^- emission (0.579 MeV). Due to its intermediate half-life, ^{64}Cu-based radiopharmaceuticals can be used with small molecules, peptides or antibodies.[6,9] ^{64}Cu can also provide a matched element PET imaging pair

with the pure β- emitter ^{67}Cu ($t_{1/2}$ = 62 h), despite the fact the decay of ^{67}Cu gives rise to three γ rays suitable for SPECT imaging.[27] There are currently four clinical trials of various ^{64}Cu radiopharmaceuticals underway,[28] three of which incorporate a monoclonal antibody as the targeting vector of choice.[28] ^{64}Cu is commercially available and can be produced in a biomedical cyclotron via proton irradiation of enriched ^{64}Ni at 12 MeV via the ^{64}Ni(p,n)^{64}Cu reaction.[6,29]

In aerobic aqueous media, copper is predominantly in its +2 oxidation state, with a $3d^9$ electronic configuration and is susceptible to Jahn-Teller distortion. Cu(II) is classified as a borderline hard cation, hence it has high affinity for borderline donor atoms such as nitrogen.[8,29] The coordination number (CN) of Cu(II) ranges between 4 – 6 with an ionic radius of 57 – 73 pm.[30] Cu(II) and its complexes are susceptible to reduction *in vivo* (redox potentials of cellular reductases range between -200 and -400 mV versus NHE). The Cu(II)/Cu(I) reduction has been suggested to be a viable cause of radiocopper loss since $3d^{10}$ Cu(I) is much more labile to ligand exchange; hence, kinetic inertness of the copper-complex is of utmost importance in radiopharmaceutical design.[6,31]

Table 1.3 Properties of selected radiometals for imaging.

Nuclide	$t_{1/2}$	Emission (branching ratio)	E_{max}	E_{avg}	Production	Modality	Ref.
^{64}Cu	12.7 h	β^+ (18%)	653 keV	278 keV	Cyclotron, ^{64}Ni(p,n)^{64}Cu	PET	6,8,13
^{68}Ga	67.7 m	β^+ (89%)	1.899 MeV	836 keV	Generator, ^{68}Ge/^{68}Ga	PET	6,12,13
^{86}Y	14.7 h	β^+ (32%)	1.221 MeV	535 keV	Cyclotron, ^{86}Sr(p,n)^{86}Y	PET	6,7,13
^{89}Zr	3.3 d	β^+ (23%)	902 keV	396 keV	Cyclotron, ^{89}Y(p.n)^{89}Zr	PET	6,13
^{111}In	2.8 d	EC (100%)		171 keV 245 keV	Cyclotron, ^{111}Cd(p,n)^{111m,g}In ^{112}Cd(p,2n)^{111m,g}In	SPECT	6,7

1.4.1.2 Gallium-68 (PET)

^{68}Ga ($t_{1/2}$ = 67.7 min) is a β^+ emitter (89%) of maximum β^+ energy 1.9 MeV.[8] ^{68}Ga-based radiopharmaceuticals are typically matched with biovectors that can localize quickly, such as small molecules, peptides, and antibody fragments.[7,32] ^{68}Ga is an attractive PET nuclide because it is produced in a commercially available ^{68}Ge/^{68}Ga generator system, and decays predominantly via β^+ emission. The half-life of the parent ^{68}Ge ($t_{1/2}$ = 270 d) allows the generator to be used for up to 1 year, with two or three elutions per day, obviating the need for an on-site cyclotron.[32] The ^{68}Ge/^{68}Ga generator system is not yet FDA-approved, this deficiency is reflected in the lack of any ^{68}Ga FDA-approved imaging agents on the market; however, four clinical trials of varying ^{68}Ga-labelled peptides or antibody fragments are on-going.[28] Given its favourable decay properties for PET and availability for widespread use by introduction of the ^{68}Ge/^{68}Ga generator, the advancement of ^{68}Ga-radiopharmacy has been a focus of many research groups, including ours. Accordingly, chelating ligands of Ga(III) are a focus in this thesis.

In aqueous solution, gallium is exclusively in its +3 oxidation state, and free hydrated $[Ga(H_2O)_6]^{3+}$ is stable only under acidic conditions.[8] Gallium has a strong affinity for hydroxide ions, and when the pH of solution is raised above ~4, insoluble $Ga(OH)_3$ begins to form. At pH > 7 $[Ga(H_2O)_6]^{3+}$ hydrolyses to the gallate anion $[Ga(OH)_4]^-$ which may result in demetallation of its complexes.[8] Ga(III) is a small and highly charged cation with ionic radius of 47 – 62 pm (CN 4 – 6),[30] and can be classified as a hard acidic cation that prefers hard donor ligands such as anionic oxygen, and nitrogen. Ga(III) can form 3 – 6 coordinate complexes; however, most successful Ga(III) ligands are hexadentate, forming (distorted) octahedral complexes, since they are known to be thermodynamically stable and kinetically inert.[8,13,25]

1.4.1.3 Yttrium-86 (PET)

With a half-life of 14.7 h ^{86}Y decays via the emission of a relatively high energy β^+ particle (32%, 1.2 MeV), and γ emission (68%, 1.08 MeV).[6,13] ^{86}Y is a proposed PET nuclide since it can be used as an imaging surrogate for estimation of the pharmacokinetics and biodistribution of pure β^- emitter ^{90}Y. The advantage of using ^{86}Y as an imaging surrogate, as opposed to other surrogates such as ^{111}In or ^{89}Zr, is that identical chelate-bioconjugates can be used in parallel since ^{86}Y and ^{90}Y share the same chemistry.[33] Currently, no FDA-approved, or clinical trials of, ^{86}Y agents exist. High specific activity ^{86}Y can be produced in a medical cyclotron by irradiating $SrCO_3$ or SrO with 8 – 15 MeV protons via the ^{86}Sr(p,n)^{86}Y reaction.[8]

Yttrium is a large second row pre-transition metal which prefers the +3 oxidation state; with ionic radius of 90 – 108 pm (CN 6 – 9),[30] it can achieve coordination numbers as high as 10. Y(III) is considered a hard acidic cation (harder than Ga(III) or In(III)), and prefers hard donor atoms such as oxygen and nitrogen.[8]

1.4.1.4 Zirconium-89 (PET)

^{89}Zr ($t_{1/2}$ = 78.4 h) is a β^+ emitter (23%, 902 keV) with an ideal half-life for labelling antibodies in immuno-PET imaging.[34] Three ^{89}Zr-labelled antibodies are in different phases of clinical trials.[28] ^{89}Zr can be produced through a ^{89}Y(p,n)^{89}Zr reaction upon irradiation of natural yttrium foil with a 14 – 14.5 MeV proton beam.[7]

A group 4 second row transition metal, zirconium forms an extremely acidic hydrated Zr^{4+} cation with a small radius of 59 – 89 pm (CN 4 – 9).[30] Hydrated Zr(IV) likely only exists in extremely dilute and acidic solutions, and tends to form multiple monomeric and polynuclear

oxo/hydroxyl species in basic media.[8] The extremely hard character of Zr(IV) means it prefers to form complexes with multidentate ligands with hard donor atoms such as anionic oxygen from carboxylic acid or phosphinic acid residues, and prefers to form eight coordinate complexes.[8,35]

1.4.1.5 Indium-111 (SPECT)

^{111}In is the next most popular metallic SPECT radioisotope after ^{99m}Tc. With a half-life of 2.8 days, ^{111}In decays via electron capture (100%) by emission of two γ rays of energies 171 and 245 keV.[8] Its half-life is long enough for incorporation into antibody-based radiopharmaceuticals, and ^{111}In has been successfully introduced into two FDA-approved pharmaceuticals, sold under the trade names Octreoscan™ and ProstaScint®. In addition there are several ^{111}In-labelled radiopharmaceuticals in early to late stage clinical trials.[28] ^{111}In is produced commercially via the ^{111}Cd(p,n)^{111}In reaction or the ^{112}Cd(p,2n)^{111}In reaction, where natural cadmium is used as the target in both cases and irradiated with a proton beam, ^{111}In is subsequently removed from the target by ion exchange or solvent extractions.[8]

Indium is a group 13 element, and in aerobic aqueous media is only stable in the +3 oxidation state; its size (62 – 92 pm for CN 4 – 8 respectively[30]) means In(III) can reach coordination numbers of 7 – 8. It is a fairly hard acidic cation and consequently prefers chelators with hard donor atoms.[8]

1.4.2 Radiometals for Therapy

1.4.2.1 Yttrium-90 (β^-)

^{90}Y is a widely studied radiometal for β-therapy. With a half-life of 64 hours, it decays solely via β^- emission (100%) with a maximum energy of 2.27 MeV to form ^{90}Zr after decay.[36] ^{90}Y is an attractive radionuclide for therapy because it has a long enough half-life to be transported for clinical use and can be coupled to large targeting vectors such as antibodies; furthermore, the lack of γ-emission reduces the radiation dose to clinicians and patients.[8] The FDA-approved agent sold under the trade name Zevalin® is a ^{90}Y-labelled monoclonal antibody in β^- therapy of non-Hodgkin's lymphoma. The success of Zevalin® has sparked an increase in the number of ^{90}Y clinical trials, most of which are small variations or combination therapy protocols of the already approved agent.[28] ^{90}Y is produced commercially in a ^{90}Sr/^{90}Y generator system where the ^{90}Sr is adsorbed on a solid support and ^{90}Y can be eluted in high specific activities.[36] The well-established coordination chemistry of Y(III) was discussed earlier for ^{86}Y.

1.4.2.2 Lutetium-177 (β^-)

^{177}Lu ($t_{1/2}$ = 6.6 days) decays via the emission of three low energy β^- emissions with energies of 176 (12%), 384 (9%), and 497 keV (79%) used for radiotherapy.[37] In addition ^{177}Lu also emits two γ rays with maximum energies of 208 (11%) and 113 (6.6%) keV that can be used for SPECT imaging and dosimetry calculations.[36,37] ^{177}Lu has a long enough half-life that is best suited with biomolecules of long biological half-lives and the nuclide can be distributed to hospitals in remote regions. The low β^- energy emission is favourable for treating small metastases whilst minimizing kidney doses.[37] Despite its relatively long half-life, the radionuclide is part of one clinical trial in late phase II investigating the therapeutic potential of a ^{177}Lu-labelled peptide (^{177}Lu-DOTA-Octreotate) for treatment of neuroendocrine tumours.[28]

^{177}Lu is most commonly produced in a medium flux reactor via irradiation of enriched ^{176}Lu (via the ^{176}Lu(n,γ)^{177}Lu reaction); this method gives ^{177}Lu in high yields with medium to high specific activities at low cost.[36,37]

Lutetium is last in the lanthanide group and has the smallest atomic radius (86 – 103 pm for CN 6 – 9 respectively[30]), its most common oxidation state is +3 and Lu(III) commonly forms complexes of coordination number 9.[37]

Table 1.4 Properties of selected radiometals for radiotherapy.

Nuclide	$t_{1/2}$	Emission (branching ratio)	E_{max}	E_{avg}	Production	Comment	Ref.
^{67}Ga	3.3 d	Auger (4.7 yield[a])		6.26 keV	^{68}Zn(p, 2n)^{67}Ga	Imaging γ radiation (93, 185 & 300 keV)	15,17,38
^{111}In	2.8 d	Auger (14.7 yield[a])		6.75 keV	Cyclotron, ^{111}Cd(p,n)^{111m,g}In ^{112}Cd(p,2n)^{111m,g}In	Imaging γ radiation (171 & 245 keV)	17
^{201}Tl	3.0 d	Auger (36.9 yield[a])		15.27 keV	^{203}Tl(p, 3n)^{201}Pb^{201}Tl	Imaging γ radiation (167 &135 keV)	15,17
^{203}Pb	2.2 d	Auger (23.3 yield[a])		11.63 keV	^{203}Tl(p,n)^{203}Pb ^{203}Tl(d, 2n)^{203}Pb	Imaging γ radiation (279 & 401 keV)	15,17
^{213}Bi	45.7 m	α (2%) β$^-$ (98%)	5.87 MeV α 5.55 MeV α		Generator, ^{225}Ac/^{213}Bi	Imaging γ radiation (440 keV)	6,15,38
^{225}Ac	10.0 d	α (100%)	5.83 MeV α 5.79 MeV α 5.73 MeV α		n-capture of ^{232}Th→^{233}U→^{225}Ac	Imaging γ radiation (86 & 440 keV)	15,38,39
^{90}Y	2.7 d	β$^-$ (100%)	2.27 MeV β$^-$	935 keV β$^-$	Generator, ^{90}Sr/^{90}Y	No imaging radiation	7,15,36, 38
^{177}Lu	6.6 d	β$^-$ (100%)	497 keV β$^-$ 384 keV β$^-$ 176 keV β$^-$		^{176}Lu(n,γ)^{177}Lu	Imaging γ radiation (208 & 113 keV)	15,38
^{186}Re	3.7 d	β$^-$ (91%)	1.02 MeV β$^-$		^{185}Re(n,γ)^{186}Re	Imaging γ radiation (137 keV)	36,40
^{188}Re	17.0 h	β$^-$ (100%)	2.10 MeV β$^-$		Generator, ^{188}W/^{188}Re	Imaging γ radiation (155 keV)	40,41
^{212}Pb	10.2 h	β$^-$ (100%)	570 keV β$^-$ 6.09 MeV α[b] 6.05 MeV α[b]		Generator, ^{224}Ra/^{212}Pb	Imaging γ radiation	42

[a]Auger yield = mean number of Auger electrons per decay. [b]Decay from ^{212}Bi daughter.

1.4.2.3 Rhenium-186/188 (β^-)

^{188}Re ($t_{1/2}$ = 17.0 h) is a high energy β^- emitter (100%, E_{max} = 2.1 MeV) that has many accompanying γ-ray emissions from the depopulation of excited daughter states and the 155 keV γ can be used for imaging.[40,41] ^{186}Re ($t_{1/2}$ = 3.7 d) is a moderate energy β^- emitter (E_{max} = 1.02 MeV, 91%) with an accompanying 137 keV γ-ray that can be used for imaging.[36] ^{188}Re can be obtained from a ^{188}W/^{188}Re generator, similar in design to the commonly used ^{99m}Tc generator; Na[^{188}Re(V)O_4] can be eluted from the generator in high specific activity with saline. The half-life of the parent ^{188}W ($t_{1/2}$ = 60 d) permits the generator to be used for 2 – 6 months.[36,40] The production of ^{186}Re is reactor-based via irradiation of ^{185}Re with neutrons (^{185}Re(n,γ)^{186}Re) yielding low to medium specific activity ^{186}Re.[36,40] Of the two isotopes, ^{188}Re has garnered the most attention and is part of a completed Phase I trial for treatment of lung carcinomas, and a Phase I trial in recruiting stage for treatment of hepatocellular carcinomas.[28]

Rhenium, a group 7 transition metal, is a congener of Technetium. As a consequence Re shares parallel chemistry and isostructural complexes with Tc, and much of the same coordination chemistry employed in Tc radiopharmaceuticals can be adapted for Re. Although it is worth nothing that $[ReO_4]^-$, the starting eluent from ^{188}Re production, is significantly harder to reduce than the ^{99m}Tc analogue, $[TcO_4]^-$.[40] Rhenium exists in a range of oxidation states from +7 to -1, with an ionic radius of 53 – 63 pm (CN 6) for the +7 to +4 ions.[30] Much of the progress of Re(I) and Tc(I) radiopharmaceuticals has focused around the $[M(I)(CO)_3]$ core. This *fac*-$[M(CO)_3(H_2O)_3]^+$ 'tricarbonyl core' has been thoroughly discussed and reviewed elsewhere.[40,43]

1.4.2.4 Actinium-225 (α)

^{225}Ac has a 10 day half-life and can be incorporated into a radiopharmaceutical for α therapy. ^{225}Ac has been proposed to be used as an *in vivo* generator of its daughter isotope ^{213}Bi,

also an α-emitter. This method has been developed by the Memorial Sloan-Kettering Cancer Center.[44] The decay of a single ^{225}Ac (~ 6 MeV α particle) goes predominantly through 6 daughters until it cascades to stable ^{209}Bi producing in total 4 α and 3 β^- emissions, and 2 useful γ emissions, the ^{213}Bi 440 keV γ emission can be used for imaging and dosimetry studies. Some of the intermediate daughters in the decay include ^{221}Fr ($t_{1/2}$ = 4.8 min), ^{217}At ($t_{1/2}$ = 32.3 ms), and ^{213}Bi ($t_{1/2}$ = 45.6 min), each of which emits an α particle.[45] ^{225}Ac can be produced by natural decay of ^{223}U, or by accelerator-based methods.[45] Actinium-225 has been incorporated primarily into antibody-based agents, two of which (^{225}Ac-Lintuzumab, and ^{225}Ac-humanized anti-CD33 mAb (HuM195)) are currently in clinical trials.[28]

There are no stable isotopes of actinium, as a result the chemistry of actinium is virtually unknown; however, the longer lived isotope ^{227}Ac ($t_{1/2}$ = 21.8 y) could potentially be used to help elucidate the chemistry of actinium. The use of actinium in radiopharmaceuticals has a history of unfavourable radiolabelling chemistry and poor metal-chelate stability,[46] and the lack of an appropriate chelator that can stably bind the nuclide as well as control the fate of the daughters remains a challenge. Actinium isotopes in radiopharmaceuticals are typically +3 ions with a documented ionic radius of 112 pm (CN 3).[30] The large size is likely suited to large polydentate macrocyclic chelators of high denticity, since most commonly used chelates for Ac(III) (*vide infra*) range between 8 – 12 coordinate.[45,47]

1.4.2.5 Bismuth-213 (α)

Bismuth-213 is an α emitter with a half-life of 45.6 min and decays through two different pathways: via α emission (2%, 5.8 MeV) followed by two 2 β^- emissions, or β^- emission (98%) followed by an α emission (8.4 MeV) and subsequent β^- emission to stable ^{209}Bi.[44] In addition, a 440 keV (26%) photon emission can be used for dosimetry studies. ^{213}Bi can be

generator produced from the decay of ^{225}Ac in the $^{225}Ac/^{213}Bi$ generator.[48] A clinically-used generator has been developed that can supply ^{213}Bi for 10 – 15 days.[44] Despite its relatively short half-life, a ^{213}Bi-labelled antibody agent (^{213}Bi-HuM195 (humanized anti-CD33)) was part of a clinical trial investigating the use of this agent in combination therapy with chemotherapy and has since completed.[28,49]

Bismuth is typically found in its +3 oxidation, with an ionic radius of 96 – 117 pm (CN 5 – 8).[30] Bi(III) has high affinity for oxygen and nitrogen donors, and also forms stable complexes with sulfur and halogens (especially iodide).[50] The large multidentate ligand CHX-A"-DTPA (N_3O_5) (*vide infra*) has been used in many of the labelling studies of ^{213}Bi-antibody conjugates,[44,48] and forms a dianionic octadentate complex with Bi(III).[51]

1.4.2.6 Lead-212 (α source)

^{212}Pb ($t_{1/2}$ = 10.6 hours) is a β^- emitter (100%, 570 keV) widely studied for α-particle therapy, because it is the immediate parent radionuclide of the α-emitter ^{212}Bi ($t_{1/2}$ = 60.6 m). ^{212}Pb-labelled mAbs can thus act as *in vivo* generators of ^{212}Bi, extending the short half-life of ^{212}Bi.[42] The bioconjugate ^{212}Pb-TCMC-trastuzumab is in Phase I clinical trials for treatment of cancers that express the HER-2 antibody receptor.[28] The readily obtained $^{224}Ra/^{212}Pb$ generator can be used for on-site production of either ^{212}Pb or ^{212}Bi, each can be specifically eluted by controlling the acid strength of the eluent. Due to the short half-life of ^{224}Ra ($t_{1/2}$ = 3.7 d), the generator must be regenerated after 1 – 2 weeks.[42]

Lead is as a post-transition metal with ionic radius of 119 – 149 ppm (2+ ion, CN 6 – 12).[30] Radionuclides of lead are found in their +2 oxidation state, classified as a borderline acid according to Pearson's hard-soft acid-base theory. The most common chelator of Pb(II) for

radiopharmaceuticals, TCMC (*vide infra*), employs an octadentate ligand set with nitrogen and oxygen donor atoms.[52]

1.4.2.7 Auger Electron Emitters

Based on the LET and effective range of this radiation, Auger electron emissions are only effective as therapeutics if they can be internalized in the cell nucleus; this remains a great challenge. There are currently no FDA-approved agents or on-going clinical trials of radio-therapeutic Auger electron emitters. ^{111}In, a popular SPECT radionuclide, also has an Auger electron emission (6.75 keV) that has been used for therapy studies in one clinical trial of a radiolabelled tumour targeting peptide (Octreoscan, ^{111}In-DTPA-D-Phe-Octreotide).[28,37] Other Auger electron emitters such as ^{201}Tl ($t_{1/2}$ = 3.04 days, 15.27 keV), ^{203}Pb ($t_{1/2}$ = 2.16 days, 11.63 keV), and ^{67}Ga ($t_{1/2}$ = 3.26 days, 6.26 keV),[17] better known for their accompanying imaging decays used in SPECT, have also recently gained some attention as potential Auger electron therapeutic nuclides,[17,18] but will not be a focus of this chapter.

1.5 Bifunctional Chelates (BFCs)

It is of utmost importance that the correct chelator matches a specific radiometal. Important properties of the metal-chelate complex as they relate to radiopharmaceutical design, such as thermodynamic stability, kinetic inertness, and complexation kinetics, must be evaluated (*vide supra*). The overall charge of the metal-chelate complex should also be taken into consideration since it may influence the biodistribution of the radiopharmaceutical. This is of less concern for bioconjugates of large molecular weight (e.g. monoclonal antibodies); however, for radiopharmaceuticals conjugated to peptides, small molecules, or antibody

fragments, the metal-chelate complex plays a significant role in the overall pharmacokinetic behaviour of the system due to its relative size when compared to the targeting vector.

Common ligands utilised in radiopharmaceuticals can be grouped into two classes: acyclic (open chain) or macrocyclic (closed chain). Generally, acyclic chelates are less kinetically inert than macrocyclic complexes, even when thermodynamic stability (log K_{ML}) is comparable;[8,25] however, recent reports in the literature show good examples of acyclic chelators that exhibit both high thermodynamic stability with a specific metal and excellent kinetic inertness *in vitro*.[53,54] Acyclic chelators typically have faster metal-binding kinetics compared to macrocyclic analogues, a significant advantage for shorter-lived isotopes.

Despite the unique coordination chemistries of each metal, a few common chelators are used universally across a wide range of radiometals. Most notably, the tri- and tetraaza-based amino carboxylate macrocyclic chelators NOTA (N_3O_3) and DOTA (N_4O_4) and acyclic chelator DTPA (N_3O_5) have been often used in radiolabelling experiments with many of the metals discussed herein despite less than optimal properties with many metals. Their prevalence in radiochemistry may stem from convenience rather than 'best fit' for a metal because their bifunctional analogues are commercially available. Recently, the trend is leaning towards metal-specific chelators that exhibit fast radiochemical labelling under mild conditions, high thermodynamic stability, and kinetic inertness in hopes to improve tumour-to-background ratios by eliminating radionuclide loss *in vivo*. Below, brief discussions of the most common chelating ligands used in radiopharmaceutical applications are presented (Tables 1.5 and 1.6) with some new emerging examples.

1.5.1 Acyclic Chelators

EDTA (N_2O_4) (ethylenediaminetetraacetic acid) and DTPA (N_3O_5) (diethylenetriaminepentaacetic acid) are the most commonly exploited acyclic chelates in radiopharmaceutical chemistry. DTPA (Table 1.5) has been used extensively for labelling of a variety of radiometals such as Cu(II) (CN 6, log K_{ML} = 21.4),[8] Ga(III) (CN 6, log K_{ML} = 25.5),[8] In(III) (CN 7, log K_{ML} = 29.5),[8] Y(III) (CN 8, log K_{ML} = 22.0),[8] and Zr(IV) (CN 8, log K_{ML} = 35.8).[8] Its large binding sphere and hard oxygen donor set make it a good candidate for making stable metal-ligand complexes with larger hard acidic cations. DTPA derivatives have been successfully incorporated into three FDA-approved radiopharmaceuticals (^{111}In based agents Octreoscan™ and ProstaScint®, and ^{90}Y agent Zevalin) and it is the chelate in the most prescribed Gd MRI agent Magnevist™.[3] More recently, a modified DTPA chelate, CHX-A"-DTPA (N_3O_5) (Table 1.5), has shown great promise for In(III), Y(III) and Bi(III) isotopes; *p*-SCN-Bz-CHX-A"-DTPA (Table 1.5) is a commercial product and has been used in several clinical trials of ^{111}In, ^{90}Y, and ^{213}Bi.[28,50] CHX-A"-DTPA incorporates a more rigid chiral cyclohexyl (CHX-A") fragment into the backbone of DTPA in order to pre-organize the geometry of the donor atoms in hopes of improving kinetic inertness of the resulting metal complex.

DFO (O_6) (desferrioxamine) (Table 1.5) is an acyclic chelator well-known for its application in iron chelation therapy; it possesses three hydroxamate groups for chelating metals and a terminal primary amine that can be used for conjugation to biomolecules. Due to the similarities between high spin Fe(III) and Ga(III), DFO also forms gallium complexes of high thermodynamic stability and has proven useful for conjugation to peptides and small molecules.[31] One application of DFO lies in its ability to label Zr(IV); it is the most popular choice for zirconium radiochemistry.[34] Neither thermodynamic stability constants nor crystal structure with Zr(IV) have yet been reported, nonetheless DFO has the ability to bind zirconium

isotopes efficiently and rapidly. Excellent *in vitro* stability of the proposed $[Zr(DFO)(H_2O)_2]^+$ complex has been documented (with less than 2% demetallation after seven days in serum);[34] however, recent small animal PET studies with a ^{89}Zr-DFO-antibody demonstrate instability *in vivo* evinced by elevated uptake of ^{89}Zr in bone.[55]

H_2dedpa (N_4O_2) (1,2-bis{[[6-(carboxy)pyridine-2-yl]methyl]amino}-ethane) and its analogues (Table 1.5) are new additions to the class of acyclic chelates introduced by our group over the past five years. The hexadentate and octadentate ligands were originally published by Rodriguez-Blas and coworkers as ligands for magnetic resonance imaging (MRI) and binding to divalent metals Pb(II), Cd(II), and Zn(II).[56–58] H_2dedpa has since been repurposed for Ga(III) complexation, and was found to exhibit exceptionally high thermodynamic stability with Ga^{3+} ($\log K_{ML} = 28.1$),[54] and labels gallium isotopes quantitatively in 10 minutes at room temperature at high specific activities. Moreover, $[^{68}Ga(dedpa)]^+$ demonstrated high kinetic inertness *in vitro* and *in vivo*, remaining up to 97% intact for 2 hours when incubated with excess *apo*-transferrin.[54]

An octadentate H_2dedpa analogue with two additional carboxylic acid arms, H_4octapa (N_4O_4) (*N,N'*-bis(6-carboxy-2-pyridylmethyl)-ethylenediamine-*N,N'*-diacetic acid), has also been reported by our group to form kinetically inert complexes with In(III) and Lu(III), and may be a valuable alternative to the acyclic chelator DTPA for use with ^{111}In.[53,59] These ligands which include picolinic acid moieties as chelating arms have since been termed the "pa" family of chelating ligands and have been expanded to include analogues of varying geometry, denticity and donor atom type for use with varying radiometals such as ^{64}Cu, ^{89}Zr, $^{89/90}$Y, and ^{177}Lu.[60–63]

Table 1.5 Selected acyclic chelators highlighting relevant coordinating metals, thermodynamic stability constants (log K_{ML}), and bifunctional analogues (coupling moiety highlighted in blue).

Chelate	Native Donor Set	Metal Ions (log K_{ML})	Bifunctional Analogues
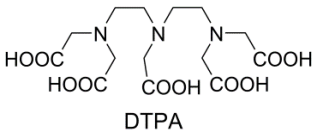 DTPA	N_3O_5	Cu(II) (21.4)[8] Ga(III) (25.5)[8] In(III) (29.5)[8] Y(III) (22.0)[8] Zr(IV) (35.8)[8] Bi(III) (35.6)[50]	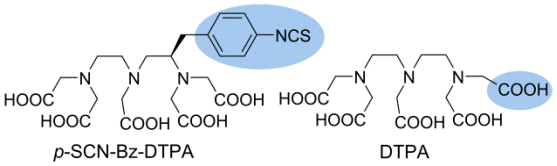 *p*-SCN-Bz-DTPA DTPA
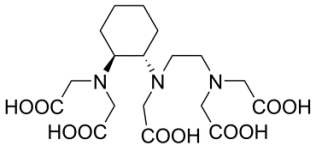 CHX-A"-DTPA	N_3O_5	In(III) Bi(III) Ac(III) Lu(III) Y(III)	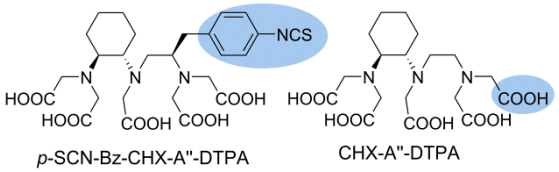 *p*-SCN-Bz-CHX-A"-DTPA CHX-A"-DTPA
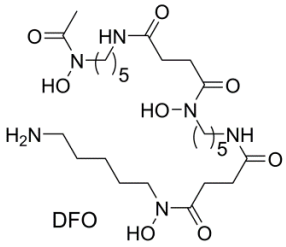 DFO	O_6	Ga(III) (28.6)[8] Zr(IV)	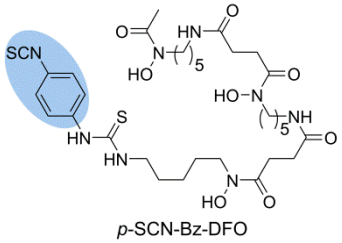 *p*-SCN-Bz-DFO
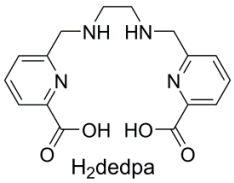 H_2dedpa	N_4O_2	Ga(III) (28.1)[54]	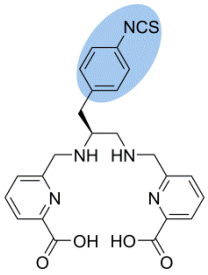 *p*-SCN-Bz-H_2dedpa

1.5.2 Macrocyclic Chelators

The popular tri- and tetraaza-based amino carboxylate macrocyclic chelators NOTA (1,4,7-triazacyclononane-1,4,7-triacetic acid) and DOTA (1,4,7,10-tetraazacyclododecane-1,4,7,10-tetraacetic acid) (Table 1.6), together with their bifunctional derivatives, form a class of 'gold standards' that have been used extensively in the labelling of a variety of radiometals

for imaging and therapy. NOTA and DOTA are in themselves BFCs; one of the pendant carboxylic acid arms can be used in a conjugation strategy to form a peptide bond with a biomolecule. This direct method alters the native binding sphere and donor-ability of the chelators. Alternatively, an extra carboxylic pendant arm is added (to form NODASA/NODAGA and DOTASA/DOTAGA) or a separate conjugation moiety (*p*-SCN-Bz) is incorporated at a position that will minimize the effect on the metal binding ability of the ligand (to form *p*-SCN-Bz-DOTA or *p*-SCN-Bz-NOTA) (Table 1.6).

NOTA (N_3O_3) has the smaller binding pocket of the two; it is most commonly used for gallium(III) isotopes (log K_{ML} = 31.0)[64] and is gaining popularity for copper(II) isotopes (log K_{ML} = 21.6)[64] where it forms hexadentate complexes with each.[29,64] The [Ga(NOTA)] complex is also extremely stable to acid dissociation, and remained unchanged by NMR after 60 days in 6 M HNO_3.[65] NOTA has become particularly attractive for Ga^{3+} because of its ability to label gallium isotopes nearly quantitatively at room temperature and the high *in vivo* stability of the resulting complex.

DOTA (N_4O_4) and its derivatives play an important role in clinical applications as it forms stable complexes with a variety of trivalent radiometals, such as ^{68}Ga (log K_{ML} = 21.3),[8] $^{86/90}$Y (log K_{ML} = 24.3),[8] ^{111}In (log K_{ML} = 23.9),[8] ^{177}Lu (log K_{ML} = 25.5),[64] and divalent nuclide ^{64}Cu (log K_{ML} = 22.3).[64,66] Cu-DOTA conjugates are only moderately stable *in vivo* and demetallate, evinced by high liver accumulation of free copper.[29,31] DOTA has also been used extensively for labelling gallium isotopes, despite its less than optimal stability and need for heating to label quantitatively. Also, a variety of DOTA derivatives have been tested as BFCs for ^{225}Ac with some success.[46]

Table 1.6 Selected macrocyclic chelators highlighting relevant coordinating metals, thermodynamic stability constants (log K_{ML}), and bifunctional analogues (coupling moiety highlighted in blue).

Chelate	Native Donor Set	Metal Ions (log K_{ML})	Bifunctional Analogues
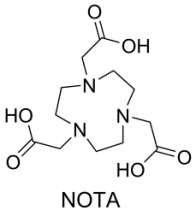 NOTA	N_3O_3	Cu(II) (21.6)[8] Ga(III) (31.0)[8] In(III) (26.2)[8]	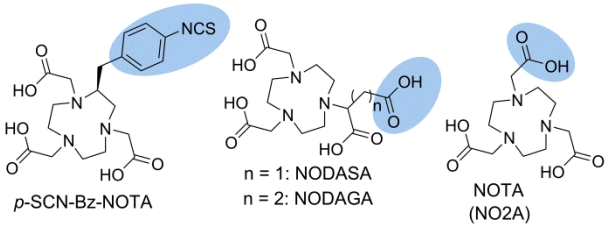 *p*-SCN-Bz-NOTA; n = 1: NODASA; n = 2: NODAGA; NOTA (NO2A)
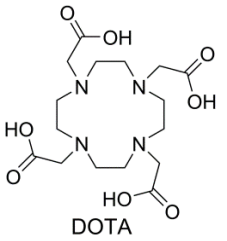 DOTA	N_4O_4	Cu(II) (22.3)[8] Ga(III) (21.3)[8] In(III) (23.9)[8] Y(III) (24.4)[8] Lu(III) (25.5)[64] Zr(IV) Ac(III)	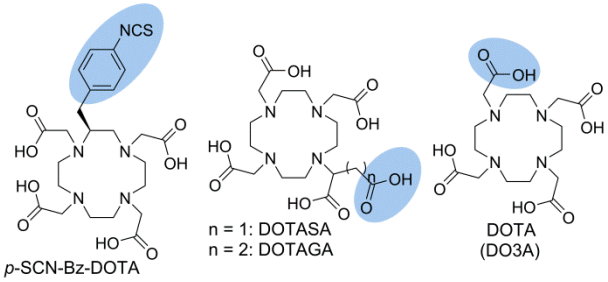 *p*-SCN-Bz-DOTA; n = 1: DOTASA; n = 2: DOTAGA; DOTA (DO3A)
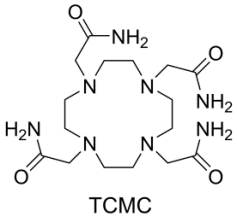 TCMC	N_4O_4	Pb(II)	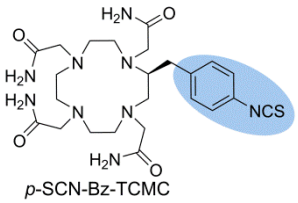 *p*-SCN-Bz-TCMC
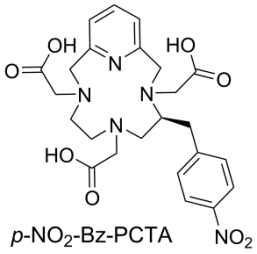 *p*-NO_2-Bz-PCTA	N_4O_3	Ga(III) Cu(II) (19.1)[67]	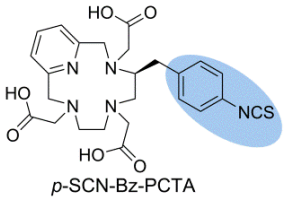 *p*-SCN-Bz-PCTA
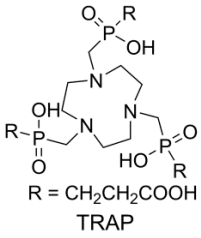 R = CH_2CH_2COOH TRAP	N_3O_3	Ga(III) (26.2)[68]	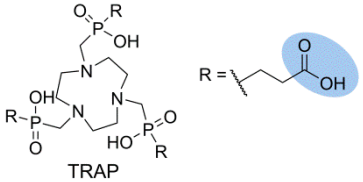 TRAP; R =

Table 1.6 Cont'd. Selected macrocyclic chelators highlighting relevant coordinating metals, thermodynamic stability constants (log K_{ML}), and bifunctional analogues (coupling moiety highlighted in blue).

Chelate	Native Donor Set	Metal Ions (log K_{ML})	Bifunctional Analogues
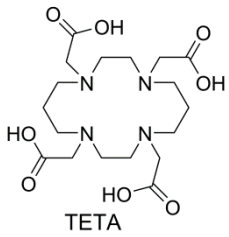 TETA	N_4O_4	Cu(II) (21.9)[8] Ga(III) (19.7)[8] In(III) (21.9)[8] Y(III) (14.8)[8] Lu(III) (15.3)[64]	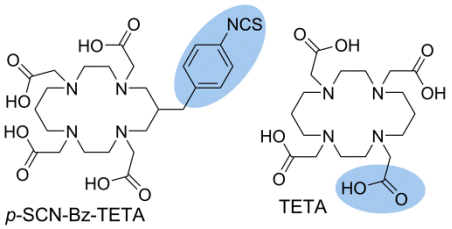 *p*-SCN-Bz-TETA TETA
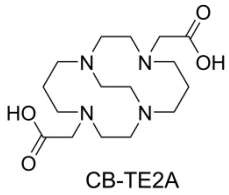 CB-TE2A	N_4O_2	Cu(II) Ga(III) In(III)	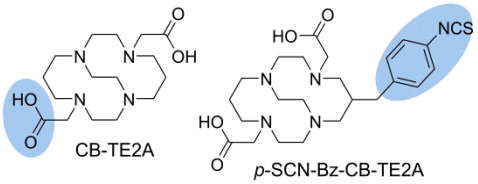 CB-TE2A *p*-SCN-Bz-CB-TE2A
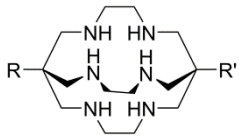 Sar derivatives	N_6	Cu(II) Ga(III)	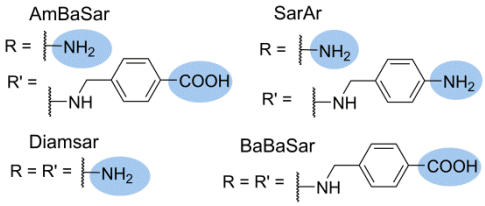 AmBaSar SarAr Diamsar BaBaSar
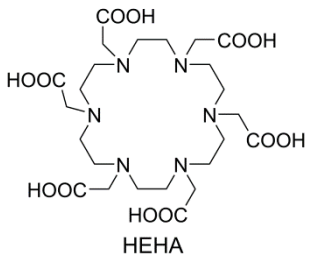 HEHA	N_6O_6	Ac(III)	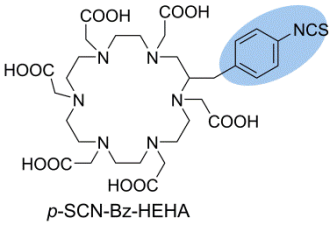 *p*-SCN-Bz-HEHA

Furthermore, an *N,N,N,N*-tetraamide analogue of DOTA, TCMC (N_4O_4) (1,4,7,10-tetraaza-1,4,7,10-tetra-(2-carbamoyl methyl)-cyclododecane), displays favourable stability *in vitro* and *in vivo* with Pb(II) isotopes compared to DOTA,[42,52] and is the chelate of choice in a ^{212}Pb clinical trial.[28] TCMC fully encapsulates the Pb(II), forming an octadentate complex with 4 nitrogen, and 4 amide oxygen donors.

The 12-membered tetraaza macrocycle, *p*-NO_2-Bz-PCTA (N_4O_3) (PCTA = 3,6,9,15-tetraazabicyclo[9.3.1]pentadeca-1(15),11,13-triene-3,6,9-triacetic acid) (Table 1.6) exhibits favourable labelling and stability properties for copper (log K_{ML} = 19.1)[67] and gallium isotopes.[31] The chelate incorporates a *p*-nitrobenzyl moiety that can be converted into an isothiocyanate for attachment of targeting groups. *p*-NO_2-Bz-PCTA exhibits much faster complex formation compared to DOTA for gallium with the ability to rapidly and efficiently label ^{68}Ga (> 96% RCY) at room temperature in 10 minutes, and exhibits high kinetic inertness *in vitro* when incubated with *apo*-transferrin (less than 10% transchelated with transferrin after 4 hours).[69] *In vivo*, the biodistribution of ^{68}Ga-labelled *p*-NO_2-Bn-PCTA is similar to that of the analogous *p*-NO_2-Bz-DOTA complex, circulating in the blood and excreted through the kidneys over 4 hours, suggesting *p*-NO_2-Bz-PCTA may be an improved alternative to DOTA in Ga based radiopharmaceutical development.[69] The chelate can also rapidly and efficiently label ^{64}Cu (> 98% RCY) in 5 minutes at room temperature.[70]

TRAP (previously known as PrP9, Table 1.6) (N_3O_3) (1,4,7-triazacyclononane phosphinic acid) is a new addition to the family of macrocyclic chelators for gallium; it is derived from a NOTA-type framework with phosphinic acid arms replacing the carboxylic acid arms. TRAP shares strong thermodynamic stability with Ga(III) (log K_{ML} = 26.2),[68] and has the ability to incorporate ^{68}Ga nearly quantitatively (>95% RCY) at low concentrations in even strongly acidic media in 5 minutes at 60 °C.[68,71] In addition, the three carboxylic pendant arms attached to the phosphinic acids provide a convenient way for introduction of three targeting groups through a peptide bond conjugation strategy.

The tetraazamacrocycle TETA (N_4O_4) (1,4,8,11-tetraazacyclotetradecane-1,4,8,11-tetraacetic acid) (Table 1.6) has been extensively used for Cu(II) radiopharmaceuticals. Cu(II) shares a similar thermodynamic stability with TETA and DOTA (log K_{ML} = 21.9 and 22.3,

respectively)[8] although $[Cu(TETA)]^{2-}$ complexes are more kinetically inert compared to $[Cu(DOTA)]^{2-}$, but still suffer from radiocopper loss *in vivo*.[72,73]

To improve on the stability of the TETA framework, the cross-bridged analogue CB-TE2A (N_4O_2) (1,4,8,11-tetraazabicyclo[6.6.2]hexadecane-4,11-diyl)diacetic acid) (Table 1.6) exhibits greatly improved stability of copper complexes; however, labelling CB-TE2A with Cu(II) isotopes requires rigorous heating (>90 °C) and prolonged reaction times (~1 h), which impedes its use with thermally sensitive biomolecules.[29,31]

The sarcophagine type bifunctional chelators (N_6) (sarcophagine = Sar = 3,6,10,13,16,19-hexaazabicyclo[6.6.6]icosane) (Table 1.6) are the most recent addition to the class of ligands employed for radiocopper labelling, but have also been evaluated for ^{68}Ga.[31] Sarcophagines have the ability to label micromolar concentrations of ^{64}Cu quantitatively at room temperature in minutes.[29] In addition, the [Cu(Sar)] complexes exhibit high *in vitro* kinetic inertness against mouse serum (>98% intact after 4 hours).[74] These characteristics make Sar cages a promising scaffold for incorporation into copper-radiopharmaceuticals of thermally sensitive biomolecules.[29,31] Labelling with ^{68}Ga, however, requires heating at 85 °C for 30 min.[31]

The large 12-coordinate (N_6O_6) ligand HEHA (1,4,7,10,13,16-hexaazacyclohexadecane-1,4,7,10,13,16-hexaacetic acid) (Table 1.6) has been investigated primarily for radiolabelling of the large radiometal ^{225}Ac, and has been successfully conjugated with a variety of antibodies.[47] Radiolabelling with ^{225}Ac at 37 °C, yields RCYs of 60-85% after 30 minutes. The bioconjugates exhibited adequate stability in bovine serum at 37 °C during early time points; however, later time points suggest more than one-third of the ^{225}Ac-HEHA-bioconjugate degraded or transchelated with serum proteins.[47,75]

1.6 Linker – Bioconjugation Strategies

The placement and mode of attachment of the BFC to the biomolecule is important; it is crucial that this conjugation does not interfere with the binding ability of the chelate to metal ion, or the affinity of the biomolecule for its intended target. Often the targeting vectors are sensitive biomolecules which risk degradation when heated, so it is best if the conjugation strategy occurs rapidly at mild temperatures to retain the integrity of the targeting vector. Predominantly, four conjugation strategies are employed extensively in radiopharmaceutical construction: amide, thiourea, thioether, and click chemistry triazole bonds (Figure 1.4). Often biomolecules have primary amines or free thiols in their structure for conjugation to a BFC, so all that remains is to introduce a conjugation moiety on the chelate that is compatible with the functional group(s) on the biomolecule.

Amide bond formation involves coupling of a carboxylic acid to a primary amine with the aid of a coupling agent such as HATU (*O*-(7-azabenzotriazol-1-yl)-*N*,*N*,*N*′,*N*′-tetramethyluronium hexafluorophosphate), HOBt (hydroxybenzotriazole) or EDC (1-ethyl-3-(3- dimethylaminopropyl)carbodiimide), or a carboxylic acid activated with a succinimidyl (NHS) ester is coupled to a primary amine without the need for additional coupling agents.[13] Many of the chelators used in radiochemistry have several carboxylic arms, and selective amide formation with one of the arms can be accomplished by controlling the mole ratios of chelate to targeting vector, and/or using protecting group chemistry to shield the other carboxylic acid pendant arms from conjugating with the primary amine on the biomolecule. Amide bond formation is the most popular conjugation strategy used in peptide-bioconjugates; the peptide coupling reaction is often done on a solid peptide resin followed by full deprotection of the chelate and cleavage from the resin.

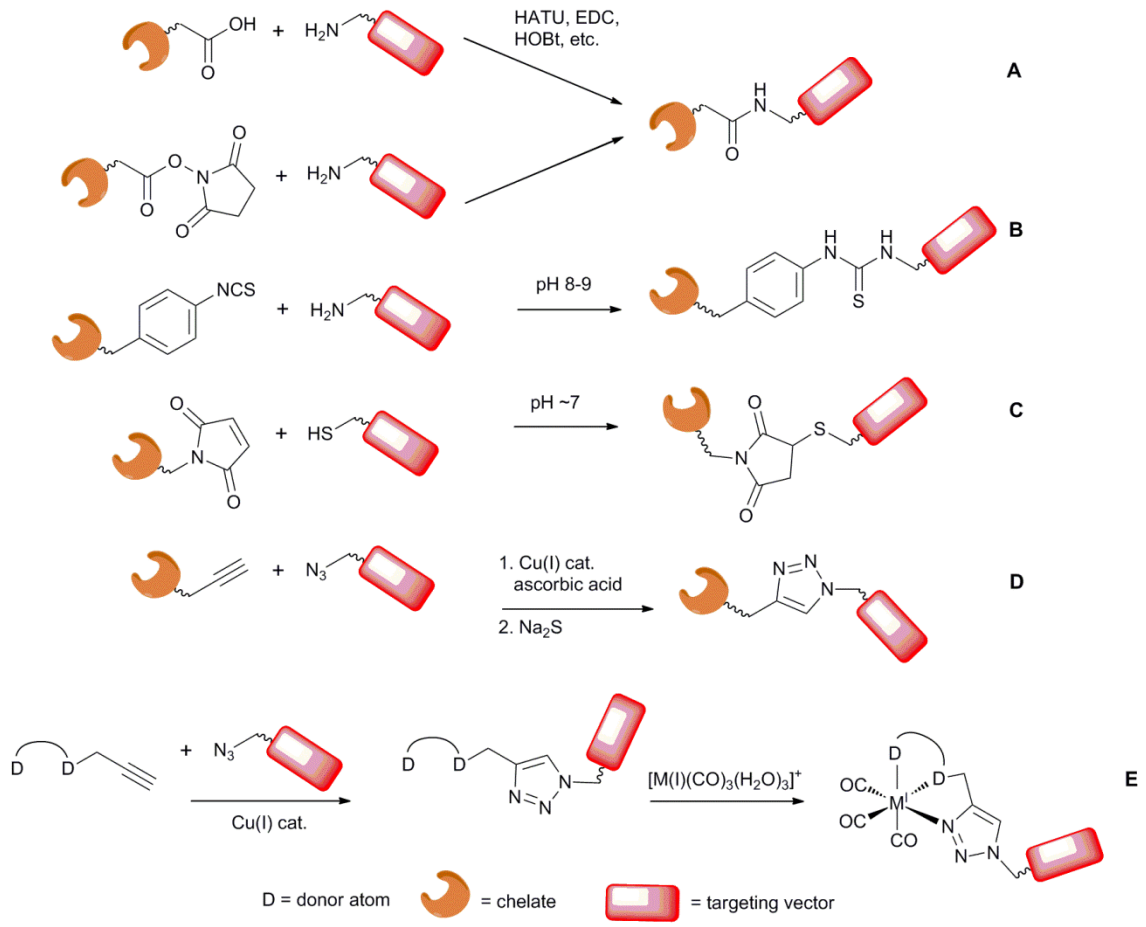

Figure 1.4 Four common types of bioconjugation bond forming reactions employed in radiopharmaceutical design: A. peptide; B. thiourea; C.thioether; and D. triazole-click. E. "Click-to-chelate" method for M(I) = Re(I)/Tc(I).

Thioether bond formation links a thiol with a maleimide and occurs under mild conditions (pH 7.2 to 7.4) without the need for heating or catalyst. This reaction has been used for coupling of both peptides and proteins, where thiol groups are naturally present and used for conjugation to a BFC that has been functionalized with a maleimide.[76] Thiourea bond formation couples an isothiocyanate to a primary amine; this reaction must be done in slightly basic conditions (pH 8-9) where the deprotonated amine is required for reactivity.[76] Generally,

thiourea bond formation is slower than thioether coupling,[76] but both reactions can be accomplished on the fully deprotected ligand.

The copper-catalyzed 1,3-dipolar Huisgen cycloaddition occurs between terminal alkynes and azides to form a 1,4-substituted triazole, and is often termed the "click" reaction.[76] Use of a Cu(I) catalyst leads to fast reaction times, and controls the regioselectivity of the reaction. Furthermore, both functional groups (azide and alkyne) are stable to most common coupling conditions and can be introduced into the chelate or biomolecule with relative ease.[76] Although a copper catalyst in a reaction involving a chelate can lead to copper complexation, copper is readily removed by quenching the reaction with Na_2S to precipitate the cupric sulfide. The resulting triazole carries electron-rich nitrogen atoms, which in some cases can act as additional donor atom(s) to the metal ion.[62,77] This method, dubbed "click-to-chelate", was first developed for the attractive *fac*-$[M(I)(CO_3)(L)_3]^+$ tricarbonyl core (M(I) = Re/Tc(I)) and has recently been extended for use with other radiometals.[62,77] It can provide an elegant method for adding the necessary donor atoms for the metal through the N3 of the 1,2,3-triazole ring while simultaneously incorporating the targeting vector (Figure 1.4).[78]

1.7 Targeting Vectors

The physiological traits of cancer suit the use of radiopharmaceuticals for the specific detection and treatment of the complex disease. When a cell becomes cancerous a cascade of biochemical responses occurs, and as a result the diseased cells exhibit many biomarkers that, although present in normal cells, are either mutated or over-expressed.[66,79,80] Various surface receptors are over-expressed in particular tumour types, and radiolabelled biomolecules that bind to these receptors can be used to visualize tumours scintigraphically, or deliver a therapeutic radiation dose to them specifically (Figure 1.5). There has been tremendous

progress in the identification of these over-expressed surface receptors (antigens) and the native ligands (biomolecules) that bind to them.[64,81] The choice of targeting vector is crucially important in the development of a successful radiopharmaceutical, since the effectiveness of targeted therapies depends on the molecular target expression in the patient. The antigen must be sufficiently over-expressed compared to neighbouring healthy tissue so as to create a positive response, and the biomolecule must bind specifically with high affinity to the desired antigen.[15,75]

There are also passive ways to target cancer cells based on such unique characteristics as the enhanced vascular permeability of tumour blood vessels, and poor lymphatic drainage systems, known collectively as the enhanced permeability and retention (EPR) effect, or tumour microenvironment such as reduced pH or reduced oxygen concentration.[82] Herein we will focus on the use of biomolecules (antibodies, peptides, and antibody fragments) that target over-expressed receptors on the surface of cancer cells.

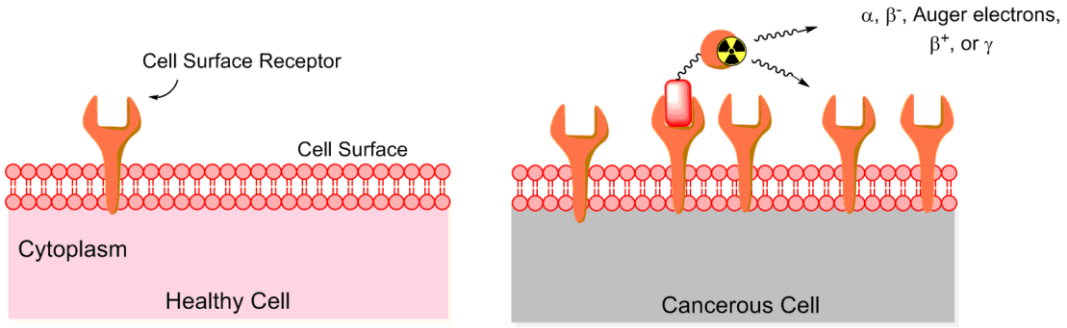

Figure 1.5 Cartoon depiction of targeting over-expressed cell surface receptors in cancerous tissue with radiopharmaceuticals.

1.8 Biomolecules

Many biomolecules have been used to target surface receptors on cancer cells. Most commonly peptides, antibodies, antibody fragments, small molecules,[80] and more recently,

nanoparticles[83] have been conjugated to a BFC. Each class of biomolecule has different biological properties, such as varying biological half-lives, and these properties must be matched with the physical properties of the radionuclide. In general, molecular size greatly influences circulation time; the larger the molecule the longer it will take to accumulate in tumours. In order to produce a clear image or minimize radiation dose to healthy tissue, the radiopharmaceutical should specifically accumulate at high levels within the tumour target sites and unbound agent should clear from the blood within a time frame compatible with the radioactive half-life of the nuclide.[15] A few of the most popular targeting vectors of choice for radiopharmaceuticals are discussed below, highlighting their strengths and weaknesses, as well as important factors affecting their potential for use in radiopharmaceuticals.

1.8.1 Antibodies

An antibody (Ab), also known as an immunoglobulin (Ig), is a large Y-shaped protein of relatively high molecular weight (140-160 kDa).[80] Upon their discovery, monoclonal antibodies (mAbs) were termed "magic bullets" because they were thought to be widely applicable in cancer therapy; however, their use to date remains limited due to reduced accumulation in tumours and relatively slow blood clearance (3-4 weeks) resulting in only moderate tumour-to-background ratios.[15] Nonetheless, there are four FDA-approved radiolabelled mAbs on the market, Bexxar (^{131}I agent), Zevalin (^{90}Y-labelled ibritumomab tiuxetan), ProstaScint® (^{111}In agent), and a ^{99m}Tc agent,[3] in addition there are dozens of clinical trials currently testing the efficacy of radiolabelled antibodies.[28] Because of their long biological half-lives *in vivo*, the antibody must be matched with a radioisotope that has a comparably long half-life, in order to allow for tumour accumulation and non-specific clearance. ^{89}Zr ($t_{1/2}$ = 3.3 days) has been

suggested as a good suitor for immunoPET, and much effort is being made towards a ^{89}Zr-immuno-conjugate.[84]

Another consequence of their large size, mAbs have multiple functional groups available on their surface making it difficult to control the number and location of BFC attachments in conjugation reactions; often multiple chelates can be attached to a single antibody. The number of chelates attached per antibody can be deduced through an isotopic dilution method and is controlled by altering the BFC to antibody molar ratios.[13] It is usually favourable to introduce as much radioactive-binding capability as possible without negatively affecting the binding affinity of the antibody to its antigen.

1.8.2 Peptides

Peptides have a broad range of biological targets and have desirable pharmacokinetic characteristics, such as high uptake in target tissue and rapid clearance from blood and non-target tissue, that are favourable for incorporation into a radiopharmaceutical. Moreover, peptides can be easily chemically modified and radiolabelled in many ways, and have garnered much interest as targeting vectors for radiopharmaceutical purposes. FDA-approved Octreoscan™ (^{111}In-DTPA-octreotide) is one example of a radiolabelled peptide used in SPECT imaging.[3] The fast localization and clearance of peptides suggests they are well suited to radioisotopes of short half-life; in this respect much effort is being made towards peptide bioconjugates of ^{68}Ga ($t_{1/2}$ = 68 min) with several clinical trials in progress.[28]

Most naturally occurring peptides are prone to rapid enzymatic degradation; in order to improve their metabolic stability, peptides have been engineered that incorporate non-natural amino acid residues, amino alcohols, or cyclic peptides, these modifications must not affect the

native binding affinity of the peptide for the antigen.[64,85,86] A spacer can also be introduced to the end of the peptide before it is conjugated to the BFC, in order to minimize or eliminate any interference between the two moieties, or act as a pharmacokinetic modifier. Most commonly used spacers include short amino acid sequences (dimer or trimer of β-Ala, Gly, or N^{ε}-amino hexanoic acid), low molecular weight polyethylene glycol (PEG), or hydrocarbon chains.[85] The length, flexibility, hydrophobicity and charge should be considered when selecting an appropriate spacer, as its introduction can greatly influence the biodistribution of the radiopharmaceutical.[85]

Solid-phase peptide synthesis (SPPS) is widely used and can easily prepare peptides with a variety of modifications.[87] The appropriate binding site can be introduced on the end of the peptide, and the point of conjugation to BFC can be controlled, and is typically set at 1:1 chelate to peptide.

1.8.3 Other Biomolecules and Targeting Vectors

Other biomolecules being investigated as targeting moieties in radiopharmaceuticals include antibody fragments, oligonucleotides,[88] and nanoparticles.[82,83] With the addition of these biomolecules, there is a large library of targeting vectors with varying pharmacokinetic properties to choose from.

Advances in protein engineering have led to a range of antibody fragments of varying sizes with corresponding varying pharmacokinetic properties that can be used as targeting vectors in radiopharmaceutical design. Examples of antibody fragments include scFv (single-chain variable fragment, 25 kDa), diabodies (50 kDa), Fab (fragment, antigen binding, 55 kDa), minibodies (80 kDa), and $F(ab')_2$ (110 kDa); each is comprised of different domains of an intact

mAb and nevertheless retains the specificity and affinity of the parental antibody.[89,90] Affibodies are the newest type of antibody fragment that have been exploited as an antibody mimetic; they are engineered molecules of 58 amino acid residues (6-7 kDa) with a three-α-helical bundle structure derived from one of the binding domains of a fully intact antibody. In general, the biological half-life of antibody fragments is inversely proportional to the molecular weight of the molecule. With their reduced size antibody fragments exhibit faster blood clearance (<10 h for an Affibody compared to 3 – 4 weeks for the full mAb),[91] which means faster acquisition times for imaging purposes, and lower non-specific radiotoxicity for therapeutic isotopes. In turn, the isotopes used with antibody fragments can have shorter half-lives. For example, a ^{68}Ga-labelled antibody fragment, F(ab')$_2$-trastuzumab, has shown great promise for PET imaging of solid tumours that express the HER-2/*neu* receptor,[92] and is currently in clinical trials.

The use of nanoparticles as targeting vectors in nuclear medicine does not rely on the ability of the particle to bind to an over expressed surface receptor; instead the biodistribution of nanoparticles is dominated by their large size and ability to take advantage of the EPR effect of cancer tissue (*vide supra*), where 'leaky' vessels of poorly vascularized tumours allow for the uptake and retention of large macromolecules. To improve the tumour-targeting ability of nanoparticles, traditional targeting vectors, such as peptides or antibodies, are often introduced onto their surface.[93]

1.9 Biological Targets

For an antigen to be selected as an appropriate target it must be readily accessible, highly overexpressed and preferably expressed only within the desired target tissue.[15] In addition, some antigens internalize their binding ligands and as a consequence trap the

radiopharmaceutical in the cell. This trait is attractive for radiotherapy, where complex and multi-daughter decay pathways of therapeutic nuclides complicate the stability of the metal-chelate complex. For Auger electron emitters that must reach the nucleus to cause cell death, internalization into the cytoplasm is the first step in entering the nucleus. An exhaustive review of all antigens that have been targeted with radiopharmaceuticals is beyond the breadth of this introduction, nor is it a focus of this thesis. Some comprehensive reviews outlining the peptide[64,66,85,87,94–96] and antibody[15,38] binding antigens can be found elsewhere. Instead some of the most popular antigens being investigated will be outlined and accompanied with a few specific examples highlighting the potential of radiometals in the field of imaging and treatment of cancers.

Common peptide binding antigens found on human cancers include the integrin, somatostatin (SST), Gastrin-releasing peptide (GRP), Melanocortin 1 (MC1), and cholecystokinin 2 (CCK2)/gastrin receptors. Frequently targeted antibody receptors include HER-2/*neu*, Epidermal Growth Factor (EGF), and Vascular Endothelial Growth Factor (VEGF). Many of these receptors are found on a variety of cancer types presenting a broader platform for their use in the clinic.[38,85]

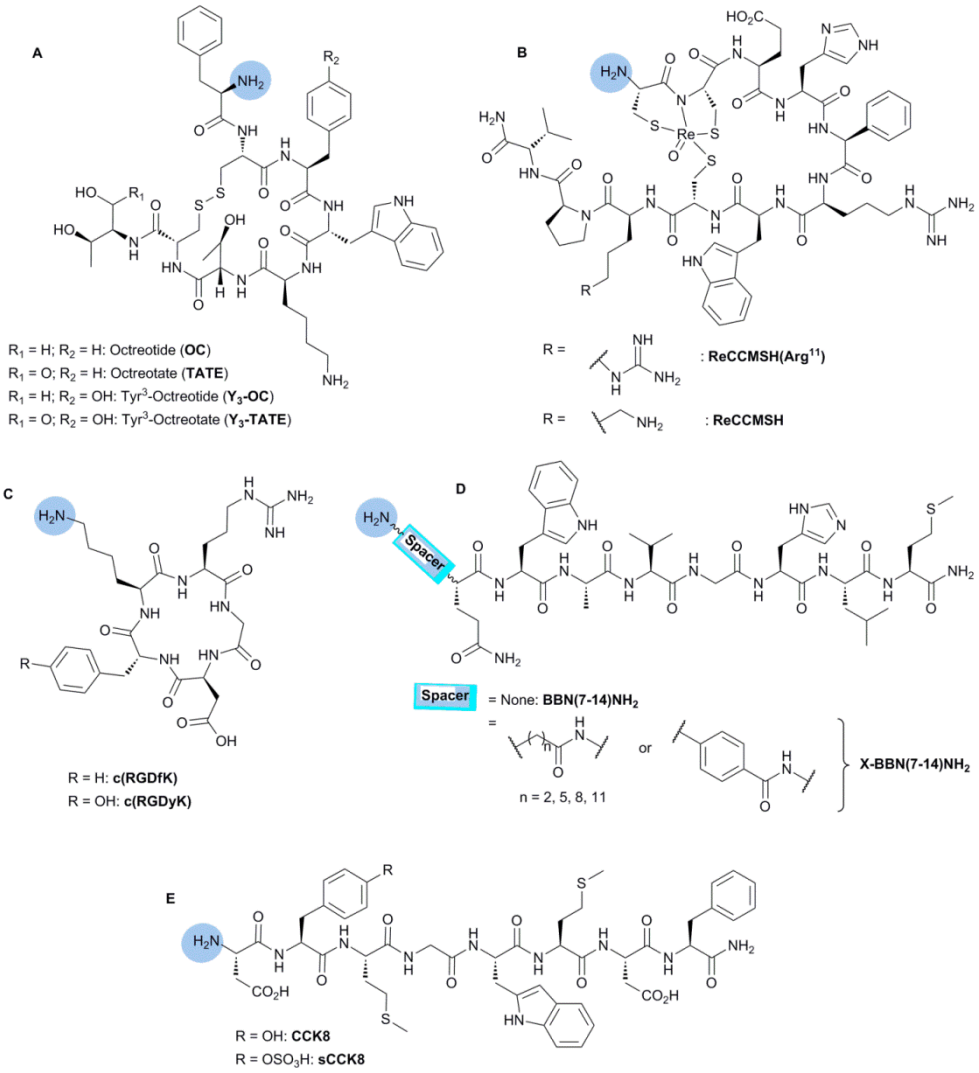

Figure 1.6 Selected targeting peptides for surface receptors used commonly in radiopharmaceutical design: A. somatostatin (SST), B. melanocortin 1 (MC1), C. $\alpha_v\beta_3$ integrin, D. gastrin-releasing peptide (GRP), and E. cholecystokinin 2(CCK2)/gastrin. Moiety used in conjugation reactions highlighted in blue.

In most cases the receptor's native targeting molecule is not an appropriate choice for use *in vivo* due to rapid degradation (of peptides) or slow blood circulation time (of mAbs); thus, analogues of native ligands have been fabricated which retain the binding avidity to the target antigen, while exhibiting favourable pharmacokinetic behaviour *in vivo*.

The naturally occurring cyclic neuropeptide somatostatin (SST) that binds the SST receptor with high affinity is rapidly degraded *in vivo* by enzymes, eliminating its potential for use *in vivo*. Analogues of the SST peptide, such as octreotide (OC) and octreotate (TATE) (Figure 1.6), are stable to enzymatic degradation while maintaining high binding affinity and specificity for the SST receptor. ^{68}Ga-DOTA-TOC (^{68}Ga-DOTA-Tyr^{3}-octreotide) is a popular example of a radiolabelled peptide which targets the SST receptor; the success of this radiopharmaceutical has stimulated much of the development of ^{68}Ga radiopharmacy and the ^{68}Ge/^{68}Ga generator.[32,97] Despite NOTA forming complexes with gallium of higher stability and faster radiolabelling chemistry than DOTA,[97] the latter was chosen as the BFC and generated a promising biodistribution of the labelled bioconjugate. This example demonstrates the importance of finding a balance between metal-complex stability without compromising the biodistribution of the biovector.

Integrin receptors are a popular class of cell surface receptors that have been implicated in many human cancers and utilised as a target for tumour-targeting radiopharmaceuticals.[8,64] The $\alpha_v\beta_3$ integrin receptor is the most popular, and has been extensively targeted with the cyclic peptide RGD (Arg-Gly-Asp)[98] (Figure 1.6). A variety of radiolabelled-RGD bioconjugates have been investigated for their ability to selectively image or treat $\alpha_v\beta_3$ integrin receptor-positive tumours using radiometals such as ^{177}Lu,[99] ^{64}Cu,[100] ^{111}In,[101] ^{68}Ga,[102] or ^{90}Y.[103]

Recently, the targeting ability of a peptidomimetic ligand LLP2A, which targets the less explored $\alpha_4\beta_1$ integrin receptor with high affinity, has been investigated.[104] The peptide was labelled with ^{64}Cu using a second generation cross-bridged macrocycle CB-TE1A1P (a CB-TE2A derivative where one pendant arm has been replaced with a methane phosphinic acid pendant arm) and evaluated against the corresponding CB-TE2A-bioconjugate.[31] The chelate-

bioconjugate CB-TE1A1P-LLP2A was prepared on a peptide resin and subsequently labelled with ^{64}Cu. Quantitative labelling was achieved after 60 min at room temperature or after 5 min at 90 °C; a marked improvement from the first generation analogue CB-TE2A, well known for its sluggish labelling kinetics with copper isotopes requiring heating at 90 °C for 1 hour (68% RCY). Small animal model studies with ^{64}Cu-CB-TE1A1P-LLP2A showed dramatically improved tumour-to-background contrast compared to the ^{64}Cu-CB-TE2A analogue. This example highlights the advantages of exploring new BFCs with improved binding kinetics.

Another popular antigen targeted by radiolabelled peptides is the melanocortin-1 (MC-1) receptor, which is a promising melanoma-specific target that binds the linear tridecapeptide α-melanocyte stimulating hormone (α-MSH) with nanomolar affinity.[66] These receptors are over expressed on the surface of human malignant melanomas, which bind and internalize their ligands leading to their sequestration in the cytoplasm. Much like other native peptides, α-MSH is degraded *in vivo* by enzymes, hence several synthetic candidate peptides have been tested as analogues[66,105] (Figure 1.6). A report recently evaluated an α-MSH analogue, Re(Arg^{11})CCMSH, labelled with ^{111}In, ^{86}Y, and ^{68}Ga in PET/SPECT imaging of melanoma;[106] this rhenium cyclized peptide analogue of α-MSH has also been studied by other groups.[107] The melanoma targeting peptide-bioconjugate CHX-A"-DTPA-Re(Arg^{11})CCMSH was prepared on a solid-phase peptide resin. ^{111}In-labelling was accomplished at 40 °C for 40 minutes, ^{86}Y-labelling at 75 °C for 30 minutes, and ^{68}Ga-labelling at 85°C for 20 minutes, to obtain RCYs >95% and radiochemical purity >95% for all nuclides with little or no purification. All three agents were able to selectively target melanoma tumours, and clearly image the lesions. The biodistribution studies showed rapid tumour uptake after 2 hours, and excess radioactivity in non-target tissues was eliminated and excreted mainly through the kidneys.

The gastrin-releasing peptide receptor (GRPr), another popular peptide specific antigen found on a wide variety of human cancers such as lung, prostate, and breast cancer, exhibits high affinity for the 14 amino acid peptide bombesin (BBN).[8] Various modifications that increase metabolic stability, influence binding properties or biodistribution behaviour of the native bombesin peptide have been made (Figure 1.6), and exploited in conjugation reactions to BFCs.[66,108] Recently, a new conjugate of bombesin, JMV594, as an antagonist for targeting the GRPr for SPECT imaging with ^{111}In was explored.[109] In addition, a positively charged spacer (4-amino-1-carboxymethyl-piperidine) was attached between the BFC and peptide to act as a pharmacokinetic modifier. The DOTA-linker-JMV594 bioconjugate was prepared on a peptide resin and subsequently labelled with ^{111}In at 95°C for 30 min (RCY >95%). Biodistribution studies showed that ^{111}In-DOTA-JMV594 was taken up quickly by the tumour and pancreas; however, uptake in the pancreas washed out over longer time points, while radioactivity remained in the tumour.[109] These results suggest ^{111}In-DOTA-JMV594 may be a good candidate for testing in humans.

The HER-2/*neu* receptor is over expressed in 25-30% of human breast cancers[8] and is a popular target in radiopharmaceuticals; several radiometals (^{111}In, ^{64}Cu, ^{89}Zr, and ^{212}Pb) conjugated to the monoclonal antibody trastuzumab (sold under the trade name Herceptin), known to target the HER-2/*neu* receptor, or analogous antibody fragments (^{68}Ga) can be found in clinical trials.[28] In a study by Costantini et al., the effect of known radiosensitizing drugs (methotrexate, paclitaxel, and doxorubicin) on the effectiveness of the Auger emitter ^{111}In was studied in a ^{111}In-DTPA-NLS-trastuzumab bioconjugate.[110] The γ emission of ^{111}In was used in dosimetry studies and SPECT imaging of the radiotherapeutic agent. The therapeutic effects of Auger electron emitters have been limited in the past due to poor localization in the cell nucleus, where the radioactivity is at an active range to cause cell death. Combination therapy

with radiosensitizing drugs to amplify the lethal effects of ionising radiation has been proposed as a way to increase the therapeutic effectiveness of radiotherapy. ^{111}In-DTPA-NLS-trastuzumab, is equipped with two targeting vectors; trastuzumab for specific targeting of the HER-2/*neu* receptor, and a synthetic 13 mer nuclear-localization sequence (NLS) which promotes nuclear importation after HER-2 mediated internalization into the cancer cell. Synthesis of the bioconjugate resulted in the chelate:mAb:NLS-peptide ratio of 15:1:60. ^{111}In-labelling was accomplished at room temperature for 60 minutes to achieve radiochemical purity > 97% after filtration purification.[110] The study found the co-administration of the radiosensitizing drugs increases the efficacy of the targeted Auger electron radiotherapy of ^{111}In-DTPA-NLS-trastuzumab.[110]

Despite some success with radiolabelled monoclonal antibodies, most still suffer from poor tumour-to-background ratios and sluggish blood clearance. To overcome these limitations, many research groups are investigating mAb fragments that can target these antibody specific receptors. The epidermal growth factor receptor (EGFr) is an attractive target antigen that is over expressed in a wide range of tumours including human breast cancer, and small cell carcinoma of the head and neck; it binds the primary ligands epidermal growth factor (EGF) and transforming growth factor-β (TGFβ), two mAbs.[80] A recent study implemented the anti-EGFR Affibody $Z_{EGFR:1907}$ in a ^{177}Lu-radiotherapeutic.[91] In previous studies radiolabelled-$Z_{EGFR:1907}$ showed excellent targeting to EGFR-positive tumours, but persistent and high renal uptake. In an attempt to improve the pharmacokinetic properties, a second targeting vector was added (large protein human serum albumin (HSA)), to keep the radiopharmaceutical in blood circulation and away from the renal system. A DO3A-HSA-$Z_{EGFR:1907}$ bioconjugate was prepared with 1-5 Affibodies per HSA protein introduced. Labelling of ^{177}Lu was performed at 39°C for 1 hour (>70% RCY) after purification. An *in vitro* stability assay of ^{177}Lu-DO3A-HSA-

$Z_{EGFR:1907}$ against an excess of mouse serum resulted in >95% of the probe intact at 4 hours, and >80% intact at longer time points (24-168 h). Biodistribution studies showed long retention of the radiopharmaceutical in the tumour and good tumour contrast in SPECT images. ^{177}Lu-DO3A-HSA-$Z_{EGFR:1907}$ showed lower uptake in the kidneys compared to the ^{177}Lu-DO3A-$Z_{EGFR:1907}$ alone,[91] but instead high and persistent liver uptake was seen which may suggest the introduction of such a large protein has influenced the pharmacokinetic and metabolic behaviour of the radiopharmaceutical towards the liver.

These few examples represent a span of target antigens and biomolecules, nonetheless some broadly applicable conclusions can be drawn. Specifically, small changes in one system can lead to large impacts on the pharmacokinetic behaviour and biodistribution of the radiopharmaceutical *in vivo*, and a unique balance must be made between all components. In this regard, it is difficult to introduce both the radiometal and BFC onto the biomolecule without hindering the targeting ability of the biovector. Moreover, *in vitro* and *in vivo* evaluation methods for bioconjugates vary throughout the literature and it can be difficult to compare results across different studies. Caution should also be taken when analysing biodistribution data that have been extracted from small animal models; promising results there do not always translate well to human patients.

The array of antigens being targeted by radiometallated bioconjugates covers a broad spectrum of human cancers, with some being over-expressed in multiple cancer types thus expanding their applicability in the clinic. The infinite number of metal-chelate-linker-biomolecule combinations available to the radiochemist indicate the field of radiopharmaceuticals has the potential to be widely used providing diagnosis and treatment catered to individual patients.

1.10 Concluding Remarks

Radiometals in nuclear oncology encompass a wide range of γ and β^+ emitters for imaging with SPECT and PET respectively, and α, β^-, and Auger electron emitters for therapy, some of which have been successfully incorporated into FDA-approved radiopharmaceuticals. Radiometals possess a number of advantages over traditional 'organic' radioisotopes: an array of possible emissions and half-lives that span a range needed to ask and answer those questions researchers and clinicians want to address while also being able to match biological and radiological half-lives, and the ability to introduce the radionuclide through quick and convenient coordination bonds *via* the BFC method. The modular assembly of the BFC method allows for a vast and quickly advancing field of treatments that are patient specific. With new biomarkers, radiometals, and chelating strategies available, there is now a plethora of combinations available for radiopharmaceutical design.

Despite the FDA-approval of a few successful metal-based radiopharmaceuticals for SPECT imaging and β^- therapy in the last decade, there is still no approved radiometal-based PET imaging agent, or radiotherapeutic agent of α or Auger electron emitters on the market. In part, the standard regulatory and financial barriers slow new metallo-radiopharmaceuticals from entering the clinic. As new cost-efficient methods for the production and wide-spread distribution of these radiometals are developed, new agents will undoubtedly be produced that demonstrate value to the clinician and patient and these barriers will slowly diminish, turning these originally 'non-traditional' isotopes into standard convention.

1.11 Thesis Overview and Aims

With the important concepts relevant to radiometals for radiopharmaceuticals now presented, we now set out to study new chelating ligands for radiochemistry applications. The

recent success of the acyclic ligands H_2dedpa for Ga(III) and H_4octapa with In(III)/Lu(III) (*vide supra*) developed by the Orvig group has led to interest in further exploiting these promising scaffolds; as such much of this thesis will focus on the synthesis, characterization, and evaluation of new H_2dedpa and/or H_4octapa analogues.

Perhaps the most promising next generation PET isotope is the generator-produced nuclide ^{68}Ga; the translation of ^{68}Ga-tracers into the clinic will be reliant on finding new and efficient chelation/radiolabeling strategies for Ga(III). The Orvig group's previous findings which identified the hexadentate acyclic chelate H_2dedpa as a promising ligand for further elaboration into a ^{68}Ga radiopharmaceutical[54] has motivated much of the work in this thesis. The particular aims, herein, are to incorporate the "bare" chelate H_2dedpa into a small molecule tracer. Through ligand design and extensive synthetic effort, new H_2dedpa (and one new H_4octapa) analogues will be studied which:

- introduce chirality and rigidity onto the ligand backbone to produce chelates which may form metal complexes of even higher thermodynamic stability and kinetic inertness
- target hypoxia by incorporation of the nitroimidazole vector onto the ligand scaffold
- have novel handles for "bifunctionality" of the H_2dedpa scaffold
- form cationic lipophilic complexes that may be useful as myocardial perfusion imaging agents
- have varying donor atom connectivity to form an alternative hexadentate "pa"-type ligand

Chapter 2 explores the effect of substituting the ethylenediamine backbone of H_2dedpa and H_4octapa with chiral 1*R*,2*R*-trans-cyclohexanediame (*CHX*) to generate acyclic chelating

ligands of greater rigidity (H_2*CHX*dedpa and H_4*CHX*octapa), and their use for gallium and indium radiopharmacy was evaluated. In Chapter 3 and 4 we functionalize these "bare" ligands with the targeting vector nitroimidazole (NI) and evaluate their feasibilities as PET imaging agents of hypoxia using radioisotopes of gallium or copper. A further modification of the H_2dedpa scaffold is made in Chapter 5 to yield a novel bifunctional chelating ligand with the potential for including multiple targeting vectors; this scaffold is tagged with a fluorophore and assessed as a potential bimodal imaging agent for optical and nuclear imaging. In Chapter 6, we take advantage of the cationic complex formed by H_2*CHX*dedpa and Ga(III), and decorate the periphery of the ligand with lipophilic appendages via the 'integrated approach' to form complexes of varying lipophilicity in an attempt to mimic the routinely used SPECT agents for myocardial perfusion imaging. The geometry and donor atom connectivity is altered from the native H_2dedpa scaffold in Chapter 7 to produce a new "pa" ligand which forms neutral complexes with trivalent metals, and is assessed for use in $^{67/68}$Ga radiochemistry. Finally, Chapter 8 summarizes and concludes the body of work with an outlook on where emphasis should be made in developing this class of acyclic chelating ligands in the future.

Chapter 2: H_2*CHX*dedpa and H_4*CHX*octapa – Chiral Acyclic Chelating Ligands for $^{67/68}$Ga and ^{111}In Radiopharmaceuticals

This chapter is an adaptation of published work, and is reproduced in part, with permission from Ramogida, C. F.; Cawthray, J. F.; Boros, E.; Ferreira, C. L.; Patrick, B. O.; Adam, M. J.; Orvig, C., H_2*CHX*dedpa and H_4*CHX*octapa – Chiral Acyclic Chelating Ligands for $^{67/68}$Ga and ^{111}In Radiopharmaceuticals. *Inorg. Chem*. **2015**, *54* (4), 2017-2031, Copyright 2015 American Chemical Society.

2.1 Introduction

The use of "non-traditional" radiometals in nuclear medicine has blossomed over the past decade into a well-established field that shows great utility for the diagnosis and targeted therapy of a variety of diseases, especially in the field of oncology.[6,8,13,25,29,34,37,111–114] Radioisotopes of Ga(III), In(III), Cu(II), Y(III), and Zr(IV) give a flavor of the myriad radiometal ions that have been exploited in radiopharmaceutical design; their inherent array of nuclear decay properties and half-lives lends them well to target a variety of molecular processes, as discussed in detail in Chapter 1.[6,8,13,25,29,34,37,111–114] Two clinically important isotopes are the positron emitter ^{68}Ga for positron-emission tomography (PET) imaging, and ^{111}In, a gamma-emitter for single-photon emitted computed tomography (SPECT) imaging and Auger electron therapy.

^{68}Ga, with a short half-life suitable for imaging agents that localize quickly, such as small molecules and peptides ($t_{1/2}$ = 67.7 min), and its predominant β^+ emission (89%, 1.9 MeV maximum energy), has become an attractive isotope for incorporation into positron-emission

tomography (PET) imaging agents.[8,13,25,32,113] Moreover, the nuclide ^{68}Ga can be commercially produced and distributed via a ^{68}Ge/^{68}Ga generator system; the half-life of the generator-parent ^{68}Ge ($t_{1/2}$ = 270 d) is sufficiently long such that the generator can be used for six months to one year before replacement,[97,105] obviating the need for an on-site cyclotron. Therefore, the ^{68}Ge/^{68}Ga generator has the potential to become as ubiquitous as the clinically important ^{99}Mo/^{99m}Tc generator, and the ^{68}Ga from these generators is already being used in patients throughout Europe. The lack of an FDA-approved ^{68}Ge/^{68}Ga generator is hindering the advancement of many ^{68}Ga agents toward the clinic in North America, but progress is steady.

^{111}In has a half-life of ~ 2.8 days, is produced by cyclotron (^{111}Cd(p,n)^{111}In), and decays via electron capture (EC, 100%) emitting γ-rays with energies of 171 and 245 keV, which are sufficient for SPECT imaging, as well as Auger electrons that can be used for therapy.[8,113] The radiometal ^{111}In is commercially available and has been incorporated into the clinically relevant agents Octreoscan™ and ProstaScint®, with many more ^{111}In-based radiopharmaceuticals in clinical trials.[3] It is the second most popular SPECT radiometal next to ^{99m}Tc.

The utility of radiometals such as ^{111}In and ^{68}Ga in nuclear medicine is strongly dependent on a chelating ligand that exhibits rapid radiometal incorporation and strong kinetic inertness to prevent unintentional transchelation and/or demetalation of the coordination complex *in vivo*.[13,114] The tri- and tetra-aza-based aminocarboxylate macrocyclic chelators 1,4,7-triazacyclononane-1,4,7-triacetic acid (NOTA (N_3O_3)) and 1,4,7,10-tetraazacyclododecane-1,4,7,10-tetraacetic acid (DOTA (N_4O_4)), developed by Maecke and co-workers,[115–117] persist as the "gold-standards" in the field of radiometal chelation. NOTA and DOTA are used in many applications with their radiochemical properties ranging from sufficient to superb for many radiometals, including but not limited to ^{64}Cu, ^{68}Ga, ^{111}In, $^{86/90}$Y, and ^{177}Lu.[114] The preorganized donor atoms of these macrocyclic (closed-chain) systems result in metal complexes of often

very high stability; however, elevated temperatures and extended reaction times are often required to quantitatively label radiometals – a major downfall of these ligands, especially when denaturing of sensitive biomolecules and decay of short-lived radionuclides are at stake.

Many acyclic (open-chain) ligands such as diethylenetriaminepentaacetic acid (DTPA (N_3O_5)) and ethylenediaminetetraacetic acid (EDTA (N_2O_4)) have been extensively evaluated for use with a variety of radiometals,[74,118] and despite their rapid and quantitative radiometal incorporation, they suffer from poor kinetic inertness *in vitro*, a common characteristic of acyclic ligands. A structural modification of DTPA to give CHX-A"-DTPA (Figure 2.1) through incorporation of a 1,2-trans-cyclohexanediamine backbone to preorganize the donor atoms has proven to increase the kinetic inertness of its resulting metal complexes.[119,120] CHX-A"-DTPA has been used extensively with many radiometals including $^{86/90}$Y,[120,121] ^{177}Lu,[122,123] and $^{212/213}$Bi,[50] and some with ^{111}In,[121] and in most cases showed increased stability (kinetic inertness) *in vivo* compared to the analogous DTPA complexes.

The importance of choosing the appropriate chelate-radiometal pair in radiopharmaceutical construction has been emphasised throughout this thesis. Most importantly, the chelate must be chosen to match the unique coordination chemistries of each metal; as such there is increasing interest in the development of new ligands that stably bind the variety of radiometal isotopes that have potential use in diagnostic imaging and targeted radiotherapy.[31,114,124] Many groups,[69–71,125–130] including ours, have sought to find new ligands with improved properties for radiometal chelation - such as fast and mild radiolabeling conditions, high thermodynamic stability, and exceptional kinetic inertness *in vivo*. A selection of these new and emerging ligands are evaluated in Chapter 1. To this end, our group has extensively studied a variety of acyclic (linear) chelators based on the pyridine carboxylate scaffold (Figure 2.1), which we have termed the "pa" family of chelators[19,53,54,59–63] – with the

most promising entries of the family being the acyclic chelator H_2dedpa and octadentate version H_4octapa. We first reported the acyclic chelating ligand H_2dedpa (N_4O_2) that binds gallium isotopes quantitatively and under mild conditions with high specific activities (10 min, RT, 9.8 mCi/nmol).[54] Bifunctional H_2dedpa derivatives were conjugated to the cyclic peptide RGD[19,131] and evaluated with both ^{68}Ga and ^{64}Cu. Moreover, monocationic Ga-dedpa derivatives with lipophilic appendages were evaluated as myocardial perfusion agents.[132] The octadentate version, H_4octapa (N_4O_4), was investigated for use with indium isotopes[53,59] and exhibited properties that rivaled those of DOTA, the current industry gold standard for indium chelation. The main advantage of the pa ligands lies in their ability to quantitatively label radiometals quickly and under mild conditions (a trait often lacking in the macrocyclic gold standards NOTA and DOTA); yet despite both being acyclic (open chain) ligands, complexes of H_2dedpa and H_4octapa exhibit surprisingly high kinetic inertness *in vitro* and *in vivo*.

The work presented herein is a study to investigate the effect of an added structural modification onto the backbone of these linear chelating agents. By substitution of a chiral 1*R*,2*R*-trans-cyclohexanediamine in place of the ethylenediamine backbone in the native scaffolds of H_2dedpa and H_4octapa, an augmented preorganization of the donor atoms has been enforced, which may positively affect the *in vitro/in vivo* kinetic inertness of the resulting metal complexes. Moreover, the replacement of ethylenediamine with a slightly more lipophilic cyclohexanediamine backbone may alter the pharmacokinetics and biodistribution of the resultant radiotracers *in vivo*. This work has drawn inspiration from the acyclic chelator CHX-A"-DTPA, which showed much better kinetic inertness with yttrium, lutetium, and bismuth isotopes compared to the native DTPA derivative.[51,119]

The chelating agents investigated herein include the hexadentate (N_4O_2) derivatives H_2*CHX*dedpa, and H_2*CHX*dedpa-bb, which is a model compound where benzyl groups were

added to the secondary nitrogen atoms as placeholders for targeting vectors, and octadentate (N_4O_4) derivative H_4*CHX*octapa (Figure 2.1). Much like H_2dedpa and H_4octapa, H_2*CHX*dedpa has been previously investigated by other groups for coordination to divalent transition metals,[56,57] but to our knowledge, its coordination properties with Ga(III) have never been investigated. In addition, H_4*CHX*octapa is a novel ligand that has not been previously reported.

Presented herein are the synthesis, characterization, coordination chemistry, thermodynamic stability, radiolabeling, and *in vitro* human serum stability of the three cyclohexyl-pa ligands. These studies are used collaboratively to evaluate the potential of the *CHX*-pa chelates as bifunctional chelating agents in radiopharmaceutical design.

Figure 2.1 (Top) Structures of ligand standards NOTA, DOTA, DTPA, and CHX-A"-DTPA used extensively with a variety of radiometals; (Bottom) "pa" ligands H_2dedpa, H_4octapa and novel *CHX*-pa ligands discussed in Chapter 2.

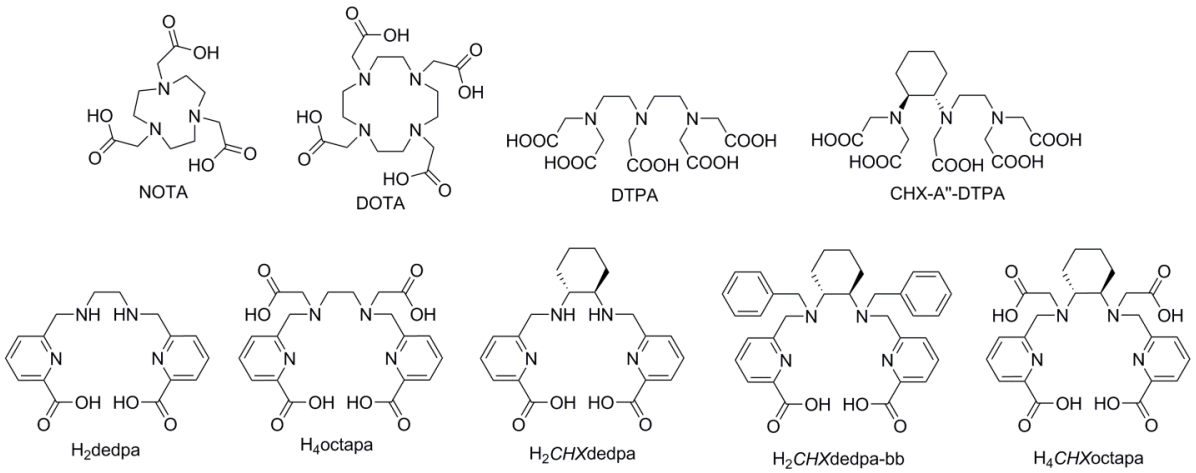

2.2 Results and Discussion

As seen in the example of the ligand CHX-DTPA and the differential stability of its four isomers,[120] stereochemistry can greatly influence metal-ligand complex stability *in vivo*. Herein

we chose to focus the study on one isomer (1*R*, 2*R*) of the *CHX*-pa chelates in order to eliminate any discrepancies in stability that different isomers may have, and directly compare their metal ion coordinating abilities to the previously reported achiral ethylenediamine versions.

Scheme 2.1 Synthesis of precursors **2.1**, **2.2**, **2.3**, H_2*CHX*dedpa, **2.5**, and H_4*CHX*octapa.[a]

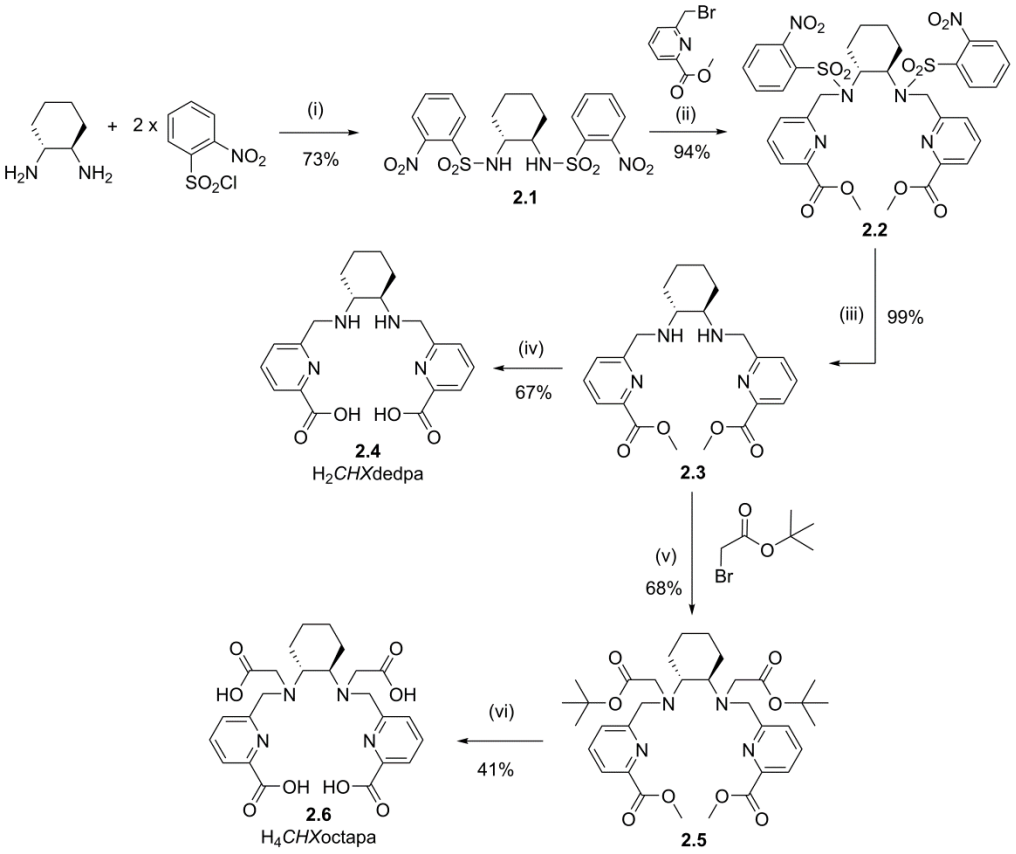

[a]Reagents and conditions: (i) THF, $NaHCO_3$, 0 °C – RT, 18 h; (ii) CH_3CN, K_2CO_3, methyl-6-bromomethylpicolinate (2 equiv), 65 °C, 48 h; (iii) THF, K_2CO_3, thiophenol (2.05 equiv), 72 h; (iv) HCl (6 M), reflux, 18 h; (v) CH_3CN, Na_2CO_3, *tert*-butylbromoacetate (2 equiv), 60 °C, 18h; (vi) HCl (6 M), reflux, 18 h.

2.2.1 Synthesis and Characterization

Like H_2dedpa, H_2*CHX*dedpa has been previously synthesized and evaluated for its chelation properties with divalent metals Zn(II), Cd(II) and Pb(II);[56] however, its chelation properties with gallium(III) have not yet been investigated.

Our group recently reported a novel synthesis of H_2dedpa and H_4octapa using the uncommon 2-nitrobenzenesulfonamide (nosyl) protecting group,[59] which allowed for facile and efficient preparation of both nonfunctionalized and functionalized ligands. The use of this protecting group resolved issues with the original synthetic route via the reductive amination step, which led to unwanted simultaneous reduction of the methoxy ester group. The synthesis of H_4octapa or H_2dedpa began with protection of ethylenediamine (en) using 2 equiv of 2-nitrobenzenesulfonyl chloride.[59] Herein, we prepared H_2*CHX*dedpa in an analogous fashion (Scheme 2.1), with the enantiomerically pure diamine starting material 1*R*,2*R*-(-)-cyclohexanediamine being used in the first protection step with 2-nitrobenzenesulfonyl chloride to yield **2.1** in 73% yield. The addition of a cyclohexyl ring on the backbone of the ethylenediamine core caused **2.1** to be more soluble than the ethylenediamine derivative previously reported, hence crystallization was not achieved and a column chromatography purification step was required to isolate the final protected diamine **2.1**. Subsequently, methyl-6-bromomethyl picolinate was used as alkylating agent, with excess base to yield **2.2** in high yield (94%) after column purification. The following deprotection of nosyl groups with thiophenol was nearly quantitative (99%) to yield Me_2*CHX*dedpa **2.3**. Intermediate **2.3** could then be deprotected in refluxing HCl overnight to produce H_2*CHX*dedpa as an HCl salt (46% cumulative yield in four steps), or used in a subsequent *N*-alkylation with *tert*-butyl bromoacetate (Scheme 2.1) to yield the protected version of *CHX*octapa^{4-}, **2.5**. Finally, **2.5** could

be deprotected in refluxing HCl to give H_4*CHX*octapa as an HCl salt (19% cumulative yield over five steps).

Scheme 2.2 Synthesis of precursors **2.7**, **2.8**, and H_2*CHX*dedpa-bb.[a]

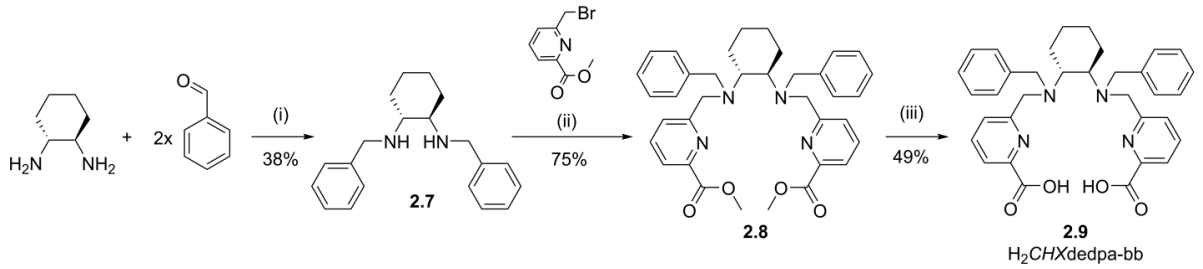

[a]Reagents and conditions: (i) a. Ethanol, 0 °C – reflux, 18h, b. Ethanol, 0 °C, $NaBH_4$, 2 h; (ii) CH_3CN, K_2CO_3, methyl-6-bromomethyl picolinate (2.1 equiv), reflux, 72 h; (iii) THF/H_2O (3:1), LiOH, RT, 2 h.

As a model for potential bifunctional derivatives of *CHX*dedpa^{2-}, the dibenzylated derivative H_2*CHX*dedpa-bb (**2.9**) was synthesized (Scheme 2.2). The benzyl groups act as placeholders for potential targeting vectors, which could be either introduced by alkylation of the 2° amines of Me_2*CHX*dedpa (**2.3**), or the benzyl groups could instead be in the form of 4-nitrobenzyl groups, which would be subsequently converted to the reactive isothiocyanate for further conjugation to targeting vectors bearing reactive primary amines. A similar *N*-alkylated derivative of H_2dedpa was evaluated previously, H_2dedpa-bb-NO_2, and found to exhibit reduced stability compared to that of H_2dedpa.[54] Thus, H_2*CHX*dedpa-bb was used to make direct comparisons to the stability trends of H_2dedpa versus H_2dedpa-bb, and to determine the effect the cyclohexyl ring will have on stability of the resultant metal complex. The preparation of H_2*CHX*dedpa-bb (**2.9**) began with benzyl protection of 1*R*,2*R*-(-)-cyclohexanediamine with 2 equiv of benzaldehyde, followed by *in situ* reduction with sodium borohydride to produce **2.7**. Next, methyl-6-bromomethyl picolinate was added in an alkylation step to **2.7** to yield the

methyl-protected ligand Me$_2$*CHX*dedpa-bb (**2.8**) in 75% yield. Finally, methyl ester deprotection was accomplished in basic conditions via the addition of LiOH in water/tetrahydrofuran (THF) at room temperature. The lithium salts were removed by semipreparative RP-HPLC, and the ligand was converted to its HCl salt by redissolving in dilute HCl (aqueous). This milder deprotection route was necessary to preserve the integrity of the ligand, since refluxing **2.8** in aqueous HCl resulted in debenzlyation and a mixture of products.

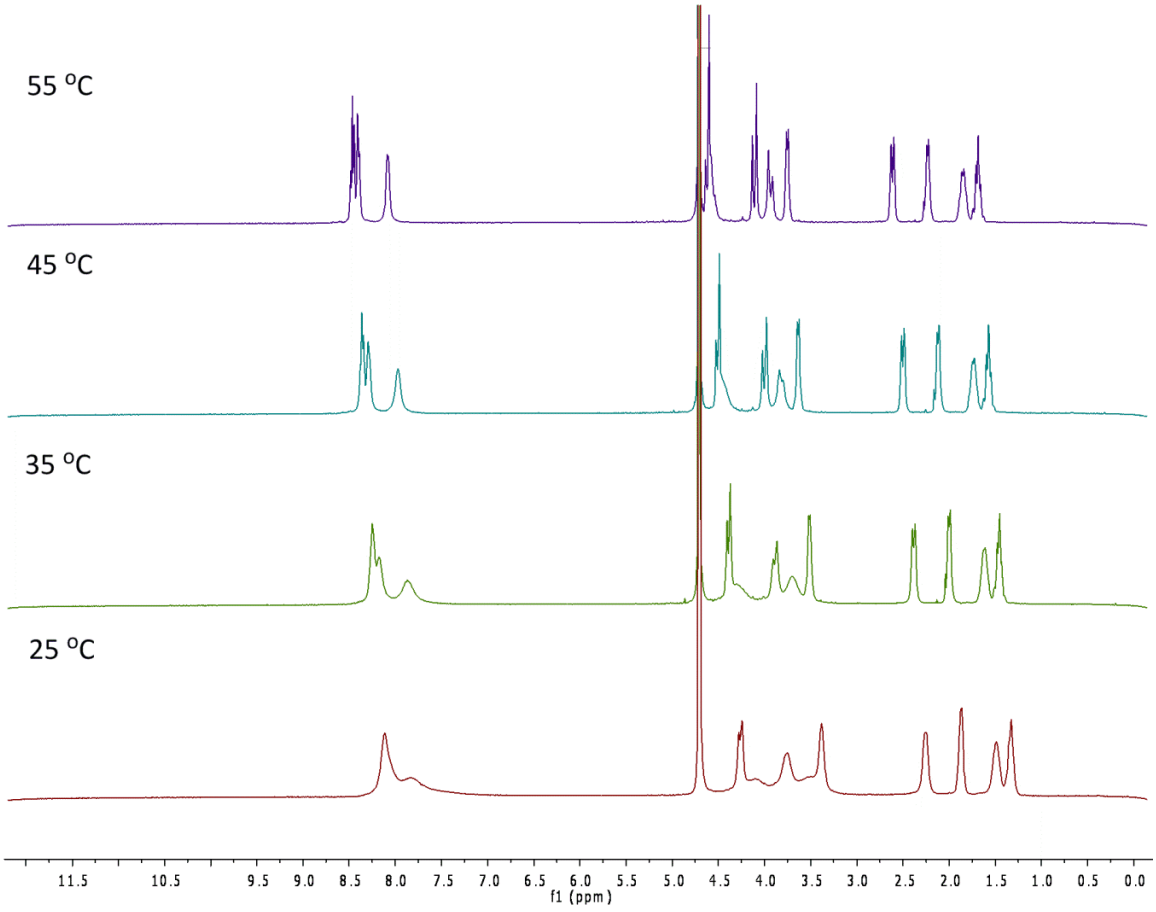

Figure 2.2 Variable-temperature ^{1}H NMR spectra of **2.6** H$_4$*CHX*octapa at 25 – 55 °C in D$_2$O (400 MHz).

Following synthesis, the HCl salts of all three ligands were successfully metallated with $Ga(ClO_4)_3$ and/or $In(ClO_4)_3$. All proligands and their metal complexes were fully characterized using ^{1}H NMR, ^{13}C NMR, ^{1}H-^{1}H COSY NMR, HSQC NMR, and high-resolution electrospray ionization mass spectrometry (HR-ESI-MS). It is interesting to note that the ^{1}H NMR spectra of the HCl salt of H_4*CHX*octapa (**2.6**) exhibited very broad and hard to resolve peaks at 25 °C which precluded ^{13}C NMR spectra collection; thus, variable-temperature (VT) NMR experiments from 25 – 55 °C in D_2O were performed (Figure 2.2). An apparent sharpening of peaks began at 35 °C and continued as the temperature rose to 55 °C, to appear finally as sharply resolved peaks. After resolution of peaks at 55 °C was observed, a ^{13}C NMR spectrum was obtained at this temperature. One explanation for this solution behavior is that there is strong intramolecular hydrogen bonding, possibly augmented by the presence of HCl, also evinced by the density functional theory (DFT) structure of H_4*CHX*octapa (Appendix, Figure A.1). This may also explain the slightly higher pK_a (*vide infra*) values of the ligand nitrogen atoms of H_4*CHX*octapa compared to H_4octapa; these were also corroborated by ^{1}H NMR pH titrations at 55 °C (Appendix, Figure A.2).

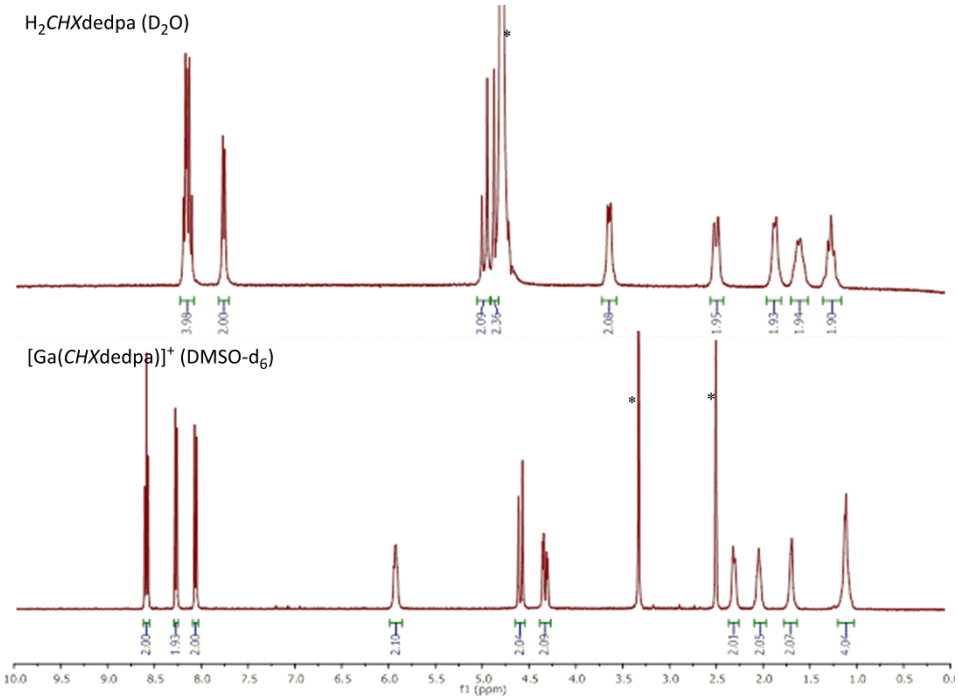

Figure 2.3 ^{1}H NMR spectra at ambient temperature of (top) H_2*CHX*dedpa (300 MHz) and (bottom) [Ga(*CHX*dedpa)][ClO_4] (400 MHz) showing diastereotopic splitting present in both the free ligand and Ga-complex. *Residual solvent peak.

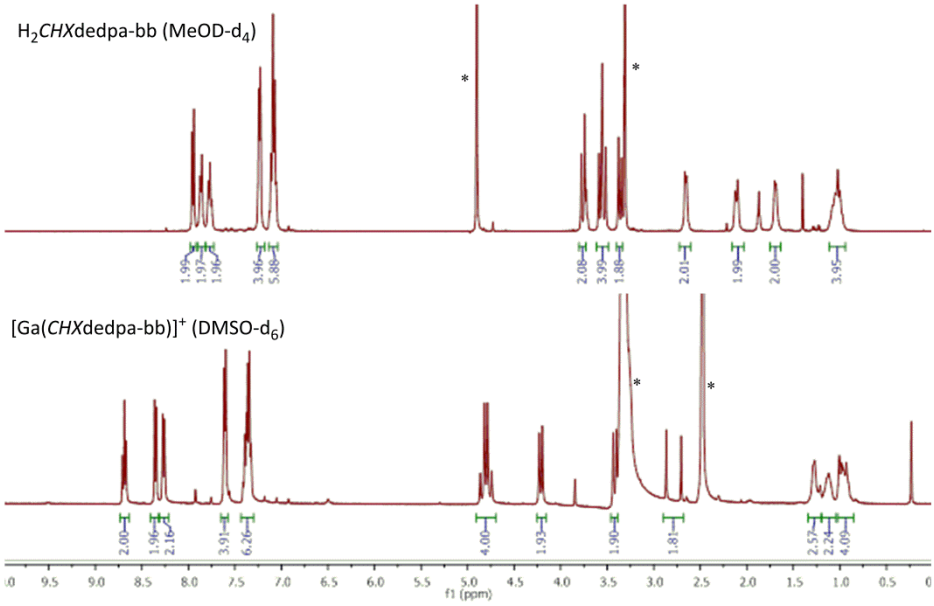

Figure 2.4 ^{1}H NMR spectra at ambient temperature and 400 MHz of (top) H_2*CHX*dedpa-bb and (bottom) [Ga(*CHX*dedpa-bb)][ClO_4]. *Residual solvent peak.

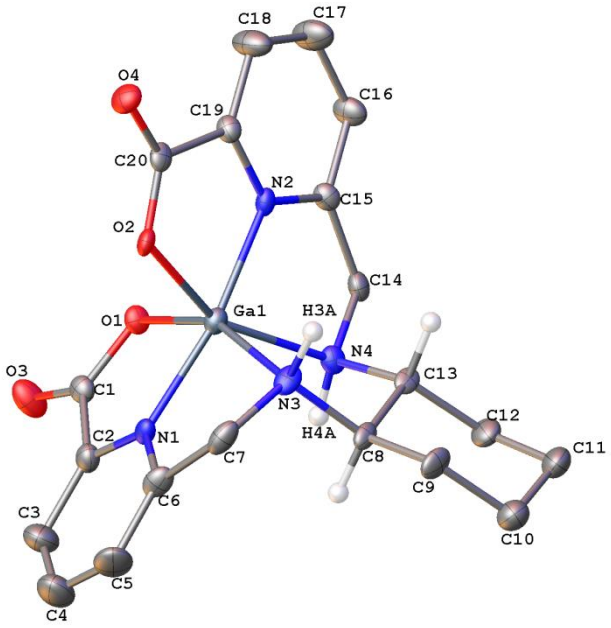

Figure 2.5 Solid-state X-ray crystal structure of the cation in [Ga(*CHX*dedpa)][ClO_4]; only one crystallographically independent unit shown, perchlorate anion omitted for clarity. Ellipsoids drawn with 50% probability.

Table 2.1 Selected bond lengths (Å) and angles (°) in the X-ray structure of [Ga(*CHX*dedpa)]$^+$ with comparison to that of [Ga(dedpa)]$^+$.[54]

bond	length (Å) [Ga(*CHX*dedpa)]$^+$ [a]	length (Å) [Ga(dedpa)]$^+$	bond	length (Å) [Ga(*CHX*dedpa)]$^+$ [a]	length (Å) [Ga(dedpa)]$^+$
Ga-N(1)$_{pyr}$	1.968	1.9868(16)	Ga-N(4)$_{en}$	2.105	2.1132(16)
Ga-N(2)$_{pyr}$	1.961	1.9903(16)	Ga-O(1)	1.992	1.9708(13)
Ga-N(3)$_{en}$	2.110	2.1115(16)	Ga-O(2)	1.982	1.9828(13)
angle	degree (°) [Ga(*CHX*dedpa)]$^+$ [a]	degree (°) [Ga(dedpa)]$^+$	angle	degree (°) [Ga(*CHX*dedpa)]$^+$ [a]	degree (°) [Ga(dedpa)]$^+$
O(1)-Ga-O(2)	101.1	101.39(6)	N(1)-Ga-N(3)	78.9	77.82(6)
O(1)-Ga-N(1)	79.6	80.14(6)	N(2)-Ga-N(3)	111.2	108.92(6)
O(2)-Ga-N(1)	94.1	94.02(6)	O(1)-Ga-N(4)	93.3	90.32(6)
O(1)-Ga-N(2)	91.5	94.73(6)	O(2)-Ga-N(4)	154.7	155.64(6)
O(2)-Ga-N(2)	80.0	79.64(6)	N(1)-Ga-N(4)	109.0	109.11(6)
N(1)-Ga-N(2)	167.7	170.97(6)	N(2)-Ga-N(4)	79.0	78.15(6)
O(1)-Ga-N(3)	155.7	153.44(6)	N(3)-Ga-N(4)	83.1	83.12(6)
O(2)-Ga-N(3)	91.7	94.78(6)			

[a]An average of the three independent units of [Ga(*CHX*dedpa)][ClO_4] was calculated.

The ^{1}H and ^{13}C NMR of all pro-ligands H_2*CHX*dedpa, H_2*CHX*dedpa-bb, and H_4*CHX*octapa revealed the expected C_2 symmetry with half-integrations of the resonances present and typical diastereotopic splitting of hydrogen atoms observed α to the chiral centre due to the inclusion of the chiral cyclohexane ring. The ^{1}H NMR spectra at 25 °C of all Ga(chelate) complexes revealed sharp and distinct coupling patterns, and could be perceived as one electronically unique isomer in solution at ambient temperature. The C_2 symmetry seen in the pro-ligands H_2*CHX*dedpa and H_2*CHX*dedpa-bb seems to be conserved in the Ga(chelate) complexes (Figure 2.3 and 2.4, respectively). In addition, X-ray quality crystals of [Ga(*CHX*dedpa)][ClO_4] were obtained by slow evaporation in methanol/water, the structure of which validated the solution NMR data. The solid state structure of [Ga(*CHX*dedpa)][ClO_4] (Figure 2.5) exhibited the predicted N_4O_2 hexadentate coordination with Ga(III). There were three crystallographically independent complexes in the asymmetric unit; a comparison of relevant averaged Ga-L bond lengths and angles of $[Ga(dedpa)]^+$ are compared with $[Ga(CHXdedpa)]^+$ in Table 2.1. There is very good correlation between the bond lengths and angles around the metal centres of the $[Ga(CHXdedpa)]^+$ and $[Ga(dedpa)]^+$ cations, with a maximum difference in bond length and angle of 0.032 Å and 3.3°, respectively, between all relevant Ga-L or L-Ga-L bond lengths and angles of *CHX*$dedpa^{2-}$ and $dedpa^{2-}$ complexes (calculated using an average of the three independent units in $[Ga(CHXdedpa]^+$). Because of the minor differences in bond lengths and angles, differences in dihedral angles of the two Ga-complexes were also inspected; the largest difference of 9.4° is seen in the N_{en}-C_{alk}-C_{pyr}-N_{pyr} (N(3)-C(7)-C(6)-N(1)) angle between $[Ga(dedpa)]^+$ and molecule 1 of $[Ga(CHXdedpa)]^+$, while all other relevant dihedral angles show much less variance. Though minor differences in the solid-state structures of $[Ga(CHXdedpa)]^+$ and $[Ga(dedpa)]^+$ exist, differences in stability of the metal-complexes based solely on their solid-state structures cannot be discerned. Moreover, caution should always be taken when making predictions for solution-state properties based on solid-state data.

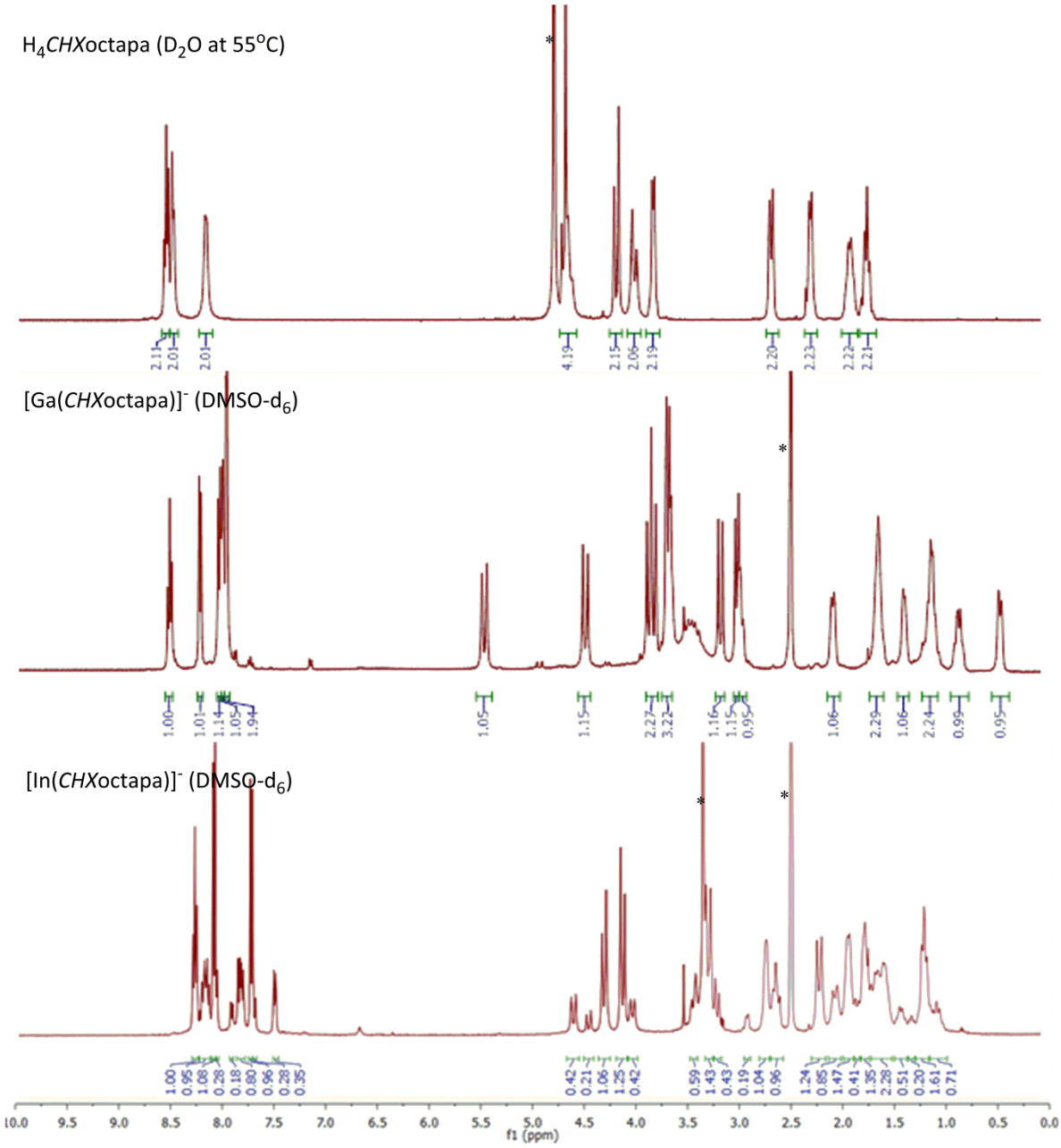

Figure 2.6 ^{1}H NMR spectra of (top) H$_4$*CHX*octapa (400 MHz at 55°C), (middle) [Ga(*CHX*octapa)]$^-$ (400 MHz at 25°C) showing diastereotopic splitting, and predominantly one isomer in solution, and (bottom) [In(*CHX*octapa)]- (400 MHz at 25 °C) showing multiple isomers in solution. *Residual solvent peak.

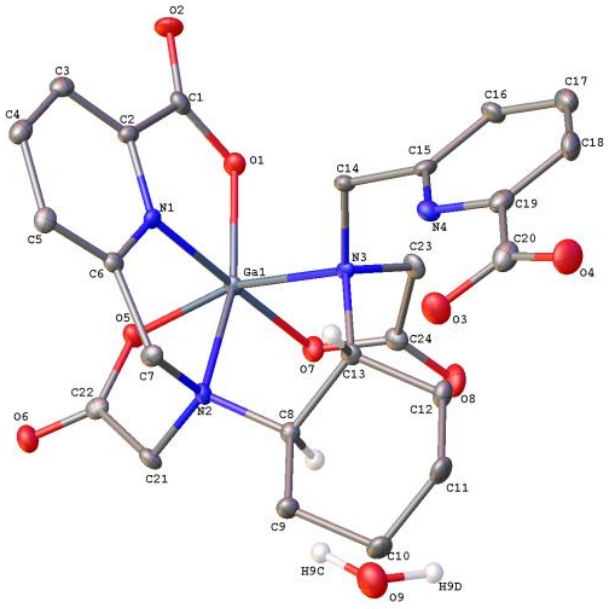

Figure 2.7 Solid-state structure of [Ga(H*CHX*octapa)]H_2O. Ellipsoids drawn with 50% probability.

Table 2.2 Selected bond lengths (Å) and angles (°) in the X-ray structure of [Ga(H*CHX*octapa)].

Bond	Length (Å)	Angle	Degree (°)	Angle	Degree (°)
Ga-N(1)$_{pyr}$	1.999(3)	O(7)-Ga-O(5)	92.89(13)	O(5)-Ga-N(2)	82.94(12)
Ga-N(2)$_{en}$	2.152(4)	O(7)-Ga-O(1)	100.01(14)	O(1)-Ga-N(2)	160.52(13)
Ga-N(3)$_{en}$	2.174(3)	O(5)-Ga-O(1)	97.22(12)	N(1)-Ga-N(2)	79.77(14)
Ga-O(1)$_{pyr\text{-}COO}$	1.894(3)	O(7)-Ga-N(1)	177.73(14)	O(7)-Ga-N(3)	82.81(13)
Ga-O(5)$_{Ac\text{-}COO}$	1.953(3)	O(5)-Ga-N(1)	89.13(13)	O(5)-Ga-N(3)	163.34(12)
Ga-O(7)$_{Ac\text{-}COO}$	1.894(3)	O(1)-Ga-N(1)	80.75(14)	O(1)-Ga-N(3)	99.37(13)
		O(7)-Ga-N(2)	99.44(13)	N(1)-Ga-N(3)	94.96(13)
				N(2)-Ga-N(3)	81.92(12)

Conversely, the solution NMR spectra of [Ga(*CHX*octapa)]$^-$ suggest the formation of one asymmetric isomer in solution, evinced by the apparent inequivalency of the two sets of pyridine-carboxylate hydrogens in the ^{1}H NMR spectrum (Figure 2.6), and 24 signals in the ^{13}C NMR spectrum, correlating to each carbon atom on the ligand backbone being electronically distinct. The splitting pattern of the pyridine-carboxylate hydrogen atoms suggests that one picolinate acid arm is uncoordinated. Indeed, this result is corroborated with the solid state

structure of [Ga(H*CHX*octapa)] (Figure 2.7, Table 2.2), which displays a six-coordinate complex with an N_3O_3 donor set provided by an oxygen atom from each acetate carboxylate arm (2 x $O_{Ac\text{-}COO}$), both nitrogen atoms from the *CHX*-en backbone (2 x N_{en}), and one picolinate arm providing a nitrogen and oxygen donor (1 x $O_{pry\text{-}COO}$, 1 x N_{pyr}), whilst the second picolinic acid arm is situated well away from the coordination sphere. Moreover, the absence of a counter ion in the crystallographic unit suggests the Ga-complex is neutral, and hence the uncoordinated picolinic acid is protonated in the solid state structure. At physiological pH (~7.4), it would be expected that this uncoordinated picolinic acid arm would be deprotonated and the overall complex charge to be monoanionic.

H_4*CHX*octapa was also metallated with In(III) to make direct comparisons between H_4octapa and its cyclohexyl derivative. The solution state ^{1}H NMR spectrum of [In(*CHX*octapa)]$^-$ portrays multiple (static) isomers in solution (Figure 2.6). On the basis of examination of the ^{1}H-^{1}H correlations of the COSY NMR (Appendix, Figure A.3 and A.4) and ^{1}H-^{13}C correlations of the HSQC NMR (Appendix, Figure A.5) spectra, the mixture of isomers can be interpreted to be one major symmetric isomer, which may be the eight-coordinate structure, and one (or two) minor asymmetric isomer(s), which may be a seven-coordinate structure in solution, likely with one acetate carboxylate ($O_{Ac\text{-}COO}$) unbound.

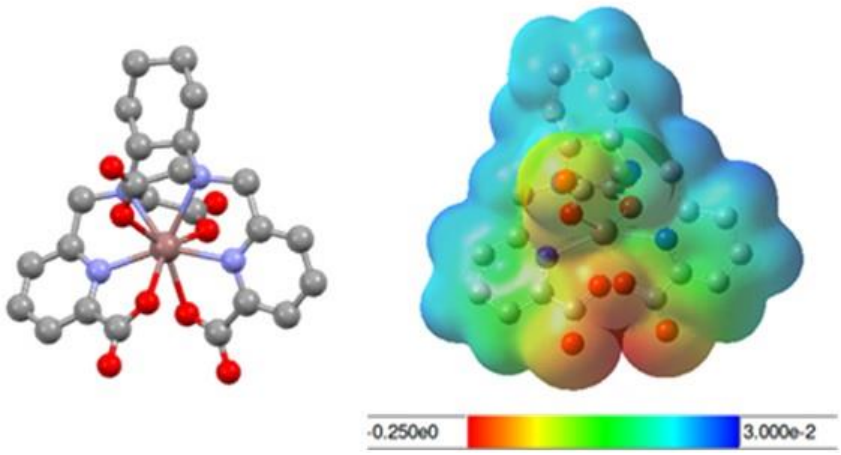

Figure 2.8 DFT structure of the anion [In(*CHX*octapa)]$^-$ showing eight-coordinate structure (left), and the molecular electrostatic potential (MEP) of the complex mapped onto the electron density (right) (positive = blue, negative = red, representing a maximum potential of 0.03 au, and a minimum of -0.25 au, mapped onto electron density isosurfaces of 0.002 Å^{-3}). Performed using the B3LYP functional employing the 6-31+G(d,p) basis set for first- and second-row elements and LanL2DZ for In^{3+} with water as solvent (PCM).

Table 2.3 Comparison of relevant bond lengths (Å) and angles (deg) of DFT-calculated In^{3+} complexes of H_4octapa[60] and H_4*CHX*octapa.

Bond length (Å)	[In(*CHX*octapa)]$^-$	[In(octapa)]$^-$
In-$O_{pyr\text{-}COO}$	2.309	2.295/2.294
In-$O_{Ac\text{-}COO}$	2.224	2.200/2.201
In-N_{pyr}	2.244	2.241
In-N_{en}	2.496	2.538
N_{en}-In-N_{en} angle (deg)	76.1	74.8

2.2.2 DFT Structures and Molecular Electrostatic Potential Maps

A solid-state structure of the likely monoanionic complex [In(*CHX*octapa)]$^-$ was not obtained; instead DFT calculations (modeled in water) were performed at the B3LYP level of theory utilizing the 6-31+g(d,p) basis set for the lighter atoms and effective core potential approximation (LanL2DZ) for In^{3+}. The DFT structure of [In(*CHX*octapa)]$^-$ (Figure 2.8) reveals an eight-coordinate symmetric complex with approximate C_2 symmetry, showing tight binding of In^{3+}. The electrostatic potential map of the complex exhibits a symmetric and relatively even

surface charge distribution. A very similar DFT structure was observed for [In(octapa)]$^-$;[53] in fact, close quantitative comparison of the In-O or In-N bond lengths and relevant N_{en}-In-N_{en} angle reveals very little difference between the two calculated structures (Table 2.3). The biggest differences in bond lengths arise from the In-N_{en} bonds, in which the [In(*CHX*octapa)]$^-$ complex exhibits bonds that are 0.042 Å shorter than the analogous In-N_{en} bonds in [In(octapa)]$^-$.

2.2.3 Thermodynamic Stability

Stepwise protonation constants (pK_a) (Table 2.4), formation constants (log K_{ML}), and pM values (-log[M^{n+} free]) (Table 2.5) have been determined for H_2*CHX*dedpa and H_4*CHX*octapa and some metal complexes. Values of pM are a more relevant comparative indicator of the extent to which a metal complex is formed in solution as it takes into consideration metal-ligand association, ligand basicity and metal ion hydrolysis at the biologically relevant pH of 7.4. The higher the pM value, the lower the concentration of free unbound metal ions in solution under the specified conditions (10 μM total ligand, 1 μM total metal ion, pH 7.4, 25 °C).

Table 2.4 Step-wise protonation constants (pK_as) of L = *CHX*dedpa^{2-} and *CHX*octapa^{4-}, including values for previously reported achiral analogues dedpa^{2-} and octapa^{4-} for comparison.

	*CHX*dedpa^{2-}	dedpa^{2-} [a]	*CHX*octapa^{4-}	octapa^{4-} [a]
[H_6L]/[H_5L][H]			1.91(8)	ND
[H_5L]/[H_4L][H]			1.82(6)	2.79(4)
[H_4L]/[H_3L][H]	2.40(9)	2.59(6)	2.24(2)	2.77(4)
[H_3L]/[H_2L][H]	2.99(8)	3.06(6)	3.94(2)	3.77(2)
[H_2L]/[HL][H]	6.47(8)	6.30(5)	5.40(2)	5.59(6)
[HL]/[L][H]	9.23(5)	9.00(3)	9.23(1)	8.59(4)

[a]Previously reported values for H_2dedpa[54] and H_4octapa.[53] ND = not determined.

The largest variances in pK_a values of dedpa^{2-} versus *CHX*dedpa^{2-}, and octapa^{4-} versus *CHX*octapa^{4-} both arise from the protonation of an N_{en} atom. In both cases, the first N_{en} pK_a value of the *CHX*-pa ligand was more basic (9.23 for both *CHX*dedpa^{2-} and *CHX*octapa^{4-}) compared to the native achiral ligand (9.00 and 8.59 for dedpa^{2-} and octapa^{4-}, respectively). These small differences in ligand basicity may arise from the added structural rigidity of the *CHX*-en backbone compared to the more flexible en backbone.

In vivo, there are many endogenous ligands that can compete for metal-binding from the desired radiometal-complex. Specifically, the iron binding protein *apo*-transferrin also has a high binding affinity for Ga(III) and In(III), because of the physical similarities between Ga(III)/In(III) and Fe(III). Therefore, it is important that the thermodynamic stabilities of the metal-chelate complex be higher than those for any endogenous ligands such as metal-bound transferrin. The thermodynamic stability constant of [Ga(*CHX*dedpa)]$^{+}$ was determined to be log K_{ML} = 27.61(8) (pM = 26.7), a comparably high value compared to Ga-transferrin or Ga-DOTA (Table 2.5), yet slightly lower (by less than one order of magnitude) than that previously found for [Ga(dedpa)]$^{+}$ (log K_{ML} = 28.11(8), pM = 27.4[54]). One might have expected that the introduction of a "cyclohexyl" backbone would have resulted in a more rigid chelate with pre-organized donor atoms leading to a higher thermodynamic stability constant; nonetheless, the thermodynamic stability value of [Ga(*CHX*dedpa)]$^{+}$ is still exceptionally high compared to the *in vivo* Ga(III)-competitor transferrin.

The thermodynamic stability constant (log K_{ML}) of *CHX*octapa^{4-} with Ga(III) was determined to be 22.32(20) (pM = 21.4), still a comparably high value, but lower than the corresponding dedpa^{2-} or *CHX*dedpa^{2-} values, confirming the obvious - the octadentate derivative would be better suited to larger metal ions such as In^{3+}, Y^{3+}, and Lu^{3+}.

Much like [In(octapa)]$^{-}$ (log K_{ML} = 26.76(14), pM = 26.5), [In(*CHX*octapa)]$^{-}$ flaunts exceptionally high thermodynamic stability constants (log K_{ML} = 27.16(9), pM = 26.3) that exceed those of In-NOTA, In-DOTA, or In-transferrin.

Thermodynamic stability constants are an important factor when evaluating metal-chelate pairs; however, they often do not correlate well with *in vivo* stability, and serum competition studies are essential experiments to evaluate kinetic inertness of the metal complexes.

Table 2.5 Formation constants (log K_{ML}) and pM[a] values for Ga^{3+} and/or In^{3+} complexes of *CHX*dedpa^{2-}, *CHX*octapa^{4-}, and relavent ligands used for comparison.

	M = Ga^{3+}		M = In^{3+}	
Ligand	log K_{ML}	pM[a]	log K_{ML}	pM[a]
dedpa^{2-} [53,54]	28.11(8)	27.4	26.60(4)	25.9
*CHX*dedpa^{2-}	27.61(8)	26.7		
octapa^{4-} [53]			26.76(14)	26.5
*CHX*octapa^{4-}	22.32(20)	21.4	27.16(9)	26.3
NOTA[133]	30.98	27.9	26.2	23.4
DOTA[134]	21.33	18.5	23.9	18.8
DTPA[135]	24.3	21.0	29.0	25.7
transferrin[136,137] [b]	20.3	21.3	18.3	18.7

[a]Calculated for 1 μM total metal ion, 10 μM total ligand, pH 7.4 at 25 °C. [b]Stability constants for highest binding site in *apo*-transferrin.

2.2.4 Radiolabeling Experiments

To determine the ability of the cyclohexyl-pa ligands to label gallium isotopes, the γ-emitter ^{67}Ga ($t_{1/2}$ = 3.26 d) was used as a model for ^{68}Ga in labeling experiments. The longer half-life of ^{67}Ga makes it more suitable for *in vitro* assays than ^{68}Ga. In addition, because of the success of octapa^{4-} with indium(III), the labeling behavior of ^{111}In with the cyclohexyl derivative *CHX*octapa^{4-} was also investigated. Representative HPLC radio-chromatograms can be found in the Appendix.

Initial radiolabeling experiments discovered H_2*CHX*dedpa could quantitatively radiolabel ^{67}Ga at ambient temperature in 10 min, showing a single sharp peak in the HPLC radiotrace at t_R = 6.8 min. Concentration dependent labeling was performed by decreasing the ligand concentration 10-fold, while holding the activity constant (~ 1 mCi ^{67}Ga), to determine the highest specific activity (S.A.) and lowest ligand concentration that would yield quantitative labeling. Unlike H_2dedpa, which exhibited quantitative radiolabeling at ligand concentrations as low as 10^{-7} M with specific activities as high as 9837 mCi/μmol at 10 min and room temperature,[54] the analogous cyclohexyl derivative H_2*CHX*dedpa only radiolabelled quantitatively (> 99% radiochemical yield (RCY)) at room temperature with ligand concentrations of 10^{-5} M (S.A. 40 mCi/μmol); at lower ligand concentrations (10^{-6} M), the RCY was 16% at 10 min and room temperature, and the solution required heating (60 °C, 30 min) to reach an RCY of 96%. Initial radiolabeling studies with the *N*-alkylated derivative H_2*CHX*dedpa-bb showed ^{67}Ga labeling of 96% at the original ligand concentration of 10^{-4} M, and when the ligand concentration was decreased 10-fold to 10^{-5} M, radiochemical yield decreased significantly to 27%. The additional benzyl arms of H_2*CHX*dedpa-bb add a degree of steric hindrance around the metal binding site, which may explain the lower radiochemical yields obtained with the *N*-alkylated derivatives. Additionally, the tertiary backbone nitrogen atoms of H_2*CHX*dedpa-bb may be inferior electronically to the secondary nitrogen atoms of H_2*CHX*dedpa, a trend previously observed for H_2dedpa and its derivatives.[54] These results suggest that adding a more rigid chiral backbone onto the chelate structure, making it a more macrocyclic-like ligand, where the cyclohexyl ring acts to preorganize the geometry of the donor atoms, with the intention of adding kinetic inertness, hampers labeling kinetics at low concentrations. The phrase “easy-in, easy-out” may be an applicable catch-phrase for describing radiometal-ligand systems, as a higher energetic barrier to getting a radiometal inside a macrocycle (e.g., heating) also often translates to a higher energetic barrier to removing the radiometal from the grasp of

the macrocycle (more kinetically inert). An appropriate and functional balance between these forces is much sought after.

Initial ^{67}Ga radiolabeling experiments with H$_4$*CHX*octapa were similar to those with H$_2$*CHX*dedpa described above. Quantitative radiolabeling (RCY 99%) was achieved at 10^{-4} and 10^{-5} M ligand concentrations with 1-6 mCi ^{67}Ga, using standard mild labeling conditions (room temperature, 10 min). The RCY decreased to 38% when the ligand concentration decreased to 10^{-6} M, with labeling conditions of 10 min at ambient temperature. Labeling yields increased to 72% when the reaction was heated at 70 °C for 1 h. Also, close examination of the labeling peak reveals an interesting split in the radiotrace, likely from different protonation states of the Ga-complex in solution; the ligand has an extra carboxylic acid arm that would not be involved in chelation if the predicted six-coordinate complex were formed and therefore could be protonated depending on the pH of the solution. Indeed, the solid-state structure of [Ga(H*CHX*octapa)] confirms this hypothesis, since the X-ray structure exhibits a six-coordinate structure with one of the pyridyl carboxylates uncoordinated to the metal center.

Labeling experiments with ^{111}In and the ligand H$_4$*CHX*octapa showed quantitative labeling of ^{111}In at 10^{-4} – 10^{-6} M ligand (RCY >99%) within 10 min at room temperature. The highest specific activity of [^{111}In(*CHX*octapa)]$^-$ obtained within 10 min at room temperature was ~670 mCi/μmol (10^{-6} M ligand), unlike [^{111}In(octapa)]$^-$, which yielded specific activities as high as 2300 mCi/μmol at 10^{-7} M ligand concentration, after 10 min at room temperature.

2.2.5 Human Serum Stability Studies

To investigate the stability of the ^{67}Ga- and ^{111}In-complexes, a 2 or 120 h competition experiment, respectively, was performed in the presence of excess human blood serum, which

contains endogenous ligands that can compete for Ga(III)/In(III) binding *in vivo/in vitro,* such as *apo*-transferrin and albumin. This assay is a preferred method of predicting the *in vivo* kinetic inertness of the radiometal ion complexes. Preliminary studies showed that the human serum competition was a harsher competition than the *apo*-transferrin challenge that was used in earlier stability studies with the ligands H_2dedpa and H_4octapa. Results for the stability of [^{67}Ga(*CHX*dedpa)]$^+$, [^{67}Ga(*CHX*dedpa-bb)]$^+$, and [^{67}Ga(*CHX*octapa)]$^-$ are compiled in Table 2.6, with H_2dedpa, NOTA, and DOTA used as ligand standards for comparison.

The [^{67}Ga(*CHX*dedpa)]$^+$ complex exhibited excellent stability with 95.7% and 90.5% of ^{67}Ga remaining chelate bound after 1 and 2 h, respectively; this is a marked improvement compared to the [^{67}Ga(dedpa)]$^+$ complex, which was only 77.8% stable after 2 h. These results clearly show the positive influence on stability that the added chiral modification and preorganization of the metal binding site has on complex stability of the dedpa^{2-} core. The [^{67}Ga(*CHX*dedpa)]$^+$ complex also exhibited higher stability (~10 % more stable) than the industry 'gold-standard' [^{67}Ga(DOTA)]$^-$ in the human serum stability challenge after 2 h.

Table 2.6 Stability of ^{67}Ga-labelled *CHX*-"pa" ligands and standards dedpa^{2-}, NOTA, and DOTA in human serum at 37 °C, with stability shown as the percentage of intact ^{67}Ga complex.

complex	1 h (%)	2 h (%)
[^{67}Ga(*CHX*dedpa)]$^+$	95.7 ± 0.7	90.5 ± 4.4
[^{67}Ga(*CHX*dedpa–bb)]$^+$	81.2 ± 3.9	82.9 ± 1.8
[^{67}Ga(*CHX*octapa)]$^-$	78.1 ± 3.7	74.7 ± 3.5
[^{67}Ga(dedpa)]$^+$	94.8 ± 3.4	77.8 ± 1.5
[^{67}Ga(NOTA)]	97.5 ± 0.7	98.0 ± 0.6
[^{67}Ga(DOTA)]$^-$	80.1 ± 0.8	80.0 ± 1.9

A small loss of stability was seen with the benzyl functionalized derivative H_2*CHX*dedpa-bb with only 83% of ^{67}Ga bound after 2 h. The loss of stability with the *N*-alkylated derivative was also seen in the native H_2dedpa derivatives previously reported, where stability dropped

from >99 to 51% for the H_2dedpa-bb-NO_2 derivative in a 2 h *apo*-transferrin challenge assay. This may suggest that functionalization at the secondary nitrogen atoms is negatively affecting the coordination sphere of the metal ion and is thus not an appropriate choice for preparing bifunctional derivatives (either due to steric bulk or electronic changes from secondary to tertiary amines, *vide supra*). Moreover, benzyl groups as a model placeholder for bifunctional derivatives may not be an appropriate choice since they introduce a great deal of steric hindrance near the metal binding core, and instead alkyl groups may be a better choice for *N*-alkylation. Nonetheless, alternate modes of functionalization may be required, for example functionalization on the pyridyl ring, or the cyclohexyl-ring to avoid loss of radiometal complex stability.

Table 2.7 Stability of ^{111}In-*CHX*octapa in human serum at 37 °C and previously reported ^{111}In-octapa derivatives, ^{111}In-DOTA, and ^{111}In-DTPA in mouse serum, with stability shown as the percentage of intact ^{111}In complex.

complex	1 h (%)	24 h (%)	120 h (%)
[^{111}In(*CHX*octapa)]$^-$	90.9 ± 0.3	90.2 ± 0.5	91.0 ± 0.2
[^{111}In(octapa)]$^-$ [53]	93.8 ± 3.6	92.3 ± 0.04	ND[a]
[^{111}In(octapa-Trastuzumab)]$^-$ [59]	ND[a]	ND[a]	94.9 ± 0.6
[^{111}In(DOTA)]$^-$ [53]	89.6 ± 2.2	89.4 ± 2.2	ND[a]
[^{111}In(DTPA)]$^{2-}$ [53]	86.5 ± 2.2	88.3 ± 2.2	ND[a]

[a]Not determined.

The ^{67}Ga-*CHX*octapa complex was 74% stable after 2 h. The additional chelating arms of the octadentate chelate, which most likely remain unbound to the metal, may create uneven charge distribution on the metal complex and an easy site for attack of endogenous ligands. Additionally, the decreased stability could simply be a result of modifying the secondary amines of *CHX*dedpa^{2-} to the tertiary amines of *CHX*octapa^{4-}, which appear to be inferior Ga(III) binding groups. It has been a recurring trend throughout our studies with Ga(III) that ligands that

possess secondary amines in their backbone (e.g., H_2dedpa) have superior stability to those that are functionalized to possess tertiary amines. This trend where the electronics of secondary versus tertiary amine binding groups strongly affects radiometal stability is also observed with ^{64}Cu binding TETA derivatives, such as CB-TE2A, MM-TE2A, and DM-TE2A, where tertiary amines are found to be far more stable than secondary amines.[127,130] One might expect that H_4*CHX*octapa would be better suited for larger metal ions that can tolerate or prefer higher denticity ligands, ions such as In^{3+}. Indeed, the [^{111}In(*CHX*octapa)]$^-$ complex showed excellent stability of 91% over 5 d against human serum (Table 2.7). This result is comparable to those obtained for mouse serum competition assays of ^{111}In-octapa complexes,[53,59] suggesting H_4*CHX*octapa is a good candidate for further testing *in vivo*.

2.3 Conclusions

Preliminary investigations of the chiral hexadentate chelating ligand H_2*CHX*dedpa (N_4O_2) with ^{67}Ga/Ga^{3+} and chiral octadentate chelating ligand H_2*CHX*octapa (N_4O_4) with ^{111}In/In^{3+} have shown them to be promising candidates for radiopharmaceutical elaboration. Both chelates retain their ability to quantitatively label their respective isotopes at room temperature within 10 min, a marked advantage over many of the macrocyclic gold standards such as NOTA and DOTA, and even some new Ga(III) ligands such as TRAP.[68,71]

In vitro human serum stability assays demonstrated H_2*CHX*dedpa to have improved stability with ^{67}Ga compared to its achiral counterpart H_2dedpa, with only 9% of ^{67}Ga transchelated to serum proteins after 2 h versus 22% for H_2dedpa. Moreover, analogous *in vitro* studies of H_4*CHX*octapa with ^{111}In demonstrated exceptional stability of the complex over 5 d – matching well with results previously obtained for H_4octapa. These stability assays suggest the added structural modification of the cyclohexyl ring onto the ligand backbone results in metal-

ligand complexes of higher stability (in the case of H_2*CHX*dedpa) or comparable stability (in the case of H_4*CHX*octapa) evaluated against their ethylenediamine analogues H_2dedpa and H_4octapa. Thermodynamic stability constants of [Ga(*CHX*dedpa)]$^+$ and [In(*CHX*octapa)]$^-$ were determined through potentiometric titrations to be log K_{ML} = 27.61(8) and 27.16(9) (pM = 26.7 and 26.3), respectively. The [Ga(*CHX*dedpa)]$^+$ thermodynamic stability constant is comparable to the high stability constant previously obtained for [Ga(dedpa)]$^+$ (log K_{ML} = 28.11(8), pM = 27.4), further exemplifying the *CHX*dedpa^{2-} scaffold as a strong Ga^{3+} ligand. The [In(*CHX*octapa)]$^-$ thermodynamic stability constant was slightly higher than the already exceptionally high stability constants of [In(octapa)]$^-$ (log K_{ML} = 26.76(14), pM = 26.5), confirming that *CHX*octapa^{4-} is a remarkably stable ligand for $^{111}In/In^{3+}$ chelation.

The fast and quantitative labeling of Ga(III) or In(III) isotopes, exceptionally high thermodynamic stability constants, and favorable *in vitro* stability together with facile and good yield syntheses make H_2*CHX*dedpa and H_4*CHX*octapa ideal candidates for incorporation into radiopharmaceutical design. H_4*CHX*octapa is of significant interest for future study with isotopes such as $^{86/90}Y$ and ^{177}Lu. To further demonstrate the stability of these radiotracers in a biological system, biodistribution data will be of significance; hence moving forward, alternate modes of functionalization of the scaffolds with the intention of making bifunctional derivatives would be of great interest for further testing *in vivo* to fully evaluate the potential of these promising scaffolds.

2.4 Experimental

2.4.1 Materials and Methods

All solvents and reagents were purchased from commercial suppliers (Sigma Aldrich, TCI America, Fisher Scientific) and were used as received. Human serum was purchased from Invitrogen. NOTA and DOTA were purchased from Macrocylics. The analytical thin-layer chromatography (TLC) plates were aluminum-backed ultrapure silica gel 60 Å, 250 μm thickness; the flash column silica gel (standard grade, 60 Å, 40-63 μm) was provided by Silicycle. ^{1}H and ^{13}C NMR spectra were recorded at 25 °C unless otherwise noted on Bruker AV300, AV400, or AV600 instruments; NMR spectra are expressed on the δ scale and referenced to residual solvent peaks. Low-resolution mass spectrometry was performed using a Waters ZG spectrometer with an ESCI electrospray/chemical-ionization source, and high-resolution electrospray-ionization mass spectrometry (HR-ESI-MS) was performed on a Micromass LCT time-of-flight instrument at the Department of Chemistry, University of British Columbia. Microanalyses for C, H, and N were performed on a Carlo Erba Elemental Analyzer EA 1108. ^{67}Ga- or ^{111}In-(chelate) human serum stability experiments were analyzed using GE Healthcare Life Sciences PD-10 desalting columns (size exclusion for MW < 5000 Da) and counted with a Capintec CRC 15R well counter. The HPLC system used for analysis and purification of nonradioactive compounds consisted of a Waters 600 controller, Waters 2487 dual wavelength absorbance detector, and a Waters delta 600 pump. Phenomenex Synergi Hydro-RP 80 Å columns (250 mm x 4.6 mm analytical or 250 mm x 21.2 mm semipreparative) were used for purification of several of the deprotected ligands. Analysis of radiolabelled complexes was carried out using a Phenomenex Synergi 4 μ Hydro-RP 80A analytical column (250 x 4.60 mm 4 μm) using a Waters Alliance HT 2795 separation module equipped with a

Raytest Gabi Star NaI (Tl) detector and a Waters 996 photodiode array (PDA). $^{67}GaCl_3$ and $^{111}InCl_3$ were cyclotron-produced and provided by Nordion as ~0.1 M HCl solutions.

2.4.2 *N,N'*-((1*R*,2*R*)-Cyclohexane-1,2-diyl)bis(2-nitrobenzenesulfonamide) (2.1)

To a stirred solution of (1*R,*2*R*)-(-)-1,2-diaminocyclohexane (0.33 g, 2.9 mmol), and $NaHCO_3$ (1.44 g, 17.2 mmol, 6 equiv) in THF (6 mL) at 0°C under N_2, a solution of 2-nitrobenzenesulfonyl chloride (1.27 g, 5.7 mmol, 2 equiv) in THF (8 mL) was added dropwise. The murky white mixture was allowed to warm to ambient temperature and stirred overnight. The reaction mixture was filtered to remove sodium bicarbonate and was subsequently concentrated *in vacuo*. The resultant orange oil was purified by column chromatography (CombiFlash R_f automated column system; 40 g HP silica; A: hexanes, B: ethyl acetate, 100% A to 100% B gradient) to yield the product **2.1** as a fluffy white solid (1.01 g, 73%) (R_f = 0.63, TLC in ethyl acetate). ^{1}H NMR (400 MHz, $CDCl_3$) δ 8.05 (dd, *J* = 7.5, 1.4 Hz, 2H), 7.75 (dd, *J* = 7.4, 1.6 Hz, 2H), 7.73 – 7.61 (m, 4H), 5.59 (d, *J* = 7.0 Hz, 2H), 3.29 – 3.15 (m, 2H), 1.79 (d, *J* = 12.7 Hz, 2H), 1.51 (d, *J* = 7.6 Hz, 2H), 1.36 – 1.21 (m, 2H), 1.12 (t, *J* = 9.7 Hz, 2H). ^{13}C NMR (101 MHz, $CDCl_3$) δ 147.6, 134.3, 134.0, 133.5, 130.6, 125.6, 57.7, 33.3, 24.1. MS (ES+) m/z = 485.2 $[M+H]^+$.

2.4.3 Dimethyl 6,6'-(((1*R*,2*R*)-cyclohexane-1,2-diylbis(((2-nitrophenyl)sulfonyl) azane-diyl))-bis(methylene))dipicolinate (2.2)

Potassium carbonate (1.5 g, 11.1 mmol, 6 equiv) was added to a stirred solution of **2.1** (0.898 g, 1.85 mmol), and methyl-6-bromomethyl picolinate[138] (0.853 g, 3.71 mmol, 2 equiv) in acetonitrile (20 mL). The mixture was stirred at 65°C for 2 d, excess salts were removed by centrifugation (4000 rpm for 10 min) and filtration, and the filtrate was concentrated *in vacuo.*

The crude product was purified by column chromatography (CombiFlash R_f automated column system; 80 g HP silica; A: hexanes, B: ethyl acetate, 100% A to 100% B gradient) to yield the product **2.2** as a fluffy off-white solid (1.37 g, 94%). ^{1}H NMR (400 MHz, $CDCl_3$) δ 7.67 (d, *J* = 7.7 Hz, 1H), 7.55 (t, *J* = 7.7 Hz, 1H), 7.40 (dt, *J* = 16.7, 8.4 Hz, 4H), 7.13 (t, *J* = 7.0 Hz, 1H), 5.01 (d, *J* = 17.5 Hz, 1H), 4.58 (t, *J* = 18.8 Hz, 1H), 4.21 (s, 1H), 3.70 (s, 3H), 2.39 (d, *J* = 7.3 Hz, 1H), 1.61 (s, 1H), 1.31 (m, 2H). ^{13}C NMR (101 MHz, $CDCl_3$) δ 164.9, 156.2, 147.2, 146.6, 136.9, 134.1, 132.7, 130.9, 126.1, 123.4, 123.2, 59.6, 53.5, 52.2, 49.6, 32.5, 25.1. MS (ES+) m/z = 821.3 $[M+K]^+$; 805.4 $[M+Na]^+$.

2.4.4 *N,N'*-[6-(Methoxycarbonyl)pyridin-2-yl]methyl-1,2-(1*R*,2*R*)-cyclohexanediamine (2.3)

To a solution of **2.2** (1.16 g, 1.48 mmol) in THF (10 mL) was added thiophenol (313 μL, 3.04 mmol, just over 2 equiv) and potassium carbonate (1.22 g, 8.88 mmol, 6 equiv). The reaction mixture was stirred at ambient temperature for 72 hours, during which time a slow colour change from faint yellow to deep yellow occurred. The salts were removed by filtration after centrifugation (4000 rpm for 10 min), and the filtrate was concentrated *in vacuo*. The crude product was purified by column chromatography (CombiFlash R_f automated column system; 24 g HP silica; A: dichloromethane, B: methanol with 2% triethylamine, 100% A to 25% B gradient) to yield **2.3** as a yellow oil (0.606 g, 99%). ^{1}H NMR (400 MHz, $CDCl_3$) δ 7.87 (d, *J* = 7.5 Hz, 2H), 7.69 (t, *J* = 7.7 Hz, 2H), 7.61 (d, *J* = 7.4 Hz, 2H), 4.06 (d, *J* = 14.9 Hz, 2H), 3.87 (d, *J* = 13.5 Hz, 2H), 3.84 (s, 6H), 2.67 (s, 2H), 2.28 – 2.19 (m, 2H), 2.05 (d, *J* = 13.1 Hz, 2H), 1.60 (d, *J* = 8.1 Hz, 2H), 1.17 – 1.04 (m, 2H), 1.03 – 0.87 (m, 2H). ^{13}C NMR (101 MHz, $CDCl_3$) δ 165.7, 161.4, 147.1, 137.3, 125.7, 123.3, 61.3, 52.7, 52.1, 31.5, 24.8. MS (ES+) m/z = 451.3 $[M+K]^+$.

2.4.5 H_2*CHX*dedpa·2HCl·2H_2O (2.4)

Compound **2.3** (0.314 g, 0.76 mmol) was dissolved in HCl (6 M, 5 mL) and refluxed overnight, during which time a white precipitate formed. The resultant mixture was cooled on ice, and the solid was isolated by vacuum filtration and washed with acetone to yield **2.4** as a white crystalline solid (0.251 g, 67%). ^{1}H NMR (300 MHz, D_2O) δ 8.15 (dt, *J* = 15.3, 7.1 Hz, 4H), 7.76 (d, *J* = 6.5 Hz, 2H), 4.98 (d, *J* = 17.1 Hz, 2H), 4.85 (d, *J* = 15.9 Hz, 2H), 3.72 – 3.56 (m, 2H), 2.50 (d, *J* = 12.5 Hz, 2H), 1.87 (d, *J* = 9.0 Hz, 2H), 1.61 (d, *J* = 8.7 Hz, 2H), 1.27 (t, *J* = 9.9 Hz, 2H). ^{13}C NMR (75 MHz, D_2O) δ 167.4, 151.6, 146.6, 140.1, 126.8, 125.7, 58.8, 47.8, 28.1, 22.7. Elemental Anal. calcd. (found) for $C_{20}H_{24}N_4O_4$·2HCl·2H_2O: C, 48.69 (48.90); H, 6.13 (5.99); N, 11.36 (11.37). HR-ESI-MS m/z for $C_{20}H_{25}N_4O_4$ ($M+H^+$) calcd. (found): 385.1876 (385.1881) (1.3 PPM).

2.4.6 Dimethyl 6,6'-(((1*R*,2*R*)-cyclohexane-1,2-diylbis((2-(tert-butoxy)-2-oxoethyl) aza-nediyl))-bis(methylene))dipicolinate (2.5)

To a solution of **2.3** (0.398 g, 0.96 mmol) in acetonitrile (8 mL), *tert*-butylbromoacetate (285 μL, 1.93 mmol, 2 equiv) and sodium carbonate (0.610 g, 5.76 mmol, 6 equiv) were added. The reaction mixture was stirred at 60°C overnight. Excess salts were removed by filtration, and the filtrate was concentrated *in vacuo*. The crude oil was purified by column chromatography (CombiFlash R_f automated column system; 24 g HP silica; A: dichloromethane, B: methanol, 100% A to 20% B gradient) to yield **2.5** as a faint yellow oil (0.423 g, 68%). ^{1}H NMR (400 MHz, $CDCl_3$) δ 8.02 (d, *J* = 7.8 Hz, 2H), 7.91 (d, *J* = 7.5 Hz, 2H), 7.55 (t, *J* = 7.7 Hz, 2H), 3.95 (s, 6H), 3.90 (d, *J* = 15.0 Hz, 2H), 3.77 (d, *J* = 15.0 Hz, 2H), 3.36 (d, *J* = 16.8 Hz, 2H), 3.25 (d, *J* = 16.8 Hz, 2H), 2.61 (s, 2H), 2.11 (d, *J* = 7.1 Hz, 2H), 1.71 (s, 2H), 1.40 (s, 18H), 1.08 (d, *J* = 5.8 Hz,

4H). ^{13}C NMR (101 MHz, $CDCl_3$) δ 171.5, 166.1, 161.8, 146.8, 137.0, 127.7, 123.6, 80.5, 61.8, 56.1, 52.9, 52.7, 28.2, 26.3, 26.0. MS (ES+) m/z = 641.6 $[M+H]^+$.

2.4.7 H$_4$*CHX*octapa·3.5HCl·0.5H$_2$O (2.6)

Compound **2.5** (0.336 g, 0.52 mmol) was dissolved in HCl (6 M, 10 mL) and refluxed overnight. The reaction mixture was concentrated *in vacuo* and purified via semipreparative RP-HPLC (gradient: A: 0.1% TFA (trifluoroacetic acid) in water, B: CH_3CN, 5 to 100% B linear gradient over 25 min, 10 mL/min, t_R = 12.5 min). Product fractions were pooled, concentrated *in vacuo*, dissolved in CH_3CN (3 mL) and HCl (3 M, 3 mL), and then concentrated *in vacuo* again to remove trifluoroacetic acid. This process was repeated two more times, the last time solvent was lyophilized to yield the HCl salt **2.6** as an off-white solid (0.136 g, 41% based on MW calculated from EA). ^{1}H NMR (400 MHz, D_2O, 55 °C) δ 8.54 (t, *J* = 7.7 Hz, 2H), 8.48 (d, *J* = 7.1 Hz, 2H), 8.16 (d, *J* = 5.4 Hz, 2H), 4.74 – 4.57 (m, 4H), 4.19 (d, *J* = 17.4 Hz, 2H), 4.01 (d, *J* = 17.1 Hz, 2H), 3.83 (d, *J* = 9.2 Hz, 2H), 2.69 (d, *J* = 12.3 Hz, 2H), 2.31 (d, *J* = 8.5 Hz, 2H), 1.93 (d, *J* = 8.9 Hz, 2H), 1.83 – 1.67 (m, 2H). ^{13}C NMR (101 MHz, D_2O) δ 172.4, 165.3, 152.5, 146.2, 143.7, 129.1, 126.2, 100.1, 63.3, 52.3, 24.5, 24.4. Elemental Anal. calcd. (found) for $C_{24}H_{28}N_4O_8$·3.5HCl·0.5H_2O: C, 45.24 (45.26); H, 5.14 (5.47); N, 8.79 (8.41). HR-ESI-MS m/z for $C_{24}H_{29}N_4O_8$ ($M+H^+$) calcd. (found): 501.1985 (501.1982) (-0.6 PPM).

2.4.8 (1*R*,2*R*)-N^1,N^2-dibenzylcyclohexane-1,2-diamine (2.7)

A solution of (1*R*,2*R*)-(-)-1,2-diaminocyclohexane (1.381 g, 12.1 mmol) and benzaldehyde (2.46 mL, 24.2 mmol, 2 equiv) in ethanol (50 mL) was stirred at 0°C for 4 h, then overnight at reflux. Formation of imine was confirmed by MS (ES+) m/z = 291.4 $[M+H]^+$, and

the reaction mixture was cooled to ambient temperature and concentrated *in vacuo*. The crude imine was purified by column chromatography (CombiFlash R_f automated column system; 80 g HP silica; A: dichloromethane, B: methanol, 100% A to 10% B gradient) to yield the intermediate imine as a faint yellow solid (1.28 g). The imine was then dissolved in ethanol (70 mL) at 0°C, and $NaBH_4$ (0.422 g, 11.2 mmol, ~2.5 equiv) was added in small portions. The mixture was stirred for 2 hours, subsequently quenched with saturated aqueous NH_4Cl (70 mL), and extracted with dichloromethane (3x90 mL). The organics were collected, dried over $MgSO_4$, and concentrated *in vacuo* to yield **2.7** as yellow oil (1.336 g, 38% over two steps). ^1H NMR (400 MHz, MeOD) δ 7.39 – 7.25 (m, 10H), 3.96 (d, *J* = 13.0 Hz, 2H), 3.76 (dd, *J* = 12.9, 7.4 Hz, 2H), 2.53 – 2.41 (m, 2H), 2.21 (d, *J* = 12.0 Hz, 2H), 1.83 – 1.71 (m, 2H), 1.34 – 1.19 (m, 4H). ^{13}C NMR (101 MHz, MeOD) δ 139.3, 129.7, 129.7, 128.7, 60.9, 50.6, 30.8, 25.7. MS (ES+) m/z = 295.5 $[M+H]^+$.

2.4.9 Dimethyl 6,6'-(((1*R*,2*R*)-cyclohexane-1,2-diylbis(benzylazanediyl))bis(methylene))-dipicolinate (2.8)

To a solution of **2.7** (0.356 g, 1.21 mmol) and methyl-6-bromomethyl picolinate[138] (0.585 g, 2.54 mmol, just over 2 equiv) in acetonitrile (20 mL), potassium carbonate (0.836 g, 6.05 mmol, 6 equiv) was added, and the resultant suspension was refluxed for 3 d. The mixture was cooled to ambient temperature, excess salts were removed by filtration, and filtrate was concentrated *in vacuo*. The crude yellow oil was purified by column chromatography (CombiFlash R_f automated column system; 80 g HP silica; A: dichloromethane, B: methanol, 100% A to 10% B gradient) to yield **2.8** as a yellow oil (0.537 g, 75%). ^1H NMR (400 MHz, $CDCl_3$) δ 7.97 (d, *J* = 7.6 Hz, 2H), 7.93 (d, *J* = 7.7 Hz, 2H), 7.65 (t, *J* = 7.6 Hz, 2H), 7.27 (d, *J* = 7.1 Hz, 4H), 7.15 – 7.07 (m, 6H), 3.98 (s, 6H), 3.84 (d, *J* = 15.2 Hz, 2H), 3.72 – 3.62 (m, 4H), 3.47 (d, *J* =

13.6 Hz, 2H), 2.73 (d, *J* = 7.0 Hz, 2H), 2.17 (d, *J* = 10.0 Hz, 2H), 1.73 (d, *J* = 5.4 Hz, 2H), 1.13 – 0.99 (m, 4H). ^{13}C NMR (101 MHz, $CDCl_3$) δ 165.8, 161.8, 147.0, 139.4, 136.6, 128.9, 127.9, 126.8, 126.2, 123.2, 59.1, 55.1, 53.9, 52.7, 25.7, 24.3. (ES+) m/z = 593.4 $[M+H]^+$.

2.4.10 H_2*CHX*dedpa-bb (2.9)

Compound **2.8** (0.308 g, 0.52 mmol) was dissolved in THF/water mixture (3:1, 12 mL), and lithium hydroxide (0.062 g, 2.60 mmol, 5 equiv) was added. The mixture was stirred at ambient temperature for 2 h, and solvent was removed *in vacuo* to yield the product as the lithium adduct. ^{1}H NMR (400 MHz, MeOD) δ 7.95 (d, *J* = 7.5 Hz, 2H), 7.87 (d, *J* = 7.4 Hz, 2H), 7.77 (t, *J* = 7.5 Hz, 2H), 7.24 (d, *J* = 6.6 Hz, 4H), 7.14 – 7.04 (m, 6H), 3.76 (d, *J* = 14.5 Hz, 2H), 3.55 (t, *J* = 14.9 Hz, 4H), 3.36 (d, *J* = 13.4 Hz, 2H), 2.66 (d, *J* = 7.8 Hz, 2H), 2.11 (d, *J* = 10.3 Hz, 2H), 1.69 (d, *J* = 6.1 Hz, 2H), 1.11 – 0.94 (m, 4H). ^{13}C NMR (101 MHz, MeOD) δ 172.8, 161.4, 155.2, 140.8, 138.9, 130.2, 129.1, 128.0, 126.3, 123.4, 60.5, 56.1, 55.1, 26.9, 25.3. The product was then purified via semipreparative RP-HPLC to remove lithium salts (gradient: A: 0.1% TFA (trifluoroacetic acid) in water, B: CH_3CN; 5 to 100% B linear gradient over 25 min, 10 mL/min, t_R = 17.9 min). The HPLC fractions were pooled, concentrated *in vacuo*, redissolved in CH_3CN (1 mL) and HCl (1 M, 3 mL), and concentrated again to drive off trifluoroacetic acid. This process was repeated two more times, and the last time solvent was removed on a lyophilizer yielding the HCl salt **2.9** as a faint yellow solid (0.143 g, 49%). Elemental Anal. calcd. (found) for $C_{34}H_{36}N_4O_4 \cdot 3.5HCl \cdot 0.5H_2O$: C, 58.23 (58.58); H, 5.82 (5.93); N, 7.99 (7.96). HR-ESI-MS m/z for $C_{34}H_{37}N_4O_4$ ($M+H^+$) calcd. (found): 565.2815 (565.2821) (1.1 PPM).

2.4.11 [Ga(*CHX*dedpa)][ClO_4]

H_2*CHX*dedpa·3HCl (**2.4**) (18.1 mg, 0.037 mmol) was dissolved in methanol/water (1:3, 2 mL); the pH of this solution was 2.5. To this clear solution $Ga(ClO_4)_3{\cdot}6H_2O$ (14.6 mg, 0.040 mmol, 1.1 equiv) in water (500 µL) was added. The pH of this solution was adjusted to 4.5 using NaOH (aq) (0.1 M), and the mixture was stirred at room temperature for 1.5 h. The resultant murky solution was concentrated *in vacuo* to a white solid. The crude product was dissolved in water/acetonitrile (4 mL: 0.5 mL) and purified by semi-preparative RP-HPLC (gradient: A: water, B: CH_3CN, 5 to 100% B linear gradient over 25 min, 10 mL/min, t_R = 11.3 min). Fractions were concentrated *in vacuo*, and further dried under vacuum overnight to give the product as a white solid (15.7 mg, 77%). ^{1}H NMR (400 MHz, DMSO) δ 8.59 (t, *J* = 7.8 Hz, 2H), 8.27 (d, *J* = 7.6 Hz, 2H), 8.06 (d, *J* = 7.9 Hz, 2H), 5.92 (dd, *J* = 10.1, 5.2 Hz, 2H), 4.59 (d, *J* = 17.4 Hz, 2H), 4.33 (dd, *J* = 17.3, 5.4 Hz, 2H), 2.31 (d, *J* = 8.3 Hz, 2H), 2.09 – 1.97 (m, 2H), 1.78 – 1.64 (m, 2H), 1.20 – 1.03 (m, 4H). ^{13}C NMR (101 MHz, DMSO) δ 162.5, 150.6, 145.5, 144.5, 127.4, 122.3, 59.0, 45.1, 28.6, 23.9. HR-ESI-MS m/z for $C_{20}H_{22}{}^{69}GaN_4O_4$ (M^+) calcd. (found): 451.0897 (451.0903) (1.3 PPM).

2.4.12 [Ga(*CHX*dedpa-bb)][ClO_4]

H_2*CHX*dedpa-bb (**2.9**) (13.5 mg, 0.024 mmol) was dissolved in methanol/water (1:1). The pH of this solution was adjusted to 3 using HCl (aq) (0.1 M). To this clear solution, a solution of $Ga(ClO_4)_3{\cdot}6H_2O$ (17.1 mg, 0.036 mmol, 1.5 equiv) in water (100 µL) was added, during which time a white precipitate formed. The pH of the solution was adjusted to 4 using NaOH (aq) (0.1 M), and stirred at ambient temperature for 3 h. The precipitate was isolated by centrifugation (4000 rpm, 10 min), the filtrate was decanted and the solid was dried under vacuum to yield the product as a white powdery solid (16.0 mg, 91%). ^{1}H NMR (400 MHz, DMSO) δ 8.69 (t, *J* = 7.8 Hz, 1H), 8.35 (d, *J* = 7.5 Hz, 1H), 8.27 (d, *J* = 7.9 Hz, 1H), 7.61 (d, *J* = 7.1

Hz, 2H), 7.37 (dq, *J* = 14.1, 6.9 Hz, 3H), 4.80 (q, *J* = 18.1 Hz, 2H), 4.21 (d, *J* = 13.4 Hz, 1H), 3.46 – 3.39 (m, 1H), 2.79 (d, *J* = 64.0 Hz, 1H), 1.24 (d, *J* = 23.6 Hz, 1H), 1.12 (s, 1H), 1.02 – 0.85 (m, 2H). ^{13}C NMR (101 MHz, DMSO) δ 162.2, 151.9, 146.6, 143.8, 132.9, 131.7, 129.3, 128.5, 127.3, 123.3, 64.5, 62.0, 49.2, 29.3, 23.5. HR-ESI-MS m/z for $C_{34}H_{34}{}^{69}GaN_4O_4$ (M^+) calcd. (found): 631.1836 (631.1837) (0.2 PPM).

2.4.13 Na[Ga(*CHX*octapa)]

H_4*CHX*octapa·2HCl·3H_2O (**2.6**) (14.6 mg, 0.023 mmol) was dissolved in methanol/water (1:1, 1 mL); the pH of this solution was ~1. To this clear solution, $Ga(NO_3)_3$·6H_2O (9.6 mg, 0.026 mmol, 1.1 equiv) in water (300 µL) was added. The pH of the solution was adjusted to 4 using NaOH (aq) (0.1 M), and the mixture was stirred at room temperature overnight, during which time a white precipitate formed. The precipitate was isolated by centrifugation (4000 rpm, 10 min), the filtrate was decanted and the solid was dried under vacuum to yield the product as a white solid (8.0 mg, 59%). ^{1}H NMR (400 MHz, DMSO) δ 8.51 (t, *J* = 7.7 Hz, 1H), 8.21 (d, *J* = 7.5 Hz, 1H), 8.03 (d, *J* = 8.3 Hz, 1H), 8.00 (d, *J* = 2.7 Hz, 1H), 7.98 – 7.93 (m, 2H), 5.46 (d, *J* = 18.9 Hz, 1H), 4.49 (d, *J* = 18.9 Hz, 1H), 3.85 (t, *J* = 17.3 Hz, 2H), 3.74 – 3.65 (m, 3H), 3.18 (d, *J* = 16.7 Hz, 1H), 3.02 (d, *J* = 12.8 Hz, 1H), 3.00 – 2.93 (m, 1H), 2.09 (d, *J* = 9.7 Hz, 1H), 1.74 – 1.60 (m, 2H), 1.40 (d, *J* = 7.6 Hz, 1H), 1.23 – 1.08 (m, 2H), 0.87 (dd, *J* = 21.2, 10.0 Hz, 1H), 0.47 (d, *J* = 10.5 Hz, 1H). ^{13}C NMR (101 MHz, DMSO) δ 170.4, 170.0, 165.5, 163.1, 153.1, 150.1, 147.5, 145.0, 143.0, 138.6, 128.9, 127.0, 124.4, 122.5, 68.0, 63.0, 62.5, 62.5, 54.4, 52.7, 28.0, 26.4, 23.7, 23.6. HR-ESI-MS m/z for $C_{24}H_{25}{}^{69}GaN_4O_8Na$ ($Ga(L)^- + H^+ + Na^+$) calcd. (found): 589.0826 (589.0831) (0.8 PPM).

2.4.14 Na[In(*CHX*octapa)]

H_4*CHX*octapa·2HCl·3H_2O (**2.6**) (8.2 mg, 0.013 mmol) was dissolved in methanol/water (1:2, 1 mL); the pH of this solution was ~1. To this clear solution, $In(ClO_4)_3$·8H_2O (8.7 mg, 0.016 mmol, 1.2 equiv) in water (200 µL) was added. The pH of this solution was adjusted to 5 using NaOH (aq) (0.1 M), and stirred at 60 °C for 2 h. The resultant clear solution was evaporated to dryness to yield Na[In(*CHX*octapa)]. HR-TOF-MS (ES-) m/z for $C_{24}H_{24}{}^{115}InN_4O_8$ calcd. (found): 611.0633 (611.0635) (0.3 PPM). Multiple isomers in solution were observed; NMR spectra can be found in the Appendix.

2.4.15 ^{67}Ga or ^{111}In Radiolabeling Studies

The ligands H_2*CHX*dedpa, H_2*CHX*dedpa-bb, H_4*CHX*octapa, and standards H_2dedpa, NOTA, and DOTA were made up as stock solutions (1 mg/mL, ~10^{-3} M) in deionized water. A 100 µL aliquot of each ligand stock solution was transferred to screw-cap mass spectrometry vials and diluted with pH 4 NaOAc (10 mM) buffer such that the final volume was 1 mL after the addition of $^{67}GaCl_3$ or $^{111}InCl_3$, to a final ligand concentration of ~10^{-4} M for each sample. An aliquot of $^{67}GaCl_3$ or $^{111}InCl_3$ (~1 mCi for labeling studies and ~3-6 mCi for serum competitions) was added to the vials containing the ligand and allowed to radiolabel at ambient temperature for 10 min (DOTA was reacted at 70 °C, 30 min), and then it was analyzed by RP-HPLC to confirm radiolabeling and calculate yields. Areas under the peaks observed in the HPLC radiotrace were integrated to determine radiolabeling yields. Elution conditions used for RP-HPLC analysis were gradient: A: 10 mM NaOAc buffer, pH 4, B: CH_3CN; 0 to 100% B linear gradient 20 min. [^{67}Ga(*CHX*dedpa)]$^+$ (t_R = 6.8 min), [^{67}Ga(*CHX*dedpa-bb)]$^+$ (t_R = 13.7 min), [^{67}Ga(*CHX*octapa)]$^-$ (t_R = 7.1 min), [^{67}Ga(NOTA)] (t_R = 3.6 min), [^{67}Ga(DOTA)]$^-$ (t_R = 3.0 min), [^{111}In(*CHX*octapa)] (t_R = 6.6 min), free ^{67}Ga or ^{111}In (t_R = 2.0 – 2.4 min).

2.4.16 Human Serum Stability Data

The compounds [^{67}Ga(*CHX*dedpa)]$^{+}$, [^{67}Ga(*CHX*dedpa-bb)]$^{+}$, [^{67}Ga(*CHX*octapa)]$^{-}$, [^{67}Ga(dedpa)]$^{+}$, [^{67}Ga(NOTA)], [^{67}Ga(DOTA)]$^{-}$, and [^{111}In(*CHX*octapa)]$^{-}$ were prepared with the radiolabeling protocol as described above. Human serum was removed from the freezer and allowed to thaw at ambient temperature. In triplicate for each ^{67}Ga- or ^{111}In-complex above, solutions were prepared in vials with 750 µL of human serum, 500 µL of ^{67}Ga- or ^{111}In-complex, and 250 µL of phosphate buffered saline (PBS), and incubated at 37°C in a water bath. At time points 1 and 2 h, 500 µL of the human serum competition mixture was removed from each vial (for ^{111}In-complex competitions 400 µL aliquots of mixture at 1, 24, and 120 h were removed), diluted to a total volume of 2.5 mL with PBS, and then counted in a Capintec CRC 15R well counter to obtain a value for the total activity to be loaded on the PD-10 column. The 2.5 mL of diluted human serum mixture was loaded onto a PD-10 column that had previously been conditioned via elution with 20 mL of PBS, and the empty vial was counted in a well counter to determine the residual activity left in the vial. The 2.5 mL of loading volume was allowed to elute into a waste container, and then the PD-10 column was eluted with 3.5 mL of PBS and collected into a separate vial. The eluent that contained ^{67}Ga or ^{111}In bound/associated with serum proteins (size exclusion for MW < 5000 Da) was counted in a well counter and then compared to the total amount of activity that was loaded on the PD-10 column to obtain the percentage of ^{67}Ga or ^{111}In that was bound to serum proteins and therefore no longer chelate-bound.

2.4.17 Solution Thermodynamics

The experimental procedures and details of the apparatus closely followed those of our previous study of H_2dedpa with Ga^{3+}.[54] Carbonate-free solutions of the titrant, NaOH, were prepared by dilution of 0.1 mol of NaOH analytical standard solution with freshly boiled MQ water (800 mL) under a stream of nitrogen. The solution was standardized using potassium hydrogen phthalate, and the extent of carbonate accumulation was periodically checked by titration with standard hydrochloric acid solution and determination of the corresponding Gran titration plot. Gallium or indium ion solutions were prepared by dilution of the atomic absorption (AA) standard. The exact amount of acid present in the gallium and indium standards was determined by titration of an equimolar solution of M(III) and Na_2H_2EDTA. The amount of acid present was determined by Gran's method. Potentiometric titrations were performed using a Metrohm Titrando 809 equipped with a Ross combination pH electrode and a Metrohm Dosino 800. Data were collected in triplicate. The titration apparatus consisted of a 10 mL water-jacketed vessel maintained at 25.0 ± 0.1 °C (water bath). Prior to and during the titration a stream of nitrogen, passed through 50% KOH, was maintained over the solution to exclude any CO_2. The ionic strength was maintained at 0.15 M using NaCl. Prior to each potentiometric titration, the electrode was calibrated using a standard HCl solution. Calibration data were analyzed by standard computer treatment provided within the program GLEE[139] to obtain the calibration parameters E_o and pK_w.

The degree of M(III) complexation at even low pH (<2) was too high to determine the stability constants by direct methods, and the ligand-ligand competition method using the known competitor, Na_2H_2EDTA, was performed instead. Protonation constants of the proligands and stability constants of Ga(III) or In(III) were calculated within the program Hyperquad[140] using previously reported methods.[54] The protonation constants (pK_a) and log

K_{ML} values with Ga(III) or In(III) for the proligands and previously reported H_2dedpa and H_4octapa for comparison are listed in Appendix Table A.1. Also included are the pM (-log[M_{free}]) values, a more relevant indicator of the extent of which a metal complex is formed in solution.

2.4.18 X-ray Crystallography

An orange plate crystal of [Ga(*CHX*dedpa)]$_3$[ClO_4]$_3$·1.5MeOH·H_2O having approximate dimensions of 0.05 x 0.14 x 0.41 mm was grown by slow evaporation in 1:1 H_2O/MeOH and mounted on a glass fiber. Data for [Ga(*CHX*dedpa)][ClO_4] were collected with graphite-monochromated Mo Kα radiation (0.71073 Å) at -173.0 °C. The material crystallizes with three crystallographically independent salt moieties in the asymmetric unit. Two perchlorate anions were disordered and were each modeled in two orientations, with restraints applied making all Cl – O distances relatively equivalent. Additionally, the material crystallizes with both water and methanol in the lattice. The asymmetric unit contains one water molecule and approximately 1.5 MeOH molecules. Measurements were made on a Bruker X8 APEX II diffractometer with graphite monochromated Mo-Kα radiation (0.71073 Å). Data were collected and integrated using the Bruker SAINT[141] software package. Data were corrected for absorption effects using the multiscan technique (SADABS[142]), with minimum and maximum transmission coefficients of 0.832 and 0.934, respectively. The data were corrected for Lorentz and polarization effects. The structure was solved by Dr. B. O. Patrick using direct methods SIR-97 and refined using SHELXL-97[143] via the WinGX[144,145] interface. All non-hydrogen atoms were refined anisotropically. All hydrogen atoms, including hydroxyl H atoms, were placed in calculated positions.

A colourless plate crystal of $C_{24}H_{24}GaN_4O_8 \cdot H_2O$ ([Ga(H*CHX*octapa)]·H_2O) having approximate dimensions 0.06 x 0.14 x 0.31 mm was grown by slow evaporation in 1:1 H_2O/DMSO and was mounted on a glass fiber. All measurements were made on a Bruker APEX DUO diffractometer with graphite monochromated Mo-Kα radiation. The data were collected at a temperature of -183.0 + 0.1°C to a maximum 2θ value of 56.7°. Data were collected in a series of ϕ and ω scans in 0.5° oscillations using 20.0-second exposures. The crystal-to-detector distance was 60.20 mm. Data were collected and integrated using the Bruker SAINT[141] software package. The linear absorption coefficient, μ, for Mo-Kα radiation is 12.45 cm-1. Data were corrected for absorption effects using the multiscan technique (SADABS[142]), with minimum and maximum transmission coefficients of 0.737 and 0.928, respectively. The data were corrected for Lorentz and polarization effects. The structure was solved by Dr. B. O. Patrick using direct methods.[146] The material crystallizes with one molecule of water in the asymmetric unit. All non-hydrogen atoms were refined anisotropically. All O—H hydrogen atoms were located in difference maps and refined isotropically. All other hydrogen atoms were placed in calculated positions. The absolute configuration, S, R, R, and R at N2, N3, C8 and C13, respectively, were determined on the basis of the refined Flack x-parameter (0.027(6)).[147]

2.4.19 Molecular Modeling

Calculations were performed by Dr. J. F. Cawthray using *Gaussian 09*(Revision D.01)[148] and visualized using either *GaussView* or *WebMO*. The molecular geometries of the ligand, H_4*CHX*octapa, the complexes with In^{3+} and associated electron densities were obtained from DFT calculations, with the B3LYP functional employing the 6-31+G(d,p) basis set for first- and second-row elements, and the ECP basis set, LANL2DZ, for indium.[149,150] Solvent (water) effects

were described through a continuum approach by means of the IEF PCM as implemented in G09. The electrostatic potential was mapped onto the calculated electron density surface.

Chapter 3: Nitroimidazole-Containing H_2dedpa and H_2*CHX*dedpa Derivatives as Potential PET Imaging Agents of Hypoxia with ^{68}Ga

This chapter is an adaptation of published work, and is reproduced in part, with permission from Ramogida, C. F.; Pan, J.; Ferreira, C. L.; Patrick, B. O.; Rebullar, K.; Yapp, D. T. T.; Lin, K.-S.; Adam, M. J.; Orvig, C., Nitroimidazole-containing H_2dedpa and H_2*CHX*dedpa derivatives as potential PET imaging agents of hypoxia with ^{68}Ga. *Inorg. Chem*. **2015**, *54* (10), 4953-4965,

3.1 Introduction

Hypoxia, a condition defined by insufficient oxygen supply to support metabolism, is an important characteristic in many diseases, playing a role in stroke, heart attack, and oncology.[151,152] It has specific consequences in oncology, since solid tumours that are hypoxic tend to be more aggressive and resistant to radiotherapy and chemotherapy compared to well oxygenated cells (normoxia).[153–158] As a consequence, hypoxia can greatly compromise a patient's survival outcome. For this reason, hypoxia is a high priority target where identification of hypoxic regions in tumours would allow appropriate therapies to be chosen for each patient, presumably improving patient prognosis. The class of compounds containing nitroimidazoles (NIs) is among the most popular strategy used for tracking and imaging hypoxia. NIs have the ability to be reduced and retained exclusively in hypoxic cells via direct competition with intracellular oxygen concentration. The accepted mechanism of action commences with the NI-tracer entering the cell; once inside the cell, one electron reduction to form the nitro radical anion ($NO_2^{\bullet-}$) can occur in all cells (normoxic and/or

hypoxic).[151,154,156,159,160] In normoxic cells, intracellular oxygen will compete for the electron and the radical anion can be back oxidized to form the native NO_2 compound, which can subsequently leave the cell freely. In hypoxic cells, the inherent insufficient oxygen supply results in incapability of back oxidation of the $NO_2^{\bullet-}$ radical, hence the nitro radical can be further reduced to form reactive species that can covalently bind to macromolecules intracellularly; the NI tracer is now irreversibly trapped inside the hypoxic cell (Figure 3.1).[151,154,156,159,160]

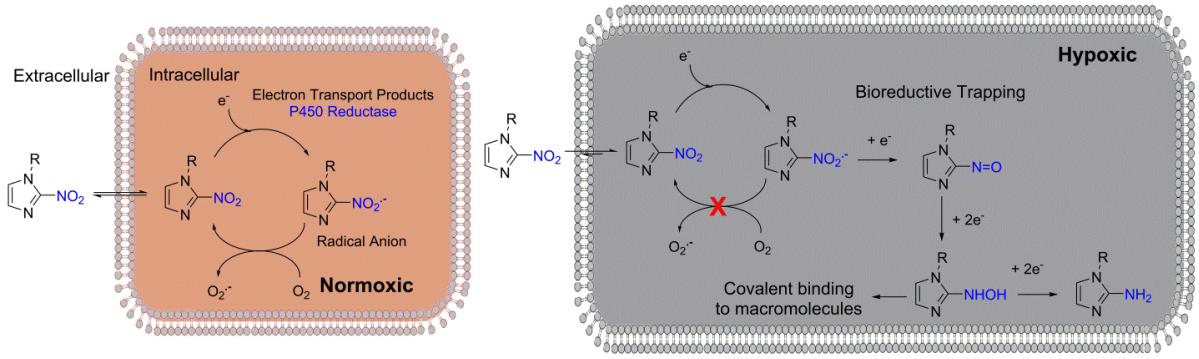

Figure 3.1 Depiction of the accepted trapping mechanism of nitroimidazoles in hypoxic cells.[151,161,162]

This bioreductive trapping mechanism has been exploited in several 2-NI ^{18}F-labelled clinical tracers such as fluoromisonidazole (F-MISO),[163,164] and more recently fluoroazomycin arabinofuranoside (FAZA)[165,166] and etanidazole pentafluoride (EF5)[167–169] used in positron emission tomography (PET) imaging of hypoxia (Figure 3.2). The relatively high lipophilicity of many ^{18}F-labelled 2-NI tracers (log *P* = 0.43 for F-MISO[170]), allows for facile penetration through the cell membrane; however, as a consequence, clearance from non-target tissue is slow resulting in high liver uptake and low tumour-to-background ratios.[158] More hydrophilic tracers that are cleared rapidly from non-target tissue would be of great interest. Other non-traditional hypoxia tracers such as Cu-diacetyl-bis(*N*4-methylthiosemicarbazone) (Cu-ATSM) (Figure 3.2),

have shown potential for imaging and therapy of hypoxia.[21,22,171] The array of radioactive copper isotopes ([60,61,62,64]Cu) in production suggests that ATSM can be radiolabelled with any copper radionuclide which best suits the intended application; nonetheless, the widespread use of these radiotracers in the clinic would be inherently restrained due to the limited availability of copper isotopes.

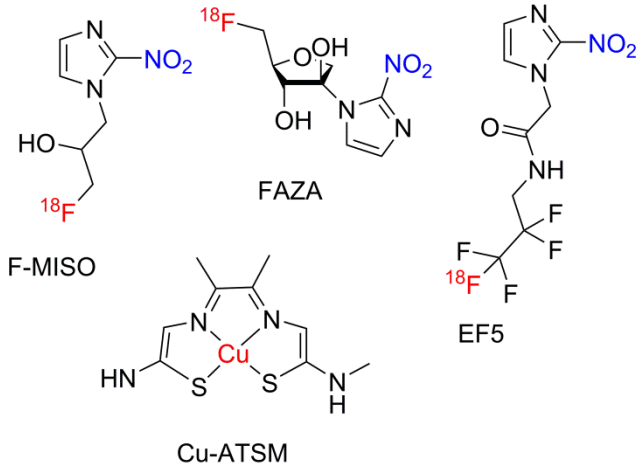

Figure 3.2 [18]F-labelled 2-nitroimidazole hypoxia tracers F-MISO, EF5, and FAZA, and non-traditional hypoxia tracer Cu-ATSM.

The positron-emitter [68]Ga has been proposed as an alternative to [18]F, since it has a high positron branching ratio (89%, E_{β^+max} = 1.9 MeV)[8] and a comparably short half-life ($t_{1/2}$ = 67.7 min compared to 118 min for [18]F). Unlike the 'organic' nuclide, [68]Ga can be incorporated into a radiotracer via a facile and efficient coordination complex. Moreover, [68]Ga is produced in a commercially available [68]Ge/[68]Ga generator system; the half-life of the parent [68]Ge ($t_{1/2}$ = 270.95 d) allows the generator to be used for up to 1 year, with two or three elutions per day providing a very cost-effective means of supplying isotope whilst obviating the need for an on-site cyclotron.[32,112–114,172]

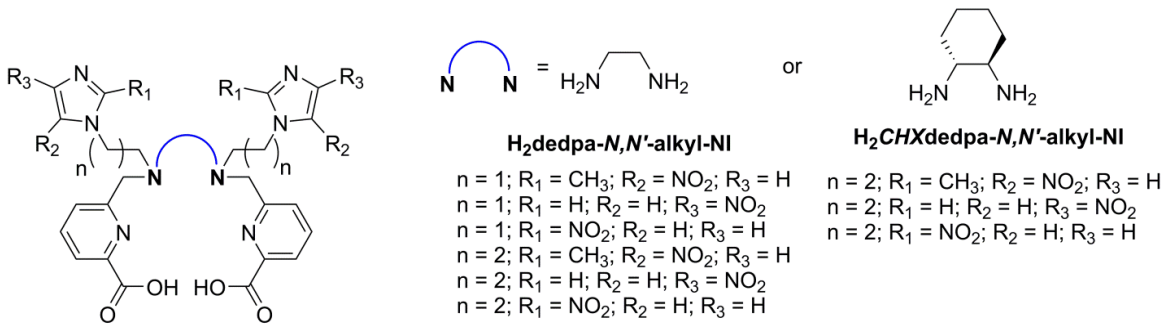

Figure 3.3 General structures of nitroimidazole-containing H_2dedpa and H_2*CHX*dedpa ligands investigated in Chapter 3.

Naturally, a hypoxia tracer incorporating ^{68}Ga would be of great interest. As a result, the hypoxia targeting moiety nitroimidazole (NI) has been successfully incorporated into the strong gallium chelators 1,4,7-triazacyclononane-1,4,7-triacetic acid (NOTA) and 1,4,7,10-tetraazacyclododecane-1,4,7,10-tetraacetic acid (DOTA) with moderate to good results.[173–175] Recently, our group has investigated an acyclic hexadentate (N_4O_2) chelator H_2dedpa (1,2-[[6-carboxy-pyridin-2-yl]-methylamino]ethane) which displays ideal properties for Ga(III) chelation and elaboration into a radiopharmaceutical for ^{68}Ga PET imaging,[54] such as mild and efficient radiolabeling of gallium isotopes (>99% radiochemical yield (RCY), 10 min at room temperature), exceptionally high thermodynamic stability constants with Ga(III) (log K_{ML} = 28.11(8)), and forms complexes of promising kinetic inertness *in vitro*. In Chapter 2, we investigated the chiral derivative H_2*CHX*dedpa (*CHX* = cyclohexyl/cyclohexane), which incorporates a 1*R*,2*R*-*trans*-cyclohexanediamine backbone in place of the ethylenediamine bridge to form a ligand with an augmented preorganization of donor atoms which restricts the flexibility around the coordinating atoms in order to form metal complexes of even higher kinetic inertness. Much like its achiral analogue H_2dedpa, H_2*CHX*dedpa forms Ga(III) complexes of exceptionally high thermodynamic stability (log K_{ML} = 27.61(8)), and exhibits even higher *in vitro* kinetic inertness.[176] In order to harness the potential of these promising scaffolds

(H_2dedpa and H_2*CHX*dedpa) for radiopharmaceutical elaboration, the chelating ligands must first be functionalized with a targeting vector which should regulate the accumulation of the radiotracer to an area of interest (as discussed in Chapter 1). In this chapter, we report H_2dedpa and H_2*CHX*dedpa chelating ligands that have been functionalized with nitroimidazole moieties as potential PET imaging agents of hypoxia with ^{68}Ga. The ligands have been functionalized via their secondary amines with alkylation using either an ethyl or propyl linker, and imidazole ring with the nitro group in the 2-, 5-, or 4-position (Figure 3.3).

The synthesis and characterization of pro-ligands and 'cold' metal complexes, electrochemical studies to determine the redox behaviors of the nitroimidazole moieties, radiolabeling experiments with both ^{67}Ga and ^{68}Ga, determination of partition coefficients (log $D_{7.4}$), *in vitro* stability, and *in vitro* cell uptake under hypoxic versus normoxic conditions were determined. In addition, preliminary in vivo small animal PET/CT imaging and biodistribution studies with one of the ^{68}Ga-tracers are presented. The studies were used collaboratively to determine the feasibility of these novel H_2dedpa-*N,N'*-alkyl-NI or H_2*CHX*dedpa-*N,N'*-alkyl-NI agents as chelating ligands for PET imaging of hypoxia with ^{68}Ga.

3.2 Results and Discussions

3.2.1 Synthesis and Characterization

A small library of nitroimidazole-containing H_2dedpa or H_2*CHX*dedpa pro-ligands containing varying alkyl chain linker length (ethyl or propyl) and varying substitution around the imidazole ring (2-, 4-, or 5-nitroimidazole) was synthesized. Changing the linker length between the ligand and nitroimidazole targeting vector can serve two purposes: 1. to make compounds of varying lipophilicity – lipophilic molecules can more easily pass the cell

membrane; however, very lipophilic compounds have a tendency to accumulate in the liver causing poor biodistribution profiles *in vivo*, thus a balance must be found; 2. to increase the distance between metal-bound chelate and targeting vector in order to reduce the chance of interference between the two independent parts of the radiotracer – the targeting vector/linker should not affect the metal-binding ability of the chelate, and the metal-complex should not affect the targeting vector's ability to be reduced and retained intracellularly. Changing the substitution of the nitro group on the imidazole ring alters the reduction potential of the nitro radical; since the retention of NI is dependent on the one-electron redox this would subsequently alter the compound's ability to be entrapped inside hypoxic tissue.

Scheme 3.1 Synthesis of 1-(ω-bromoalkyl)-nitroimidazoles (**3.7 – 3.12**).

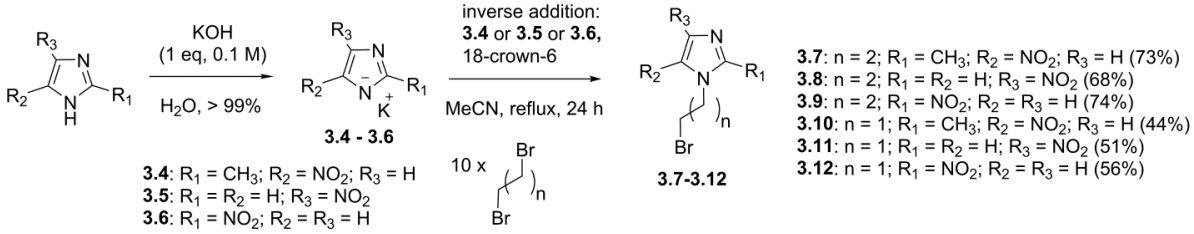

Scheme 3.2 Synthesis of H_2dedpa-*N,N'*-alkyl-nitroimidazoles (**3.19 – 3.24**) and H_2*CHX*dedpa-*N,N'*-propyl-nitroimidazoles (**3.28 – 3.30**).

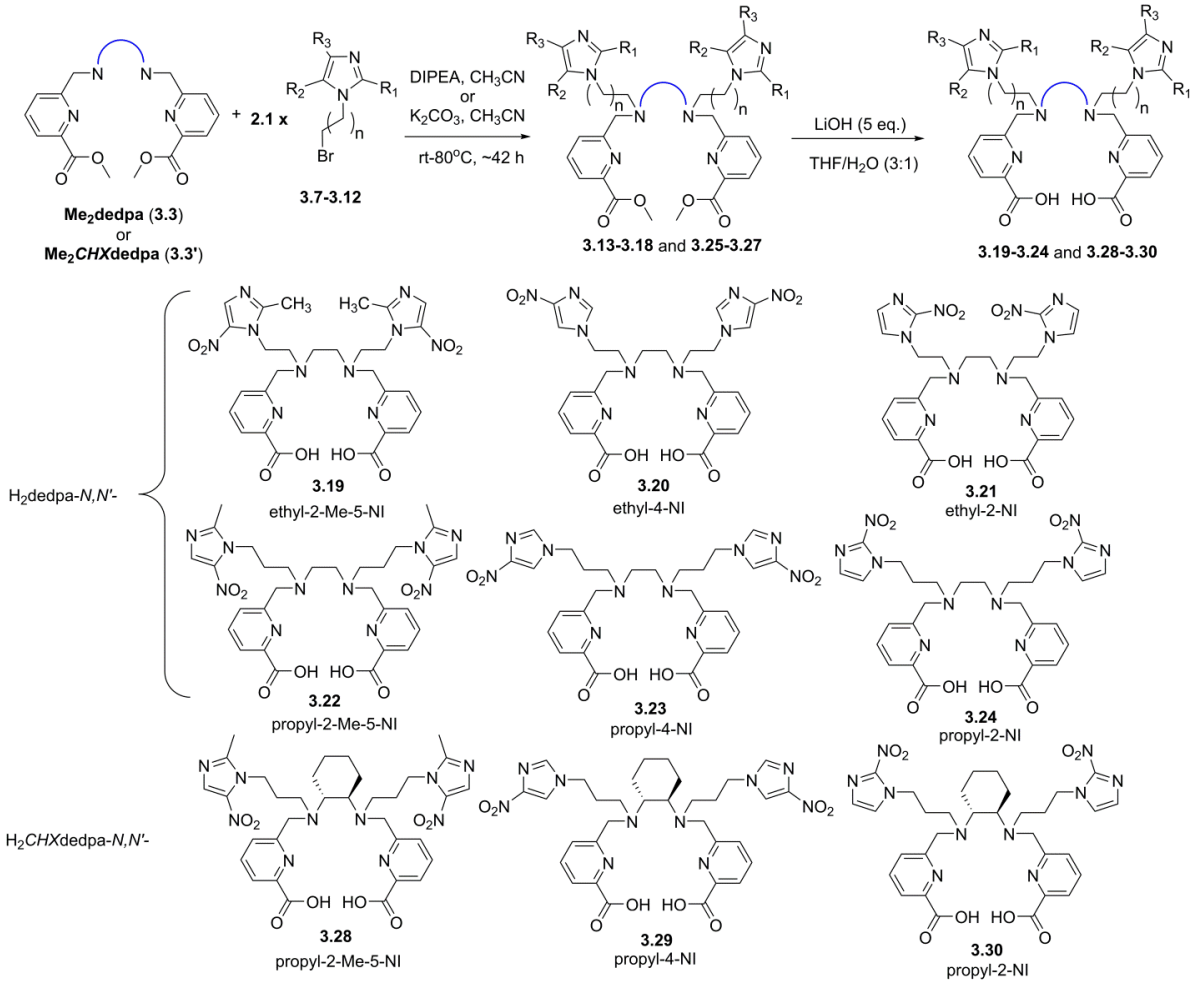

Methyl-ester protected Me_2dedpa (**3.3**) was prepared via a previously published method from our group and Me_2*CHX*dedpa (**3.3'**) was prepared as in Chapter 2.[59,176] Bromo-alkylating agents **3.7-3.12** were prepared using a previously reported synthesis of similar analogues (Scheme 3.1).[177] The alkylations of Me_2dedpa with the ethyl-linked nitroimidazoles (**3.10-3.12**) were poor yielding (10-23%) compared to the alkylation with the propyl derivatives (**3.7-3.9**) (30-69%) (Scheme 3.2). This result is due to the intrinsic electronics of the nitroimidazole ring which destabilizes the δ^+ charge on the electrophilic carbon α to the

bromine atom; hence the propyl linked derivatives were less affected by the destabilization of partial charge due to the nitroimidazole's relative distance to the electrophilic carbon and resulted in higher yielding syntheses. Considering this and the fact that the ethyl-linked derivatives may impose more of a steric hindrance around the metal-binding cavity, only the propyl-linked analogues of *CHX*dedpa^{2-} were synthesized (Scheme 3.2). Six H_2dedpa derivatives with either an ethyl or propyl linker and different substitution around the imidazole ring (**3.19-3.24**), and three H_2*CHX*dedpa derivatives with a propyl linker and varying substitution of the imidazole ring (**3.28-3.29**) were synthesized and characterized.

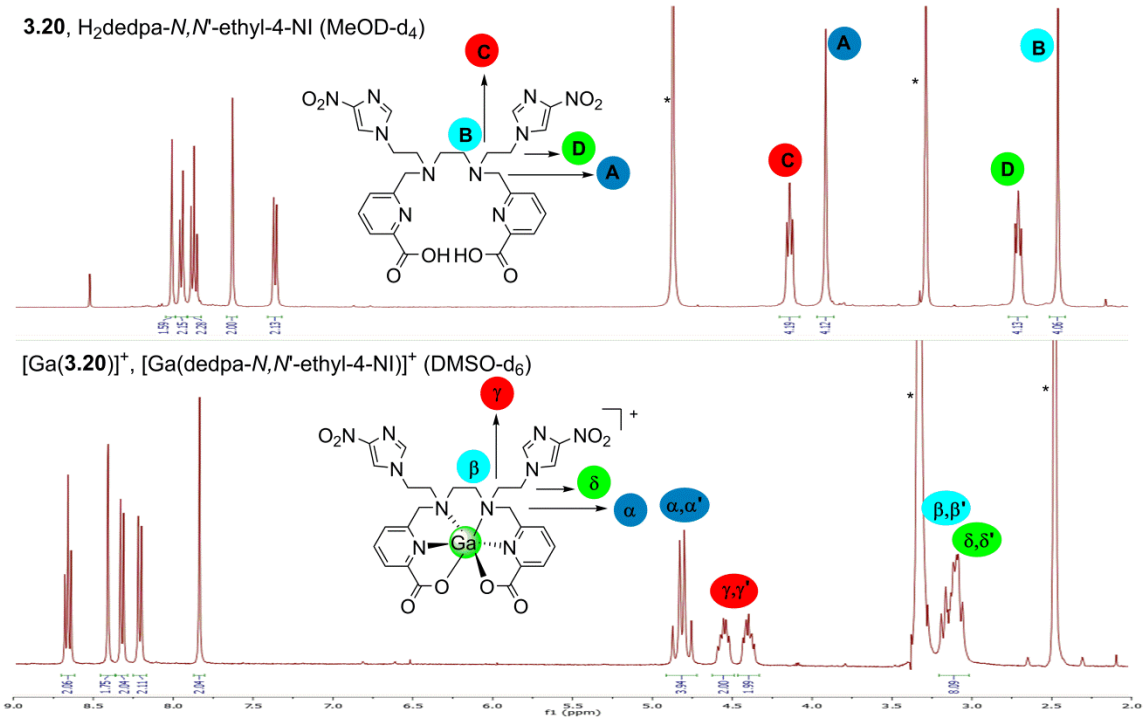

Figure 3.4 ^{1}H NMR spectrum at 25°C and 400 MHz of (top) **3.20**, H_2dedpa-*N,N'*-ethyl-4-NI and (bottom) [Ga(**3.20**)][ClO_4] highlighting diastereotopic splitting upon gallium chelation. *Residual solvent peak.

After synthesis, all nine pro-ligands were allowed to complex with 'cold' (non-radioactive) Ga(III), and characterized by $^{1}H/^{13}C$ NMR, mass spectrometry (MS), and, when successful, X-ray crystallography. ^{1}H NMR spectra of the H_2dedpa-*N,N'*-alkyl-NI pro-ligands exhibited C_{2v} symmetry, with only half the resonances present. While the C_2 symmetry is retained (only half the resonances present) in the metal complexes, diastereotopic splittings of the methylene hydrogens alpha to the pyridine ring, hydrogens in the ethylenediamine bridge, and hydrogens of the ethylene or propylene linker are observed in the ^{1}H NMR spectra of the [Ga(dedpa-*N,N'*-alkyl-NI)]$^{+}$ complexes, and are used as a diagnostic handle to confirm successful metal coordination (see Figure 3.4 for representative spectrum). The intrinsically chiral H_2*CHX*dedpa-*NN'*-alkyl-NI pro-ligands already exhibit diastereotopic splitting of hydrogens alpha to the chiral cyclohexane ring in the ^{1}H NMR spectra; nonetheless, shifts in the hydrogen resonances are observed in the [Ga(*CHX*dedpa-,*NN'*-alkyl-NI)]$^{+}$ complexes which were used to confirm Ga(III) chelation. In addition, C_2 symmetry is conserved (Appendix, Figure A.8).

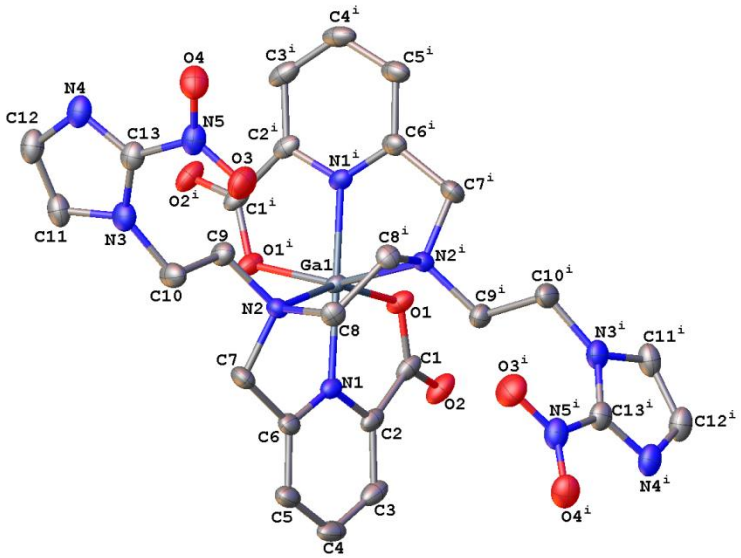

Figure 3.5 Solid-state structure of the cation in [Ga(dedpa-*N,N'*-ethyl-2-NI)][ClO_4]; counterion omitted for clarity. Ellipsoids drawn with 50% probability. Superscript i refers to the symmetry operation $-{}^{1}/_{2}-x,-{}^{3}/_{2}-y,+z$.

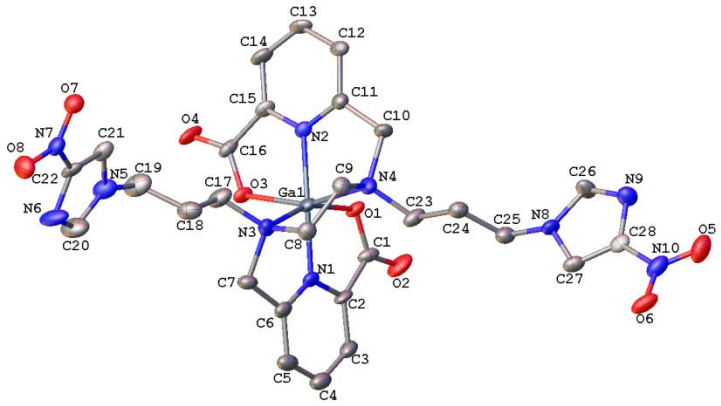

Figure 3.6 Solid-state structure of the cation in the major disordered fragment of [Ga(dedpa-*N,N'*-propyl-4-NI)][ClO4]; counterion omitted for clarity. Ellipsoids drawn with 50% probability.

X-ray quality crystals of [Ga(**3.21**)][ClO_4] ([Ga(dedpa-*N,N'*-ethyl-2-NI)][ClO_4], Figure 3.5) and [Ga(**3.23**)][ClO_4] ([Ga(dedpa-*N,N'*-propyl-4-NI)][ClO_4], Figure 3.6) were obtained through slow evaporation in water/acetonitrile (~1:4). Qualitative examination of the obtained structures confirms that the N_4O_2 coordination sphere of native $dedpa^{2-}$ ligand is retained, whilst the two nitroimidazole targeting vectors are pointing in opposite directions, away from the metal binding sphere. Only minor differences were found upon close quantitative comparison of relevant bond lengths and angles of the two novel [Ga(dedpa-*N,N'*-alkyl-NI)]$^+$ solid-state structures to the previously reported [Ga(dedpa)]$^+$ complex[54] (Table 3.1). The largest difference in relevant Ga-L bond lengths between [Ga(**3.21**)]$^+$ and the 'unfunctionalized' [Ga(dedpa)]$^+$ complex is 0.10 Å which arose from both Ga-N_{en} bonds in the *N,N'*-functionalized complex being longer than those in [Ga(dedpa)]$^+$. Comparison of all other Ga-L bonds yielded differences much less than 0.10 Å. The largest difference in relevant L-Ga-L bond angle is 5.6°. Comparison of the propyl-linked complex, [Ga(**3.23**)]$^+$, to the 'unfunctionalized' [Ga(dedpa)]$^+$ revealed very minor differences in relevant Ga-L bond lengths. The largest difference of 0.08 Å

arises from one of the Ga-$O_{pyr\text{-}COO}$ bonds in [Ga(**3.23**)]$^+$ being longer than the analogous bond in the [Ga(dedpa)]$^+$ structure, and largest L-Ga-L bond angle difference between the two complexes was only 6.6°. The lack of major changes in the solid-state structures of these novel *N,N'*-functionalized Ga-dedpa derivatives bodes well for their retention of stability *in vitro* compared to the unfunctionalized Ga-dedpa; however, caution must be taken when comparing solid-state data to reflect solution state properties, and *in vitro* stability assays are better predictors of kinetic inertness (*vide infra*).

Table 3.1 Selected bond lengths (Å) and angles (°) in solid-state structure of [Ga(dedpa-*N,N'*-ethyl-2-NI)]$^+$ and [Ga(dedpa-*N,N'*-propyl-4-NI)]$^+$ compared to previously reported [Ga(dedpa)][ClO_4].

		[Ga(dedpa-*N,N'*-ethyl-2-NI)]$^+$		[Ga(dedpa-*N,N'*-propyl-4-NI)]$^+$	
	Length (Å) [Ga(dedpa)]$^{+\,a}$	Bond	Length (Å) [Ga(3.21)]$^+$	Bond	Length (Å) [Ga(3.23)]$^+$
Ga-N_{pyr}	1.9868(16)	Ga-N(1)	1.980(2)	Ga-N(1)	1.985(9)
Ga-N_{pyr}	1.9903(16)	Ga-N(1)^i	1.980(2)	Ga-N(2)	1.996(9)
Ga-N_{en}	2.1115(16)	Ga-N(2)	2.2172(19)	Ga-N(3)	2.177(3)
Ga-N_{en}	2.1132(16)	Ga-N(2)^i	2.2172(19)	Ga-N(4)	2.183(2)
Ga-$O_{pyr\text{-}COO}$	1.9708(13)	Ga-O(1)	1.9626(16)	Ga-O(1)	2.038(12)
Ga-$O_{pyr\text{-}COO}$	1.9828(13)	Ga-O(1)^i	1.9626(16)	Ga-O(3)	2.068(10)
	Degree (°) [Ga(dedpa)]$^{+\,a}$	Angle	Degree (°) [Ga(3.21)]$^+$	Angle	Degree (°) [Ga(3.23)]$^+$
O_{COO}-Ga-O_{COO}	101.39(6)	O(1)-Ga-O(1)^i	98.52(10)	O(1)-Ga-O(3)	94.8(7)
O_{COO}-Ga-N_{pyr}	94.02(6)	O(1)^i-Ga-N(1)	98.25(7)	O(3)-Ga-N(1)	95.4(4)
O_{COO}-Ga-N_{pyr}	79.64(6)	O(1)^i-Ga-N(1)^i	81.03(8)	O(3)-Ga-N(2)	77.9(3)
N_{pyr}-Ga-N_{pyr}	170.97(6)	N(1)-Ga-N(1)^i	178.91(11)	N(1)-Ga-N(2)	168.3(3)
O_{COO}-Ga-N_{en}	94.78(6)	O(1)-Ga-N(2)^i	93.41(7)	O(3)-Ga-N(3)	95.1(4)
O_{COO}-Ga-N_{en}	155.64(6)	O(1)-Ga-N(2)	156.60(7)	O(3)-Ga-N(4)	158.3(3)
N_{pyr}-Ga-N_{en}	109.11(6)	N(1)-Ga-N(2)^i	103.47(7)	N(2)-Ga-N(3)	108.0(2)
N_{pyr}-Ga-N_{en}	78.15(6)	N(1)^i-Ga-N(2)^i	77.36(7)	N(1)-Ga-N(3)	81.9(2)
N_{en}-Ga-N_{en}	83.12(6)	N(2)^i -Ga-N(2)	83.05(10)	N(3)-Ga-N(4)	84.05(9)

^{a}Values from previously reported [Ga(dedpa)][ClO_4] complex.[54]

3.2.2 Electrochemistry

The mechanism of intracellular nitroimidazole trapping is directly dependent on the reduction ability and reduction potential (E_{red}) of the nitro group. Hence, the redox behaviors of the [Ga((*CHX*)dedpa-*N,N'*-alkyl-NI)]$^+$ complexes were determined by cyclic voltammetry in both

aqueous (0.1 M KCl, pH 7) and non-aqueous (DMSO, 0.1 M tetrabutylammonium perchlorate (TBAP)) (Figure 3.7) conditions and compared directly with the clinically relevant agents F-MISO (2-NI) and metronidazole (METRO, 5-NI, 2-(2-methyl-5-nitro-1*H*-imidazol-1-yl)ethanol).

The cyclic voltammograms (CVs) of F-MISO and METRO in non-aqueous solvent (DMSO, 0.1 M TBAP) exhibit one quasi-reversible couple at -0.993 and -1.283 V, respectively, which presumably arise from the reduction of the nitro group (NO_2) to form a nitro-radical ($NO_2^{\bullet -}$) upon falling potential sweep from 0 to approx. -2 V, and back-oxidation to the initial nitro group upon increasing potential from approx. -2 to 1.3 V. These results are corroborated by previously reported values, which also show that F-MISO (2-nitroimidazole) has a less negative (easier to reduce) reduction potential than other 5- or 4-nitroimidazole compounds (such as METRO), this difference being about 250 mV.[178,179] This trend is sustained with the novel nitroimidazole Ga-dedpa and Ga-*CHX*dedpa complexes (Ga-**3.19-3.24** or **3.28-3.30**), which also show one major quasi-reversible couple (in DMSO) at approx. -1.05 V (for 2-nitroimidazole compounds) or approx. -1.35 V (for 5- or 4-nitroimidazole compounds) (Table 3.2, Figure 3.7). Moreover, a CV of a Ga-complex with the addition of exactly one equivalent of ferrocene results in a voltammogram with the redox couple due to the nitro group of the Ga-dedpa-NI compound being almost exactly twice in amplitude to the Fc/Fc^+ couple (Appendix, Figure A.9), suggesting that both nitroimidazole groups on the dedpa-core are being reduced simultaneously and independently of each other. The addition of two 'hypoxia trapping' groups on one radiotracer may increase the probability of successful entrapment in hypoxic cells; this hypothesis has also been suggested by others.[180,181]

The CVs of standards and complexes in aqueous media (water, 0.1 M KCl, pH 7) exhibited very different voltammograms, where F-MISO and METRO show one irreversible reduction at -0.681 and -0.807 V, respectively (Figure 3.7, Table 3.3). Again, these results are

corroborated with previously reported values for F-MISO and METRO in aqueous solvent.[178,179,182] The CV of the novel [Ga(dedpa-*N,N'*-propyl-NI)]$^{+}$ complexes also exhibited irreversible reduction with E_{red}^{1} values of -0.780, -0.779, and -0.631 V for the 5-, 4-, and 2-NI compounds, respectively. The title [Ga(dedpa-*N,N'*-propyl-NI)]$^{+}$ compounds possess a larger deviation from the E_{red}^{1} of the standards (F-MISO/METRO) in aqueous solvent compared to non-aqueous solvent; the E_{red}^{1} of the 4- or 5-NI Ga-complexes were shifted positively 27 mV compared to the 5-NI clinical standard METRO, and the E_{red}^{1} of the 2-NI Ga-complex was shifted 50 mV to the positive compared to the 2-NI clinical standard F-MISO. Moreover, all of the Ga-complexes displayed a second irreversible reduction, E_{red}^{2}, at -1.13 V regardless of their nitro-substitution.

The similarity between the redox behaviors of the standards F-MISO/METRO and the novel [Ga((*CHX*)dedpa-*N,N'*-alkyl-NI)]$^{+}$ complexes in non-aqueous solvent implies that linking the nitroimidazole ring through an ethyl or propyl connection to the H_2dedpa or H_2*CHX*dedpa ligand backbone has no significant effect on the $E_{1/2}$ of the nitro-moiety, and the nitroimidazoles should be seemingly uninhibited to undergo reduction *in vitro* and/or *in vivo*.

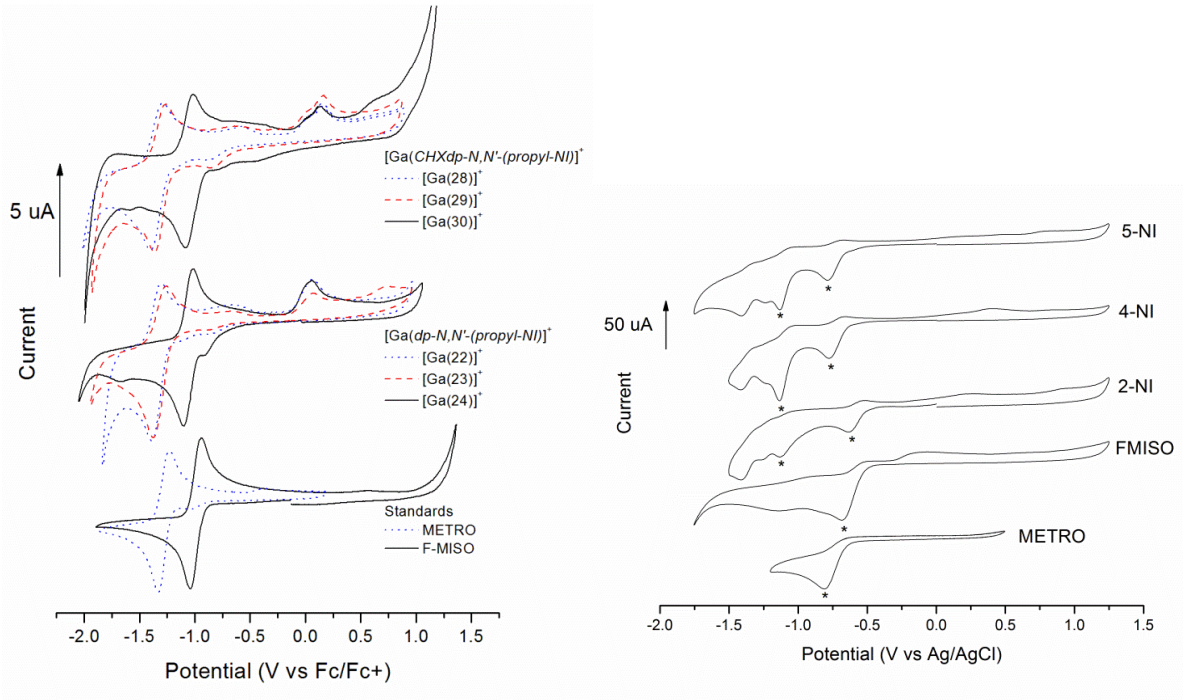

Figure 3.7 Cyclic voltammograms of [Ga((*CHX*)dedpa-*N,N'*-alkyl-nitroimidazole)]$^+$ complexes and standards in LEFT: non-aqueous solvent (DMSO, 0.1 M TBAP, 1-5 mM complex, vs Fc/Fc$^+$): [Ga(*CHX*dedpa-*N,N'*-propyl-NI)]$^+$ compounds (top), [Ga(dedpa-*N,N'*-propyl-NI)]$^+$ compounds (middle), and clinical standards F-MISO and METRO (bottom). 2-Nitroimidazole compounds (black), 5-nitroimidazole compounds (blue dotted), 4-nitroimidazole compounds (red dashed). (Legend: *dp* = dedpa, *CHXdp* = *CHX*dedpa), and RIGHT: aqueous solvent (0.1 M KCl, Ag/AgCl reference, 1-5 mM complex).

Table 3.2 E_{red}, E_{ox}, and calculated $E_{1/2}$ values for [Ga((*CHX*)dedpa-*N,N'*-alkyl-nitroimidazole)]$^+$ complexes and standards F-MISO and METRO obtained from cyclic voltammetry in DMSO (0.1 M TBAP, 1 – 5 mM complex, vs Fc/Fc$^+$).[a]

	Compound		E_{red} /V	E_{ox}/V	$E_{1/2}$ /V
2-NI	F-MISO (2-NI)		-1.045	-0.941	-0.993
	[Ga(dp-*N,N'*-propyl-2-NI)]$^+$	[Ga(**3.24**)]$^+$	-1.100	-1.021	-1.061
	[Ga(dp-*N,N'*-ethyl-2-NI)]$^+$	[Ga(**3.21**)]$^+$	-1.132	-1.067	-1.100
	[Ga(*CHX*dp-*N,N'*-propyl-2-NI)]$^+$	[Ga(**3.30**)]$^+$	-1.082	-1.013	-1.047
5- or 4-NI	METRO (2-Me-5-NI)		-1.334	-1.232	-1.283
	[Ga(*CHX*dp-*N,N'*-propyl-2-Me-5-NI)]$^+$	[Ga(**3.28**)]$^+$	-1.402	-1.291	-1.347
	[Ga(dp-*N,N'*-propyl-2-Me-5-NI)]$^+$	[Ga(**3.22**)]$^+$	-1.389	-1.300	-1.344
	[Ga(*CHX*dp-*N,N'*-propyl-4-NI)]$^+$	[Ga(**3.29**)]$^+$	-1.365	-1.266	-1.315
	[Ga(dp-*N,N'*-propyl-4-NI)]$^+$	[Ga(**3.23**)]$^+$	-1.363	-1.276	-1.319

[a]dp = dedpa; *CHX*dp = *CHX*dedpa

Table 3.3 Reduction potentials (E_{red}) for [Ga(dedpa-*N,N'*-propyl-nitroimidazole)]$^+$ complexes and standards F-MISO and METRO obtained from cyclic voltammetry in H_2O (0.1 M KCl, pH = 7, 1 – 5 mM complex, vs Ag/AgCl).[a]

Compound		E_{red}^1 /V	E_{red}^2 /V
METRO (5-NI)		-0.807	--
[Ga(dp-*N,N'*-propyl-2-Me-5-NI)]$^+$	[Ga(**3.22**)]$^+$	-0.780	-1.133
[Ga(dp-*N,N'*-propyl-4-NI)]$^+$	[Ga(**3.23**)]$^+$	-0.779	-1.133
F-MISO (2-NI)		-0.681	--
[Ga(dp-*N,N'*-propyl-2-NI)]+	[Ga(**3.24**)]$^+$	-0.631	-1.128

[a]dp = dedpa

3.2.3 $^{67/68}$Ga Radiolabeling

Initial radiolabeling studies with both ^{67}Ga and ^{68}Ga were performed on all nine of the novel NI-containing pro-ligands **3.19-3.24** and **3.28-3.30**. Gamma-emitter ^{67}Ga was used as a model for ^{68}Ga; since it has a longer half-life ($t_{1/2}$ = 3.3 days) it is a more convenient choice for *in vitro* testing. Initial results show that all H_2dedpa-*N,N'*-alkyl-NI and H_2*CHX*dedpa-*N,N'*-propyl-NI ligands were able to quantitatively bind gallium isotopes at 10^{-5} and 10^{-4} M (RCY >99%), respectively, in only 10 minutes at room temperature, displaying one sharp peak in the HPLC radio-chromatogram. For the H_2dedpa-NI complexes, at ligand concentrations of 10^{-6} M or lower, incomplete labeling was observed (RCY ~89% or less) when incubated for 10 minutes at room temperature. For the H_2*CHX*dedpa-*N,N'*-propyl-NI ligands, $^{67/68}$Ga labeling was partially incomplete (RCY 96%) at ligand concentrations of 10^{-5} M, and reduced significantly (RCY 13%) at ligand concentrations of 10^{-6} M. In comparison, quantitative $^{67/68}$Ga labeling (10 min, room temperature) of the unaltered pro-ligands H_2dedpa[54] and H_2*CHX*dedpa[176] was accomplished at ligand concentrations as low as 10^{-7} and 10^{-5} M, respectively, suggesting that conversion of the secondary amines to tertiary amines via *N,N'*-alkylation with the corresponding 1-(ω-bromoalkyl)-nitroimidazoles has impeded the labeling kinetics of the resultant ligands. Likely extended reaction times, or elevated temperatures are needed to achieve quantitative labeling at lower ligand concentrations, but these conditions were not tested.

The octanol:water partition coefficients (log $D_{7.4}$) of four selected ^{68}Ga-complexes were also determined, by mixing pre-formed ^{68}Ga-tracer in equal amounts of phosphate buffered saline (PBS, pH 7.4) and 1-octanol, separating phases, and measuring the activity in aliquots of each phase. The lipophilicity of a compound plays an important role in the pharmacokinetics *in vivo*. For many ^{18}F-labelled hypoxia tracers such as F-MISO (log P = 0.43),[170] their relatively high lipophilicity limits tumour-to-background ratios and causes unwanted liver uptake. The novel Ga-dedpa-NI tracers are substantially more hydrophilic with log $D_{7.4}$ values ranging between -2.16 and -2.76 (Table 3.4).

Table 3.4 Partition coefficients (log $D_{7.4}$) of selected ^{68}Ga-labelled dedpa-NI or *CHX*dedpa-NI complexes.

^{68}Ga-complex		**Log $D_{7.4}$**
[^{68}Ga(dedpa-*N.N'*-propyl-2-Me-5-NI)]$^+$	[Ga(**3.22**)]$^+$	-2.16 ± 0.29
[^{68}Ga(dedpa-*N.N'*-propyl-4-NI)]$^+$	[Ga(**3.23**)]$^+$	-2.63 ± 0.13
[^{68}Ga(dedpa-*N.N'*-propyl-2-NI)]$^+$	[Ga(**3.24**)]$^+$	-2.76 ± 0.19
[^{68}Ga(*CHX*dedpa-*N.N'*-propyl-2-NI)]$^+$	[Ga(**3.30**)]$^+$	-2.71 ± 0.12

3.2.4 Human *apo*-Transferrin Stability Studies

The iron transport protein, transferrin, has two sites for strong Fe(III) binding, and since Ga(III) and Fe(III) share many physical similarities, transferrin also has a strong affinity for Ga(III).[136] Consequently *apo*-transferrin is a strong competitor for Ga(III) *in vivo*, and any chelate-bound gallium must be more thermodynamically stable and kinetically inert than Ga-transferrin to prevent transchelation of radioactive gallium from the radiotracer to the endogenous protein. To investigate the stability of the ^{67}Ga-complexes, a two hour competition experiment in excess human *apo*-transferrin at 37°C was performed. This assay is a preferred method to predict *in vivo* stability of the resultant gallium-radiotracers. Results for the nine ^{67}Ga-tracers are shown in Figure 3.8. With the exception of one ethyl-linked tracer, [^{67}Ga(dedpa-*N,N'*-ethyl-2-NI)]$^+$, which remained 68% intact, all other ^{67}Ga-complexes exhibited

very good to excellent stability with the poorest being 86% intact and the highest being >99% intact after 2 hours against *apo*-transferrin. These results indicate that the chelating ligands tested herein form kinetically inert gallium complexes, suggesting they would be good candidates for further testing *in vitro* and *in vivo*. A kinetically inert metal-complex of an 'open-chain' acyclic ligand is not a common manifestation, this fact further exemplifies the uniqueness of the H_2dedpa and H_2*CHX*dedpa scaffolds as promising gallium chelating ligands in radiopharmaceutical elaboration.

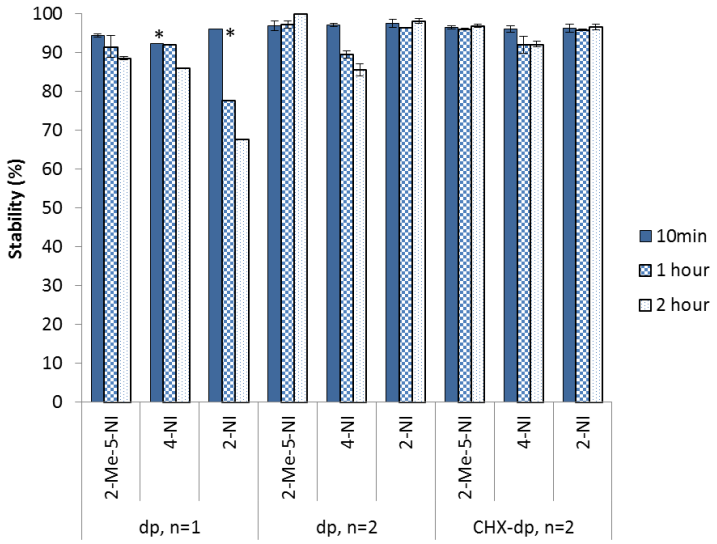

Figure 3.8 *apo*-Transferrin stability challenge assay (37°C, 2 h) of nine ^{67}Ga-labelled ((*CHX*)dedpa-*N,N'*-alkyl-NI)$^{2-}$ ligands, with stability shown as the percentage of intact ^{67}Ga complex; dp: dedpa; n = 1: ethyl linked; n = 2: propyl linked; *single experiments only, all others repeated in triplicate.

3.2.5 *In Vitro* Cell Uptake Studies

HT-29 (human colon), LCC6^{HER-2} (human breast), and CHO (Chinese hamster ovarian, data not shown) cancer cells were used in the *in vitro* cell uptake study of four ^{68}Ga-(*CHX*)dedpa-*N,N'*-propyl-NI tracers: [^{68}Ga-**3.22**, **3.23**, **3.24**, or **3.30**]$^{+}$. Cell uptake of all four

radiotracers in all three cell lines were performed under hypoxic (0.5% O_2) and normoxic (21% O_2) conditions and analyzed at time points 10, 30, 60, and 120 min.

All three cells lines showed significantly higher uptakes of all four ^{68}Ga-dedpa tracers under hypoxic compared to normoxic conditions after 30 – 60 minutes (Figure 3.9). The largest jump in uptake under hypoxic conditions occurred between 30 and 60 min for all cell lines and tracers tested. Hypoxic/normoxic ratios in LCC6^{HER-2} cells were as high as 7.9 ± 2.7 (^{68}Ga-**3.24** at 120 min), 6.3 ± 2.4 (^{68}Ga-**3.22** at 60 min), 5.8 ± 2.7 (^{68}Ga-**3.23** at 60 min), and 6.5 ± 1.7 (^{68}Ga-**3.30** at 60 min). Hypoxic/normoxic ratios in HT-29 cells were highest after 60 min for all tracers: 5.5 ± 1.7 (^{68}Ga-**3.24**), 7.3 ± 2.0 (^{68}Ga-**3.22**), 7.1 ± 2.0 (^{68}Ga-**3.23**), 4.7 ± 1.4 (^{68}Ga-**3.30**). These results are comparable with *in vitro* experiments of ^{18}F-MISO which show hypoxic (0.5% O_2) versus normoxic uptake ratios of typically 6:1.[155] Overall there were no significant differences in uptake/retention between the four ^{68}Ga-tracers tested *in vitro*, regardless of the substitution of the nitro group on the imidazole ring (2-, 4-, or 5-nitroimidazoles), suggesting that, under the constraints of the *in vitro* assay, the differences in reduction potentials of the varying 2-, 4- or 5-nitroimidazoles makes no difference in the retention of the complexes in hypoxic cells. The overall uptake/retention is likely more critically controlled by the rate at which the tracers may diffuse inside the cell, which is traditionally regulated by the lipophilicity of the complexes. Indeed, all ^{68}Ga tracers exhibited similar log $D_{7.4}$ values ranging between -2.16 and -2.76 (vide supra). The significantly higher uptake under hypoxic conditions than normoxic conditions for all four radio-ligands tested suggests that these ^{68}Ga-(*CHX*)dedpa-nitroimidazole tracers would be promising candidates for further testing *in vivo*.

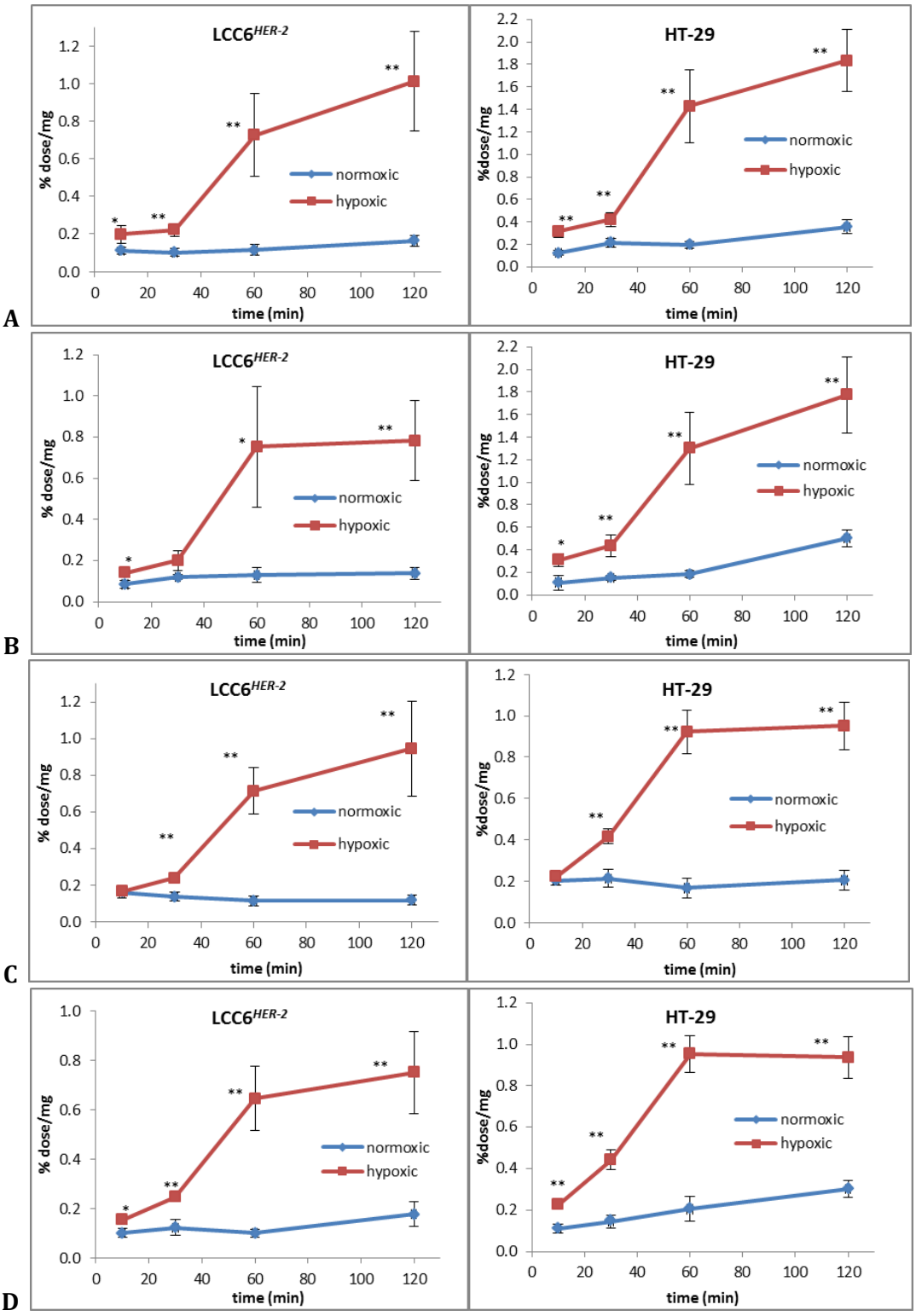

Figure 3.9 *In vitro* cell uptake studies of (A) ^{68}Ga-**3.22**, (B) ^{68}Ga-**3.23**, (C) ^{68}Ga-**3.24**, and (D) ^{68}Ga-**3.30** under normoxic (21% O_2, blue) and hypoxic (0.5% O_2, red) conditions in LCC6^{HER-2} and HT-29 cells over 120 min. Statistical analyses of uptake ratios (hypoxic/normoxic) were performed using Student's *t*-test (*p <0.05, **p <0.01, n = 3 at each time point).

3.2.6 Small Animal Dynamic PET/CT Imaging and Biodistribution

Due to the similarities between *in vitro* hypoxic uptake of the varying nitroimidazole-containing ^{68}Ga-tracers (*vide supra*), *in vivo* pharmacokinetics and biodistribution of only one of the ^{68}Ga-labelled tracers ([^{68}Ga(**3.24**)]$^{+}$) was investigated herein. Four mice bearing HT-29 colon cancer xenografts on the right shoulder were injected with [^{68}Ga(dedpa-*N.N'*-propyl-2-NI)]$^{+}$. After 14 days of growth, the resultant HT-29 tumours were unfortunately extremely small (<100 mm^3 tumour volume) or non-existent suggesting there would be negligible hypoxic tissue present and/or no blood circulation to the (non-existent) tumour. Nonetheless, two mice were imaged using dynamic positron emission tomography (PET) in conjunction with standard helical X-ray CT and sacrificed for biodistribution profiles at 2 h post-injection (p.i.), and two mice were used only for biodistribution data at 2 h p.i.

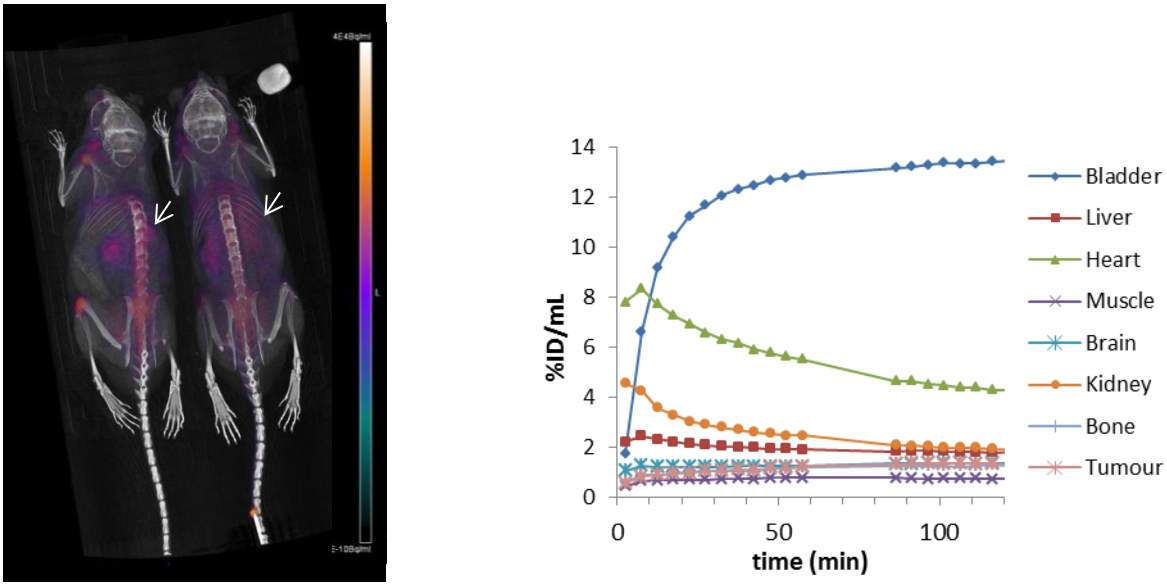

Figure 3.10 Left: Fused PET/CT image of [^{68}Ga(dedpa-*N,N'*-propyl-2-NI)]$^{+}$ showing negligible accumulation in HT-29 tumours (white arrows). Right: Time activity curve over 120 min of [^{68}Ga(dedpa-*N,N'*-propyl-2-NI)]$^{+}$ using regions-of-interest showing rapid clearance from the blood, fast renal excretion, and negligible uptake in non-target tissue.

A 2 hour dynamic PET scan was performed and reconstructed in 5 minute intervals to obtain time activity curves (TACs) for [^{68}Ga(dedpa-*N.N'*-propyl-2-NI)]$^{+}$ (Figure 3.10). TACs of the radiolabelled tracer show rapid clearance from the blood and fast renal excretion with minimal uptake in non-target tissue such as liver, muscle, bone, and brain. The diminutive tumours showed uptake within background levels, as predicted. The hydrophilic character (log $D_{7.4}$ = -2.76(19)) of [^{68}Ga(dedpa-*N.N'*-propyl-2-NI)]$^{+}$ nicely translated to rapid renal excretion and low liver uptake of the radiotracer *in vivo*. The static PET/CT image at 2 h p.i. (Figure 3.10) correlates with the results obtained from the TAC: no delineation of the (insufficiently hypoxic) tumour and minimal accumulation of radioactivity in non-target tissue such as liver with some residual activity in the blood pool. There is some indication of activity accumulation in the joints (knee, shoulder, jaw) in the static PET/CT image, which may be indicative of radiometal decomplexation and transchelation of ^{68}Ga *in vivo* to some extent. The biodistribution results (Figure 3.11) are also comparable to the TAC, suggesting rapid clearance of the radiotracer with minimal activity (<0.1 %ID/g) in all measured organs at 2 h p.i. (n = 4).

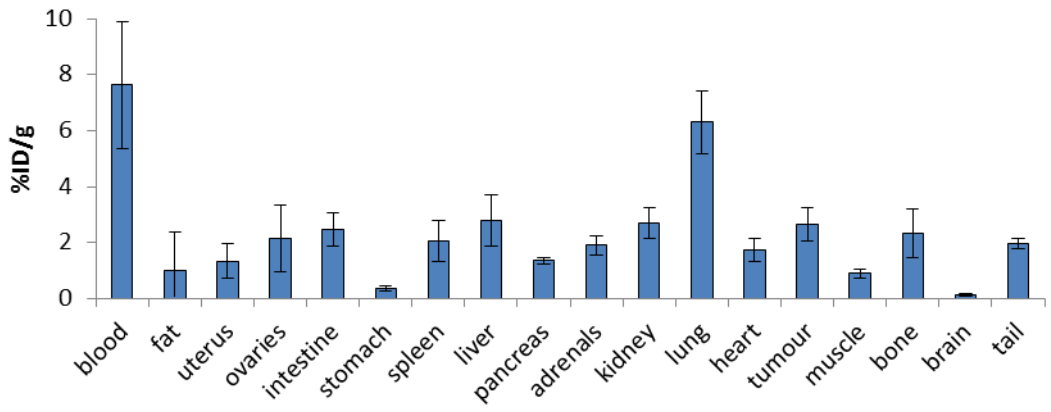

Figure 3.11 Biodistribution data for [^{68}Ga(dedpa-*N,N'*-propyl-2-NI]$^{+}$ at t = 2 h (n = 4) p.i. for selected organs and tumour (expressed as %ID/g).

3.3 Conclusions

Nine nitroimidazole-containing derivatives of the promising Ga(III) chelators H_2dedpa and H_2*CHX*dedpa were successfully synthesized and characterized. All chelating ligands retained their ability to quantitatively (>99% RCY) label $^{67/68}$Ga in 10 minutes at room temperature, a marked advantage over other nitroimidazole-macrocyclic analogues such as NI-NOTA and NI-DOTA which required heating at 100°C to accomplish quantitative labeling of gallium isotopes.[173,174] Moreover, stability assays with *apo*-transferrin suggest all propyl-linked H_2dedpa and H_2*CHX*dedpa analogues form kinetically inert gallium complexes, with stabilities ranging from 86 to >99% intact after a 2 hour *apo*-transferrin challenge assay. *In vitro* cell uptake of three [^{68}Ga(dedpa-*N,N'*-propyl-NI)]$^+$ tracers and one [^{68}Ga(*CHX*dedpa-*N,N'*-propyl-NI)]$^+$ complex with three cell lines, LCC6^{HER-2}, HT-29, and CHO, were tested under hypoxic (0.5% O_2) and normoxic conditions. All four ^{68}Ga-tracers exhibited exceptional differentiation between hypoxic and normoxic uptake after 60 minutes with ratios ranging from 4.7 to 7.9. Despite somewhat disappointing initial *in vivo* small animal PET/CT imaging and biodistribution studies which showed negligible tumour uptake of [^{68}Ga(dedpa-*N,N'*-propyl-2-NI)]$^+$ (likely attributable to the undersized tumours), the radiotracer displayed favorable renal excretion and no significant liver uptake – an advantage over lipophilic clinical hypoxia tracer ^{18}F-MISO. The results suggest that these novel H_2dedpa- and H_2*CHX*dedpa-*N,N'*-alkyl-nitroimidazole ligands would be ideal candidates for further testing *in vivo* for PET imaging of hypoxia with ^{68}Ga. More thorough *in vivo* studies with mice bearing larger (more hypoxic) tumours and directly comparing ^{18}F-MISO and ^{68}Ga-dedpa-NI uptake may be of interest moving forward.

3.4 Experimental

3.4.1 Materials and Methods

All solvents and reagents were purchased from commercial suppliers (Sigma Aldrich, TCI America, Fisher Scientific) and were used as received. Human *apo*-transferrin was purchased from Sigma Aldrich. The analytical thin-layer chromatography (TLC) plates were aluminum-backed ultrapure silica gel 60 Å, 250 μm thickness; the flash column silica gel (standard grade, 60 Å, 40-63 μm) was provided by Silicycle. ^{1}H and ^{13}C NMR spectra were recorded at 25 °C unless otherwise noted on Bruker AV300, AV400, or AV600 instruments; NMR spectra are expressed on the δ scale and were referenced to residual solvent peaks. Low-resolution mass spectrometry was performed using a Waters ZG spectrometer with an ESCI electrospray/chemical-ionization source, and high-resolution electrospray-ionization mass spectrometry (ESI-MS) was performed on a Micromass LCT time-of-flight instrument at the Department of Chemistry, University of British Columbia.

^{67}Ga(chelate) human *apo*-transferrin stability experiments were analyzed using GE Healthcare Life Sciences PD-10 desalting columns (size exclusion for MW < 5000 Da) and counted with a Capintec CRC 15R well counter. Radioactivity of ^{68}Ga-labelled tracers for *in vitro* studies was measured using a Capintec CRC-25R/W dose calibrator. The HPLC system used for analysis and purification of non-radioactive compounds consisted of a Waters 600 controller, Waters 2487 dual wavelength absorbance detector, and a Waters delta 600 pump. Phenomenex synergi hydro-RP 80 Å columns (250 mm x 4.6 mm analytical or 250 mm x 21.2 mm semipreparative) were used for purification of several of the deprotected chelators. Analysis of radiolabelled complexes was carried out using either a Phenomenex hydro-RP 80 Å column (250 mm x 4.6 mm analytical) using a Waters Alliance HT 2795 separation module equipped with a Raytest Gabi Star NaI (Tl) detector and a Waters 996 photodiode array (PDA) or

Phenomenex C18 column (5 μ, 250 x 10 mm) using an Agilent HPLC system equipped with a model 1200 quaternary pump, a model 1200 UV absorbance detector (set at 220 nm), and a Bioscan (Washington, DC) NaI scintillation detector (the radio-detector was connected to a Bioscan B-FC-1000 Flow-count system, and the output from the Bioscan Flow-count system was fed into an Agilent 35900E Interface which converted the analog signal to digital signal). $^{67}GaCl_3$ was cyclotron produced and provided by Nordion as a ~0.1 M HCl solution. ^{68}Ga was obtained from either Nordion (5-10 mCi/mL) from a generator constructed of titanium dioxide sorbent that was charged with ^{68}Ge and eluted with aqueous HCl (0.1 M),[69,183] or from an Eckert & Ziegler (Berlin, Germany) IGG100 ^{68}Ga generator and was purified according to previously published procedures[184] using DGA resin column.

Compounds **3.1 – 3.3** and **3.1'-3.3'** were prepared as previously reported.[59,176]

3.4.2 General Procedure for Preparation of Nitroimidazole Potassium Salt (3.4, 3.5, or 3.6)

A calculated quantity of KOH in aqueous solution (1 molar equiv, 0.1 M) was added to the nitroimidazole and the mixture was warmed to 60°C to dissolve the imidazole. The water was removed in *vacuo* and the imidazole salt was dried under vacuum at 115°C overnight (100%).

3.4.3 General Procedure for 1-(ω-Bromoalkyl)-nitroimidazoles (3.7-3.12)

Compounds **3.7-3.12** were synthesized as per analogues reported in the literature.[177] The nitroimidazole potassium salt (**3.4** or **3.5** or **3.6**, 1.3 mmol, 1 equiv) and 18-crown-6 (3.9 mmol, ~3 equiv) dissolved in distilled CH_3CN (75 mL) was added dropwise to a refluxing

solution of the appropriate 1,ω-dibromoalkane (13 mmol, 10 equiv) in distilled CH_3CN (100 mL) under N_2 over one hour. The resultant solution was set at reflux for 16-24 hours. The solvent was subsequently removed in *vacuo*, and the crude product was purified by column chromatography (SiO_2, EtOAc/Pet Ether 3:1).

3.4.4 1-(3-Bromopropyl)-2-methyl-5-nitroimidazole (3.7)

Beige solid (73%). ^{1}H NMR (400 MHz, $CDCl_3$) δ 7.68 (s, 1H), 4.06 (t, *J* = 6.8 Hz, 2H), 3.30 (t, *J* = 5.9 Hz, 2H), 2.33 (s, 3H), 2.29 – 2.14 (m, 2H). ^{13}C NMR (101 MHz, $CDCl_3$) δ 146.2, 144.8, 119.8, 44.8, 32.2, 28.9, 12.9.

3.4.5 1-(3-Bromopropyl)-4-nitroimidazole (3.8)

Beige solid (68%). ^{1}H NMR (400 MHz, $CDCl_3$) δ 7.81 (d, *J* = 1.3 Hz, 1H), 7.49 (d, *J* = 0.9 Hz, 1H), 4.27 (t, *J* = 6.6 Hz, 2H), 3.37 (t, *J* = 6.0 Hz, 2H), 2.43 – 2.31 (m, 2H). ^{13}C NMR (101 MHz, $CDCl_3$) δ 148.2, 136.2, 119.2, 46.0, 32.7, 28.7.

3.4.6 1-(3-Bromopropyl)-2-nitroimidazole (3.9)

Beige solid (74%). ^{1}H NMR (400 MHz, $CDCl_3$) δ 7.20 (s, 1H), 7.07 (s, 1H), 4.55 (t, *J* = 6.7 Hz, 2H), 3.33 (t, *J* = 6.1 Hz, 2H), 2.35 (p, *J* = 6.5 Hz, 2H). ^{13}C NMR (101 MHz, $CDCl_3$) δ 128.7, 126.9, 48.4, 32.5, 29.5.

3.4.7 1-(2-Bromoethyl)-2-methyl-5-nitroimidazole (3.10)

Beige solid (44%). ^{1}H NMR (300 MHz, $CDCl_3$) δ 7.79 (s, 1H), 4.36 (t, *J* = 6.0 Hz, 2H), 3.64 (t, *J* = 6.0 Hz, 2H), 2.44 (s, 3H).

3.4.8 1-(2-Bromoethyl)-4-nitroimidazole (3.11)

White solid (51%). ^{1}H NMR (400 MHz, $CDCl_3$) δ 7.85 (d, *J* = 1.5 Hz, 1H), 7.52 (d, *J* = 1.3 Hz, 1H), 4.46 (t, *J* = 5.9 Hz, 2H), 3.67 (t, *J* = 5.9 Hz, 2H). ^{13}C NMR (101 MHz, $CDCl_3$) δ 136.2, 119.1. 49.6. 29.6.

3.4.9 1-(2-Bromoethyl)-2-nitroimidazole (3.12)

Yellow solid (56%). ^{1}H NMR (300 MHz, $CDCl_3$) δ 7.22 (s, 1H), 7.13 (s, 1H), 4.78 (t, *J* = 5.9 Hz, 2H), 3.72 (t, *J* = 5.9 Hz, 2H). ^{13}C NMR (101 MHz, $CDCl_3$) δ 128.3, 127.0. 51.3, 29.6.

3.4.10 General Procedure for *N,N'*-Alkylation of Me_2dedpa (3.13-3.18)

Me_2dedpa, **3.3** (279 mg, 0.78 mmol) and the appropriate 1-(ω-bromoalkyl)-nitroimidazole (**3.7-3.12**) (1.95 mmol, 2.5 equiv) were dissolved in CH_3CN (6 mL), and potassium carbonate (572 mg, 4.14 mmol, ~5 equiv) was added. The reaction mixture was stirred at reflux for 2-3 days, subsequently cooled to room temperature and inorganic salts were filtered out. The filtrate was concentrated *in vacuo* and the crude oil was purified by column chromatography (CombiFlash R_f automated column system; 40 g HP silica; A: dichloromethane, B: methanol, 100% A to 15% B gradient).

3.4.11 Me_2dedpa-*N,N'*-ethyl-2-methyl-5-nitroimidazole (3.13)

Yellow oil (23%). ^{1}H NMR (400 MHz, MeOD) δ 7.92 (dd, *J* = 7.9, 5.4 Hz, 4H), 7.79 (s, 2H), 7.60 (dd, *J* = 5.5, 3.0 Hz, 2H), 4.40 (s, 4H), 4.29 (t, *J* = 6.0 Hz, 4H), 3.82 (s, 6H), 3.60 (s, 4H), 3.54 (t, *J* = 5.9 Hz, 4H), 2.22 (s, 6H). ^{13}C NMR (101 MHz, MeOD) δ 166.3, 156.6, 148.1, 147.0, 146.8, 140.4, 128.8, 126.0, 122.3, 57.8, 55.2, 53.6, 52.3, 44.0, 12.8. MS (ES+) m/z = 665.5 $[M+H]^+$.

3.4.12 Me_2dedpa-*N,N'*-ethyl-4-nitroimidazole (3.14)

Yellow oil (15%). ^{1}H NMR (300 MHz, MeOD) δ 8.09 (d, *J* = 1.2 Hz, 2H), 7.95 (d, *J* = 7.6 Hz, 2H), 7.80 (t, *J* = 7.7 Hz, 2H), 7.73 (d, *J* = 1.2 Hz, 2H), 7.33 (d, *J* = 7.6 Hz, 2H), 4.18 (t, *J* = 5.6 Hz, 4H), 3.96 (s, 6H), 3.80 (s, 4H), 3.37 (s, 3H), 2.89 (t, *J* = 5.6 Hz, 4H), 2.64 (s, 4H). MS (ES-) m/z = 715.5 $[M+^{79}Br]^-$.

3.4.13 Me_2dedpa-*N,N'*-ethyl-2-nitroimidazole (3.15)

Yellow oil (10%). ^{1}H NMR (300 MHz, $CDCl_3$) δ 7.97 (d, *J* = 7.7 Hz, 2H), 7.72 (t, *J* = 7.7 Hz, 2H), 7.22 (s, 2H), 7.13 (d, *J* = 7.6 Hz, 2H), 7.03 (s, 2H), 4.50 (t, *J* = 5.5 Hz, 4H), 3.97 (s, 6H), 3.79 (s, 4H), 2.85 (t, *J* = 5.5 Hz, 4H), 2.57 (s, 4H). MS (ES-) m/z = 715.4 $[M+^{79}Br]^-$.

3.4.14 Me_2dedpa-*N,N'*-propyl-2-methyl-5-nitroimidazole (3.16)

Yellow oil (34%). ^{1}H NMR (400 MHz, MeOD) δ 8.00 (s, 2H), 7.97 (d, *J* = 7.7 Hz, 2H), 7.89 (t, *J* = 7.7 Hz, 2H), 7.64 (d, *J* = 7.8 Hz, 2H), 4.03 (t, *J* = 7.1 Hz, 4H), 3.95 (s, 6H), 3.82 (s, 4H), 2.67 (s, 4H), 2.56 (t, *J* = 6.7 Hz, 4H), 2.36 (s, 6H), 2.05 – 1.93 (m, 4H). ^{13}C NMR (101 MHz, $CDCl_3$) δ

165.3, 159.4, 147.2, 145.9, 144.5, 137.4, 126.0, 123.6, 120.0, 59.6, 52.6, 51.9, 50.9, 44.6, 27.4, 12.8. MS (ES+) m/z = 693.4 $[M+H]^+$.

3.4.15 Me_2dedpa-*N,N'*-propyl-4-nitroimidazole (3.17)

Yellow oil (30%). ^{1}H NMR (400 MHz, MeOD) δ 8.12 (d, *J* = 1.3 Hz, 2H), 7.95 (dd, *J* = 7.6, 0.7 Hz, 2H), 7.87 (t, *J* = 7.7 Hz, 2H), 7.74 (d, *J* = 1.3 Hz, 2H), 7.63 (dd, *J* = 7.7, 0.7 Hz, 2H), 4.15 (t, *J* = 6.9 Hz, 4H), 3.95 (s, 6H), 3.78 (s, 4H), 2.62 (s, 4H), 2.51 (t, *J* = 6.7 Hz, 4H), 2.03 (p, *J* = 6.7 Hz, 4H). ^{13}C NMR (101 MHz, $CDCl_3$) δ 166.8, 161.6, 148.5, 148.1, 139.1, 138.4, 128.2, 124.7, 121.7, 60.6, 53.2, 53.1, 52.2, 47.2, 28.9. MS (ES+) m/z = 665.4 $[M+H]^+$.

3.4.16 Me_2dedpa-*N,N'*-propyl-2-nitroimidazole (3.18)

Yellow oil (69%). ^{1}H NMR (400 MHz, $CDCl_3$) δ 7.85 (d, *J* = 7.4 Hz, 2H), 7.67 (t, *J* = 7.8 Hz, 2H), 7.45 (d, *J* = 7.5 Hz, 2H), 7.10 (d, *J* = 0.5 Hz, 2H), 6.93 (d, *J* = 0.6 Hz, 2H), 4.37 – 4.27 (m, 4H), 3.82 (s, 6H), 3.69 (s, 4H), 2.53 (s, 4H), 2.45 (t, *J* = 6.5 Hz, 4H), 1.93 – 1.82 (m, 4H). ^{13}C NMR (101 MHz, $CDCl_3$) δ 165.4, 159.9, 147.1, 144.4, 137.3, 128.0, 126.4, 126.0, 123.5, 70.3, 60.0, 52.6, 51.5, 48.1, 27.9. MS (ES+) m/z = 665.4 $[M+H]^+$.

3.4.17 General Procedure for Methyl Ester Deprotection of 3.13-3.18

The methyl-ester protected ligand (**3.13-3.18**) (0.17 mmol) was dissolved in THF/H_2O (3:1, 6 mL), and lithium hydroxide (20 mg, 0.83 mmol, 5 equiv) was added. The reaction mixture was stirred at ambient temperature until the reaction was complete by TLC (15-30 min). (R_f(products) = ~0.06 in 10% methanol/dichloromethane). The mixture was

subsequently evaporated to dryness, and purified by semi-preparative HPLC (A: 0.1 % trifluoroacetic acid in water; B: CH_3CN; 5% to 100% B; 30 min, 10 mL/min). Product fractions were pooled and lyophilized.

3.4.18 H_2dedpa-*N,N'*-ethyl-2-methyl-5-nitroimidazole (3.19)

Beige solid (66%). ^{1}H NMR (300 MHz, DMSO) δ 8.29 (s, 2H), 7.96 (dd, *J* = 8.3, 5.2 Hz, 4H), 7.63 (dd, *J* = 5.8, 2.7 Hz, 2H), 4.46 – 4.38 (m, 4H), 4.36 (s, 4H), 3.43 (s, 4H), 3.33 (t, *J* = 6.2 Hz, 4H), 2.30 (s, 6H). ^{13}C NMR (101 MHz, DMSO) δ 165.6, 154.3, 147.6, 145.3, 145.2, 138.6, 127.3, 124.1, 122.2, 56.7, 52.4, 49.4, 42.4, 12.6. HR-ESI-MS m/z for $C_{28}H_{33}N_{10}O_8$ ($M+H^+$) calcd. (found): 637.2483 (637.2484).

3.4.19 H_2dedpa-*N,N'*-ethyl-4-nitroimidazole (3.20)

Yellow solid (98%). ^{1}H NMR (400 MHz, MeOD) δ 8.01 (d, *J* = 1.4 Hz, 2H), 7.95 (d, *J* = 7.5 Hz, 2H), 7.87 (t, *J* = 7.7 Hz, 2H), 7.63 (d, *J* = 1.5 Hz, 2H), 7.36 (d, *J* = 7.5 Hz, 2H), 4.22 – 4.08 (m, 4H), 3.91 (s, 4H), 2.77 – 2.67 (m, 4H), 2.46 (s, 4H). ^{13}C NMR (101 MHz, MeOD) δ 172.2, 159.0, 154.8, 148.6, 139.8, 138.4, 125.6, 123.2, 121.6, 60.3, 55.1, 52.0, 45.8. HR-ESI-MS m/z for $C_{26}H_{29}N_{10}O_8$ ($M+H^+$) calcd. (found): 609.2170 (609.2178).

3.4.20 H_2dedpa-*N,N'*-ethyl-2-nitroimidazole (3.21)

Yellow solid (95%). ^{1}H NMR (400 MHz, MeOD) δ 7.95 – 7.87 (m, 4H), 7.40 (d, *J* = 6.5 Hz, 2H), 7.37 (d, *J* = 1.0 Hz, 2H), 7.06 (d, *J* = 1.0 Hz, 2H), 4.51 – 4.39 (m, 4H), 4.03 (s, 4H), 2.79 – 2.66 (m, 4H), 2.53 (s, 4H). ^{13}C NMR (101 MHz, MeOD) δ 172.2, 172.1, 158.9, 139.8, 135.4, 128.7,

128.6, 125.6, 123.2, 60.7, 54.9, 52.1. HR-ESI-MS m/z for $C_{26}H_{29}N_{10}O_8$ ($M+H^+$) calcd. (found): 609.2170 (609.2177).

3.4.21 H_2dedpa-*N,N'*-propyl-2-methyl-5-nitroimidazole (3.22)

White solid (99%). ^{1}H NMR (400 MHz, MeOD) δ 8.01 (d, *J* = 7.6 Hz, 2H), 7.94 (t, *J* = 7.7 Hz, 2H), 7.90 (s, 2H), 7.58 (d, *J* = 7.4 Hz, 2H), 4.38 (s, 4H), 4.00 (t, *J* = 7.1 Hz, 4H), 3.49 (s, 4H), 3.17 – 3.09 (m, 4H), 2.29 (s, 6H), 2.23 – 2.10 (m, 4H). ^{13}C NMR (101 MHz, MeOD) δ 167.1, 156.6, 149.0, 146.8, 140.1, 128.3, 125.9, 121.7, 58.0, 53.5, 51.6, 45.6, 26.8, 12.7. HR-ESI-MS m/z for $C_{30}H_{37}N_{10}O_8$ ($M+H^+$) calcd. (found): 665.2796 (665.2792).

3.4.22 H_2dedpa-*N,N'*-propyl-4-nitroimidazole (3.23)

Yellow solid (99%). ^{1}H NMR (400 MHz, MeOD) δ 7.89 (d, *J* = 1.1 Hz, 2H), 7.85 (d, *J* = 7.6 Hz, 2H), 7.72 (t, *J* = 7.7 Hz, 2H), 7.49 (d, *J* = 1.1 Hz, 2H), 7.20 (d, *J* = 7.7 Hz, 2H), 3.77 (t, *J* = 6.9 Hz, 4H), 3.67 (s, 4H), 2.07 (s, 4H), 2.07 – 1.99 (m, 4H), 1.84 – 1.71 (m, 4H). ^{13}C NMR (101 MHz, MeOD) δ 172.2, 159.2, 154.7, 148.5, 139.7, 138.2, 125.4, 123.0, 121.4, 60.3, 51.8, 51.5, 47.6, 26.5. HR-ESI-MS m/z for $C_{28}H_{33}N_{10}O_8$ ($M+H^+$) calcd. (found): 637.2483 (637.2483).

3.4.23 H_2dedpa-*N,N'*-propyl-2-nitroimidazole (3.24)

White solid (83%). ^{1}H NMR (600 MHz, MeOD) δ 8.00 (d, *J* = 7.3 Hz, 2H), 7.95 (t, *J* = 7.7 Hz, 2H), 7.59 (d, *J* = 7.5 Hz, 2H), 7.38 (d, *J* = 0.7 Hz, 2H), 7.12 (d, *J* = 0.8 Hz, 2H), 4.45 (t, *J* = 7.2 Hz, 4H), 4.40 (s, 4H), 3.51 (s, 4H), 3.23 – 3.16 (m, 4H), 2.29 – 2.21 (m, 4H). ^{13}C NMR (151 MHz,

MeOD) δ 167.3, 156.4, 148.7, 140.1, 128.8, 128.3, 128.3, 125.9, 58.3, 53.6, 51.6, 48.7, 27.1. HR-ESI-MS m/z for $C_{28}H_{33}N_{10}O_8$ ($M+H^+$) calcd. (found): 637.2483 (637.2490).

3.4.24 Me$_2$*CHX*dedpa-*N,N'*-propyl-2-methyl-5-nitroimidazole (3.25)

To a stirred solution of Me$_2$*CHX*dedpa (**3.3'**) (220 mg, 0.53 mmol) and **3.7** (331 mg, 1.33 mmol, 2.5 equiv) in CH_3CN (~4 mL), diisopropylethylamine (462 µL, 2.65 mmol, 5 equiv) was added, and the mixture was heated to reflux for 3 days. The solvent was then concentrated *in vacuo* and the crude oil was purified by column chromatography (CombiFlash R_f automated column system; 24 g HP silica; A: dichloromethane, B: methanol, 100% A to 10% B gradient) to give **3.25** as a yellow oil (120 mg, 30%). ^{1}H NMR (600 MHz, MeOD) δ 7.97 – 7.92 (m, 4H), 7.76 (s, 2H), 7.65 (dd, *J* = 7.1, 1.1 Hz, 2H), 4.37 (d, *J* = 13.9 Hz, 2H), 3.93 (d, *J* = 14.0 Hz, 2H), 3.86 (t, *J* = 7.1 Hz, 4H), 3.56 (s, 6H), 3.55 – 3.52 (m, 2H), 3.16 – 3.06 (m, 4H), 2.27 (d, *J* = 11.5 Hz, 2H), 2.17 – 2.13 (m, 2H), 2.11 (s, 6H), 2.04 (tt, *J* = 12.1, 6.0 Hz, 2H), 1.93 (d, *J* = 8.0 Hz, 2H), 1.68 – 1.59 (m, 2H), 1.46 (t, *J* = 9.5 Hz, 2H). ^{13}C NMR (151 MHz, MeOD) δ 165.8, 157.3, 149.1, 146.7, 139.9, 129.2, 125.9, 122.0, 62.4, 54.2, 53.1, 51.0, 45.6, 28.1, 25.6, 25.5, 12.6. MS (ES+) m/z = 747.6 $[M+H]^+$.

3.4.25 Me$_2$*CHX*dedpa-*N,N'*-propyl-4-nitroimidazole (3.26)

Prepared as compound **3.25** above, but with 1-(3-bromopropyl)-4-nitroimidazole (**3.8**) as alkylating agent. Yellow oil (20%). ^{1}H NMR (400 MHz, MeOD) δ 8.05 – 7.95 (m, 4H), 7.92 (d, *J* = 1.4 Hz, 2H), 7.65 (dd, *J* = 7.4, 1.0 Hz, 2H), 7.51 (d, *J* = 1.4 Hz, 2H), 4.37 (d, *J* = 13.8 Hz, 2H), 4.05 – 3.99 (m, 4H), 3.96 (d, *J* = 13.9 Hz, 2H), 3.65 (s, 6H), 3.57 (d, *J* = 9.0 Hz, 2H), 3.20 – 3.03 (m, 4H), 2.29 (d, *J* = 12.1 Hz, 2H), 2.25 – 2.13 (m, 4H), 1.99 (d, *J* = 8.5 Hz, 2H), 1.74 – 1.59 (m, 2H), 1.51 (t,

J = 10.0 Hz, 2H). ^{13}C NMR (101 MHz, MeOD) δ 165.7, 157.1, 139.9, 138.2, 129.2, 126.0, 121.5, 62.4, 54.0, 53.1, 51.0, 46.8, 28.3, 25.6, 25.6. MS (ES+) m/z = 719.6 $[M+H]^+$.

3.4.26 Me_2*CHX*dedpa-*N,N'*-propyl-2-nitroimidazole (3.27)

To a stirred solution of Me_2*CHX*dedpa (**3.3'**) (238 mg, 0.58 mmol) and **3.9** (340 mg, 1.45 mmol, 2.5 equiv) in CH_3CN (5 mL), potassium carbonate (481 mg, 3.48 mmol, 6 equiv) was added. The reaction mixture was stirred at reflux for 2 days, subsequently cooled to room temperature and inorganic salts removed by vacuum filtration. The solvent was removed *in vacuo* and the crude oil was purified by column chromatography (CombiFlash R_f automated column system; 24 g HP silica; A: dichloromethane, B: methanol, 100% A to 10% B gradient) to give **3.27** as a yellow oil (257 mg, 62%). ^{1}H NMR (400 MHz, $CDCl_3$) δ 7.89 (dd, *J* = 7.4, 0.7 Hz, 2H), 7.64 (t, *J* = 7.6 Hz, 2H), 7.59 (d, *J* = 7.0 Hz, 2H), 7.05 (s, 2H), 6.98 (d, *J* = 0.7 Hz, 2H), 4.38 – 4.20 (m, 4H), 3.93 (d, *J* = 15.0 Hz, 2H), 3.90 (s, 6H), 3.73 (d, *J* = 15.0 Hz, 2H), 2.68 (d, *J* = 8.2 Hz, 2H), 2.64 – 2.50 (m, 4H), 1.99 – 1.92 (m, 2H), 1.92 – 1.83 (m, 4H), 1.71 (d, *J* = 6.9 Hz, 2H), 1.22 – 1.03 (m, 4H). ^{13}C NMR (101 MHz, $CDCl_3$) δ 165.6, 161.5, 147.3, 144.7, 137.3, 128.3, 126.4, 126.2, 123.6, 61.8, 56.4, 52.8, 48.6, 47.4, 29.8, 26.6, 25.8. MS (ES+) m/z = 719.5 $[M+H]^+$.

3.4.27 General Procedure for Methyl Ester Deprotection of 3.25-3.27

The methyl protected ligand (**3.25-3.27**) (0.16 mmol) was dissolved in THF/H_2O (3:1, 5 mL), and lithium hydroxide (19 mg, 0.80 mmol, 5 equiv) was added. The reaction mixture was stirred at ambient temperature until the reaction was complete by TLC (15-30 min). (R_f(products) = ~0.1 in 15% methanol/dichloromethane). The mixture was subsequently evaporated to dryness, and purified by semi-preparative HPLC (A: 0.1 % trifluoroacetic acid in

water; B: CH_3CN; 5% to 100% B; 30 min, 10 mL/min). Product fractions were pooled and lyophilized to yield the pro-ligand as a white powder (99% recovery).

3.4.28 H_2*CHX*dedpa-*N,N'*-propyl-2-methyl-5-nitroimidazole (3.28)

^{1}H NMR (400 MHz, MeOD) δ 8.03 (d, *J* = 7.6 Hz, 2H), 7.94 (t, *J* = 7.7 Hz, 2H), 7.75 (s, 2H), 7.63 (d, *J* = 7.5 Hz, 2H), 4.41 (d, *J* = 14.1 Hz, 2H), 3.94 (d, *J* = 14.2 Hz, 2H), 3.86 (t, *J* = 7.2 Hz, 4H), 3.55 (d, *J* = 9.0 Hz, 2H), 3.18 – 3.04 (m, 4H), 2.28 (d, *J* = 11.5 Hz, 2H), 2.22 (d, *J* = 3.8 Hz, 1H), 2.15 (d, *J* = 1.5 Hz, 1H), 2.14 (s, 6H), 2.11 – 2.04 (m, 2H), 1.96 (d, *J* = 8.3 Hz, 2H), 1.71 – 1.59 (m, 2H), 1.48 (t, *J* = 9.6 Hz, 2H). ^{13}C NMR (101 MHz, MeOD) δ 166.7, 156.8, 150.0, 146.7, 139.9, 128.7, 126.2, 121.6, 101.4, 62.2, 54.4, 50.9, 45.7, 28.3, 25.6, 25.3, 12.6. HR-ESI-MS m/z for $C_{34}H_{43}N_{10}O_8$ ($M+H^+$) calcd. (found): 719.3265 (719.3271).

3.4.29 H_2*CHX*dedpa-*N,N'*-propyl-4-nitroimidazole (3.29)

^{1}H NMR (400 MHz, MeOD) δ 8.08 (d, *J* = 7.7 Hz, 2H), 7.97 (t, *J* = 7.7 Hz, 2H), 7.90 (s, 2H), 7.62 (d, *J* = 7.5 Hz, 2H), 7.48 (s, 2H), 4.40 (d, *J* = 13.9 Hz, 3H), 4.06 – 3.98 (m, 4H), 3.96 (d, *J* = 14.3 Hz, 2H), 3.56 (d, *J* = 8.6 Hz, 2H), 3.18 – 3.03 (m, 4H), 2.28 (d, *J* = 11.9 Hz, 2H), 2.25 – 2.15 (m, 4H), 2.03 – 1.96 (m, 2H), 1.75 – 1.60 (m, 2H), 1.55 – 1.45 (m, 2H). HR-ESI-MS m/z for $C_{32}H_{39}N_{10}O_8$ ($M+H^+$) calcd. (found): 691.2952 (691.2957).

3.4.30 H_2*CHX*dedpa-*N,N'*-propyl-2-nitroimidazole (3.30)

^{1}H NMR (400 MHz, MeOD) δ 7.95 (d, *J* = 7.7 Hz, 2H), 7.86 (t, *J* = 7.7 Hz, 2H), 7.52 (d, *J* = 7.7 Hz, 2H), 7.11 (s, 2H), 6.91 (s, 2H), 4.35 (d, *J* = 14.2 Hz, 2H), 4.28 – 4.20 (m, 4H), 3.86 (d, *J* =

14.2 Hz, 2H), 3.49 (d, *J* = 8.8 Hz, 2H), 3.08 (dt, *J* = 12.8, 7.8 Hz, 4H), 2.21 (d, *J* = 10.4 Hz, 2H), 2.11 – 2.01 (m, 4H), 1.93 – 1.84 (m, 2H), 1.64 – 1.52 (m, 2H), 1.44 – 1.36 (m, 2H). ^{13}C NMR (151 MHz, MeOD) δ 166.6, 156.7, 149.8, 139.9, 128.7, 128.5, 128.2, 126.1, 62.2, 54.3, 51.0, 48.7, 28.3, 25.6, 25.2. HR-ESI-MS m/z for $C_{32}H_{39}N_{10}O_8$ ($M+H^+$) calcd. (found): 691.2952 (691.2952).

3.4.31 General Procedure for Gallium Complexation of Pro-ligands 3.19-3.24 and 3.28-3.30

The appropriate pro-ligand (**3.19-3.24** or **3.28-3.30**) (0.02 mmol) was dissolved in MeOH/H_2O (1:1, ~1 mL), and pH of the solution was adjusted to ~1-2 with 0.1 M HCl (aq). To this clear solution, a solution of $Ga(ClO_4)_3 \cdot 6H_2O$ (13 mg in 80 μL of H_2O, 0.03 mmol, 1.5 equiv) was added, at which time a white precipitate formed. The pH of the mixture was adjusted to 4-5 using 0.1 M NaOH (aq), and stirred at room temperature overnight to ensure quantitative complexation. The resultant white precipitate was collected by centrifugation (10 min, 4000 rpm), the filtrate was discarded and the solid pellet was further dried under vacuum to yield the gallium complex as the perchlorate salt [Ga(L)][ClO_4].

3.4.32 [Ga(dedpa-*N,N'*-ethyl-2-methyl-5-nitroimidazole)][ClO_4], [Ga(3.19)][ClO_4]

White solid (65%). ^{1}H NMR (400 MHz, DMSO) δ 8.68 (t, *J* = 7.8 Hz, 2H), 8.35 (d, *J* = 7.6 Hz, 2H), 8.31 (s, 2H), 8.25 (d, *J* = 7.9 Hz, 2H), 4.94 (d, *J* = 17.5 Hz, 2H), 4.78 (d, *J* = 17.5 Hz, 2H), 4.52 – 4.41 (m, 2H), 4.40 – 4.28 (m, 2H), 3.38 (d, *J* = 8.0 Hz, 3H), 3.17 – 3.04 (m, 6H), 2.34 (s, 6H). ^{13}C NMR (101 MHz, DMSO) δ 162.1, 150.6, 146.8, 145.6, 145.4, 143.5, 127.8, 123.5, 122.0, 55.4, 50.1, 48.5, 12.8. HR-ESI-MS m/z for $C_{28}H_{30}{}^{69}GaN_{10}O_8$ (M^+) calcd. (found): 703.1504 (703.1505).

3.4.33 [Ga(dedpa-*N,N'*-ethyl-4-nitroimidazole)][ClO_4], [Ga(3.20)][ClO_4]

White solid (70%). ^{1}H NMR (600 MHz, DMSO) δ 8.65 (t, *J* = 7.8 Hz, 2H), 8.40 (d, *J* = 1.0 Hz, 2H), 8.31 (d, *J* = 7.6 Hz, 2H), 8.20 (d, *J* = 8.0 Hz, 2H), 7.83 (d, *J* = 1.0 Hz, 2H), 4.84 (d, *J* = 17.5 Hz, 2H), 4.78 (d, *J* = 17.5 Hz, 2H), 4.58 – 4.51 (m, 2H), 4.44 – 4.35 (m, 2H), 3.17 (d, *J* = 11.4 Hz, 2H), 3.13 – 3.02 (m, 6H). ^{13}C NMR (151 MHz, DMSO) δ 162.1, 150.5, 147.0, 146.9, 143.6, 127.8, 123.6, 121.9, 55.4, 41.6. HR-ESI-MS m/z for $C_{26}H_{26}{}^{69}GaN_{10}O_8$ (M^+) calcd. (found): 675.1191 (675.1183).

3.4.34 [Ga(dedpa-*N,N'*-ethyl-2-nitroimidazole)][ClO_4], [Ga(3.21)][ClO_4]

White solid (73%). ^{1}H NMR (400 MHz, DMSO) δ 8.65 (t, *J* = 7.8 Hz, 2H), 8.32 (d, *J* = 7.6 Hz, 2H), 8.23 (d, *J* = 7.9 Hz, 2H), 7.64 (s, 2H), 7.19 (s, 2H), 5.08 – 4.97 (m, 2H), 4.89 (d, *J* = 17.3 Hz, 2H), 4.73 (d, *J* = 17.5 Hz, 2H), 4.71 – 4.63 (m, 2H), 4.10 (dd, *J* = 10.1, 5.0 Hz, 2H), 3.62 (d, *J* = 11.2 Hz, 2H), 3.25 – 3.19 (m, 2H), 3.04 (d, *J* = 11.3 Hz, 2H). ^{13}C NMR (151 MHz, DMSO) δ 162.1, 150.2, 146.9, 144.7, 143.6, 128.1, 127.9, 127.8, 123.4, 54.7, 49.6, 47.9, 42.9. HR-ESI-MS m/z for $C_{26}H_{26}{}^{69}GaN_{10}O_8$ (M^+) calcd. (found): 675.1191 (675.1202).

3.4.35 [Ga(dedpa-*N,N'*-propyl-2-methyl-5-nitroimidazole)][ClO_4], [Ga(3.22)][ClO_4]

Beige solid (68%). ^{1}H NMR (400 MHz, DMSO) δ 8.69 (t, *J* = 7.8 Hz, 2H), 8.34 (d, *J* = 7.6 Hz, 2H), 8.20 (d, *J* = 8.0 Hz, 2H), 8.09 (s, 2H), 4.68 – 4.55 (m, 4H), 3.85 (t, *J* = 7.2 Hz, 4H), 3.18 (d, *J* = 10.8 Hz, 2H), 2.86 (d, *J* = 11.3 Hz, 2H), 2.77 – 2.59 (m, 4H), 2.30 (s, 6H), 2.23 – 2.10 (m, 2H), 2.08 – 1.94 (m, 2H). ^{13}C NMR (151 MHz, DMSO) δ 162.0, 150.7, 146.8, 145.5, 144.9, 143.7, 127.8, 123.3, 121.6, 55.6, 48.6, 47.9, 44.0, 23.0, 12.6. HR-ESI-MS m/z for $C_{30}H_{34}{}^{69}GaN_{10}O_8$ (M^+) calcd. (found): 731.1817 (731.1812).

3.4.36 [Ga(dedpa-*N,N'*-propyl-4-nitroimidazole)][ClO_4], [Ga(3.23)][ClO_4]

White solid (55%). ^{1}H NMR (400 MHz, DMSO) δ 8.68 (t, *J* = 7.8 Hz, 2H), 8.33 (d, *J* = 7.5 Hz, 2H), 8.25 (s, 1H), 8.18 (d, *J* = 7.9 Hz, 2H), 7.72 (s, 2H), 4.64 (d, *J* = 17.6 Hz, 2H), 4.56 (d, *J* = 17.5 Hz, 2H), 3.94 (t, *J* = 7.1 Hz, 4H), 3.17 (d, *J* = 11.0 Hz, 2H), 2.86 (d, *J* = 11.0 Hz, 2H), 2.77 – 2.65 (m, 2H), 2.65 – 2.54 (m, 2H), 2.31 – 2.17 (m, 2H), 2.16 – 2.01 (m, 2H). ^{13}C NMR (101 MHz, $CDCl_3$) δ 162.0, 150.6, 147.0, 146.7, 143.7, 137.1, 127.8, 123.3, 121.1, 55.6, 45.0, 23.3. HR-ESI-MS m/z for $C_{28}H_{30}{}^{69}GaN_{10}O_8$ (M^+) calcd. (found): 703.1504 (703.1512).

3.4.37 [Ga(dedpa-*N,N'*-propyl-2-nitroimidazole)][ClO_4], [Ga(3.24)][ClO_4]

Off-white solid (58%). ^{1}H NMR (600 MHz, DMSO) δ 8.67 (t, *J* = 7.8 Hz, 2H), 8.36 (d, *J* = 7.6 Hz, 2H), 8.18 (d, *J* = 8.0 Hz, 2H), 7.33 (s, 2H), 7.14 (d, *J* = 0.7 Hz, 2H), 4.59 (q, *J* = 17.4 Hz, 4H), 4.40 – 4.32 (m, 2H), 4.22 – 4.14 (m, 2H), 3.16 (d, *J* = 11.4 Hz, 2H), 2.90 – 2.84 (m, 2H), 2.76 – 2.70 (m, 2H), 2.68 – 2.60 (m, 2H), 2.26 – 2.16 (m, 2H), 2.14 – 2.05 (m, 2H). ^{13}C NMR (151 MHz, DMSO) δ 162.0, 150.7, 146.6, 144.6, 143.8, 127.9, 127.8, 127.2, 123.3, 69.7, 55.4, 47.2, 40.1, 22.6. HR-ESI-MS m/z for $C_{28}H_{30}{}^{69}GaN_{10}O_8$ (M^+) calcd. (found): 703.1504 (703.1497).

3.4.38 [Ga(*CHX*dedpa-*N,N'*-propyl-2-methyl-5-nitroimidazole)][ClO_4], [Ga(3.28)][ClO_4]

White solid (60%). ^{1}H NMR (400 MHz, DMSO) δ 8.66 (t, *J* = 7.8 Hz, 2H), 8.34 (d, *J* = 7.6 Hz, 2H), 8.15 (d, *J* = 7.9 Hz, 2H), 8.01 (s, 2H), 4.93 (d, *J* = 18.4 Hz, 2H), 4.46 (d, *J* = 18.4 Hz, 2H), 3.84 – 3.74 (m, 4H), 3.11 (d, *J* = 7.4 Hz, 2H), 2.69 (dt, *J* = 25.5, 11.6 Hz, 4H), 2.77 – 2.60 (m, 4H), 2.24 (s, 6H), 2.18 (d, *J* = 10.8 Hz, 2H), 1.97 (dd, *J* = 10.7, 6.2 Hz, 2H), 1.72 (d, *J* = 3.9 Hz, 4H), 1.38 – 1.28 (m, 2H), 1.24 (d, *J* = 8.0 Hz, 2H). ^{13}C NMR (101 MHz, DMSO) δ 161.9, 151.5, 146.9, 145.4,

144.9, 143.7, 126.5, 123.4, 121.4, 63.1, 54.7, 50.8, 44.0, 27.1, 25.5, 23.7, 12.5. HR-ESI-MS m/z for $C_{34}H_{40}{}^{69}GaN_{10}O_8$ (M^+) calcd. (found): 785.2286 (785.2280).

3.4.39 [Ga(*CHX*dedpa-*N,N'*-propyl-4-nitroimidazole)][ClO_4], [Ga(3.29)][ClO_4]

White solid (78%). ^{1}H NMR (400 MHz, DMSO) δ 8.67 (t, *J* = 7.8 Hz, 2H), 8.34 (d, *J* = 7.6 Hz, 2H), 8.16 (s, 2H), 8.14 (d, *J* = 8.0 Hz, 2H), 7.64 (s, 2H), 4.94 (d, *J* = 18.4 Hz, 2H), 4.43 (d, *J* = 18.4 Hz, 2H), 3.98 – 3.79 (m, 4H), 3.11 (d, *J* = 7.5 Hz, 2H), 2.77 – 2.63 (m, 4H), 2.15 (d, *J* = 11.0 Hz, 2H), 2.10 – 1.97 (m, 2H), 1.81 – 1.63 (m, 4H), 1.43 – 1.27 (m, 2H), 1.27 – 1.13 (m, 2H). ^{13}C NMR (151 MHz, DMSO) δ 162.0, 151.5, 146.9, 143.7, 137.1, 126.6, 123.5, 121.2, 62.8, 54.9, 51.2, 45.1, 27.0, 26.0, 23.7. HR-ESI-MS m/z for $C_{32}H_{36}{}^{69}GaN_{10}O_8$ (M^+) calcd. (found): 757.1973 (757.1976).

3.4.40 [Ga(*CHX*dedpa-*N,N'*-propyl-2-nitroimidazole)][ClO_4], [Ga(3.30)][ClO_4]

White solid (67%). ^{1}H NMR (600 MHz, DMSO) δ 7.71 (t, *J* = 7.8 Hz, 2H), 7.41 (d, *J* = 7.6 Hz, 2H), 7.18 (d, *J* = 7.9 Hz, 2H), 6.34 (s, 2H), 6.14 (d, *J* = 0.8 Hz, 2H), 3.96 (d, *J* = 18.4 Hz, 2H), 3.47 (d, *J* = 18.5 Hz, 4H), 3.28 – 3.23 (m, 6H), 2.14 (d, *J* = 8.9 Hz, 6H), 1.77 (d, *J* = 8.9 Hz, 8H), 1.19 (d, *J* = 11.1 Hz, 4H), 1.16 – 1.05 (m, 4H), 0.88 – 0.80 (m, 4H), 0.76 (d, *J* = 7.1 Hz, 4H), 0.39 (s, 4H), 0.27 (d, *J* = 14.5 Hz, 6H). ^{13}C NMR (151 MHz, DMSO) δ 162.1, 151.6, 147.0, 144.6, 143.8, 128.0, 127.3, 126.7, 123.6, 69.8, 63.1, 55.1, 51.0, 47.3, 27.2, 25.5, 23.7. HR-ESI-MS m/z for $C_{32}H_{36}{}^{69}GaN_{10}O_8$ (M^+) calcd. (found): 757.1973 (757.1981).

3.4.41 X-ray Crystallography

All solid-state structures were solved by Dr. B. O. Patrick. A pink prism crystal of $C_{26}H_{26}GaN_{10}O_8 \cdot ClO_4$, [Ga(**3.21**)][$ClO_4$], having approximate dimensions of 0.14 x 0.18 x 0.28 mm was mounted on a glass fiber. All measurements were made on a Bruker X8 APEX II diffractometer with graphite monochromated Mo-Kα radiation. The data were collected at a temperature of -173.0 ± 0.1°C to a maximum 2θ value of 60.1°. Data were collected in a series of ϕ and ω scans in 0.50° oscillations with 15.0-second exposures. The crystal-to-detector distance was 39.99 mm. Data were collected and integrated using the Bruker SAINT[141] software package. Data were corrected for absorption effects using the multi-scan technique (SADABS[142]), with minimum and maximum transmission coefficients of 0.800 and 0.855, respectively. The data were corrected for Lorentz and polarization effects. The structure was solved by direct methods.[146] The complex resides on a two-fold rotation axis passing through the Ga-atom, and thus has one half-molecule in the asymmetric unit. Additionally, the perchlorate anion is also disordered about a second two-fold rotation axis. All non-hydrogen atoms were refined anisotropically. All hydrogen atoms were placed in calculated positions.

A colourless tablet crystal of $C_{28}H_{30}GaN_{10}O_{12}Cl$, [Ga(**3.23**)][$ClO_4$], having approximate dimensions of 0.08 x 0.25 x 0.25 mm was mounted on a glass fiber. All measurements were made on a Bruker X8 APEX II diffractometer with graphite monochromated Mo-Kα radiation. The data were collected at a temperature of -173.0 ± 0.1°C to a maximum 2θ value of 58.4°. Data were collected in a series of ϕ and ω scans in 0.50° oscillations with 20.0-second exposures. The crystal-to-detector distance was 40.08 mm. Data were collected and integrated using the Bruker SAINT[141] software package. Data were corrected for absorption effects using the multi-scan technique (SADABS[142]), with minimum and maximum transmission coefficients of 0.760 and 0.931, respectively. The data were corrected for Lorentz and polarization effects.

The structure was solved by direct methods.[146] The material crystallizes with significant disorder to both the complex and the ClO_4 counterion. Additional regions of unresolvable electron density were treated by the PLATON/SQUEEZE[185] program to generate a 'solvent-free' data set. The amount of electrons removed from the entire cell (203) is consistent with approximately 1 solvent CH_3CN molecule per asymmetric unit. All non-hydrogen atoms were refined anisotropically. All hydrogen atoms were placed in calculated positions.

3.4.42 Electrochemical Studies

Cyclic Voltammograms (CVs) were measured using a potentiostat (PINE Instrument Company Model AFCBP1 visualized with AfterMath software) at ambient temperature. All experiments were conducted in a one-compartment 3 mL cell; oxygen was removed by bubbling N_2 gas through the solution prior to taking measurements. Non-aqueous CVs were conducted with Pt mesh counter electrode, Pt wire working electrode and Ag wire pseudo-reference electrode. In addition, 0.10 M Bu_4NClO_4 in DMSO was used as electrolyte solution. Ferrocene was added as an internal potential reference. For aqueous CVs, a Pt mesh counter electrode, glass carbon working electrode (~2 mm diameter), and saturated AgCl in KCl reference electrode were used. The electrolyte solution was 0.10 M KCl (pH 7) in water. Before use, the working electrode was polished with 0.25 μm and 0.05 μm diamond polishing paste, rinsed thoroughly with deionized water, then rinsed with methanol and left to air dry. In most experiments, a 50 μL solution of compound in DMSO was added to 3 mL of electrolyte solution in the cell to give measurement concentrations of 1-5 mM. CVs were recorded at 100 mV/s.

3.4.43 $^{67/68}$Ga Radiolabeling Studies

For initial labeling studies and human *apo*-transferrin challenge assays, all chelators were made up as stock solutions (1 mg/mL, ~10^{-3} M) in deionized water. A 100 μL aliquot of each chelator stock solution was transferred to screw-cap mass spectrometry vials and diluted with pH 4 NaOAc (10 mM for ^{67}Ga or 100 mM for ^{68}Ga) buffer such that the final volume was 1 mL after the addition of $^{67/68}GaCl_3$, to a final chelator concentration of ~10^{-4} M for each sample. An aliquot of $^{67/68}GaCl_3$ (~1 mCi for labeling studies and ~3-6 mCi for *apo*-transferrin competitions) was added to the vials containing the chelator and allowed to radiolabel at ambient temperature for 10 min, then analyzed by RP-HPLC to confirm radiolabeling and calculate yields. Areas under the peaks observed in the HPLC radiotrace were integrated to determine radiolabeling yields. Elution conditions used for RP-HPLC analysis were gradient: A: 10 mM NaOAc buffer, pH 4.5, B: CH_3CN; 0 to 100% B linear gradient 20 min. [^{67}Ga(dedpa-*N,N'*-alkyl-NI)]$^+$ ([^{67}Ga(**3.19-3.24**)]$^+$) (t_R = 8.2 – 9.4 min), [^{67}Ga(*CHX*dedpa-*N,N'*-alkyl-NI)]$^+$ ([^{67}Ga(**3.28-3.30**)]$^+$) (t_R = 10.1 – 11.0 min), free ^{67}Ga (t_R = 2.4 – 3.1 min). Preparation of ^{68}Ga-tracers for log $D_{7.4}$, *in vitro*, and *in vivo* studies was accomplished by adding $^{68}GaCl_3$ solution (0.5 mL in water) to a 4-mL glass vial preloaded with 0.7 mL of HEPES buffer (2 M, pH 5.0) and precursor (100 μg), and allowed to radiolabel at ambient temperature for 10 min. For *in vitro* experiments, no further purification was necessary. For *in vivo* studies, the reaction mixture was purified by semi-preparative RP-HPLC (Phenomenex C18, 5 μ, 250 x 10 mm) eluted with EtOH/PBS (5:95, pH 7.1) at a flow rate of 4.0 mL/min (t_R = 14.0 min).

3.4.44 Human *apo*-Transferrin Stability Data

The procedures closely followed those of a previously published method.[53,59] The radiolabelled complexes [^{67}Ga(**3.19-3.24** or **3.28-3.30**)]$^+$ were prepared with the radiolabeling

protocol as described above. In triplicate for each ^{67}Ga-complex above, solutions were prepared in vials with 500 µL of freshly prepared 1 mg/mL *apo*-transferrin in $NaHCO_3$ (10 mM, pH 7) solution, 300 µL of ^{67}Ga-complex, and 200 µL of phosphate buffered saline (PBS, pH 7.4), and incubated at 37°C in a water bath. At time points 10 min, 1 and 2 hours, 300 µL of the *apo*-transferrin competition mixture was removed from each vial, diluted to a total volume of 2.5 mL with PBS, and then counted in a Capintec CRC 15R well counter to obtain a value for the total activity to be loaded on the PD-10 column (*F*). The 2.5 mL of diluted *apo*-transferrin mixture was loaded onto a PD-10 column that had previously been conditioned via elution with 20 mL of PBS, and the empty vial was counted in a well counter to determine the residual activity left in the vial (*R*). The 2.5 mL of loading volume was allowed to elute into a waste container, and then the PD-10 column was eluted with 3.5 mL of PBS and collected into a separate vial. The eluent which contained ^{67}Ga bound/associated with *apo*-transferrin (size exclusion for MW < 5000 Da) was counted in a well counter (*E*) and then compared to the total amount of activity that was loaded on the PD-10 column to obtain the percentage of ^{67}Ga that was bound to *apo*-transferrin and therefore no longer chelate-bound using the equation: $\left(1 - \frac{E}{(F-R)}\right) \times 100$.

3.4.45 Partition Coefficients

^{68}Ga-labelled complex (30 µCi/6 µL) was added to 1.5 mL centrifuge tubes containing phosphate buffered saline (PBS) (494 µL) and 1-octanol (500 µL), mixed vigorously for 1 minute, and subsequently centrifuged to separate phases (3000 rpm, 5 min). Aliquots (100 µL) of the organic and aqueous phases were transferred and radioactivities counted in a γ-counter (Cobra II Auto Gamma, Packard). Measurements were carried out in triplicate.

3.4.46 *In Vitro* Cell Uptake Study

Cell uptake studies were carried out using LCC6$^{HER\text{-}2}$, HT-29 and CHO cell lines. LCC6$^{HER\text{-}2}$ cells were maintained in DMEM culture medium enriched with 10% fetal bovine serum (FBS) containing 500 µg/mL G148 (Geneticin) (all from Invitrogen), HT-29 cells were maintained in McCoy's 5A medium enriched with 10% FBS, and CHO cells were maintained in DMEM with 10% FBS. All cell lines were maintained in 5% CO_2 in an incubator at 37°C. For normoxic experiments, cells were subcultured for 24 hours in 24-well plates (2 x 10^5 cells/well of HT-29 and CHO, and 1 x 10^5 cells/well of LCC6$^{HER\text{-}2}$). For hypoxic experiments, cells were subcultured in 24-well plates as above for 20 hours, then transferred to a hypoxia chamber (maintained at 0.5 % O_2, remainder: 95% N_2, 5% CO_2); culture medium was replaced with fresh medium that had been allowed to equilibrate under hypoxic conditions overnight, and then the cells were pre-incubated for 4 hours under hypoxic conditions. ^{68}Ga-L_n (5 µCi/100 µL) was added to each well and incubated for 10, 30, 60, or 120 min; samples were carried out in triplicate. The medium was then decanted off, and wells were washed thrice with phosphate buffered saline (PBS), all washings were collected in counting tubes (W). The cells were then lifted with the addition of trypsin, and quantitatively transferred to counting tubes (C). The tracer uptakes were measured using a γ-counter. Percentage uptake was calculated using the equation: $\left(\frac{C}{C+W}\right) \times 100$. Each cell sample ($C$) was then pelleted, lysed (0.5 mL lysis buffer), and total protein concentrations in samples were determined using the bicinchoninic acid (BCA) method (Pierce).

3.4.47 *In Vivo* Imaging and Biodistribution

Animal experiments were approved by the University of British Columbia Animal Care Committee (Vancouver, BC, Canada). Four female immunodeficient Rag2M mice were obtained from an in-house breeding colony at the Animal Resource Centre of the BC Cancer Agency Research Centre. HT-29 tumours were inoculated by injection of 1 x 10^6 cells on the right shoulder of each mouse, and were grown for approx. 14 days. Two mice (for PET/CT imaging followed by biodistribution) were injected with 8.0 MBq, and two mice (for biodistribution only) were injected with 1.7 MBq of ^{68}Ga-labelled tracer.

A 2 hour dynamic PET/CT scan was conducted to determine the time-activity course of the radiopharmaceutical using a Siemens Inveon microPET/CT scanner. Two mice were sedated with 2% isoflurane inhalation and positioned in the scanner side-by-side on a warmed heating pad. A baseline CT scan was obtained for localization and attenuation correction before radiotracer injection.

After 2 hours post-injection, all mice were anesthetized by isoflurane inhalation, and then euthanized by CO_2 inhalation. Blood was promptly withdrawn, and the organs of interest were harvested, rinsed thrice with saline, blotted dry, and inserted into preweighted counting tubes. Tubes were reweighed to obtain exact organ weight. The radioactivity of each collected organ was counted using a γ-counter (Cobra II Auto Gamma, Packard), decay corrected and normalized to the injected dose and expressed as the percentage of injected dose per gram of tissue (%ID/g).

Chapter 4: Evaluation of H_2*CHX*dedpa, H_2dedpa- and H_2*CHX*dedpa-*N,N'*-propyl-2-NI Ligands for Cu(II) Radiopharmaceuticals

4.1 Introduction

Because of the variety and current production of copper isotopes (^{60,61,62,64,67}Cu), incorporation of Cu(II) into a radiopharmaceutical is of great interest in a research and clinical setting. The selection of copper isotopes that can be produced offers a variety of half-lives (0.16 to 62.01 h) and decay properties (β^+, β^-, or EC) which are suitable for diagnostic imaging, radiotherapy, or theranostics.[29,40] The relevant solution properties of Cu(II) were discussed in Chapter 1. Of critical importance to copper-based radiopharmaceuticals is complex stability *in vivo*, since high water-exchange rates of Cu(II) render the corresponding copper complexes particularly susceptible to substitution chemistry.[8,29,40] The development of BFCs which stably bind radio-copper isotopes have been the focus of many reviews[8,25,27,40,108,186] and research efforts have generated some new chelating ligands with promising Cu(II) coordination properties.[72,74,104,127,129,187–189] A cation of borderline hardness, Cu(II) prefers borderline soft donors; as such nitrogen-rich ligands dominate the library of relevant copper chelators (Figure 4.1).

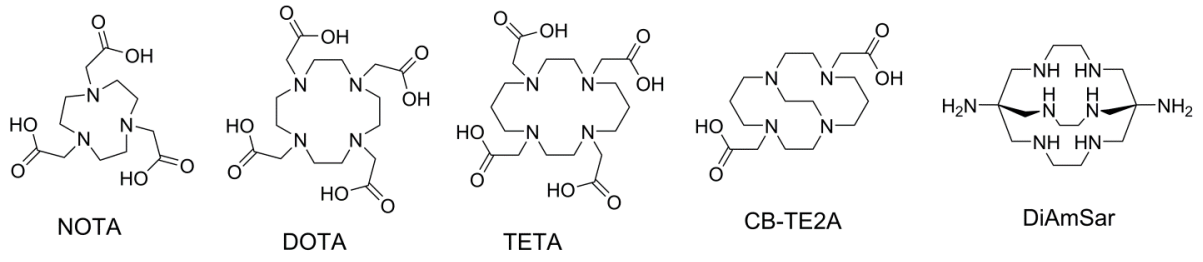

Figure 4.1 Structures of selected chelating ligands (NOTA, DOTA, TETA, CB-TE2A, and DiAmSar) used for labeling with copper isotopes.

Table 4.1 Relevant radiolabeling properties of previously investigated copper ligands.[131]

Ligand		Radiolabeling conditions	Relative stability	Log K_{ML}
NOTA	N_3O_3 (CN = 6)	30 min, 25°C	good	21.6
DOTA	N_4O_4 (CN = 8)	5 min, 25°C	moderate	22.7
TETA	N_4O_4 (CN = 8)	60 min, 25°C	moderate	21.9
CB-TE2A	N_4O_2 (CN = 6)	60 min, 95°C	good	ND[a]
DiAmSar	N_6 (CN = 6)	5-30 min, 25°C	excellent	ND[a]
H_2dedpa	N_4O_2 (CN = 6)	5-10 min, 25°C	moderate/poor	19.2

[a]ND = not determined

Previously, the hexadentate acyclic chelator H_2dedpa and its cRGDyK conjugates were investigated for their coordination potential with Cu(II)/^{64}Cu and found to possess only moderate kinetic inertness and thermodynamic stability (log K_{ML} = 19.16(5)) compared to other relevant Cu(II) ligands (Table 4.1). The decreased serum stability of the conjugates with ^{64}Cu *in vitro* within 24 h renders the dedpa^{2-} complex unsuitable for *in vivo* applications.[131] In Chapter 2, a chiral dedpa^{2-} analogue, H_2*CHX*dedpa, was studied for its coordination potential with Ga(III). The pre-organised donor atoms enforced by the cyclohexanediamine backbone resulted in a metal complex of higher kinetic inertness compared to the achiral analogue H_2dedpa. Herein, we hypothesize that this trend in increased stability of [Ga(*CHX*dedpa)]$^+$ compared to [Ga(dedpa)]$^+$ would transfer to complexes with other metals such as Cu(II). Correspondingly, H_2*CHX*dedpa will be investigated for its coordination capacity with Cu(II). In addition, copper complexes of an *N,N'*-alkylated derivative, H_2*CHX*dedpa-*N,N'*-propyl-2-NI (NI = nitroimidazole) and achiral *N,N'*-alkylated derivative H_2dedpa-*N,N'*-propyl-2-NI will be tested alongside [Cu(*CHX*dedpa)]. The two ligands containing NI motifs, were synthesized and complexed with Ga(III) in Chapter 3, and tested for their potential as ^{68}Ga PET hypoxia imaging agents, given that NI can be reduced and retained exclusively in hypoxic tissue via direct competition with intracellular oxygen concentration. Complexation with Cu(II) of the two NI-containing H_2dedpa and H_2*CHX*dedpa ligands would form neutrally charged complexes. In

general, neutral complexes more readily cross the cell membrane and since the hypoxia trapping ability of the above complexes is dependent on intracellular uptake it was hypothesized that [Cu(*CHX*dedpa-*N,N'*-propyl-2-NI)] and [Cu(dedpa-*N,N'*-propyl-2-NI)] may exhibit superior uptake in hypoxic tissue compared to the analogous mono-cationic Ga-complexes.

4.2 Results and Discussion

4.2.1 Synthesis and Characterization of Copper Complexes

The copper(II) complexes of *CHX*dedpa^{2-}, (dedpa-*N,N'*-propyl-2-NI)$^{2-}$, and (*CHX*dedpa-*N,N'*-propyl-2-NI)$^{2-}$ were prepared by mixing equimolar amounts or $CuCl_2$ with appropriate pro-ligand in aqueous solution. Upon addition of Cu(II), a rapid colour change of the solution from light blue to deep turquoise occurs, additionally, copper complexes of the two *N,N'*-propyl-2-NI containing ligands produced blue precipitates. All three complexes were purified by RP-HPLC to remove excess salts. The paramagnetic Cu(II) complexes obviated NMR spectroscopic data collection. Mass spectrometry easily identified the $[M+H]^+$ or $[M+Na]^+$ peaks which displayed the characteristic isotope distribution associated with $^{63}Cu/^{65}Cu$.

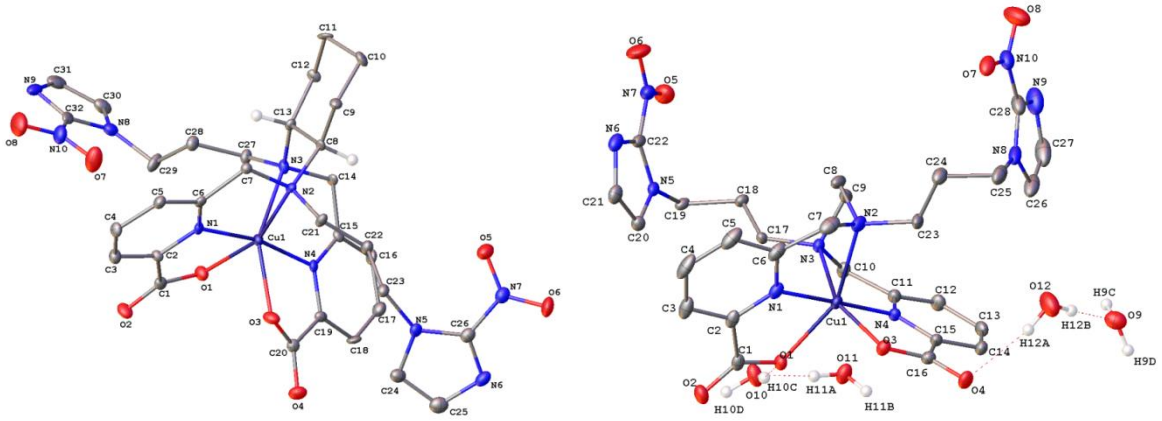

Figure 4.2 Solid state X-ray structure of [Cu(*CHX*dedpa-*N,N'*-propyl-2-NI)] (left) and [Cu(dedpa-*N,N'*-propyl-2-NI)]·4H_2O (right). Ellipsoids drawn at 50% probability.

Deep blue crystals suitable for X-ray diffraction and solid-state structure determination of [Cu(dedpa-*N,N'*-propyl-2-NI)] and [Cu(*CHX*dedpa-*N,N'*-propyl-2-NI)] were obtained through slow evaporation in water and methanol or water and acetonitrile (1:1). Both complexes form distorted octahedral complexes with the N_4O_2 donor atoms from the $dedpa^{2-}$ or *CHX*$dedpa^{2-}$ ligand. A comparison of relevant Cu-L bond lengths of the previously reported [Cu(dedpa)] structure to the two new Cu-complexes presented herein reveals the new structures to exhibit more symmetric bond lengths around the metal ion (Table 4.2). The asymmetric bond lengths in [Cu(dedpa)] were due to Jahn-Teller distortion, typical for octahedral Cu(II) complexes.[131] The individual bond lengths in each pair of related bonds associated with Cu-N_{en}, Cu-N_{pyr}, or Cu-O_{COO} vary in the [Cu(dedpa)] complex, e.g. the Cu-N_{en} bond length values differ by ~0.2 Å (2.317 and 2.136 Å, respectively), whilst the analogous bonds in the [Cu(dedpa-*N,N'*-propyl-2-NI)] and [Cu(*CHX*dedpa-*N,N'*-propyl-2-NI)] complexes appear to be more symmetric, e.g. Cu-N_{en} bond lengths differ by 0.06 and 0.03 Å, respectively.

Table 4.2 Selected bond lengths (Å) and angles (°) in the X-ray structure of [Cu(*CHX*dedpa-*N,N'*-propyl-2-NI)] and [Cu(dedpa-*N,N'*-propyl-2-NI)] with comparison to that of [Cu(dedpa)].[131]

	Complex	[Cu(dedpa)]	[Cu(*CHX*dedpa-*N,N'*-propyl-2-NI)]	[Cu(dedpa-*N,N'*-propyl-2-NI)]
	Bond	Length (Å)	Length (Å)	Length (Å)
$Cu\text{-}N_{en}$	Cu(1)-N(2)	2.3171(13)	2.311(4)	2.3173(14)
	Cu(1)-N(3)	2.1364(13)	2.342(4)	2.2562(13)
$Cu\text{-}N_{pyr}$	Cu(1)-N(1)	2.0008(12)	1.937(4)	1.9664(13)
	Cu(1)-N(4)	1.9386(13)	1.968(4)	1.9263(13)
$Cu\text{-}O_{COO}$	Cu(1)-(O1)	2.3014(11)	2.110(3)	2.2128(12)
	Cu(1)-(O3)	2.0430(10)	2.230(3)	2.0741(11)
	Angle	Degree (°)	Degree (°)	Degree (°)
$N_{pyr}\text{-}Cu\text{-}N'_{pyr}$	N(4)-Cu(1)-N(1)	173.30(5)	168.42(16)	178.59(6)
$N_{pyr}\text{-}Cu\text{-}N_{en}$	N(4)-Cu(1)-N(3)	78.65(5)	77.39(15)	78.45(5)
	N(1)-Cu(1)-N(2)	76.82(5)	78.49(14)	78.01(6)
$N_{pyr}\text{-}Cu\text{-}N'_{en}$	N(1)-Cu(1)-N(3)	104.83(5)	112.92(14)	101.18(5)
	N(4)-Cu(1)-N(2)	109.55(5)	110.03(14)	103.22(6)
$N_{en}\text{-}Cu\text{-}N'_{en}$	N(3)-Cu(1)-N(2)	81.37(5)	76.32(11)	80.04(5)
$N_{pyr}\text{-}Cu\text{-}O'_{COO}$	N(1)-Cu(1)-O(3)	96.18(5)	93.11(14)	99.90(5)
	N(4)-Cu(1)-O(1)	97.86(5)	92.49(14)	100.52(5)

Although not as apparent as in [Cu(dedpa)], the [Cu(dedpa-*N,N'*-propyl-2-NI)] structure also exhibits a small Jahn-Teller distortion evinced through slight elongation of $Cu\text{-}N_{en}(2)$ and Cu-O(1) bonds (2.32 and 2.21 Å, respectively) compared to the remaining Cu-L bond lengths. Similarly, the [Cu(*CHX*dedpa-*N,N'*-propyl-2-NI)] structure shows slightly elongated bonds along $Cu\text{-}N_{en}(3)$ and Cu-O(3) (2.34 and 2.23 Å, respectively) (Figure 4.3).

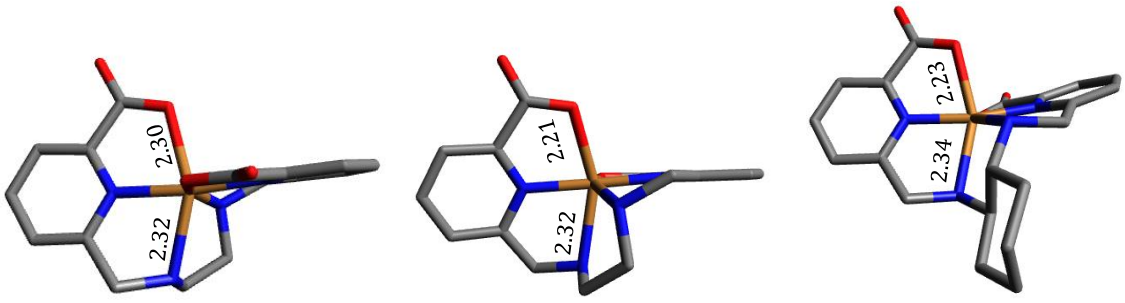

Figure 4.3 Selected bond lengths in side-on view of [Cu(dedpa)][131] (left), [Cu(dedpa-*N,N'*-propyl-2-NI)] (middle) and[Cu(*CHX*dedpa-*N,N'*-propyl-2-NI)] (right), highlighting Jahn-Teller distortion of the Cu(II) d^9 complexes. H atoms, and *N,N'*-propyl-2-NI motifs omitted for clarity.

4.2.2 Electrochemistry

Reasons for evaluating the electrochemical behaviour of the Cu-dedpa complexes were two-fold: firstly, cyclic voltammograms (CVs) were obtained in order to evaluate the reduction potential of the nitroimidazole (NI) motifs to ensure swapping the metal in the coordination complex would not alter the electronic environment of the NI appendages. Secondly, CVs can also give insight into the ability of the Cu(II)-complex to withstand bioreductive-induced decomplexation *in vivo*. The drastically different coordination preferences of Cu(I) and Cu(II) suggests that if reduction of a Cu(II)-complex can occur *in vivo* the Cu(I) products become susceptible to demetallation or disproportionation resulting in loss of radioactive copper *in vivo*.[8,29,190]

The cyclic voltammogram of [Cu(dedpa-*N,N'*-propyl-2-NI)] in DMSO (0.1 M TBAP) displays one irreversible reduction at -0.850 V and one quasi-reversible redox cycle $E_{1/2}$ = -1.068 V (Figure 4.4). The peak cathodic current (i_{pa}) of the first reduction (at -0.850 V) is approximately half the amplitude of the adjacent quasi-reversible couple (-1.068 V) suggesting the first irreversible reduction represents the addition of one electron likely due to reduction of Cu(II) to Cu(I), whilst the second quasi-reversible couple represents a two electron process due to the simultaneous reduction of the two nitroimidazole motifs. Comparing the CV of the analogous Ga-complex reveals that the quasi-reversible $NO_2/NO_2^{\bullet-}$ couple is in alignment with the Cu-complex ($E_{1/2}$ = -1.061 and -1.068 V, respectively) (Figure 4.4). Hence, changing the metal in the coordination complex of (dedpa-*N,N*-propyl-2-NI)$^{2-}$ seems to have negligible effect on nitroimidazole reduction.

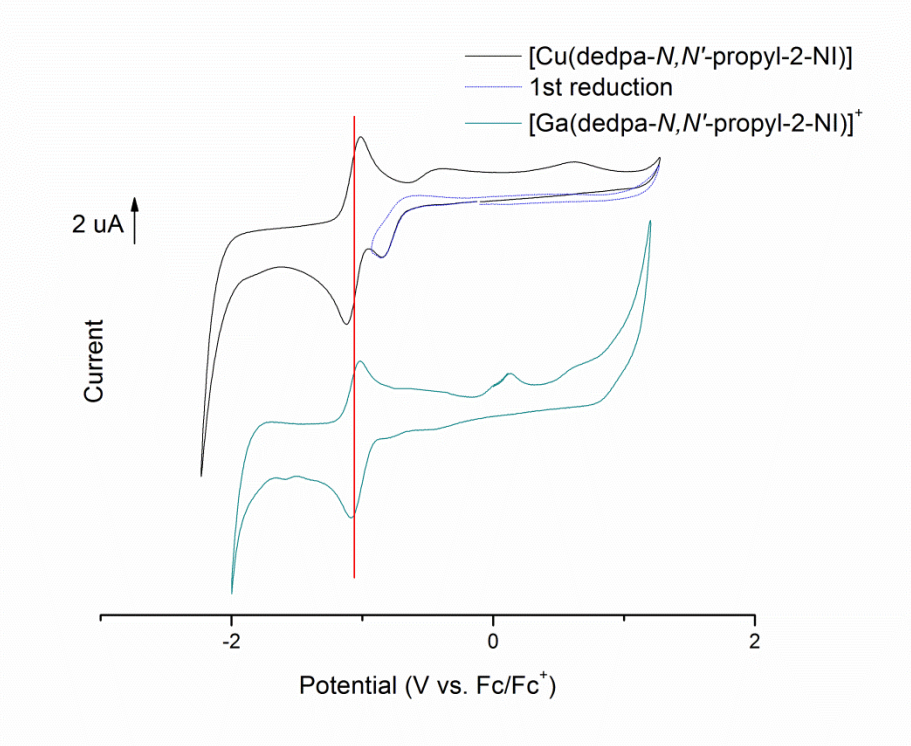

Figure 4.4 Cyclic voltammogram of [Cu(dedpa-*N,N'*-propyl-2-NI)] and [Ga(dedpa-*N,N'*-propyl-2-NI)] for comparison, performed in non-aqueous solvent (DMSO, 0.1 M TBAP, 1- 5 mM complex) with ferrocene added as internal potential standard.

The cyclic voltammogram was found to be reproducible over multiple cycles, without decreasing of intensities of all peaks, including the irreversible peak assigned to Cu(II)/Cu(I) reduction. The reproducibility of the Cu(II)/Cu(I) reduction over multiple reduction and reoxidation cycles implies there is no copper loss throughout the course of the cycles. The previously reported CV data for [Cu(dedpa)] also exhibited an irreversible, but reproducible reduction in aqueous conditions (0.1 M NaOAc, pH 7).[131] It has been previously reported (with Cu(II)-DOTA, -TETA, -CB-DO2A, and –CB-TE2A complexes) that complexes which exhibit irreversible and unreproducible cyclic voltammograms indicate a loss of copper upon reduction.[190]

4.2.3 Acid Mediated Decomplexation Studies

Aqueous acid-assisted decomplexation of [Cu(*CHX*dedpa)] (6 M HCl, 90 °C) was established using HPLC methods previously reported for the [Cu(dedpa)] complex.[131] Much like [Cu(dedpa)], [Cu(*CHX*dedpa)] was found to rapidly dissociate in acid solution ($t_{1/2} \leq 5$ min), suggesting reduced kinetic stability consistent with other Cu-complexes of DOTA, TETA, NOTA, or cyclam. Although being a convenient and frequently-used indicator for the relative kinetic inertness of copper complexes, acid-decomplexation studies do not accurately mimic any relevant *in vivo* environment and their results should also be interpreted with caution. Serum challenge assays with radioactive copper complexes are a more relevant indicator of kinetic inertness *in vivo* and can be analysed at varying time points. Regrettably, at the time of these studies, copper isotopes (^{64}Cu or ^{62}Cu) were not available and consequently radiolabeling of the ligands as well as serum stability assays were not performed.

4.3 Conclusions

The H_2*CHX*dedpa scaffold along with H_2*CHX*dedpa-*N,N*'-propyl-2-NI and H_2dedpa-*N,N*'-propyl-2-NI were investigated for their capability to coordinate Cu(II). The solid-state X-ray structures of [Cu(*CHX*dedpa-*N,N*'-propyl-2-NI)] and [Cu(dedpa-*N,N*'-propyl-2-NI)] revealed the predicted 6-coordinate structure with the Cu(II) ion encapsulated by the N_4O_2 binding sphere of the ligand. Electrochemical studies of [Cu(dedpa-*N,N*'-propyl-2-NI)] revealed a quasi-reversible redox couple in the cyclic voltammogram at -1.068 V (DMSO, vs. Fc/Fc^+) associated with the reduction and reoxidation of the nitroimidazole motifs. A second independent irreversible but reproducible reduction at -0.850 V was associated with the Cu(II) to Cu(I) reduction. Rapid decomplexation of [Cu(*CHX*dedpa)] was observed in an acid-decomplexation reaction ($t_{1/2} \leq 5$

min) at 90 °C suggesting a reduced kinetic inertness compared to other well-known copper ligands such as CB-TE2A which boasts a 154 h half-life with copper (5 M HCl, 90 °C).[190]

The unavailability of copper radioisotopes impeded radiolabeling experiments and subsequent *in vitro* and *in vivo* experiments on H_2*CHX*dedpa, H_2*CHX*dedpa-*N,N'*-propyl-2-NI and H_2dedpa-*N,N'*-propyl-2-NI. Future work should entail such experiments in order to unambiguously evaluate *CHX*dedpa^{2-} as a ligand for Cu radiopharmaceuticals.

4.4 Experimental

4.4.1 Materials and Methods

The materials and methods closely followed those outlined in Chapters 2 and 3. Pro-ligands H_2*CHX*dedpa, H_2*CHX*dedpa-*N,N'*-propyl-2-NI, and H_2dedpa-*N,N'*-propyl-2-NI were synthesized according to Chapters 2 and 3. The HPLC system used for purification of compounds and for analysis of acid-decomplexation studies consisted of a Waters 600 controller, Waters 2487 dual wavelength absorbance detector, and a Waters delta 600 pump. Phenomenex Synergi Hydro-RP 80 Å columns (250 mm x 4.6 mm analytical or 250 mm x 21.2 mm semipreparative) were used for purification of copper complexes and acid-decomplexation studies.

4.4.2 [Cu(*CHX*dedpa)]

H_2*CHX*dedpa·2HCl·2H_2O[176] (17.0 mg, 0.034 mmol) was dissolved in methanol/water (1:3, 1 mL) to which $CuCl_2$·2H_2O (6.2 mg, 0.036 mmol, 1.1 equiv) in water (400 µL) was added. The pH of the deep blue solution was adjusted to ~5 using 0.1 M NaOH (aq), and the reaction

mixture was subsequently stirred overnight. The clear blue solution was purified by semi-preparative RP-HPLC (A: H_2O, B: CH_3CN, 5 – 100% B over 25 min, 10 mL/min, t_R = 13.5 min) and product fractions were pooled and concentrated *in vacuo* to yield the product as a blue solid (12.1 mg, 80%). HR-ESI-MS m/z for $C_{20}H_{23}{}^{63}CuN_4O_4$ ($M+H^+$) calcd. (found) 446.1015 (446.1009) (-1.3 PPM).

4.4.3 [Cu(*CHX*dedpa-*N,N'*-propyl-2-NI)]

H_2*CHX*dedpa-*N,N'*-propyl-2-NI (12.1 mg, 0.018 mmol) was dissolved in methanol/water (500 µL, 1:1), and a solution of $CuCl_2{\cdot}2H_2O$ (3.9 mg, 0.022 mmol, 1.3 equiv) in methanol/water (250 µL, 1:1) was added. The pH of this bright blue solution was adjusted to 6 – 7 with 0.1 M NaOH (aq) and stirred at ambient temperature overnight. The resultant murky blue solution was purified by semi-preparative RP-HPLC (A: H_2O, B: CH_3CN, 5 – 100% B over 25 min, 10 mL/min, t_R = 16.0 min) and product fractions were pooled and concentrated *in vacuo* to yield the product as a blue solid (6.0 mg, 45%). X-ray quality crystals were obtained through slow evaporation in water/CH_3CN (1:1). HR-ESI-MS m/z for $C_{32}H_{36}{}^{63}CuN_{10}O_8Na$ ($M+Na^+$) calcd. (found) 774.1911 (774.1905) (-0.8 PPM).

4.4.4 [Cu(dedpa-*N,N'*-propyl-2-NI)]

H_2dedpa-*N,N'*-propyl-2-NI (29.7 mg, 0.047 mmol) was dissolved in methanol/water (1 mL, 1:1), and a solution of $CuCl_2{\cdot}2H_2O$ (12.4 mg, 0.073 mmol, 1.5 equiv) in methanol/water (500 µL, 1:1) was added. The pH of the resultant bright blue solution was adjusted to 5 and the solution stirred at ambient temperature overnight during which time a blue precipitate formed. The reaction mixture was purified by semi-preparative RP-HPLC (A: H_2O, B: CH_3CN, 5 – 100% B

over 25 min, 10 mL/min, t_R = 14.2 min) and product fractions were pooled and concentrated *in vacuo* to yield the product as a blue solid (14.6 mg, 45%). X-ray quality crystals were obtained through slow evaporation in water/methanol (1:1). HR-ESI-MS m/z for $C_{28}H_{30}{}^{63}CuN_{10}O_8Na$ ($M+Na^+$) calcd. (found) 720.1442 (720.1439) (-0.4 PPM).

4.4.5 Cyclic Voltammetry

The procedures closely followed those of Chapter 3. Cyclic Voltammograms (CVs) were measured using a potentiostat (PINE Instrument Company Model AFCBP1 visualized with AfterMath software) at ambient temperature. All experiments were conducted in a one-compartment 3 mL cell; oxygen was removed by bubbling N_2 gas through the solution prior to taking measurements. CVs were conducted with Pt mesh counter electrode, Pt wire working electrode and Ag wire pseudo-reference electrode. In addition, 0.10 M Bu_4NClO_4 in DMSO was used as electrolyte solution. Ferrocene was added as an internal potential reference. Before use, the working electrode was polished with 0.25 μm and 0.05 μm diamond polishing paste, rinsed thoroughly with deionized water, then rinsed with methanol and left to air dry. In most experiments, a 50 μL solution of compound in DMSO was added to 3 mL of electrolyte solution in the cell to give measurement concentrations of 1-5 mM. CVs were recorded at 100 mV/s.

4.4.6 X-ray Crystallography

All structures were solved by Dr. B. O. Patrick.

A green irregular crystal of $C_{32}H_{37}N_{10}O_8Cu$ ([Cu(*CHX*dedpa-*N,N'*-propyl-2-NI)]) having approximate dimensions of 0.09 x 0.10 x 0.18 mm was mounted on a glass fiber. All measurements were made on a Bruker X8 APEX II diffractometer with graphite

monochromated Mo-Kα radiation. The data were collected at a temperature of -173.0 ± 2°C to a maximum 2θ value of 57.4°. Data were collected in a series of ϕ and ω scans in 0.50° oscillations with 15.0-second exposures. The crystal-to-detector distance was 59.85 mm. The structure was solved by direct methods.[146] The material crystallizes as a twin, with twin law (0 1 0 1 0 0 0 0 -1). The absolute configuration was confirmed on the basis of the refined Flack x-parameter [0.006(6)].[191] All hydrogen atoms were placed in calculated positions. Data were collected and integrated using the Bruker SAINT[141] software package. The linear absorption coefficient, μ, for Mo-Kα radiation is 7.76 cm^{-1}. Data were corrected for absorption effects using the multi-scan technique (SADABS[142]), with minimum and maximum transmission coefficients of 0.817 and 0.933, respectively. The data were corrected for Lorentz and polarization effects. All refinements were performed using the SHELXL-2012[143] via the Olex2[192] interface.

A blue blade crystal of $C_{28}H_{30}N_{10}O_8.4{\cdot}2[H_2O]$ ([Cu(dedpa-*N,N'*-propyl-2-NI)]$2H_2O$) having approximate dimensions of 0.03 x 0.09 x 0.25 mm was mounted on a glass fiber. All measurements were made on a Bruker APEX DUO diffractometer with graphite monochromated Mo-Kα radiation. The data were collected at a temperature of -183.0 ± 0.1°C to a maximum 2θ value of 60.1°. Data were collected in a series of ϕ and ω scans in 0.5° oscillations using 20.0-second exposures. The crystal-to-detector distance was 50.04 mm. The structure was solved using an analogous method as was used above for the previous structure. Additionally, there appears to be a partially occupied water site (with an occupancy of ~0.19). The position of this water seems to induce some disorder in the structure, by virtue of a O—H...N hydrogen bond. All non-hydrogen atoms were refined anisotropically. All O—H hydrogen atoms were located in difference maps and refined isotropically. H-atom coordinates were allowed to refine; however, isotropic thermal parameters were restrained to be 1.5 times that of its water oxygen. The hydrogen atoms on O13 were placed in calculated positions. All other

hydrogen atoms were placed in calculated positions. All refinements were performed using the SHELXL-2013[143] via the OLEX2[192] interface.

4.4.7 Acid-Decomplexation Studies

A solution of 6 M HCl was heated to 90 °C. To solutions of [Cu(*CHX*dedpa)] (2 mg in 100 μL water, one vial per time point) stirring at 90 °C, the preheated 6 M HCl solution was added (200 μL) and 100 μL aliquots were removed from the solution at time points 0, 2, 5, and 10 min and injected into the HPLC equipped with an analytical-grade column (A: H_2O, B: CH_3CN, 5 – 100% B over 25 min, 10 mL/min, t_R (intact copper complex) = 13.5 min). Disappearance of the initial peak indicative of [Cu(*CHX*dedpa)] was monitored. Area under the peaks obtained from the HPLC chromatograms (at 254 nm) were calculated and compared to those of the control (pre-formed [Cu(*CHX*dedpa)] at neutral pH).

Chapter 5: Novel "Bi-modal" H_2dedpa Derivatives for Radio- and Fluorescence Imaging

This chapter is an adaptation of a manuscript in preparation, Ramogida, C. F; Murphy, L.; Cawthray, J. F.; Ross, J. D.; Adam, M. J.; Orvig, C., Novel "bi-modal" H_2dedpa derivatives for radio- and fluorescence imaging. Expected submission date May-June **2015**.

5.1 Introduction

Other than nuclear medicine as a means to image disease, a variety of other imaging modalities are available to the researcher or clinician and have been used to varying success. In addition to nuclear techniques SPECT and PET (which are discussed in detail in Chapter 1), ultrasound, computed tomography (CT), magnetic resonance imaging (MRI), and optical imaging are among the choices for use in clinic. Each modality possesses specific advantages as far as depth penetration, resolution, and image acquisition time (Table 5.1). Fluorescence and nuclear imaging techniques possess characteristics on opposite sides of the spectrum – resolution down to nm scale and real-time imaging can be achieved with optical imaging, where PET and SPECT techniques allow for resolution only in the mm range and relatively long acquisition times are required (several minutes); the use of optical imaging is limited by its minimal penetration in tissue (mm – cm), by contrast nuclear modalities have unlimited penetration allowing whole body imaging.[193,194] The fusion of fluorescent and nuclear modalities into one imaging agent would take advantage of the strengths of each technique. For example, whole-body imaging using radio-imaging via PET to determine localization of the tumour can be supplemented by fluorescence techniques to inform clinicians (through

endoscopy or surgical excision) of tumour boundaries by illuminating the cancerous cells. The synergistic blend of imaging modalities to produce bi-modal and/or multi-modal agents has been acknowledged as a promising new facet of molecular imaging with broadened applicability, and has been extensively reviewed.[193–195] Specifically, the development of bimodal radio- and fluorescent imaging probes is emerging as a potentially powerful new technique.[196,197]

Table 5.1 Comparison of imaging modalities with corresponding penetration through tissue, resolution of technique, and acquisition timescale.[193]

Modality	**Penetration**	**Resolution**	**Timescale for acquisition/ observation**
CT	whole body	μm	min
MRI	whole body	μm	min-hour
PET	whole body	mm	min-hour
SPECT	whole body	mm	min-hour
Fluorescence microscopy (optical)	mm – cm	nm	sec
Ultrasound	whole body except lungs	μm	sec

In this chapter, a bi-modal H_2dedpa derivative has been prepared for the first time. This novel compound possesses two attached fluorophores suitable for fluorescence microscopy imaging, and retains the N_4O_2 binding sphere provided by the H_2dedpa ligand for coordination to $^{68}Ga^{3+}$ for PET imaging. A second analogue which also contains two 2-nitroimidazole (2-NI) moieties was also prepared to investigate the specific uptake of the probe in hypoxic tissue, given that 2-NI can be reduced and retained exclusively in hypoxic cells via direct competition with intracellular oxygen concentration. The 2-NI trapping mechanism was discussed in detail in Chapters 3 and 4. Much effort has been made by others to make a fluorescent probe of hypoxia.[157,198–201] The ability of the new H_2dedpa BFCs to label gallium isotopes was investigated, followed by assessment of their kinetic inertness via an *apo*-transferrin stability

assay. Finally, the optical properties of the novel "bi-modal" probes were evaluated in a 3D tumour spheroid *in vitro* model with confocal fluorescence microscopy.

5.2 Results and Discussion

5.2.1 Synthesis and Characterization of Pro-ligands and Metal Complexes

Scheme 5.1 Synthesis of novel pyridyl-functionalized H_2dedpa BFCs H_2dedpa-propyl$_{pyr}$-NH_2 (**5.8**) and H_2dedpa-propyl$_{pyr}$-NH_2-(*N,N*'-propyl-2-NI) (**5.10**).[a]

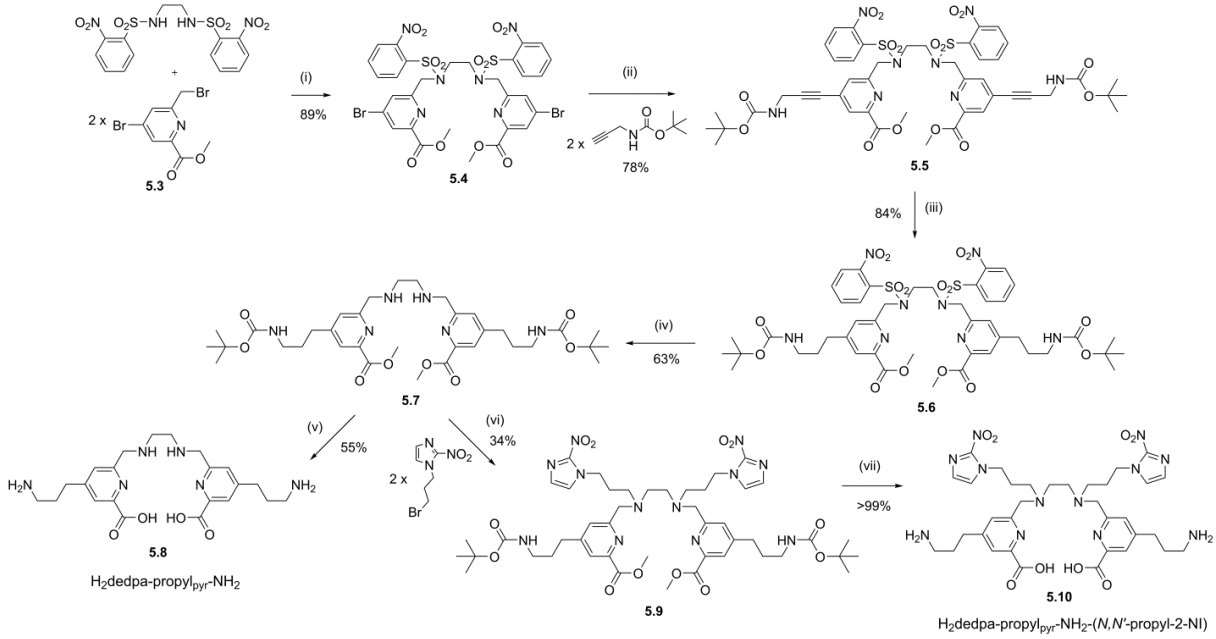

[a] Reagents and conditions: (i) DMF, Na_2CO_3, RT, 3 d; (ii) THF, Et_3N, $Pd(PPh_3)_2Cl$, CuI, N_2, 60°C, 18 h; (iii) EtOAc, Pd/C, H_2, RT, 2 x 24 h; (iv) THF, thiophenol, K_2CO_3, RT, 4 d; (v) THF/water (3:1), LiOH, RT, 1 h, then 4 M HCl/dioxane/THF (3:2:1), RT, 18 h; (vi) CH_3CN, K_2CO_3, 55°C, 4 d; (vii) same as (v).

In an attempt to fully harness the potential of H_2dedpa for radiopharmaceutical elaboration, much effort has been made towards developing new and facile synthetic routes towards preparation of bifunctionalized analogues of the native unfunctionalized scaffold.

These bifunctional chelating ligands (BFCs) should possess reactive groups for bioconjugation to targeting vectors. Herein, a novel BFC based on the strong Ga(III) chelate H_2dedpa has been developed (compound **5.8**) where bis-functionalization has been introduced through the 4-position of each pyridyl group (Scheme 5.1).

Preparation of the novel BFC (**5.8**), began with the conversion of chelidamic acid to methyl 4-bromo-6-(bromomethyl)picolinate (**5.3**) in three steps (55% overall yield). This bromo-picolinate was used in *N*,*N*'-alkylation of 2-nitrobenzenesulfonamide (nosyl) protected ethylenediamine[59] to yield **5.4** in high yield (89%). The di-bromo substituents on the nosyl-protected Me_2dedpa precursor **5.4** were cross-coupled to *tert*-butyl-prop-2-yn-1-ylcarbamate (Boc-N propargylamine) using Sonogashira methodology to yield **5.5** (78% yield). In order to prevent unwanted nucleophilic addition of thiophenol to the alkynes, the alkyne bonds were reduced under mild conditions (10% Pd on activated carbon, H_2) to produce the analogous alkane product **5.6** (84% yield) before nosyl-deprotection was performed. The alkyne reduction reaction was monitored closely and quenched before reduction of the nitro moieties off the nosyl groups began. Both nosyl groups were removed through the addition of thiophenol under basic conditions to yield protected pro-ligand **5.7** (63% yield). Methyl ester and N-Boc deprotections were performed in one-pot to yield the novel bifunctional H_2dedpa analogue H_2dedpa-propyl$_{pyr}$-NH_2 (**5.8**) (26% overall yield in 5 steps). Compound **5.8** contains two primary amines as reactive sites for further conjugation to biomolecules.

The protected pro-ligand **5.7** was also further functionalized off the secondary amines with 1-(3-bromopropyl)-2-nitroimidazole, followed by complete deprotection to give **5.10**; this scaffold now contains 2-nitroimidazoles, which are common trapping moieties in hypoxic tissue as seen in Chapters 3 and 4, as well as two primary amines situated off the 4-position of the pyridyl rings which can be used in further bioconjugation reactions.

Scheme 5.2 Synthesis of bi-modal H_2dedpa derivatives H_2dedpa-propyl$_{pyr}$-FITC (**5.11**) and H_2dedpa-propyl$_{pyr}$-FITC-(*N,N'*-propyl-2-NI) (**5.12**) and corresponding Ga-complexes.

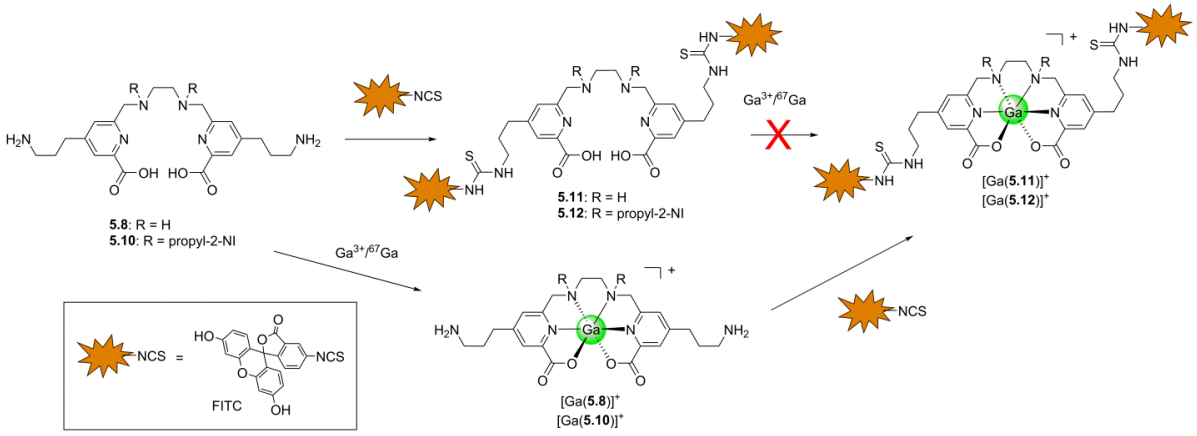

As a proof-of-principle, fluorescein isothiocyanate (FITC) was conjugated to the reactive primary amines of BFCs **5.8** and **5.10** (Scheme 5.2) through thiourea bond formation, to generate "bi-modal" imaging probes. FITC is a commercially available fluorophore ($\lambda_{ex}/\lambda_{em}$ = 490/525 nm) used commonly as a dye in fluorescence microscopy and cell biology because of its high absorptivity, excellent fluorescence quantum yield, and good water solubility. The pro-ligand **5.11** contains both the promising backbone H_2dedpa (N_4O_2) for chelation to radiometals $^{67/68}$Ga, as well as the fluorophore FITC for optical imaging. Similarly, **5.12** also contains both the chelating backbone (N_4O_2) and fluorophore, but also 2-nitroimidazole moieties which will act as hypoxia targeting/trapping vectors.

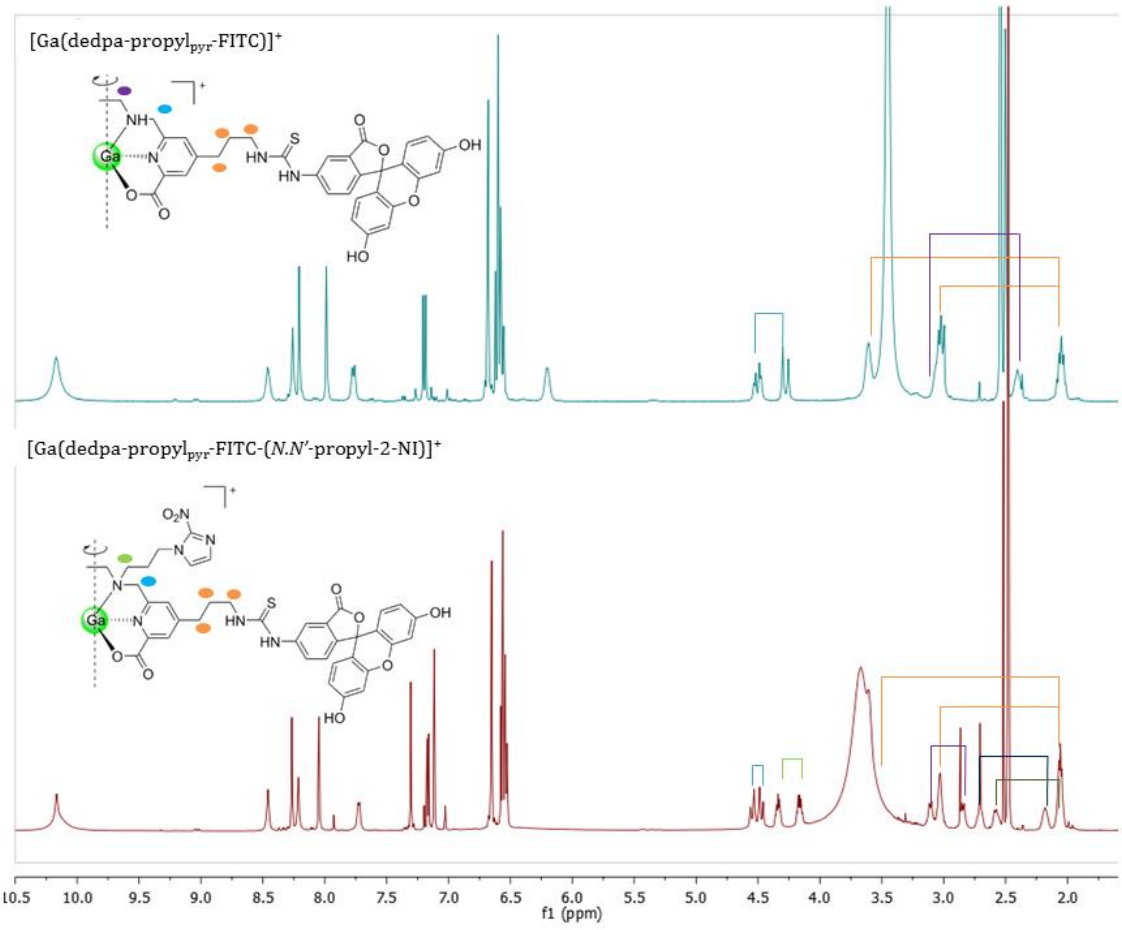

Figure 5.1 ^{1}H NMR spectra of (top) [Ga(dedpa-propyl$_{pyr}$-FITC)]$^+$ ([Ga(**5.11**)]$^+$) and (bottom) [Ga(dedpa-propyl$_{pyr}$-FITC-(*N,N'*-propyl-2-NI)]$^+$ ([Ga(**5.12**)]$^+$) in DMSO-d$_6$ (400 MHz, 25°C) highlighting diastereotopic splitting due to gallium complexation.

Complexation of each pro-ligand (**5.11** and **5.12**) with non-radioactive gallium was also attempted, but was unsuccessful. No evidence of metal complexation was observed by ESI-MS, NMR, or HPLC analysis, even when the reaction mixture was heated to reflux overnight. Instead, the 'fluorophore-free' precursors **5.8** and **5.10** were allowed to complex with Ga(III) under the mild conditions previously used for unfunctionalized H_2dedpa (Scheme 5.2). The Ga-precursors [Ga(**5.8**)]$^+$ and [Ga(**5.10**)]$^+$ were isolated and fully characterized by HR-ESI-MS, and NMR spectroscopy. Diagnostic diastereotopic splitting of hydrogens in the ethylenediamine bridge was tracked by NMR spectroscopy. These two Ga-complexes were then successfully conjugated

to FITC under basic conditions, and purified by RP-HPLC to give [Ga(**5.11**)]$^+$ and [Ga(**5.12**)]$^+$ as bright yellow solids. Again, the diastereotopic splitting of hydrogens in the metal complexes was identified in the ^{1}H NMR spectrum (Figure 5.1). The absorption and emission spectra of [Ga(dedpa-propyl$_{pyr}$-FITC)]$^+$, [Ga(**5.11**)]$^+$, revealed excitation and emission peaks at 492 and 527 nm respectively (Figure 5.2), which are typical for wavelengths of the FITC dye.

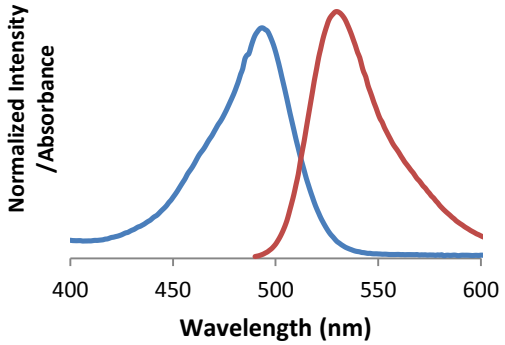

Figure 5.2 Excitation (blue) and emission (red, λ_{ex} = 490 nm) spectra of [Ga(**5.11**)]$^+$, [Ga(dedpa-propyl$_{pyr}$--FITC)]$^+$, in PBS (pH 7.4).

5.2.2 ^{67}Ga Radiolabeling Studies

As was done in previous chapters (2 and 3), the γ-emitter ^{67}Ga ($t_{1/2}$ = 3.26 d) was used in initial radiolabeling studies of the novel bi-modal ligands **5.11** and **5.12** to determine their abilities to complex gallium isotopes. Unfortunately, neither fluorescent ligand (**5.11** or **5.12**) displayed any ^{67}Ga labeling (radiochemical yield ~0%) under 10 min and room temperature reaction conditions. Extended reaction times and elevated temperatures (1 h, 85°C) did not result in an increase in radiolabeling yield. Although disappointing, this result was not surprising since direct complexation of the ligands **5.11** and **5.12** with non-radioactive gallium

was also futile (*vide supra*). It is hypothesized that the added structural 'bulk' introduced by two fluorescein molecules (MW = 389.3 ea.) dangling from the 4-position of each pyridyl ring impedes the movement/reorganization of donor atoms of the metal binding sphere of the linear H_2dedpa chelate, thus obstructing metal complexation.

Consequently, precursors without the fluorescent probe (**5.8** and **5.10**) were labelled with ^{67}Ga as a model. Both displayed quantitative ^{67}Ga labeling (RCY > 99%) under reaction conditions commensurate with unfunctionalized H_2dedpa and its 2-NI derivatives found in Chapter 3 (10 min at room temperature, 10^{-4} to 10^{-5} M ligand).

5.2.3 Human *apo*-Transferrin Stability Studies

Because radiolabeling of the final 'bi-modal' probes **5.11** and **5.12** was unsuccessful, ^{67}Ga-labelled precursors **5.8** and **5.10** were tested in a human *apo*-transferrin stability assay, and were used as a model to assess the kinetic inertness of the bi-modal H_2dedpa derivatives. The unaltered H_2dedpa ligand previously demonstrated exceptional stability in a human *apo*-transferrin stability assay remaining >99% intact after 2 h,[54] this result is compared to ligand **5.8** from this work where propyl linkers in the 4-position of the pyridyl rings have been added to introduce bifunctionality of the native H_2dedpa scaffold (Table 5.1). [^{67}Ga(**5.8**)]$^+$ exhibited slightly reduced stability after 2 h compared to [^{67}Ga(dedpa)]$^+$ (93 versus >99% intact). A similar trend was seen when comparing analogues which include 2-NI moieties (**5.10** and H_2dedpa-*N,N'*-propyl-2-NI): [^{67}Ga(**5.10**)]$^+$ was approximately 27% less stable than the corresponding complex in which there is no pyridyl functionalization ([^{67}Ga(dedpa-*N,N'*-propyl-2-NI)]$^+$). These results suggest that functionalization of H_2dedpa at the 4-position of the pyridyl rings leads to complexes of (somewhat) reduced kinetic inertness. The propyl linker serves as a weak electron donor and introduces some degree of steric 'bulk' around the metal binding

pocket of the ligand. These steric and electronic effects imposed by the addition of the alkyl linker seemed to have translated to ligands of reduced stability compared to their unfunctionalized analogues.

Table 5.1 *apo*-Transferrin stability challenge assay (37°C, 2 h) of ^{67}Ga-labelled pyridyl-functionalized dedpa^{2-} ligands **5.8** and **5.10**, and non-functionalized dedpa^{2-} standards for comparison, with stability shown as the percentage of intact ^{67}Ga complex.

Complex	15 min (%)	1 h (%)	2 h (%)
[^{67}Ga(**5.8**)]$^{+}$	99.0 ± 0.9	92.3 ± 2.3	92.7 ± 2.2
[^{67}Ga(**5.10**)]$^{+}$	87.8 ± 3.1	82.3 ± 2.4	72.4 ± 2.0
[^{67}Ga(dedpa)]$^{+}$ [54]	>99	>99	>99
[^{67}Ga(dedpa-*N,N*-propyl-2-NI)]$^{+}$ [a]	97.6 ± 1.2	97.2 ± 0.9	>99

[a]Previously reported values from Chapter 3.

5.2.4 *In Vitro* 3D Spheroid Imaging

The uptakes of the novel fluorescent Ga-dedpa probes were tested in a multicellular spheroid model and visualized using confocal microscopy. Spheroids are multicellular 3-dimensional structures of cancerous cells that act as *in vitro* tumour models.[202] Multicellular spheroids can effectively simulate the features of solid tumours *in vivo* such as tumour micro-environment, cell-cell interactions, and the extracellular matrix; accordingly, they have found great utility for screening of potential drug candidates.[203–206] It has been shown that cells on the periphery of the spheroid actively proliferate and act as well-oxygenated healthy (normoxic) cells, while diffusion of oxygen near the centre of the spheroid is limited and hence cells at the centre are hypoxic.[206] Thus 3D spheroids are a good model for visualising the distribution and targeting ability of fluorescent drugs in hypoxic conditions.

Spheroids were dosed with both Ga-complexes, [Ga(**5.11**)]$^{+}$ and [Ga(**5.12**)]$^{+}$ at concentrations of 50, 10, and 2.5 μM and incubated for 1, 2, or 4 hours to track the course of fluorescence uptake over time. The only difference between these two fluorescent probes is the

addition of two 2-NI moieties on [Ga(**5.12**)]$^{+}$. It was hypothesized that the addition of hypoxia trapping functionalities onto [Ga(**5.12**)]$^{+}$ would result in specific uptake of the fluorescent probe in the hypoxic core of the spheroid, whilst [Ga(**5.11**)]$^{+}$ would display no such preference in cell uptake. Pro-ligands, **5.11** and **5.12**, and FITC were also dosed as controls. After removal of excess fluorescent probe and washing of spheroids with phosphate buffered saline, each was imaged using fluorescence confocal microscopy. Spheroids used for imaging were grown for either 5 or 7 days. As spheroids mature their cells pack more densely in the core resulting in reduced oxygen diffusion near the centre of the spheroid, hence older spheroids tend to be more hypoxic.[202]

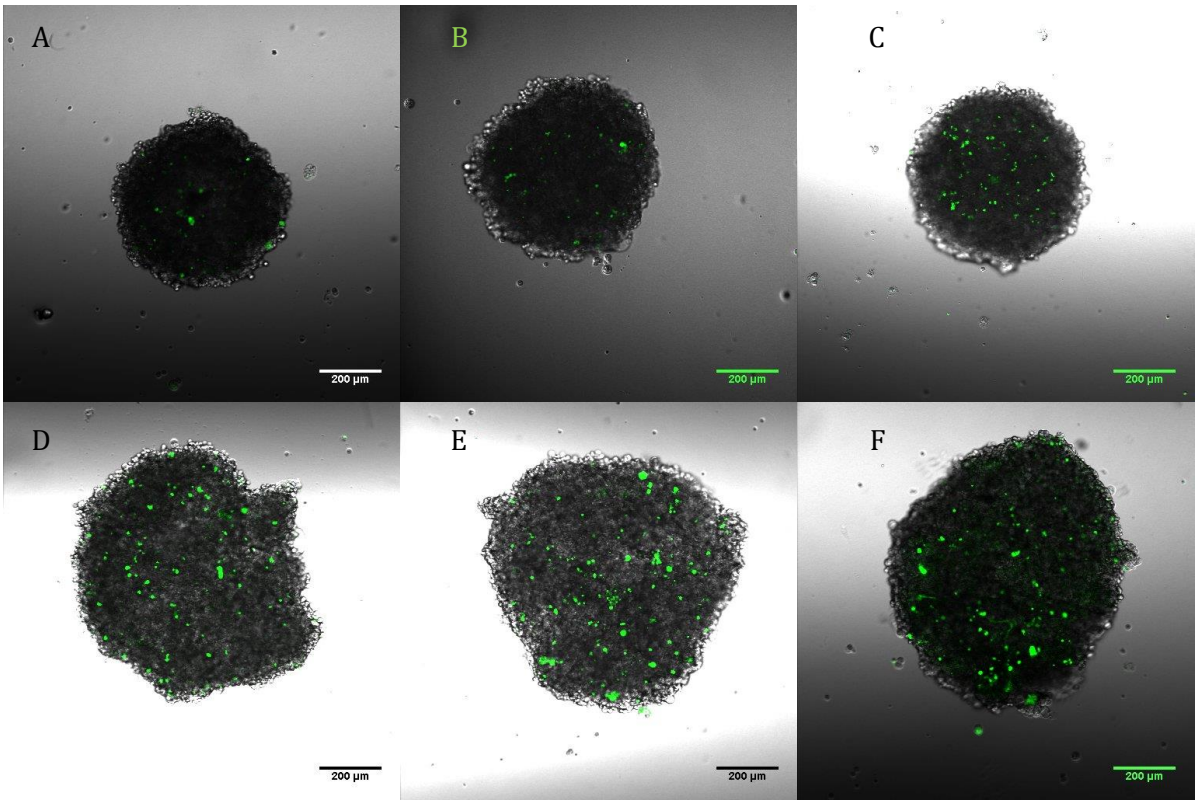

Figure 5.3 Overlaid fluorescence (green) and optical (grey) images of 3D tumour spheroids (5 days old) treated with 10 µM [Ga(dedpa-propyl$_{pyr}$-FITC-(*N*,*N*'-propyl-2-NI))]$^{+}$, [Ga(**5.12**)]$^{+}$ (top row) or [Ga(dedpa-propyl$_{pyr}$-FITC)]$^{+}$, [Ga(**5.11**)]$^{+}$ (bottom row) incubated for (A,D) 1h, (B,E) 2 h, or (C,F) 4 h.

Spheroids (grown for 5 days) treated with [Ga(dedpa-propyl$_{pyr}$-FITC-(*N,N'*-propyl-2-NI))]$^+$ yielded confocal microscopy images with slight observable uptake of tracer, but no discernable elevated uptake of the 2-NI probe in the central hypoxic core of the spheroid over the course of 4 hours (Figure 5.3). Fluorescence images of 'negative control' [Ga(dedpa-propyl$_{pyr}$-FITC)]$^+$ exhibited some non-specific uptake evinced by even distribution of fluorescence throughout the spheroid over the course of 4 hours. Due to the qualitative nature of the fluorescent images, it was impossible to discern real differences in probe uptake between [Ga(**5.11**)]$^+$ and [Ga(**5.12**)]$^+$ with 5 day old spheroids. Nonetheless, the results show that the novel fluorescent probes [Ga(**5.11**)]$^+$ and [Ga(**5.12**)]$^+$ were successfully imaged using fluorescence confocal microscopy in an *in vitro* 3D spheroid model.

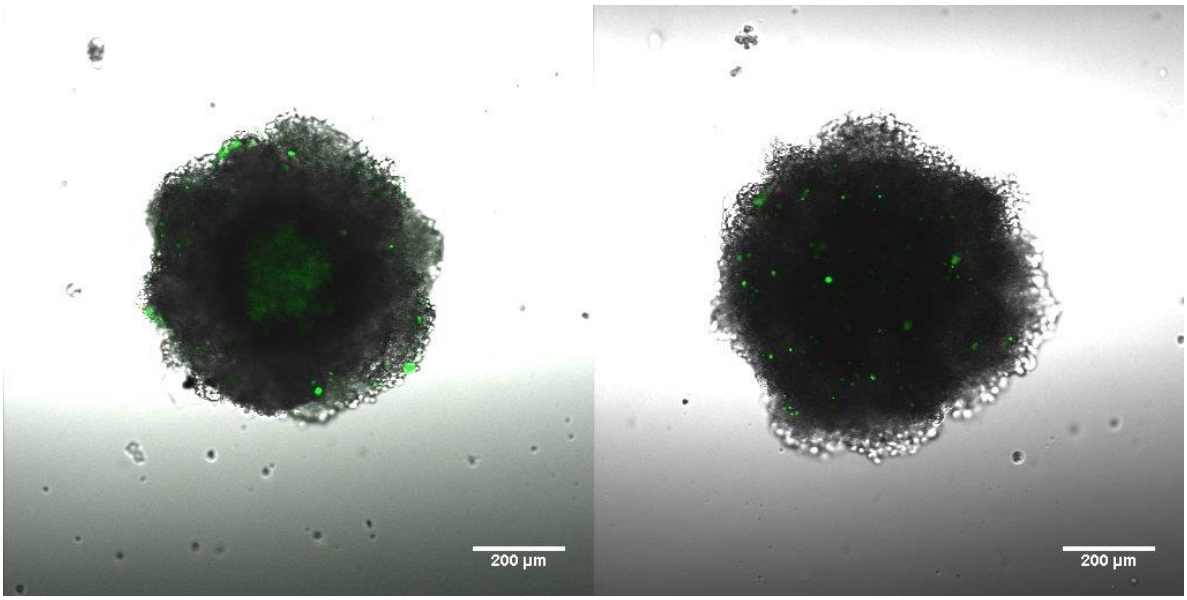

Figure 5.4. Overlaid fluorescence (green) and optical (grey) images of 3D tumour spheroids (7 days old) dosed with (left) [Ga(dedpa-propyl$_{pyr}$-FITC-(*N,N'*-propyl-2-NI))]$^+$, [Ga(**5.12**)]$^+$, (right) negative control [Ga(dedpa-propyl$_{pyr}$-FITC)]$^+$, [Ga(**5.11**)]$^+$ (10 µM complex for 2 h). Highlighting elevated uptake of 2-NI fluorescent probe (left) in the central hypoxic core of the spheroid, compared to the negative control compound without 2-NI moieties (right).

Spheroids grown for 7 days were similarly treated with 10 μM of both [Ga(dedpa-propyl$_{pyr}$-FITC-(*N,N'*-propyl-2-NI))]$^+$ and [Ga(dedpa-propyl$_{pyr}$-FITC)]$^+$ for 2 hours. It is evident that the 2-NI-containing probe ([Ga(**5.12**)]$^+$) exhibits elevated and concentrated localization near the central hypoxic core of the spheroid compared to the negative control [Ga(**5.11**)]$^+$ which displays only some residual non-specific uptake distributed evenly throughout the spheroid (Figure 5.4). These results clearly demonstrate the ability of [Ga(dedpa-propyl$_{pyr}$-FITC-(*N,N'*-propyl-2-NI))]$^+$ to specifically localize at the hypoxic region within the spheroid model. The evident difference between probe uptakes in 5 or 7 day old spheroids may suggest that younger spheroids (5 days old) are not sufficiently hypoxic to warrant 2-NI trapping.

5.3 Conclusions

Herein we report the preparation of a novel bifunctional analogue of the promising Ga(III) chelate H_2dedpa using Sonogashira cross-coupling chemistry. This H_2dedpa bifunctional chelate (BFC) has been altered to encompass two propyl-NH_2 functionalities at the 4-position of each pyridyl ring (H_2dedpa-propyl$_{pyr}$-NH_2). The two primary amines in the H_2dedpa BFC **5.8** are sufficient for bioconjugation to targeting vectors bearing compatible reactive groups, such as an isothiocyanate. This new BFC was used in a conjugation reaction with the commercially available fluorophore FITC to generate a fluorescent H_2dedpa conjugate, as proof-of-principle. This "bi-modal" agent was evaluated for its potential as a combined ^{68}Ga PET and optical fluorescent imaging agent. A second H_2dedpa analogue, which also contains two 2-NI moieties as a hypoxia marker in addition to the FITC fluorophore, was also successfully synthesized and characterized.

The addition of bulky fluorophores suspended off each pyridyl ring of H_2dedpa precluded metal-complexation, and consequently resulted in unsuccessful ^{67}Ga radiolabeling.

This result will ultimately limit the utility of these novel H_2dedpa fluorescent probes in future studies. Still, the 'fluorescent-free' precursors **5.8** and **5.10** were successfully radiolabelled with ^{67}Ga (>99% RCY, 10 min, RT), suggesting the new BFC, H_2dedpa-propyl$_{pyr}$-NH_2 (**5.8**), may be a promising candidate for conjugation with other lighter molecular weight targeting vectors. Human *apo*-transferrin stability assays of ^{67}Ga-labelled radiotracers **5.8** and **5.10** indicated that these BFCs form gallium complexes of good to moderate stability (93 and 72% intact after 2 h, respectively).

For the first time a novel fluorescent H_2dedpa derivative was synthesized, characterized, and successfully imaged using confocal fluorescence imaging in an *in vitro* 3D spheroid model. Fluorescence imaging using spheroids treated with a derivative in which the hypoxia marker 2-nitroimidazole was integrated resulted in specific localization of the fluorescent tracer in the central hypoxic core of the spheroid.

5.4 Experimental

5.4.1 Materials and Methods

The materials and methods follow closely those outlined in Chapters 2 through 4. Fluorescein isothiocyanate (FITC) was purchased from Sigma-Aldrich and used as received.

5.4.2 Dimethyl 4-bromopyridine-2,6-dicarboxylate (5.1)

Compound **5.1** was prepared via a slightly modified version from previously published.[207] Chelidamic acid monohydrate (2.20 g, 10.9 mmol) and PBr_5 (23.4 g, 54.3 mmol, 5 equiv) were heated neat to 90°C under N_2 for 2 hours. The deep red melt was then cooled to

room temperature, and $CHCl_3$ (25 mL) was added. The solution was filtered, and filtrate was cooled on ice (0°C), while methanol (90 mL) was slowly added. Crystallization was induced with scratching, and the crystalline solid was collected by vacuum filtration and further dried under vacuum to yield **5.1** as a crystalline white solid (2.82 g, 86%). ^{1}H NMR (300 MHz, $CDCl_3$) δ 8.45 (s, 2H), 4.02 (s, 6H).

5.4.3 Methyl 4-bromo-6-(hydroxymethyl)picolinate (5.2)

Compound **5.1** (5.61 g, 20.5 mmol) was stirred in methanol/CH_2Cl_2 (200 mL: 50 mL) on ice (0°C), and $NaBH_4$ (1.17 g, 30,8 mmol, 1.5 equiv) was added in small portions. The reaction mixture was stirred at 0°C for 1.5 hours, until complete by TLC (R_f (product) = 0.5, R_f (starting material) = 0.63 in 100% ethyl acetate), subsequently quenched with sat. $NaHCO_3$ (100 mL), and phases separated. The aqueous phase was extracted further with CH_2Cl_2 (4 x 50 mL); all organics were collected, dried over $MgSO_4$ and concentrated *in vacuo* to yield the crude product **5.2** as a white solid (4.79 g, 95%). The product was used in the next step without purification.

5.4.4 Methyl 4-bromo-6-(bromomethyl)picolinate (5.3)

Compound **5.2** (4.79 g, 19.5 mmol) was suspended with stirring in $CHCl_3$ (220 mL) at 0°C. To this solution, PBr_3 (2.94 mL, 31.1 mmol, 1.6 equiv) was added, and the mixture was stirred at room temperature for 3.5 hours. The yellow solution was subsequently cooled to 0°C, and quenched with aq. K_2CO_3 (200 mL). The organic phase was separated, and the aqueous layer was further extracted with CH_2Cl_2 (2 x 120 mL). The organics were collected, dried over $MgSO_4$ and concentrated *in vacuo*. The crude solid was purified by column chromatography (CombiFlash R_f automated column system; 80 g HP silica; A: hexanes, B: ethyl acetate, 100% A

to 100% B gradient) to yield **5.3** as a white solid (4.27 g, 67%). ^{1}H NMR (400 MHz, $CDCl_3$) δ 8.21 (d, *J* = 1.6 Hz, 1H), 7.86 (d, *J* = 1.6 Hz, 1H), 4.59 (s, 2H), 4.02 (s, 3H). ^{13}C NMR (101 MHz, $CDCl_3$) δ 164.39, 158.74, 148.69, 134.78, 130.31, 128.03, 53.50, 32.24. MS (ES+) m/z = 310.1 $[M+H]^+$.

5.4.5 Dimethyl 6,6'-((ethane-1,2-diylbis(((2-nitrophenyl)sulfonyl)azanediyl))bis(methylene))bis(4-bromopicolinate) (5.4)

Compound **5.3** (889 mg, 2.88 mmol, 2 equiv) and *N,N'*-(ethane-1,2-diyl)bis(2-nitrobenzenesulfonamide)[59] (619 mg, 1.44 mmol) were dissolved in dimethylformamide (7 mL), and Na_2CO_3 (915 mg, 8.64 mmol, 6 equiv) was added. The reaction mixture was stirred at room temperature for 3 days; subsequently diethyl ether (20 mL) and water (20 mL) were added. The white precipitate that formed upon addition was collected by vacuum filtration, washed with excess water and diethyl ether, and further dried under vacuum to yield **5.4** as a white solid (1.13 g, 89%). ^{1}H NMR (300 MHz, $CDCl_3$) δ 8.06 (m, 4H), 7.65 (m, 8H), 4.73 (s, 4H), 3.95 (d, *J* = 11.8 Hz, 6H), 3.60 (s, 4H). ^{13}C NMR (101 MHz, DMSO) δ 163.6, 157.9, 147.9, 147.5, 134.7, 133.6, 132.5, 131.4, 130.0, 128.5, 126.5, 124.4, 52.8, 52.1, 47.4. HR-ESI-MS m/z for $C_{30}H_{26}{}^{79}Br_2N_6NaO_{12}S_2$ $(M+Na^+)$ calcd. (found) 906.9315 (906.9296).

5.4.6 Dimethyl 6,6'-((ethane-1,2-diylbis(((2-nitrophenyl)sulfonyl)azanediyl))bis(methylene))bis(4-(3-((tert-butoxycarbonyl)amino)prop-1-yn-1-yl)picolinate) (5.5)

Compound **5.4** (420 mg, 0.47 mmol) was suspended in freshly distilled THF (20 mL) and triethylamine (8 mL) in a Schlenk flask under N_2. The vessel underwent three freeze-pump-thaw cycles to eliminate any oxygen, then *tert*-butyl prop-2-yn-1-ylcarbamate (273 mg, 1.76 mmol, 3.7 equiv), bis(triphenylphospine)palladium(II) dichloride (33 mg, 0.047 mmol, 10

mol%), and copper iodide (18 mg, 0.095 mmol, 20 mol%) were all added quickly. The flask was heated to 60°C and stirred overnight. The resultant murky brown solution was cooled to room temperature, filtered, washed with CH_2Cl_2 and concentrated *in vacuo*. The crude product was purified by column chromatography (CombiFlash R_f automated column system; 24 g HP silica; A: hexanes, B: ethyl acetate, 100% A to 100% B gradient) to yield **5.5** as a brown fluffy solid (382 mg, 78%). ^{1}H NMR (400 MHz, $CDCl_3$) δ 8.03 – 7.98 (m, 2H), 7.82 (s, 2H), 7.68 – 7.56 (m, 6H), 7.37 (s, 2H), 4.63 (s, 4H), 4.13 (d, *J* = 4.2 Hz, 4H), 3.87 (s, 6H), 3.49 (s, 4H), 1.42 (s, 18H). ^{13}C NMR (101 MHz, $CDCl_3$) δ 164.68, 156.64, 155.42, 147.88, 147.60, 133.94, 133.29, 132.33, 132.08, 131.18, 127.27, 126.21, 124.26, 92.89, 80.22, 79.41, 53.48, 53.06, 52.90, 47.10, 28.34. HR-ESI-MS m/z for $C_{46}H_{51}N_8O_{16}S_2$ ($M+H^+$) calcd. (found) 1035.2864 (1035.2865).

5.4.7 Dimethyl 6,6'-((ethane-1,2-diylbis(((2-nitrophenyl)sulfonyl)azanediyl))bis(methylene))bis(4-(3-((tert-butoxycarbonyl)amino)propyl)picolinate) (5.6)

Compound **5.5** (382 mg, 0.37 mmol) was dissolved in ethyl acetate (40 mL), and palladium on activated carbon (10% Pd, 46 mg) was added. The system was sealed and charged with hydrogen gas several times. The solution was stirred under hydrogen at room temperature for 24 hours, after which time the catalyst was filtered off and replaced anew, with further stirring for an additional 24 hours. The solid catalyst was filtered off, and filtrate was concentrated *in vacuo* to obtain **5.6** as a brown solid (325 mg, 84%). ^{1}H NMR (400 MHz, $CDCl_3$) δ 8.22 (m, 2H), 7.81 (s, 2H), 7.60-7.70 (m, 6H), 7.39 (s, 2H), 4.73 (s, 4H), 3.94 (s, 6H), 3.50 (s, 4H), 3.14 (quart, *J* = 8 Hz, 4H), 2.67 (t, *J* = 8 Hz, 4H), 1.79 (quint, *J* = 8 Hz, 4H), 1.45 (s, 18 H). ^{13}C NMR (101 MHz, $CDCl_3$) δ 165.3, 156.3, 156.0, 153.5, 148.1, 147.6, 133.6, 132.6, 132.0, 131.5, 126.0, 124.6, 124.0, 79.4, 53.2, 52.8, 46.4, 40.0, 32.4, 30.5, 28.4. HR-ESI-MS m/z for $C_{46}H_{59}N_8O_{16}S_2$ ($M+H^+$) calcd. (found) 1043.3490 (1043.3472).

5.4.8 Dimethyl 6,6'-((ethane-1,2-diylbis(azanediyl))bis(methylene))bis(4-(3-((tert-butoxy-carbonyl)amino)propyl)picolinate) (5.7)

Compound **5.6** (324 mg, 0.31 mmol) was dissolved in THF (10 mL), and thiophenol (65 μL, 0.64 mmol, 2.05 equiv), followed by K_2CO_3 (257 mg, 1.86 mmol, 6 equiv), was added. The reaction mixture was stirred at room temperature for 4 days; subsequently the excess salts were removed by centrifugation (10 min, 4000 rpm) and the filtrate was concentrated *in vacuo*. The crude product was purified by column chromatography (CombiFlash R_f automated column system; 12 g HP silica; A: dichloromethane, B: methanol with 2% triethylamine, 100% A to 25% B gradient) to obtain **5.7** as a dirty yellow oil (132 mg, 63%). ^{1}H NMR (400 MHz, $CDCl_3$) δ 7.83 (s, 2H), 7.43 (s, 2H), 4.01 (s, 4H), 3.96 (s, 6H), 3.15 (quart, J = 8 Hz, 4H), 2.85 (s, 4H), 2.70 (t, J = 8 Hz, 4H), 1.84 (quint, J = 8 Hz, 4H, quint), 1.43 (s, 18H). ^{13}C NMR (101 MHz, $CDCl_3$) δ 165.9, 160.2, 155.9, 152.6, 147.5, 125.7, 123.8, 79.3, 54.7, 52.8, 48.7, 39.9, 32.3, 30.5, 28.4. HR-ESI-MS m/z for $C_{34}H_{53}N_6O_8$ ($M+H^+$) calcd. (found) 673.3925 (673.3928).

5.4.9 6,6'-((Ethane-1,2-diylbis(azanediyl))bis(methylene))bis(4-(3-aminopropyl) picolinic acid) (5.8)

Compound **5.7** (73 mg, 0.11 mmol) was dissolved in THF/water (3:1, 4 mL), and lithium hydroxide (11 mg, 0.43 mmol, 4 equiv) was added. The reaction mixture was stirred at room temperature for 1 hour, and subsequently concentrated *in vacuo.* The resulting solids were redissolved in 4 M HCl/dioxane/THF (3:2:1, 8 mL), and stirred at room temperature overnight. The reaction mixture was then concentrated *in vacuo* and purified by semi-preparative RP-HPLC (gradient: A: 0.1% TFA (trifluoroacetic acid) in water, B: CH_3CN, 5 to 100% B linear gradient over 25 min, 10 mL/min, t_R = 8.6 min). Product fractions were pooled, and lyophilized

to yield **5.8** as an off-white solid (26 mg, 55%). ^{1}H NMR (400 MHz, D_2O) δ 8.03 (s, 2H), 7.57 (s, 2H), 4.62 (s, 4H), 3.69 (s, 4H), 3.01 (t, *J* = 8 Hz, 4H), 2.83 (t, *J* = 8 Hz, 4H), 2.02 (quint, *J* = 8 Hz, 4H). ^{13}C NMR (101 MHz, D_2O) δ 168.5, 154.1, 150.9, 148.0, 126.3, 125.3, 50.2, 44.0, 38.9, 31.3, 27.1. HR-ESI-MS m/z for $C_{22}H_{33}N_6O_4$ ($M+H^+$) calcd. (found) 445.2563 (445.2570).

5.4.10 Dimethyl 6,6'-((ethane-1,2-diylbis((3-(2-nitro-1H-imidazol-1-yl)propyl)azane-diyl))bis(methylene))bis(4-(3-((tert-butoxycarbonyl)amino)propyl)picolinate) (5.9)

Compound **5.7** (60 mg, 0.089 mmol) and 1-(3-bromopropyl)-2-nitro-1*H*-imidazole (46 mg, 0.20 mmol, 2.2 equiv) were dissolved in acetonitrile (4 mL), and K_2CO_3 (49 mg, 0.36 mmol, 4 equiv) was added. The reaction mixture was stirred at 55 °C for 4 days, subsequently cooled to room temperature, filtered to remove excess salts and concentrated in vacuo. The crude product was purified by column chromatography (CombiFlash R_f automated column system; 4 g HP silica; A: dichloromethane, B: methanol, 100% A to 30% B gradient) to yield **5.9** as a yellow oil (30 mg, 34%). ^{1}H NMR (400 MHz, $CDCl_3$) δ 7.82 (s, 2H), 7.38 (s, 2H), 7.19 (d, *J* = 9.4 Hz, 2H), 7.07 (s, 2H), 4.42 (t, *J* = 7.2 Hz, 4H), 3.93 (s, 6H), 3.77 (s, 4H), 3.13 (dd, *J* = 13.2, 6.7 Hz, 4H), 2.71 – 2.66 (m, 4H), 2.63 (s, 4H), 2.54 (s, 4H), 2.02 – 1.92 (m, 4H), 1.81 (dt, *J* = 14.6, 7.2 Hz, 4H), 1.40 (s, 18H). ^{13}C NMR (101 MHz, $CDCl_3$) δ 165.92, 156.13, 152.83, 147.58, 144.87, 128.47, 126.58, 126.25, 124.18, 79.35, 60.30, 52.96, 51.83, 51.44, 48.39, 40.08, 32.52, 30.81, 28.49, 28.32. MS (ES+) m/z = 979.6 $[M+H]^+$.

5.4.11 6,6'-((Ethane-1,2-diylbis((3-(2-nitro-1H-imidazol-1-yl)propyl)azanediyl)) bis(methylene))bis(4-(3-aminopropyl)picolinic acid) (5.10)

Compound **5.9** (30 mg, 0.03 mmol) was dissolved in THF/water (3:1, 4 mL), and lithium hydroxide (3 mg, 0.12 mmol, 4 equiv) was added. The mixture was stirred at room temperature until methyl deprotection was deemed complete by mass spectrometry (MS (ES+) m/z = 951.7 $[M+H]^+$, about 1 hour), and subsequently concentrated *in vacuo*. The residue was redissolved in 4 M HCl/dioxane/THF (3:2:1, 3 mL) and stirred at room temperature overnight. The reaction mixture was subsequently concentration *in vacuo*, redissolved in water and purified by semi-preparative RP-HPLC (gradient: A: 0.1% TFA (trifluoroacetic acid) in water, B: CH_3CN, 5 to 100% B linear gradient over 25 min, 10 mL/min, t_R = 12.7 min). Product fractions were pooled, and lyophilized to yield **5.10** as an off-white solid (23 mg, 100%). ^{1}H NMR (400 MHz, MeOD) δ 7.92 (s, 2H), 7.49 (s, 2H), 7.42 (s, 2H), 7.11 (s, 2H), 4.49 – 4.44 (m, 4H), 4.42 (s br, 4H), 3.58 (s br, 4H), 3.22 (s br, 4H), 3.03 – 2.97 (m, 4H), 2.85 – 2.79 (m, 4H), 2.26 (s br, 4H), 2.03 (dd, *J* = 14.5, 7.1 Hz, 4H). ^{13}C NMR (101 MHz, MeOD) δ 167.19, 154.65, 149.02, 145.91, 128.84, 128.39, 128.13, 125.83, 119.13, 116.24, 59.26, 58.15, 53.66, 51.67, 40.08, 32.60, 28.84, 27.12. HR-ESI-MS m/z for $C_{34}H_{47}N_{12}O_8$ ($M+H^+$) calcd. (found) 751.3640 (751.3635) (-0.7 PPM).

5.4.12 H_2dedpa-propyl$_{pyr}$-FITC (5.11)

To a solution of **5.8** (3.5 mg, 0.008 mmol) in water (0.3 mL), a solution of fluorescein isothiocyanate (FITC) (6.1 mg, 0.016 mmol, 2.1 equiv) in DMF/water (3:1, 1.2 mL) was added. To this yellow mixture, triethylamine (5.5 µL, 5 equiv) was added at which time the solution turned drastically brighter orange in colour. The reaction mixture was stirred at ambient temperature under darkness for 18 hours. The reaction mixture was subsequently concentration *in vacuo*, redissolved in CH_3CN and purified by RP-HPLC (gradient: A: 0.1 % TFA

(trifluoroacetic acid) in water, B: CH_3CN; 5 to 100% B linear gradient over 25 min, 1 mL/min, t_R (mono-FITC) = 16.7 min, t_R (product) = 18.7 min, t_R (FITC) = 23.4 min). Product fractions were pooled and lyophilized to yield the product as a yellow solid (3.2 mg, 33%). Purity was confirmed by HPLC re-injection of an aliquot of final collected product. HR-ESI-MS m/z for $C_{64}H_{55}N_8O_{14}S_2$ ($M+H^+$) calcd. (found) 1223.3279 (1223.3286) (0.6 PPM).

5.4.13 H_2dedpa-propyl$_{pyr}$-FITC-(*N,N'*-propyl-2-NI) (5.12)

Compound **5.10** (4.0 mg, 0.005 mmol) was dissolved in DMF/water (2:1, 0.3 mL) and FITC (4.6 mg, 0.012 mmol, 2.2 equiv) in DMF (0.1 mL) was added. To this murky yellow solution, triethylamine (3 μL, 4 equiv) was added at which time the solution turned clear and became drastically brighter orange in colour. The reaction mixture was stirred at ambient temperature excluded from light for 20 hours. The reaction mixture was subsequently concentration *in vacuo*, redissolved in CH_3CN and was purified by RP-HPLC (gradient: A: 0.1 % TFA (trifluoroacetic acid) in water, B: CH_3CN; 5 to 100% B linear gradient over 25 min, 1 mL/min, t_R (product) = 18.4 min). Product fractions were pooled and lyophilized to yield the product as a bright yellow solid (2.9 mg, 36%). Purity was confirmed by HPLC re-injection of an aliquot of final collected product. HR-ESI-MS m/z for $C_{76}H_{69}N_{14}O_{18}S_2$ ($M+H^+$) calcd. (found) 1529.4356 (1529.4352) (-0.3 PPM).

5.4.14 [Ga(dedpa-propyl$_{pry}$-NH_2)][NO_3], [Ga(5.8)][NO_3]

To a solution of **5.8** (5.6 mg, 0.013 mmol) in water/methanol (2:1, 0.5 mL), a solution of $Ga(NO_3)_3{\cdot}6H_2O$ (5.0 mg, 0.014 mmol, 1.1 equiv) in water (0.2 mL) was added. The pH of this solution was adjusted to 5 using aq. NaOH (0.1 M), and subsequently stirred at 60°C for 40 min.

The solvent was then removed in vacuo to yield [Ga(**5.8**)][NO_3] as a white solid. The product was used in subsequent steps without further purification. ^{1}H NMR (400 MHz, D_2O) δ 8.28 (s, 2H), 8.00 (s, 2H), 4.70 (d, *J* = 17.8 Hz, 2H), 4.42 (d, *J* = 17.8 Hz, 2H), 3.32 (d, *J* = 9.9 Hz, 2H), 3.12 (dd, *J* = 14.5, 6.8 Hz, 8H), 2.67 (d, *J* = 10.0 Hz, 2H), 2.24 – 2.09 (m, 4H). ^{13}C NMR (150 MHz, D_2O) δ 167.5, 164.0, 152.8, 144.9, 129.3, 125.9, 50.9, 48.6, 40.7, 34.1, 28.8. HR-ESI-MS m/z for $C_{22}H_{30}{}^{69}GaN_6O_4$ (M^+) calcd. (found) 511.1584 (511.1577).

5.4.15 [Ga(dedpa-propyl$_{pyr}$-NH$_2$-(*N,N'*-propyl-2-NI)][NO_3], [Ga(5.10)][NO_3]

The gallium complex was prepared as above for [Ga(**5.8**)][NO_3] using **5.10** and was isolated as a white solid. ^{1}H NMR (400 MHz, D_2O) δ 8.33 (s, 2H), 8.02 (s, 2H), 7.38 (s, 2H), 7.19 (s, 2H), 4.65 (d, *J* = 17.1 Hz, 2H), 4.47 (t, *J* = 6.0 Hz, 4H), 4.44 (d, *J* = 9.7 Hz, 2H), 3.25 (d, *J* = 11.4 Hz, 2H), 3.17 (dd, *J* = 11.2, 4.0 Hz, 8H), 2.86 (d, *J* = 11.1 Hz, 2H), 2.83 (d, *J* = 9.9 Hz, 2H), 2.49 – 2.38 (m, 2H), 2.38 – 2.23 (m, 4H), 2.21 (dt, *J* = 15.8, 7.9 Hz, 4H). ^{13}C NMR (101 MHz, D_2O) δ 163.31, 161.78, 148.80, 141.29, 126.83, 126.67, 125.98, 122.89, 116.28, 113.39, 54.35, 45.33, 37.26, 30.81, 25.33, 21.41. HR-ESI-MS m/z for $C_{34}H_{44}{}^{69}GaN_{12}O_8$ (M^+) calcd. (found) 817.2661 (817.2659) (-0.2 PPM).

5.4.16 [Ga(dedpa-propyl$_{pyr}$-FITC)][NO_3], [Ga(5.11)][NO_3]

To a solution of [Ga(**5.8**)][NO_3] (7.2 mg, 0.013 mmol) in water (0.5 mL), a solution of FITC (11.0 mg, 0.028 mmol, 2.2 equiv) in DMF/water (2:1, 0.3 mL) was added. To this murky yellow solution, triethylamine (7 μL, 4 equiv) was added at which time the solution turned clear and became bright orange in colour. The reaction mixture was stirred at ambient temperature under darkness for 18 hours. The solution volume was reduced by ~2/3 by evaporation with

blowing air, then the crude mixture was purified by RP-HPLC (gradient: A: 0.1 % TFA (trifluoroacetic acid) in water, B: CH_3CN; 5 to 100% B linear gradient over 25 min, 1 mL/min, t_R (product) = 18.0 min). Product fractions were pooled and lyophilized to yield the product as a bright yellow solid (10.7 mg, 63%). Purity was confirmed by HPLC re-injection of an aliquot of final collected product. HR-ESI-MS m/z for $C_{64}H_{52}{}^{69}GaN_8O_{14}S_2$ (M^+) calcd. (found) 1289.2300 (1289.2291) (-0.7 PPM).

5.4.17 [Ga(dedpa-propyl$_{pyr}$-FITC-(*N,N'*-propyl-2-NI)][NO_3], [Ga(5.12)][NO_3]

The final product was prepared as above for [Ga(**5.11**)][NO_3] using **5.12** and was isolated as a bright yellow solid (5.2 mg, 45%, t_R (product) = 18.5 min). Maldi-TOF MS (ES+) m/z = 1595.6 [M^+].

5.4.18 3D Tumour Spheroids Cell Culture and Compound Dosing

DLD-1 human colon carcinoma cells were maintained in Advanced DMEM (Invitrogen) and supplemented with 2% FBS and 2 mM Glutamine in a humidified incubator at 37°C and 5% CO_2. Spheroid culture procedures followed those of a previously reported protocol.[206,208] Spheroids were formed by plating 100 µL of a 1.5 × 10^5 cell ml^{-1} single cell suspension of DLD-1 cells onto agarose (0.75%) coated 96 well plates and they were allowed to aggregate for 5 to 7 days which resulted in the formation of one spheroid per well. Stock solutions (S_o) of [Ga(**5.11**)]$^+$, [Ga(**5.12**)]$^+$, **5.11**, and **5.12**, and FITC were made up in media with 6% DMSO to an original concentration of approx. 0.6 mM. Aliquots of each stock solution (S_o) were used to make working solutions (S_{100}, S_{20}, S_5) of 100, 20, and 5 µM for each compound. These were dosed in triplicate for each independent compound, concentration, and time point. At the time

of dosing, 50 µL of medium from each well containing a spheroid was replaced with 50 µL of each working solution S_{100}, S_{20} or S_5 such that the final concentration of compound in the well was 50, 10, or 2.5 µM, respectively (final concentration of DMSO in each well did not exceed 1%). Dosed spheroids were then incubated at 37°C for 1, 2, or 4 hours. At the end of each incubation period, spheroids were transferred to 1.5 mL Eppendorf tubes and washed thrice with phosphate buffered saline (PBS, pH 7.4, 3 x 200µL) to remove excess compound. Spheroids were then transferred to a 96-well imaging plate.

5.4.19 Confocal Microscopy Imaging

Confocal images were taken on an Olympus Fluoview FV1000-inverted laser scanning confocal microscope located in the Life Sciences Centre at the University of British Columbia. The microscope was equipped with an Olympus UPLAPO 10x/0.40 air objective lens, UPLAPO 40x/1.00 oil objective lens and PLAPO 60x/1.40 water objective lens. A scan rate of 4.0 µs pixel^{-1} with Kalman averaging was used. The argon 488nm laser had the following excitation and emission ranges: Ex 488 nm: Em 500–550 nm. Images were processed with ImageJ software, and displayed images are all at a depth (measurement along z-axis) of 144.3 µm.

Chapter 6: "Cardiobling v. 2.0" – Lipophilic Cationic Ga(III) Complexes Based on the H_2*CHX*dedpa Ligand for PET Imaging of Myocardial Perfusion

6.1 Introduction

Myocardial perfusion imaging (MPI) is a common and powerful technique used to illustrate the function of the heart muscle. Its main application is in diagnosis of coronary artery disease (CAD) and is of great importance for early detection of heart disease, one of the leading causes of death in the western world.[209] The aim of MPI is to visualise the perfusion of the heart muscle; this blood flow analysis relies on the ensuing accumulation of a radiopharmaceutical in the heart. Areas with good blood circulation will show increased radionuclide uptake compared to areas with poor flow or damaged tissue, thus defining the extent and severity of disease.[209–212]

MPI is dominated by the use of ^{99m}Tc labelled agents for SPECT imaging. The FDA approved radiopharmaceuticals ^{99m}Tc-Sestamibi (Cardiolite), ^{99m}Tc-Tetrofosmin (Myoview), and ^{99m}Tc-Teboroxime (Figure 6.1) are among the most popular agents used clinically. It is believed that the elevated myocardium accumulation of these ^{99m}Tc tracers is rooted in the physical properties of the complexes: these are highly lipophilic and monocationic or neutral charged complexes which contain at least two ether-like linkages.[212,213] Limitations such as low first-pass extraction and high liver uptake of such agents have led to interest in developing new radiopharmaceuticals for MPI. The ideal perfusion radiotracer should have high heart uptake and retention, with minimal liver and lung uptake to create diagnostically useful images.[212]

The advantageous properties of β+ emitter ^{68}Ga make it an ideal candidate for incorporation into a ^{68}Ga-based MPI agent for PET. A ^{68}Ga-based perfusion imaging agent would possess the specific advantages of spatial resolution obtainable by PET compared to SPECT, whilst relying on the convenience of a generator-produced isotope. Consequently, much effort has been made towards development of new lipophilic, cationic Ga-complexes with intentions of improving myocardium retention and limiting liver uptake.[132,214–216] Specifically, bis- and tris(salicylaldimine) chelators such as tris(4,6-dimethoxysalicylaldimin-*N,N'*-bis(3-aminopropyl)-*N,N'*-ethylenediamine (BAPEN)[214,217] and its derivatives[215,216,218] (Figure 6.1) showed some promising properties for myocardial perfusion imaging with ^{68}Ga, but non-trivial labeling procedures have limited the progression of these ligands towards the clinic.

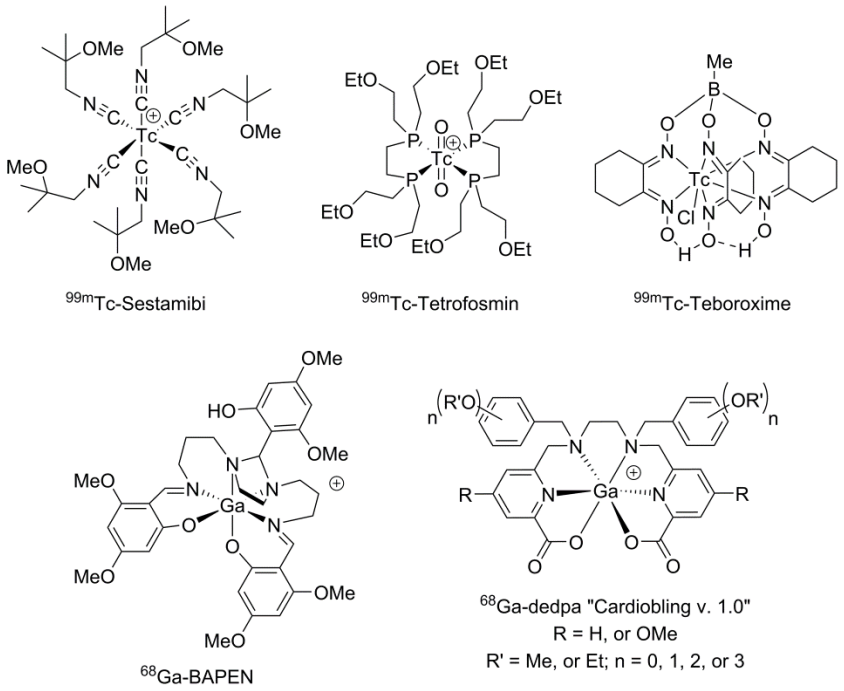

Figure 6.1 Commercially available ^{99m}Tc SPECT agents (top) and recently investigated ^{68}Ga PET agents (bottom) for myocardial perfusion imaging.

Our recent reports of the promising acyclic hexadentate $^{67/68}$Ga chelator H_2dedpa which forms a monocationic complex with Ga(III) sparked interest in developing derivatives which could potentially lead to compounds of increased and prolonged heart uptake.[132] A small library of H_2dedpa analogues of varying lipophilicity which possess benzyl residues and a variety of methoxy or ethoxy substituents was evaluated *in vivo*.[132] Despite modest biodistribution results showing initial high uptake and slow clearance from the liver, two complexes showed persistent heart uptake over the course of 2 h. These conclusions have motivated us to develop a second class of dedpa^{2-} 'Cardiobling' analogues which possess varying degrees of lipophilicity.

In this Chapter, we report five new derivatives of the chiral acyclic chelator H_2*CHX*dedpa (which was originally studied in Chapter 2), and one new derivative of H_2dedpa which have been functionalized to include varying lipophilic appendages. These analogues contain either diethyl ether –like or benzyl linkages with varying number of methoxy groups added onto the benzyl or 4-position of the picolinate moieties (Figure 6.2). Moreover, the cyclohexanediamine backbone of *CHX*dedpa^{2-} inherently introduces a degree of added lipophilicity. The addition of ether groups was found to reduce radiotracer liver uptake of cationic ^{99m}Tc complexes resulting in improved target/background ratios.[212] Herein, we hope to take advantage of this theory with some of our derivatives by incorporating such ether linkages in our ligands. Indeed, many of the structural components that have been added to this new class of compounds (**6.12 – 6.16**, and **6.19**) have been strategically chosen to mimic other ^{99m}Tc and ^{68}Ga MPI agents under investigation. The gallium coordination potential, labeling properties, *in vitro* stability, and log *P* of the six chelating ligands will be explored to assess their potential as myocardial perfusion imaging agents.

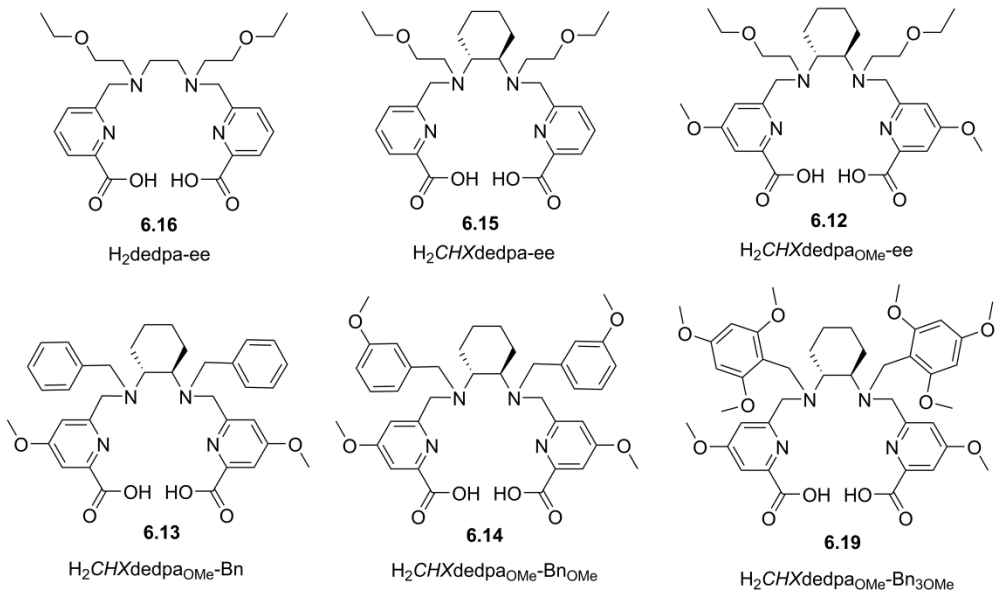

Figure 6.2 Structures of lipophilic dedpa^{2-} and *CHX*dedpa^{2-} analogues synthesized in Chapter 6 (**6.12-6.16**, and **6.19**).

6.2 Results and Discussion

6.2.1 Ligand Synthesis and Characterization

The synthesis of pro-ligands **6.12-6.14,** and **6.19** required the use of methyl 6-(bromomethyl)-4-methoxypicolinate (**6.4**) which was prepared using a previously reported synthesis.[132] Using the methoxy-modified bromo-picolinate (**6.4**), the precursor **6.6** was prepared using nosyl protection/deprotection chemistry (Scheme 6.1) analogous to that used in Chapter 2. The precursor **6.6** was nicknamed 'Me_2*CHX*$dedpa_{OMe}$' since it is similar to the analogue Me_2*CHX*dedpa (synthesized in Chapter 2) in which there are no methoxy (OMe) groups appended to the 4-position of the picolinate moieties.

Scheme 6.1 Synthesis of precursor **6.6**, Me_2*CHX*$dedpa_{OMe}$.[a]

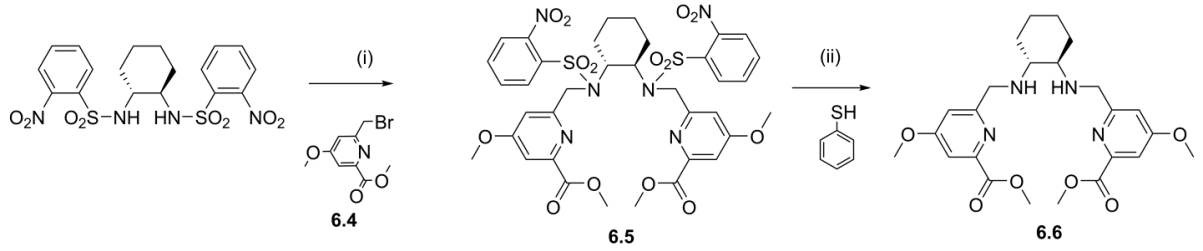

[a]Reagents and conditions: (i) methyl 6-(bromomethyl)-4-methoxypicolinate (2 equiv), K_2CO_3, CH_3CN, 65°C, 3 d; (ii) thiophenol (2.1 equiv), K_2CO_3, THF, RT, 3 d.

A similar synthetic pathway was used to prepare five ligands (**6.12 – 6.16**) (Scheme 6.2). Preparation began with *N,N'*-alkylation of Me_2dedpa,[54,59] Me_2*CHX*dedpa,[176] or Me_2*CHX*$dedpa_{OMe}$ (**6.6**) with a slight excess of the appropriate bromo-alkylating agent under basic condition (K_2CO_3) to yield the methyl ester protected precursors **6.7 – 6.11**. For alkylation reactions with 1-bromo-2-ethoxyethane (Br-ee), 2-ethoxyethane (ee) also replaced the methyl protecting group of one or both of the carboxylic acid(s) which resulted in a mixture of products (Figure 6.3). For precursors **6.7** and **6.10**, separation and isolation of the over-alkylated products via column chromatography was not possible, consequently ^{1}H and ^{13}C NMR spectra of pure compound were not collected. Nonetheless, hydrolysis of all ester protected ligands was accomplished in the final deprotection step using lithium hydroxide in order to yield all five ligands **6.12 – 6.16** as pure compounds after RP-HPLC purification.

Scheme 6.2 Synthesis of pro-ligands H_2*CHX*dedpa$_{OMe}$-ee (**6.12**), H_2*CHX*dedpa$_{OMe}$-Bn (**6.13**), H_2*CHX*dedpa$_{OMe}$-Bn$_{OMe}$ (**6.14**), H_2*CHX*dedpa-ee (**6.15**), and H_2dedpa-ee (**6.16**).[a]

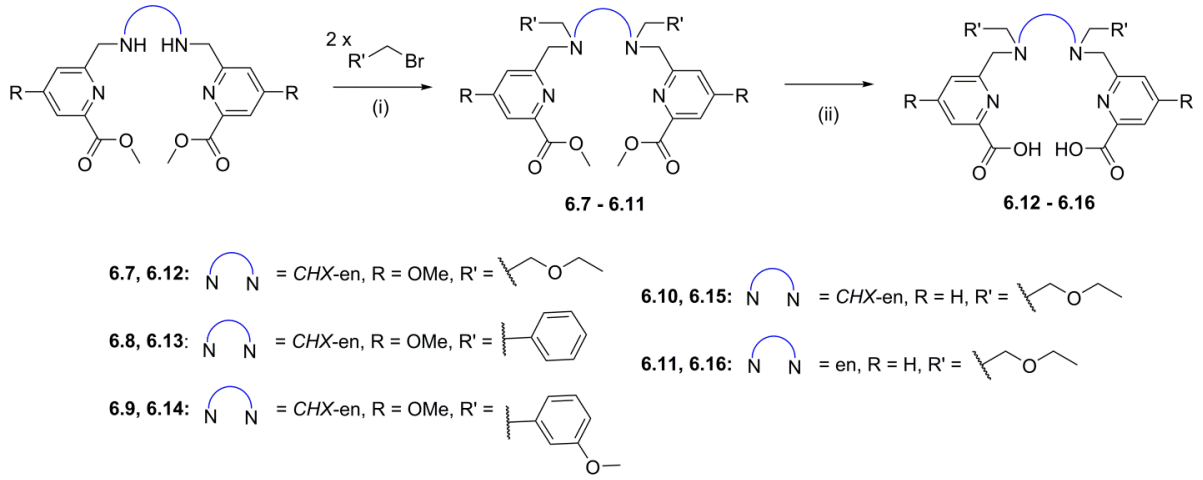

[a]Reagents and conditions: (i) Na_2CO_3, CH_3CN, 75°C, 2 d; (ii) LiOH (5 equiv), THF/H_2O (3:1), RT, 30 min.

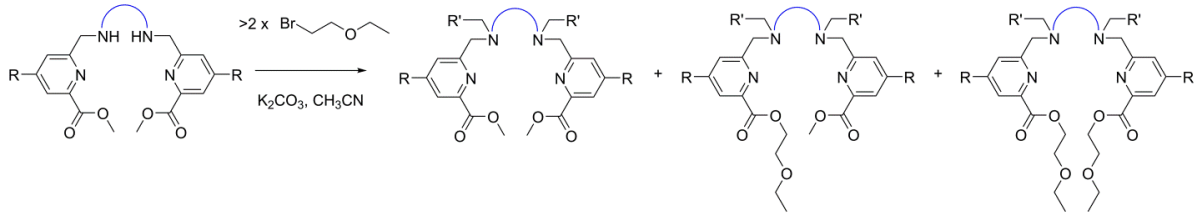

Figure 6.3 Addition of 1-bromo-2-ethoxyethane to 2° amines as well as replacement of methyl-esters which was observed during *N,N'*-alkylation reactions with Me_2dedpa, Me_2*CHX*dedpa, or Me_2*CHX*dedpa$_{OMe}$.

The sixth ligand **6.19** was synthesized in three steps (Scheme 6.3) through imine formation followed by reductive amination of 2,4,6-trimethoxybenzaldehyde with (1*R*, 2*R*)-(-)-cyclohexanediamine to yield **6.17** which was subsequently used in an *N,N'*-alkylation reaction with methyl 6-(bromomethyl)-4-methoxypicolinate (**6.4**). Finally, the methyl-ester protected ligand **6.18** was deprotected using lithium hydroxide as was done for the previous ligands to give H_2*CHX*dedpa$_{OMe}$-Bn$_{3OMe}$ (**6.19**).

Scheme 6.3 Synthesis of pro-ligand H_2*CHX*dedpa$_{OMe}$-Bn$_{3OMe}$ (**6.19**).[a]

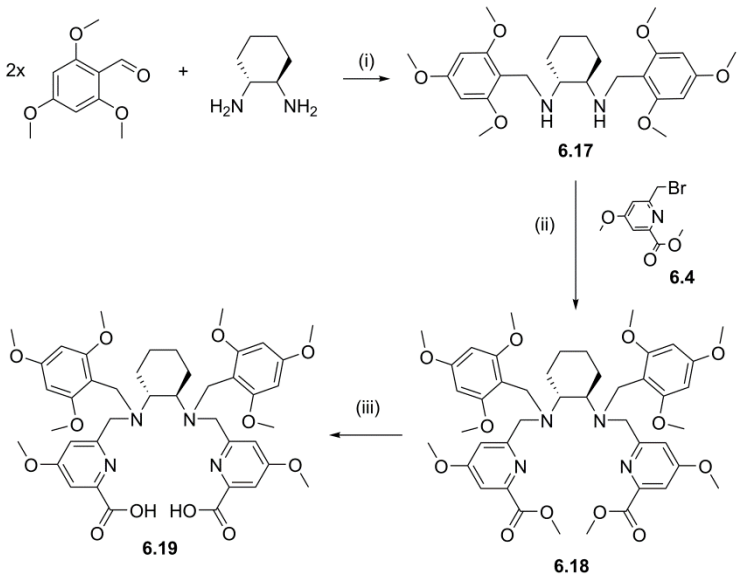

[a]Reagents and conditions: (i) a. ethanol, 0°C to RT, 18 h; b. $NaBH_4$, 0°C, 1.5 h; (ii) methyl 6-(bromomethyl)-4-methoxypicolinate (2.1 equiv), Na_2CO_3, CH_3CN, reflux to RT, 2 d. (iii) LiOH (5 equiv), THF/H_2O (3:1), RT, 30 min.

^{1}H NMR spectra of several pro-ligands at 25°C revealed very broad and unresolvable peaks which precluded ^{13}C NMR spectrum collection. It was hypothesized that intramolecular hydrogen-bonding of the acidified ligand was the cause of such peak broadening; however, NMR samples in deuterated water adjusted to pD of >7.5 using NaOD resulted in only a slight sharpening of peaks. Consequently, variable-temperature (VT) NMR was used to collect ^{1}H NMR spectra of the ligands at temperatures 25 to 75°C, and resulted in an apparent sharpening of peaks with increasing temperatures (Figure 6.4 and 6.5); ^{13}C NMR spectra were also obtained at the highest temperature.

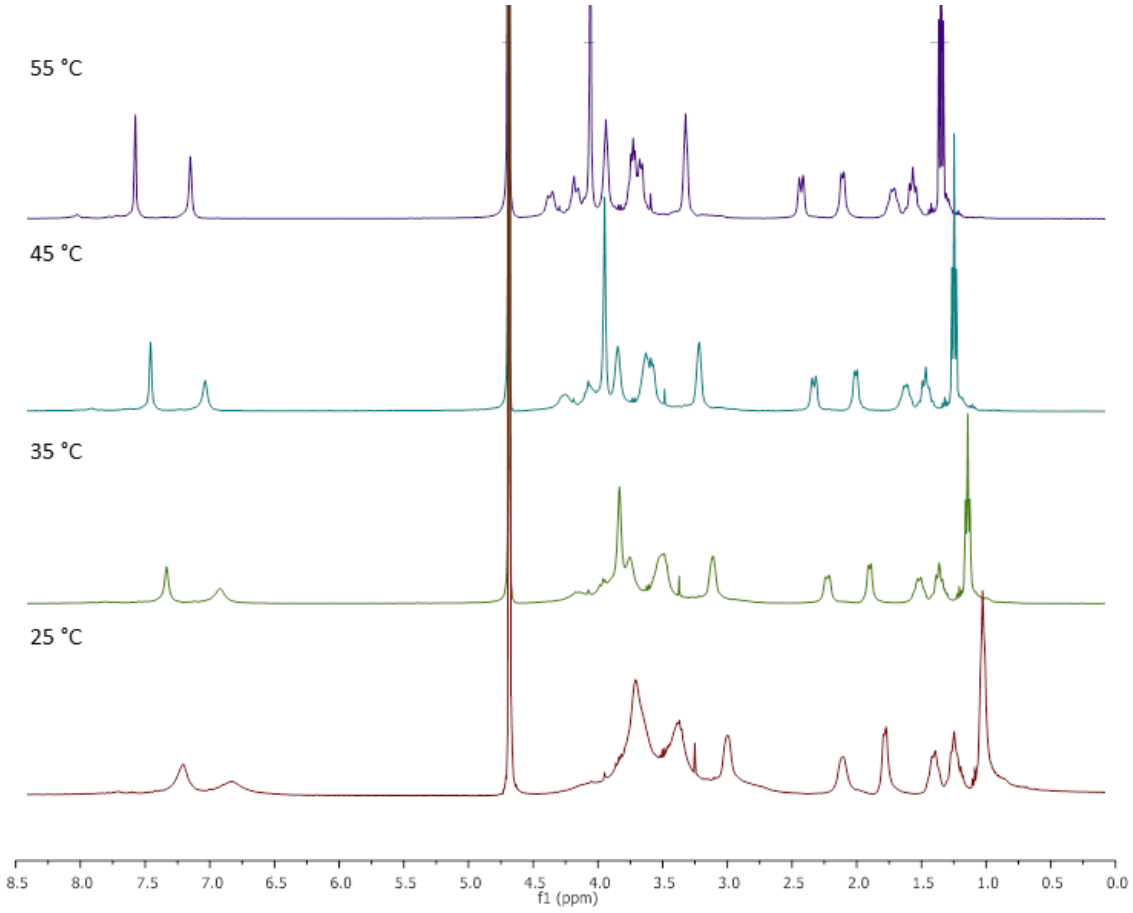

Figure 6.4 Variable temperature (VT) ^{1}H NMR spectra of H_2*CHX*dedpa$_{OMe}$-*N,N'*-ee (**6.12**) (400 MHz, D_2O, 25 – 55°C).

6.2.2 Ga(III) Complexation

After successful characterization of all six pro-ligands, preparation of metal complexes was attempted with non-radioactive Ga(III). The dedpa^{2-} and *CHX*dedpa^{2-} based ligands **6.12 – 6.16** and **6.19** reported herein were all able to complex Ga(III). In most cases, upon addition of appropriate equivalency of $Ga(ClO_4)_3$ salt solution to a solution of pro-ligand, precipitate formation was observed; the precipitate was isolated and its identity as the Ga-complex was confirmed by HR ESI-MS, and NMR spectroscopy. ^{1}H NMR spectra of two ligands and their corresponding Ga-complexes are represented in Figures 6.6 and 6.7.

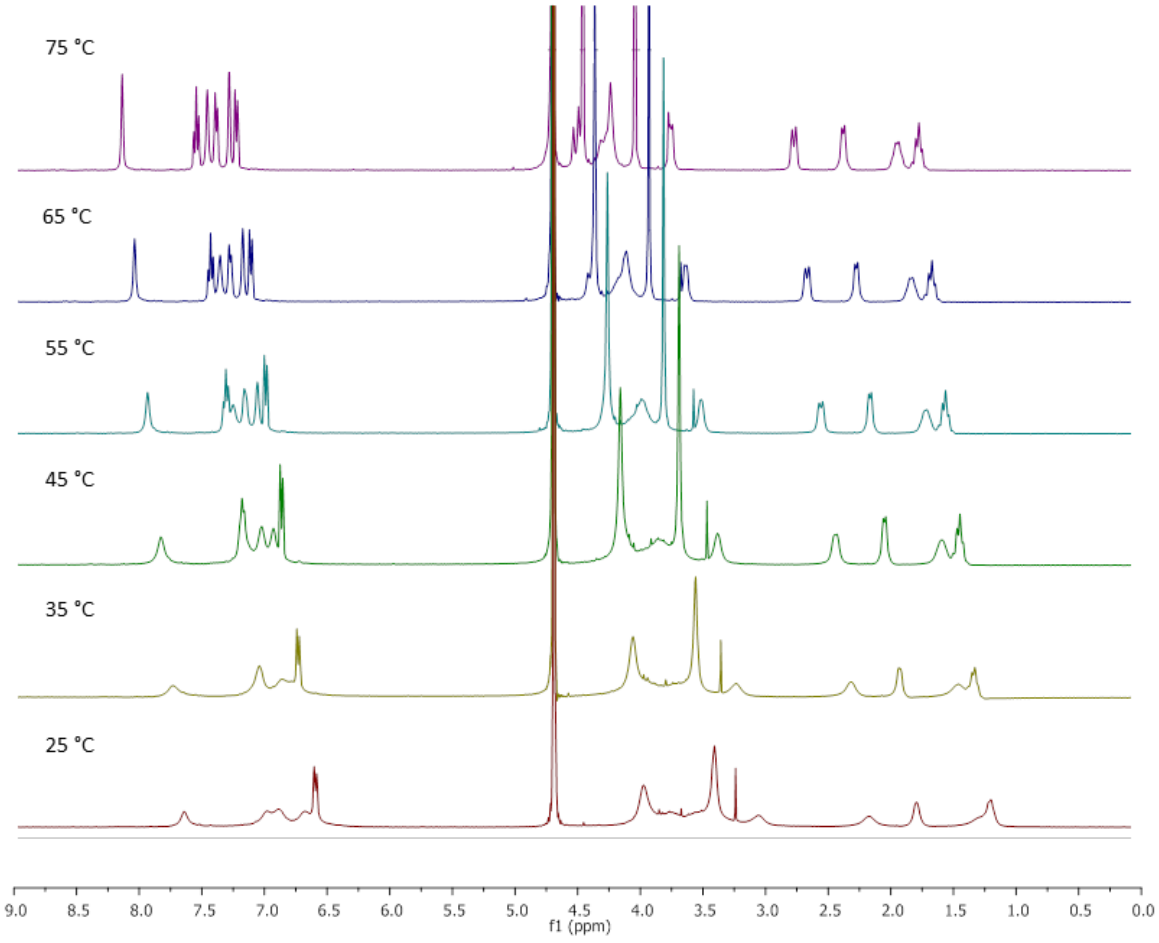

Figure 6.5 VT ^{1}H NMR spectra of H_2*CHX*dedpa$_{OMe}$-*N,N'*-Bn$_{OMe}$ (**6.14**) (400 MHz, D_2O, 25 – 75°C).

The diagnostic diastereotopic splitting of hydrogens upon metal-complexation is seen in the NMR spectra of the dedpa^{2-} based ligand **6.16** (Figure 6.6). The two singlets (labelled A and B), assigned to the methylene hydrogens alpha to the pyridine ring and the hydrogens on the ethylenediamine bridge, respectively, of the ligand **6.16**, become diastereotopic upon gallium complexation and each singlet splits into two doublets (labelled α, α' and β,β').

Diastereotopic splitting is visible in pro-ligands **6.12 – 6.15, 6.19** due to the inherently chiral nature of the *CHX*dedpa^{2-} ligands. Nonetheless, shifts in the ^{1}H resonances of the solution NMR data (Figure 6.7) can be used to confirm successful Ga(III) complexation.

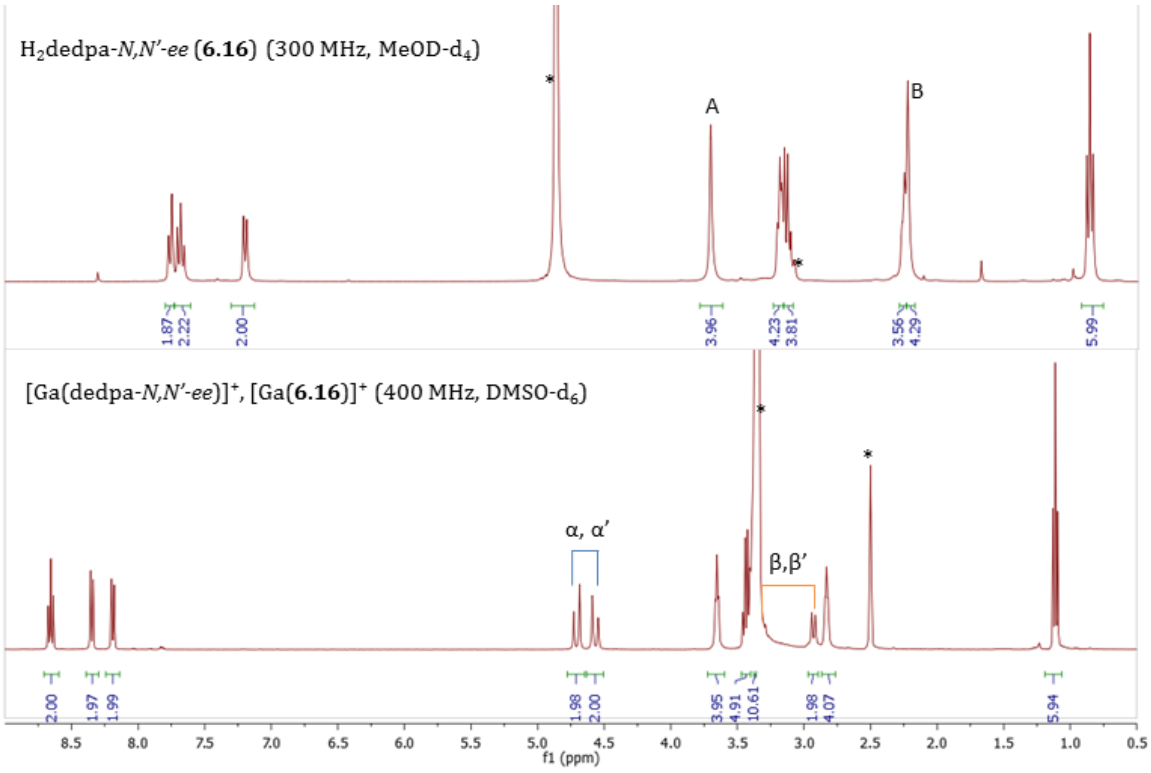

Figure 6.6. ^{1}H NMR spectra at 25 °C of (top) H$_2$dedpa-*N,N'-ee* (**6.16**, 300 MHz, MeOD-d$_4$) and (bottom) [Ga(**6.16**)]$^{+}$ (400 MHz, DMSO-d$_6$), highlighting diastereotopic splitting of hydrogen resonances upon Ga-complexation. Peak A (top spectrum) splits into peaks α and α' (bottom spectrum), and peak B (top spectrum) splits into peaks β and β' (bottom spectrum). *Residual solvent peak.

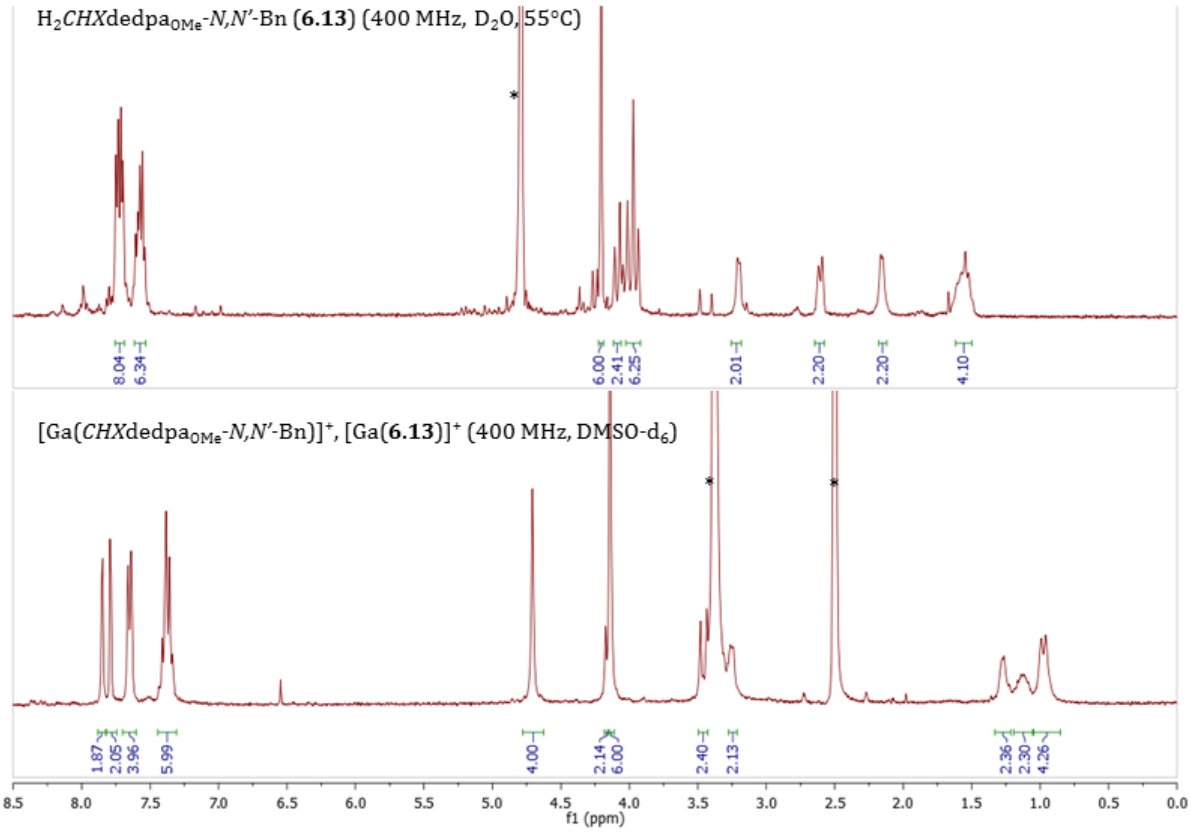

Figure 6.7. ^{1}H NMR spectra of (top) H_2dedpa$_{OMe}$-*N,N'*-Bn (**6.13**, 400 MHz, D_2O, 25°C) and (bottom) [Ga(**6.13**)]$^{+}$ (400 MHz, DMSO-d_6, 25°C), highlighting shifts in hydrogen resonances upon metal-complexation. *Residual solvent peak.

6.2.3 ^{67}Ga Radiochemistry and Log *P* Determination

With a half-life of 3.26 days, ^{67}Ga is used as a longer-lived surrogate for ^{68}Ga complexes, and can be used in studies requiring longer time points by monitoring its γ-emission. In all cases, the concentration of chelator used for radiolabeling is in great excess relative to the radioisotope. Initial radiolabeling reactions were performed with ligand concentrations of 10^{-4} M and 1 mCi of ^{67}Ga in NaOAc buffer at pH 4.5, the reaction mixture was left for 10 min at room temperature prior to injection into the HPLC.

Both *CHX*dedpa^{2-} ligands that possess 2-ethoxyethane functionalities off the secondary amines (**6.12** and **6.15**) displayed one major sharp peak in the radio-chromatogram (95, 99% RCY, respectively) assigned to the ^{67}Ga-labelled complex. The remaining three *CHX*dedpa$_{OMe}^{2-}$ ligands which possess benzyl functionalities attached to the secondary amines with none, one, or three methoxy groups per benzene ring (**6.13, 6.14, and 6.19**, respectively) display very atypical ^{67}Ga labeling radiotraces. Despite the lack of free radioisotope present in the HPLC radio-chromatogram (evinced by absence of a peak at t_R = 2 – 3 min), three sharp peaks of varying intensity are present over a span of approx. 3 min (Table 6.1, Figure 6.8). It is possible that small impurities in the ligand solution are able to complex with ^{67}Ga more efficiently that the desired ligand, resulting in multiple peaks in the radio-chromatogram. Ligand impurities, even in small concentrations relative to the pure ligand, can greatly affect labeling efficiency/yield since radiolabeling conditions require the concentration of the chelator be in great excess compared to the radioisotope. The peak with the latest retention time in the RP-HPLC radio-trace is believed to be the desired ^{67}Ga-complex, since the chelating ligand will likely be the most lipophilic molecule in the reaction mixture which will subsequently form the most lipophilic ^{67}Ga-complex. Given the shorter retention times of the two additional radio-peaks, the impurities are believed to be the mono-alkylated and non-alkylated by-products. The chelator purity was deemed sufficiently pure post-purification by RP-HPLC by re-injection of a small aliquot of chelator which resulted in one sharp peak, so it seemed surprising that the ^{67}Ga radio-traces of the above chelating ligands exhibited three peaks of similar intensity. A second hypothesis is also plausible, one in which multiple radiolabeling peaks arise from ligand radiolysis. If ligand radiolysis is indeed occurring during the course of the radiolabeling reaction, these ligands would be deemed sufficiently unstable and unfit for further testing *in vitro* or *in vivo*. The steric bulk imposed by the benzyl groups on pro-ligands **6.13, 6.14,** and **6.19** may also contribute to the instability of the chelators, resulting in ease of radiolysis.

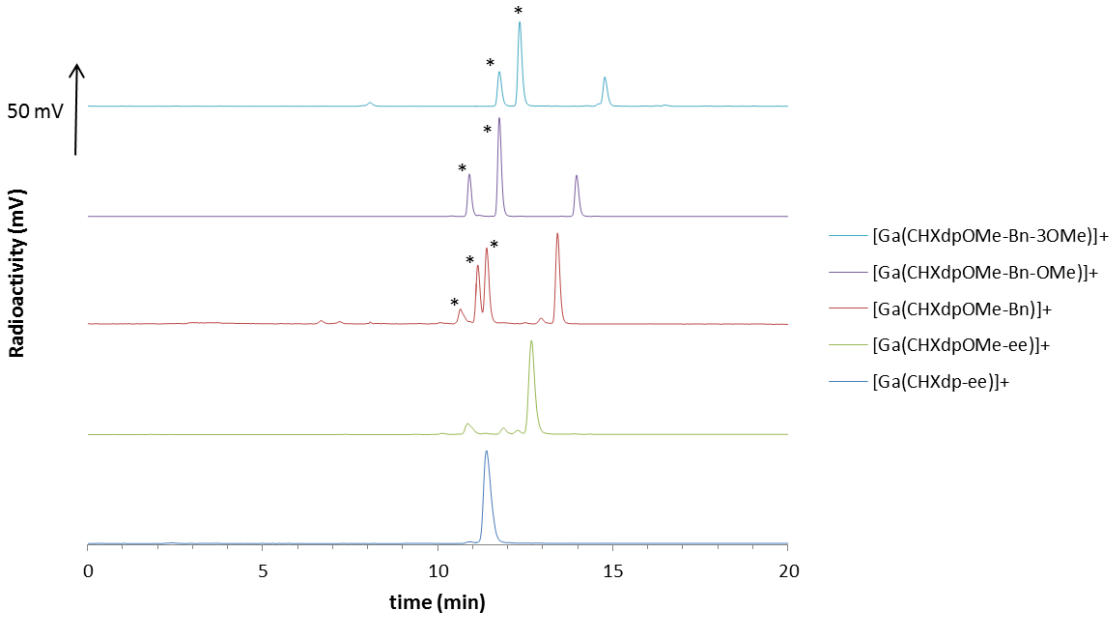

Figure 6.8 HPLC radio-chromatograms of ^{67}Ga labelling reactions with lipophilic *CHX*dedpa^{2-} chelators (top to bottom) **6.19**, **6.14**, **6.13**, **6,12**, and **6.15**. * = peaks from ligand impurities or ligand radiolysis.

Determination of partition coefficients (log *P*) for myocardial perfusion imaging agents is of particular importance because it is believed that differences in heart uptake and liver clearance are caused by the compound lipophilicity which affects the ability to cross the plasma and mitochondrial membranes (the accepted mechanism of heart uptake).[212] It has been hypothesized that cationic ^{99m}Tc radiotracers should exhibit log P values ranging from 0.5 – 1.2 in order to achieve optimal myocardium retention and fast liver clearance concurrently;[212] therefore, we sought to find a ^{68}Ga-*CHX*dedpa complex which exhibited a partition coefficient within this range.

Due to the presence of multiple species in the ^{67}Ga-labeling reactions of benzyl functionalized ligands **6.13**, **6.14**, **6.19**, (*vide supra*) log *P* values were not determined, since the

value obtained through experimental procedures would not accurately depict the lipophilicity of the desired radiometal-ligand complex but instead would be influenced by the mixture of the relatively hydrophilic ^{67}Ga by-products present in the reaction mixture. Log *P* of the two ^{67}Ga-*CHX*dedpa ligands functionalized with ee groups (**6.12**, and **6.15**) were determined to be -1.53 and -1.76, respectively. The added lipophilic character of [^{67}Ga(**6.12**)]$^{+}$ due to the addition of two extra methoxy groups off the 4-position of the picolinate moiety are represented by a shift of 0.23 log *P* units compared to [^{67}Ga(**6.15**)]$^{+}$ (derivative in which there is no additional methoxy groups). The comparatively hydrophilic nature of the two evaluated complexes renders their log *P* values well out of the optimal range predicted by Liu.[212]

Table 6.1 Radiolabeling yields, corresponding HPLC radio-chromatogram retention times, and log *P* values for ^{67}Ga-labelled *CHX*dedpa^{2-} chelators **6.12** – **6.15**, and **6.19**.

Complex	t_R/min (RCY/%)	Log *P*
[^{67}Ga(**6.12**)]$^{+}$; [^{67}Ga(*CHX*dedpa$_{OMe}$-ee)]$^{+}$	12.68 (93)	-1.53
[^{67}Ga(**6.13**)]$^{+}$; [^{67}Ga(*CHX*dedpa$_{OMe}$-Bn)]$^{+}$	11.15* (20), 11.40* (27), 13.42 (32)	ND[a]
[^{67}Ga(**6.14**)]$^{+}$; [^{67}Ga(*CHX*dedpa$_{OMe}$-Bn$_{OMe}$)]$^{+}$	10.91* (23), 11.76* (53), 13.97 (24)	ND[a]
[^{67}Ga(**6.15**)]$^{+}$; [^{67}Ga(*CHX*dedpa-ee)]$^{+}$	11.50 (99)	-1.76
[^{67}Ga(**6.19**)]$^{+}$; [^{67}Ga(*CHX*dedpa$_{OMe}$-Bn$_{3OMe}$)]$^{+}$	11.76* (23), 12.34* (54), 14.77 (21)	ND[a]

*Retention time of ^{67}Ga-labelled by-products produced from ligand impurities or ligand radiolysis. [a]Not determined.

6.2.4 Human *apo*-Transferrin Stability Studies

Selected ^{67}Ga-complexes were investigated for their stability in a human *apo*-transferrin challenge. Compared to unaltered [^{67}Ga(dedpa)]$^{+}$ which remained 99% intact after 2 hours,[54] the new *CHX*dedpa^{2-} derivatives with *N,N*-functionalization displayed moderately reduced stabilities of 86, 80, and 81% for [^{67}Ga(**6.12**)]$^{+}$, [^{67}Ga(**6.14**)]$^{+}$, and [^{67}Ga(**6.15**)]$^{+}$ after 2 hours, respectively. It should be noted that the [^{67}Ga(**6.14**)]$^{+}$ labeling reaction used for the stability assay contained a mixture of labelled products; as such the results of the transferrin challenge are representative of the bulk and not the desired single ^{67}Ga-chelate complex. The *in vitro*

stability of the pure ^{67}Ga-complex ([^{67}Ga(*CHX*dedpa$_{OMe}$-Bn$_{OMe}$)]$^{+}$) may differ from the stability of the other side products in the mixture, such as the mono-alkylated ligand.

Table 6.2 *In vitro* stability of selected ^{67}Ga-labelled *CHX*dedpa^{2-} complexes (**6.12**, **6.14**, **6.15**) against human *apo*-transferrin (37 °C, 2 h), with stability shown as the percentage of intact ^{67}Ga complex.

Complex	15 min (%)	1 h (%)	2 h (%)
[^{67}Ga(**6.12**)]$^{+}$; [^{67}Ga(*CHX*dedpa$_{OMe}$-ee)]$^{+}$	85.0	85.9	85.6
[^{67}Ga(**6.14**)]$^{+}$; [^{67}Ga(*CHX*dedpa$_{OMe}$-Bn$_{OMe}$)]$^{+}$ [a]	97.5	82.9	80.0
[^{67}Ga(**6.15**)]$^{+}$; [^{67}Ga(*CHX*dedpa-ee)]$^{+}$	86.3	84.8	81.4

[a]Multiple ^{67}Ga products present in reaction mixture.

6.3 Conclusions

The synthesis and characterization of six new lipophilic derivatives of H_2dedpa or H_2*CHX*dedpa for the purpose of myocardial perfusion imaging were described. All six derivatives were screened for their ability to bind Ga(III) and retained hexadentate N_4O_2 binding. Initial radiolabeling experiments with ^{67}Ga resulted in abnormal radiolabeling HPLC chromatograms in which three ^{67}Ga-labelled products were formed for the *N,N'*-benzyl functionalized ligand derivatives. Further investigation is needed to identify the additional by-product peaks as ligand impurities or ligand radiolysis products. The latter would render the novel benzyl-functionalized *CHX*dedpa^{2-} ligands sufficiently unstable to warrant further evaluation *in vivo*. Ligand derivatives which were *N,N'*-ethyl ether functionalized displayed the predicted single sharp peak in the ^{67}Ga radio-chromatogram. Partition coefficients of selected *CHX*dedpa^{2-} *N,N*-ethyl ether functionalized ligands were determined to be in the range of -1.5 to -1.8, and are not in the predicted suitable log *P* range for myocardial perfusion imaging agents. Nonetheless, selected ^{67}Ga-*CHX*dedpa complexes were sufficiently stable (> 80%) in a 2 h *apo*-transferrin challenge assay, suggesting that alternative *N,N*-alkylated derivatives which would introduce more lipophilic character would be of interest in future studies.

6.4 Experimental

6.4.1 Materials and Methods

The materials and methods closely followed those from Chapters 2 and 3.

Scheme 6.4 Synthesis of precursors **6.1 – 6.4**.

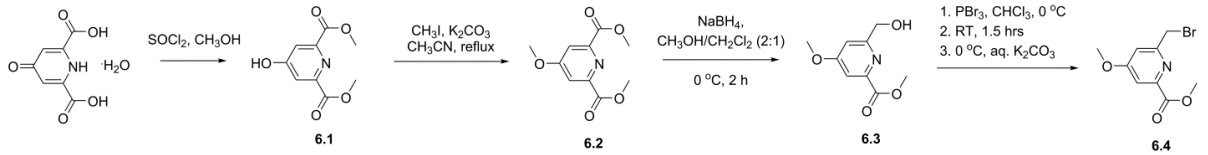

Precursors **6.1 – 6.4** (Scheme 6.4) were prepared using a modified synthesis according to literature protocol of a similar analogue.[219]

6.4.2 Dimethyl 4-hydroxypyridine-2,6-dicarboxylate (6.1)

Chelidamic acid (4.00 g, 19.9 mmol) was suspended in methanol (40 mL) at -10 °C. To this murky solution, thionyl chloride (11.4 mL, 157 mmol, ~ 8 equiv) was added slowly. The solution, which turned clear upon addition, was stirred and allowed to warm to room temperature overnight. The reaction mixture was then refluxed for 2 hours, subsequently cooled to room temperature and concentrated *in vacuo*. The resulting solids were redissolved in hot ethanol, and cooled in freezer to recrystallize. The recrystallized product was collected by vacuum filtration, and the filtrate was concentrated to half-volume, and the recrystallization procedure was repeated to recover more solid product (2.597 g, 62%). ^{1}H NMR (400 MHz,

MeOD) δ 7.88 (s, 2H), 5.01 (s, 3H). ^{13}C NMR (101 MHz, MeOD) δ 174.8, 161.5, 145.4, 117.7, 54.8. MS (ES+) m/z = 212.3 $[M+H]^+$.

6.4.3 Dimethyl 4-methoxypyridine-2,6-dicarboxylate (6.2)

Compound **6.1** (1.941 g, 9.2 mmol) and potassium carbonate (3.9 g, 28.2 mmol, ~3 equiv) were suspended in acetonitrile (50 mL). To this solution, methyl iodide (1.15 mL, 18.4 mmol, 2 equiv) was added, and the murky solution was stirred at reflux overnight. The resultant mixture was cooled to room temperature, filtered by vacuum filtration to remove excess salts and the filtrate was concentrated *in vacuo*. The crude solid was purified by column chromatography (CombiFlash R_f automated column system; 80 g HP silica; A: hexanes, B: ethyl acetate, 100% A to 100% B gradient) to yield the product as a white solid (1.384 g, 67%). ^{1}H NMR (400 MHz, $CDCl_3$) δ 7.62 (d, J = 4.9 Hz, 2H), 3.84 (s, 6H), 3.83 (s, 3H). ^{13}C NMR (101 MHz, $CDCl_3$) δ 167.0, 164.4, 149.2, 113.4, 55.5, 52.5.

6.4.4 Methyl 6-(hydroxymethyl)-4-methoxypicolinate (6.3)

Compound **6.2** (1.384 g, 6.15 mmol) was dissolved in methanol/dichloromethane (2:1, 90 mL) and cooled to 0 °C. Sodium borohydride (0.233 g, 6.15 mmol) was added in small portions, and the reaction mixture was stirred at 0 °C for 2.5 hours. The reaction mixture was quenched with water (50 mL), and the organics were decanted and collected. The aqueous phase was extracted with dichloromethane (8 x 50 mL), organics were collected, dried over $MgSO_4$ and all the organics were concentrated *in vacuo*. The crude product was purified by column chromatography (CombiFlash R_f automated column system; 40 g HP silica; A: hexanes, B: ethyl acetate, 100% A to 100% B gradient) to yield the product as a white solid (0.871 g,

72%). ^{1}H NMR (400 MHz, $CDCl_3$) δ 7.40 (d, *J* = 2.3 Hz, 1H), 7.03 (d, *J* = 2.2 Hz, 1H), 4.70 (s, 2H), 3.84 (s, 3H), 3.79 (s, 3H). ^{13}C NMR (101 MHz, $CDCl_3$) δ 167.2, 165.5, 163.0, 148.3, 110.4, 109.0, 64.7, 55.5, 52.8.

6.4.5 Methyl 6-(bromomethyl)-4-methoxypicolinate (6.4)

To a solution of **6.3** (0.74 g, 3.75 mmol) in chloroform (50 mL) at 0 °C, PBr_3 (0.42 mL, 4.50 mmol, 1.2 equiv) was added. The reaction mixture was allowed to warm to room temperature and stirred for 1.5 hours, while monitoring the reaction progress by TLC (R_f = 0.63, EtOAc). The mixture was subsequently quenched with cold saturated K_2CO_3 (40 mL), transferred to a separatory funnel and the organic layer was collected. The aqueous layer was then washed with dichloromethane (3 x 50 mL). The organic fractions were collected and dried over $MgSO_4$. The organic solution was concentrated *in vacuo* to yield the product as a pink solid (0.70 g, 71%). ^{1}H NMR (300 MHz, $CDCl_3$) δ 7.60 (d, *J*=2.3 Hz, 1 H), 7.17 (d, *J*=2.3 Hz, 1 H), 4.59 (s, 2 H), 4.01 (s, 3 H), 3.93 (s, 3 H). ^{13}C NMR (75 MHz, $CDCl_3$) δ 166.6, 164.6, 158.1, 148.5, 112.0, 110.3, 55.2, 52.4, 32.8.

6.4.6 Dimethyl 6,6'-((((1*R*,2*R*)-cyclohexane-1,2-diyl)bis(((2-nitrophenyl)sulfonyl) azane-diyl))bis(methylene))bis(4-methoxypicolinate) (6.5)

To a stirred solution of *N*,*N*'-((1*R*,2*R*)-cyclohexane-1,2-diyl)bis(2-nitrobenzene-sulfonamide)[176] (0.28 g, 0.58 mmol, 1 equiv) and K_2CO_3 (0.48 g, 3.6 mmol, 6 equiv) in CH_3CN (10 mL), methyl 6-(bromomethyl)-4-methoxypicolinate (**6.4**) (0.31 g, 1.16 mmol, 2 equiv) in CH_3CN (5 mL) was added, and the reaction mixture was stirred at reflux for 20 hours. The excess inorganic salts were subsequently removed by centrifugation (4000 rpm, 10 min) and filtration,

and the filtrate was concentrated *in vacuo*. The crude product was purified by column chromatography (CombiFlash R_f automated column system; 24 g HP silica; A: hexanes, B: ethyl acetate, 70% A to 100% B gradient) to yield the product as a yellow solid (0.46 g, 94%). (TLC R_f (product) = 0.67, 100% EtOAc). ^{1}H NMR (300 MHz, $CDCl_3$) δ 7.92 (d, *J* = 7.7 Hz, 2H), 7.54 (m, 4H), 7.42 (m, 4H), 7.23 (m, 2H), 5.05 (d, *J* = 16.7 Hz, 2H), 4.61 (d, *J* = 16.7 Hz, 2H), 4.34 (s, 2H), 3.90 (s, 6H), 3.86 (s, 6H), 2.21 (d, *J* = 7.0 Hz, 2H), 1.71 (m, 2H), 1.42 (m, 2H). ^{13}C NMR (75 MHz, $CDCl_3$) δ 166.8, 165.4, 158.5, 148.2, 147.7, 133.7, 133.0, 131.9, 131.3, 123.5, 111.5, 59.7, 55.8, 52.6, 50.2, 32.2, 25.2. MS (ES+) m/z = 881.4 $[M+K]^+$.

6.4.7 Dimethyl 6,6'-((((1*R*,2*R*)-cyclohexane-1,2-diyl)bis(azanediyl))bis(methylene)) bis(4-methoxypicolinate) (6.6)

To a solution of dimethyl **6.5** (0.46 g, 0.54 mmol, 1 equiv) and K_2CO_3 (0.90 g, 6.52 mmol, 12 equiv) in tetrahydrofuran (20 mL), thiophenol (116 μL, 1.14 mmol, 2.1 equiv) was added and the mixture was stirred at room temperature for 70 hours. The inorganic salts were subsequently filtered out after centrifugation (4000 rpm, 10 min) and the filtrate was concentrated *in vacuo*. The crude product was purified by column chromatography (CombiFlash R_f automated column system; 12 g HP silica; A: dichloromethane, B: 2% triethylamine in methanol, 100% A to 10% B gradient) to yield the product as a yellow oil (0.25 g, 99%). ^{1}H NMR (300 MHz, $CDCl_3$) δ 7.40 (d, *J* = 2.1 Hz, 2H), 7.10 (d, *J* = 2.1 Hz, 2H), 3.99 (d, *J* = 15.0 Hz, 2H), 3.83 (d, *J* = 15.0 Hz, 2H), 3.81 (s, 6H), 3.72 (s, 6H), 3.01 (s, 2H), 2.23 (d, *J* = 8.7 Hz, 2H), 2.01 (m, 2H), 1.58 (d, *J* = 7.5 Hz, 2H), 1.07 (dd, *J* = 17.8, 8.9 Hz, 2H), 0.96 – 0.86 (m, 2H). ^{13}C NMR (75 MHz, $CDCl_3$) δ 166.9, 165.7, 163.0, 148.6, 110.9, 110.0, 61.2, 55.4, 52.7, 52.0, 31.4, 24.7. MS (ES+) m/z = 473.4 $[M+H]^+$.

6.4.8 Me$_2$*CHX*dedpa$_{OMe}$-*N,N'*-ee (6.7)

To a solution of Me$_2$*CHX*dedpa$_{OMe}$ (**6.6**) (79 mg, 0.17 mmol, 1 equiv) in CH_3CN (2 mL), 1-bromo-2-ethoxyethane (66 µL, 0.58 µmol, 3.5 equiv) and Na_2CO_3 (106 mg, 1.00 mmol, 6 equiv) were added. The reaction mixture was stirred at 80 °C for 96 h. Excess salts were removed by centrifugation (4000 rpm for 10 min) and the filtrate was concentrated *in vacuo*. The crude product was purified by column chromatography (CombiFlash R_f automated column system; 24 g HP silica; A: DCM, B: methanol, 100% A to 20% B gradient) and the product (yellowish oil (122 mg)) was obtained as a mixture of product **6.7** and over-alkylated products where 2-ethoxyethane is attached to the ester function(s). The mixture could not be further separated. MS (ES+) m/z = 639.6 $[M+Na]^+$.

6.4.9 Me$_2$*CHX*dedpa$_{OMe}$-*N,N'*-Bn (6.8)

To a solution of Me$_2$*CHX*dedpa$_{OMe}$ (**6.6**) (110 mg, 0.220 mmol) in CH_3CN (2 mL), bromobenzene (68 µL, 0.576 mmol, 2.5 equiv) and Na_2CO_3 (0.15 g, 1.38 mmol, 6 equiv) were added. The reaction mixture was stirred at 60°C for 36 hours. Excess salts were removed by centrifugation (4000 rpm for 10 min) and filtration; the filtrate was concentrated *in vacuo*. The crude product was purified by column chromatography (CombiFlash R_f automated column system; 24 g HP silica; A: DCM, B: methanol, 100% A to 30% B gradient) to afford the product as a brown oil (0.135 g, 80%). ^{1}H NMR signals were broad and could not be integrated. ^{13}C NMR (101 MHz, $CDCl_3$) δ 166.9, 165.2, 163.5, 148.8, 139.6, 129.1, 128.0, 126.9, 111.8, 109.5, 59.3, 55.4, 53.5, 53.6, 46.4, 25.5, 24.5. MS (ES+) m/z = 653.6 $[M+H]^+$.

6.4.10 Me_2*CHX*dedpa$_{OMe}$-*N,N'*-Bn$_{OMe}$ (6.9)

To a stirred solution of Me_2*CHX*dedpa$_{OMe}$ (**6.6**) (0.39 g, 0.80 mmol) in CH_3CN (8 mL) were added Na_2CO_3 (0.53 g, 5.00 mmol, ~6 equiv) and 1-bromomethyl-3-methoxybenzene (243 µL, 1.7 mmol, 2 equiv). The mixture was stirred at 60 °C overnight, after which excess salts were removed by centrifugation (4000 rpm for 10 min) and filtration; the filtrate concentrated *in vacuo*. The crude product was purified by column chromatography (CombiFlash R_f automated column system; 24 g HP silica; A: dichloromethane, B: methanol, 100% A to 20% B gradient) to give the product as a yellow oil (0.48 g, 85%). HR-ESI-MS *m/z* for $C_{40}H_{49}N_4O_8$ $(M+H)^+$ calcd. (found): 713.3550 (713.3548) (-0.3 PPM).

6.4.11 Me_2*CHX*dedpa-*N,N'*-ee (6.10)

To a solution of Me_2*CHX*dedpa[176] (0.231 g, 0.56 mmol, 1 equiv) dissolved in CH_3CN (5 mL), 2-bromoethyl ethyl ether (133 µL, 1.18 mmol, 2.1 equiv) and Na_2CO_3 (0.356 g, 3.36 mmol, 6 equiv) were added. The reaction mixture was stirred at 75°C for 48 h, subsequently cooled to RT and the salts were removed by vacuum filtration; the filtrate was concentrated *in vacuo*. The crude product was purified by column chromatography (CombiFlash R_f automated column system; 24 g HP silica; A: dichloromethane, B: methanol, 100% A to 10% B gradient) to yield the product as a fluffy off-white solid (0.185 g) in a mixture also containing over-alkylated products where 2-ethoxyethane is attached to the ester function(s). The mixture could not be further separated. MS (ES+) m/z = 557.4 $[M+H]^+$.

6.4.12 Me$_2$dedpa-*N,N'*-ee (6.11)

To a solution of Me$_2$dedpa[54,59] (0.151 g, 0.42 mmol, 1 equiv) and K_2CO_3 (0.349 g, 2.52 mmol, 6 equiv) in CH_3CN (5 mL), 2-bromoethyl ethyl ether (119 µL, 1.05 mmol, 2.5 equiv) was added. The mixture was stirred for 24 h at room temperature. Inorganic salts were filtered out by centrifugation and filtration; the organic solution was concentrated *in vacuo*. The product was purified by column chromatography (CombiFlash R_f automated column system; 12 g HP silica; A: dichloromethane, B: methanol, 100% A to 5% B gradient) to yield pure product (0.159 g, 75%). ^{1}H NMR (300 MHz, $CDCl_3$) δ 7.94 – 7.86 (m, 2H), 7.75 – 7.65 (m, 4H), 3.92 (s, 4H), 3.90 (s, 6H), 3.42 (t, *J* = 5.3 Hz, 4H), 3.32 (q, *J* = 7.0 Hz, 4H), 2.74 (d, *J* = 11.7 Hz, 8H), 1.05 (t, *J* = 7.0 Hz, 6H). ^{13}C NMR (75 MHz, $CDCl_3$) δ 165.8, 147.0, 137.4, 126.3, 123.5, 68.5, 66.4, 60.8, 54.3, 53.0, 52.8, 15.1. MS (ES+) m/z = 503.3 $[M+H]^+$, 525.3 $[M+Na]^+$.

6.4.13 (1*R*,2*R*)-*N*^{1},*N*^{2}-bis(2,4,6-trimethoxybenzyl)cyclohexane-1,2-diamine (6.17)

To a solution of (1*R*, 2*R*)-(-)-cyclohexanediamine (0.162 g, 1.42 mmol, 1 equiv) in ethanol (8 mL) at 0°C, a solution of 2,4,6-trimethoxybenzaldehyde (0.557 g, 2.84 mmol, 2 equiv) in ethanol/methanol (1:1, 20 mL) was added. The reaction mixture was stirred overnight and allowed to warm to RT. Bis-imine formation was confirmed by ES-MS (*m/z* = 471.4 $[M+H]^+$), and the solution was again cooled to 0°C on ice. Sodium borohydride (0.17 g, approx. 3 equiv) was added to the reaction mixture in small portions, and the mixture was stirred for 1.5 hours. The mixture was then quenched with saturated NH_4Cl (20 mL), and extracted with dichloromethane (3 x 40 mL). The organics were collected, dried over $MgSO_4$ and concentrated *in vacuo* to yield the product as a faint yellow solid (0.675 g, >99%) which was used in the subsequent step without further purification. ^{1}H NMR (400 MHz, MeOD) δ 6.22 (s, 4H), 4.10 (d, *J* = 12.5 Hz, 2H), 3.82 (s, 6H), 3.79 (d, *J* = 12.5 Hz, 2H), 3.71 (s, 12H), 2.48 (s, 2H), 2.24 (d, *J* = 7.3

Hz, 2H), 1.81 (s, 2H), 1.30 (d, *J* = 6.3 Hz, 4H). ^{13}C NMR (75 MHz, MeOD) δ 163.4, 160.7, 105.0, 91.6, 61.1, 56.2, 56.0, 39.2, 29.9, 25.5. MS (ES+) m/z = 475.4 $[M+H]^+$.

6.4.14 Me_2*CHX*$dedpa_{OMe}$- *N,N'*-Bn_{3OMe} (6.18)

To a solution **6.7** (0.276 g, 0.58 mmol, 1 equiv) and methyl 6-(bromomethyl)-4-methoxypicolinate (**6.4**) (0.322, 1.23 mmol, 2.1 equiv) in CH_3CN (30 mL), Na_2CO_3 (0.355 g, 3.35 mmol, 5.6 equiv) was added, and the reaction mixture was stirred at reflux for 6 hours and subsequently at RT for 2 days. The excess salts were removed by vacuum filtration, and the filtrate was concentrated *in vacuo*. The crude product was purified by column chromatography (CombiFlash R_f automated column system; 24 g HP silica; A: dichloromethane, B: methanol, 100% A to 10% B gradient) to yield the product as a fluffy white solid (0.382 g, 79%). ^{1}H NMR (400 MHz, $CDCl_3$) δ 7.89 (s, 2H), 7.59 (s, 2H), 5.87 – 5.75 (m, 4H), 4.67 (d, *J* = 14.2 Hz, 2H), 4.30 (d, *J* = 13.8 Hz, 2H), 4.10 (d, *J* = 13.7 Hz, 2H), 4.00 (s, 6H), 3.87 (s, 6H), 3.76 (d, *J* = 15.3 Hz, 4H), 3.68 (s, 6H), 3.46 (s, 12H), 3.30 (d, *J* = 9.1 Hz, 2H), 2.16 (d, *J* = 11.9 Hz, 2H), 1.82 (d, *J* = 8.1 Hz, 2H), 1.44 – 1.34 (m, 2H), 1.12 – 1.03 (m, 2H). ^{13}C NMR (101 MHz, $CDCl_3$) δ 167.0, 165.4, 161.8, 159.8, 157.5, 149.1, 113.6, 109.6, 102.1, 90.1, 61.2, 56.1, 55.4, 55.2, 53.5, 52.5, 52.2, 44.6, 26.0, 25.0. MS (ES+) *m/z* = 833.7 $[M+H]^+$.

6.4.15 General Procedure for Methyl Ester Deprotection

To a stirred solution of methyl ester-protected ligand (**6.7 – 6.11, 6.18**) (approx. 60 mg) in THF/water (3:1, 4 mL), LiOH (12 mg, approx. 5 equiv) was added. The reaction mixture was stirred at ambient temperature for 1.5 h or until reaction progress was complete (confirmed by absence of starting material peak in MS, and disappearance of starting material spot on TLC (R_f

(product)< R_f (starting materials)) in 10% MeOH/dichloromethane). The reaction mixture was concentrated *in vacuo* and used without further purification, or purified by semi-preparative RP-HPLC (A: CH_3CN, B: 0.1 % trifluoroacetic acid (TFA) in water, 5 – 100% A linear gradient, 25 min, 10 mL/min). Product fractions were lyophilized to yield the ligand as a white solid (80 – 99% yield).

6.4.16 H_2*CHX*dedpa$_{OMe}$-*N,N'*-ee (6.12)

^{1}H NMR (400 MHz, D_2O, 55°C) δ 7.67 (s, 2H), 7.25 (s, 2H), 4.46 (d, *J* = 13.0 Hz, 2H), 4.26 (d, *J* = 12.0 Hz, 2H), 4.16 (s, 6H), 4.09 – 3.97 (m, 4H), 3.89 – 3.79 (m, 4H), 3.76 (d, *J* = 7.8 Hz, 2H), 3.49 – 3.34 (m, 4H), 2.53 (d, *J* = 11.5 Hz, 2H), 2.21 (d, *J* = 8.2 Hz, 2H), 1.88 – 1.74 (m, 2H), 1.66 (t, *J* = 9.9 Hz, 2H), 1.44 (t, *J* = 7.0 Hz, 6H). ^{13}C NMR (101 MHz, D_2O, 55°C) δ 172.1, 167.8, 156.6, 155.9, 118.4, 115.5, 111.9, 109.3, 67.0, 62.4, 56.1, 24.6, 24.4, 14.5. HR-ESI-MS *m/z* for $C_{30}H_{45}N_4O_8$ $(M+H)^+$ calcd. (found): 589.3237 (589.3237).

6.4.17 H_2*CHX*dedpa$_{OMe}$-*N,N'*-Bn (6.13)

^{1}H NMR (400 MHz, D_2O, 55°C) δ 7.72 (dd, *J* = 13.9, 6.2 Hz, 8H), 7.61 – 7.53 (m, 6H), 4.20 (s, 6H), 4.09 (d, *J* = 15.4 Hz, 2H), 4.03 – 3.92 (m, 6H), 3.20 (d, *J* = 6.7 Hz, 2H), 2.60 (d, *J* = 11.0 Hz, 2H), 2.16 (d, *J* = 6.9 Hz, 2H), 1.62 – 1.50 (m, 4H). ^{13}C NMR (101 MHz, D_2O, 55°C) 129.8, 128.5, 127.5, 110.7, 108.2, 100.1, 60.0, 55.9, 54.6, 54.3, 25.9, 23.9. HR-ESI-MS *m/z* for $C_{36}H_{41}N_4O_6$ $(M+H)^+$ calcd. (found): 625.3026 (625.3020).

6.4.18 H_2*CHX*dedpa$_{OMe}$-*N,N'*-Bn$_{OMe}$ (6.14)

^{1}H NMR (400 MHz, D_2O, 75°C) δ 8.22 (s, 2H), 7.63 (t, *J* = 7.8 Hz, 2H), 7.54 (s, 2H), 7.47 (d, *J* = 7.3 Hz, 2H), 7.37 (s, 2H), 7.31 (d, *J* = 8.3 Hz, 2H), 4.60 (d, *J* = 16.3 Hz, 2H), 4.55 (s, 6H), 4.38 (d, *J* = 18.2 Hz, 2H), 4.33 (s, 4H), 4.13 (s, 6H), 3.84 (d, *J* = 8.3 Hz, 2H), 2.86 (d, *J* = 12.0 Hz, 2H), 2.47 (d, *J* = 8.8 Hz, 2H), 2.10 – 1.97 (m, 2H), 1.93 – 1.80 (m, 2H). ^{13}C NMR (101 MHz, D_2O, 75°C) δ 160.16, 153.42, 149.07, 131.06, 123.55, 116.97, 114.87, 113.66, 111.83, 100.12, 60.57, 57.75, 56.08, 55.36, 51.87, 24.52, 23.98. HR-ESI-MS *m/z* for $C_{38}H_{45}N_4O_8$ $(M+H)^+$ calcd. (found): 685.3237 (685.3231).

6.4.19 H_2*CHX*dedpa-*N,N'*-ee (6.15)

^{1}H NMR (400 MHz, MeOD) δ 8.10 (d, *J* = 7.4 Hz, 2H), 8.01 (t, *J* = 7.5 Hz, 2H), 7.80 (d, *J* = 7.2 Hz, 2H), 4.48 (d, *J* = 14.0 Hz, 2H), 4.06 (d, *J* = 14.1 Hz, 2H), 3.79 – 3.66 (m, 4H), 3.56 – 3.48 (m, 2H), 3.41 – 3.33 (m, 2H), 3.27 – 3.16 (m, 4H), 3.16 – 3.05 (m, 2H), 2.38 (d, *J* = 10.8 Hz, 2H), 1.99 (d, *J* = 6.4 Hz, 2H), 1.94 – 1.76 (m, 2H), 1.70 – 1.56 (m, 2H), 1.51 – 1.32 (m, 4H), 1.12 (s, 4H), 0.96 (t, *J* = 6.5 Hz, 6H). MS (ES+) *m/z* = 529.5 $[M+H]^+$, 535.5 $[M+Li]^+$.

6.4.20 H_2dedpa-*N,N'*-ee (6.16)

^{1}H NMR (300 MHz, MeOD) δ 7.76 (d, *J* = 7.5 Hz, 2H), 7.68 (t, *J* = 7.6 Hz, 2H), 7.20 (d, *J* = 7.4 Hz, 2H), 3.71 (s, 4H), 3.24 – 3.16 (m, 4H), 3.18 – 3.06 (m, 4H), 2.29 – 2.24 (m, 4H), 2.23 (s, 4H), 0.86 (t, *J* = 7.0 Hz, 6H). ^{13}C NMR (75 MHz, MeOD) δ 172.2, 159.5, 154.5, 139.6, 125.5, 123.0, 68.1, 67.3, 61.3, 53.9, 51.6, 15.5. MS (ES+) *m/z* = 475.3 $[M+H]^+$, 481.3 $[M+Li]^+$, 497.3 $[M+Na]^+$.

6.4.21 H_2*CHX*dedpa$_{OMe}$-*N,N'*-Bn$_{3OMe}$ (6.19)

^{1}H NMR (400 MHz, MeOD) δ 7.65 – 7.43 (m, 4H), 5.88 (s, 4H), 3.91 (s, 6H), 3.68 (d, *J* = 26.7 Hz, 2H), 3.63 (s, 6H), 3.55 (d, 2H), 3.48 (s, 12H), 3.32 (d, *J* = 14.2 Hz, 4H), 2.55 (br s, 2H), 2.24 – 1.98 (m, 2H), 1.73 – 1.54 (m, 2H), 1.09 – 0.90 (m, 4H). HR-ESI-MS *m/z* for $C_{42}H_{52}N_4O_{12}$ $(M+H)^+$ calcd. (found): 805.3660 (805.3658) (-0.2 PPM).

6.4.22 General Procedure for Ga(III) Complexation of Pro-ligands (6.12-6.16, 6.19)

A solution of pro-ligand (**6.12-6.16, 6.19**) (0.02 mmol) in water/methanol (1:1, 2 mL) was adjusted to pH 2-3 using 0.1 M HCl (aq). A solution of $Ga(ClO_4)_3 \cdot 6H_2O$ (0.03 mmol, 1.5 equiv) in water (500 μL) was added to this solution, and the pH was then adjusted to 4-4.5 with 0.1 M NaOH (aq). The reaction mixture was stirred at room temperature overnight, over which time a white precipitate formed. The solid was subsequently isolated by centrifugation (4000 rpm, 10 min) and dried further under vacuum to yield the Ga-complex as a white solid (55 - 89% yield).

6.4.23 [Ga(*CHX*dedpa$_{OMe}$-*N,N'*-ee)][ClO_4], [Ga(6.12)][ClO_4]

^{1}H NMR (300 MHz, DMSO) δ 7.76 (s, 2H), 7.75 – 7.70 (m, 2H), 4.87 (d, *J* = 17.7 Hz, 2H), 4.27 (d, *J* = 17.8 Hz, 1H), 4.11 (s, 6H), 3.39 – 3.16 (m, 8H), 2.99 (d, *J* = 3.9 Hz, 2H), 2.88 – 2.75 (m, 2H), 2.16 (d, *J* = 9.7 Hz, 2H), 1.77 – 1.64 (m, 2H), 1.44 – 1.29 (m, 2H), 1.26 – 1.15 (m, 2H), 1.07 (t, *J* = 6.9 Hz, 6H). ^{13}C NMR (resonances obtained from HSQC) (75 MHz, DMSO) δ 111.5, 110.1, 66.3, 63.9, 58.3, 51.5, 51.1, 49.0, 27.7, 24.2, 15.3. HR-ESI-MS *m/z* for $C_{30}H_{42}{}^{69}GaN_4O_8$ $(M)^+$ calcd. (found): 655.2258 (655.2253) (-0.8 PPM).

6.4.24 [Ga(*CHX*dedpa$_{OMe}$-*N,N'*-Bn)][ClO_4], [Ga(6.13)][ClO_4]

^{1}H NMR (300 MHz, DMSO) δ 7.87 – 7.83 (m, 2H), 7.79 (d, *J* = 1.6 Hz, 2H), 7.65 (d, *J* = 6.8 Hz, 4H), 7.45 – 7.32 (m, 6H), 4.71 (br s, 4H), 4.17 (d, *J* = 13.7 Hz, 2H), 4.14 (s, 6H), 3.46 (d, *J* = 13.7 Hz, 2H), 3.25 (2, *J* = 6.5 Hz, 4H), 1.32 – 1.21 (m, 2H), 1.20 – 1.06 (m, 2H), 1.03 – 0.90 (m, 2H). ^{13}C NMR (resonances obtained from HSQC) (75 MHz, DMSO) δ 132.1, 128.7, 112.1, 110.2, 62.5, 62.1, 58.2, 49.3, 40.1. HR-ESI-MS *m/z* for $C_{36}H_{38}{}^{69}GaN_4O_6$ $(M)^+$ calcd. (found): 691.2061 (691.2074) (2.0 PPM).

6.4.25 [Ga(*CHX*dedpa$_{OMe}$-*N,N'*-Bn$_{OMe}$)][ClO_4], [Ga(6.14)][ClO_4]

^{1}H NMR (600 MHz, DMSO) δ 7.83 (d, *J* = 6.0 Hz, 4H), 7.29 (t, *J* = 7.9 Hz, 2H), 7.25 (s, 2H), 7.19 (d, *J* = 7.4 Hz, 2H), 6.99 (dd, *J* = 8.4, 1.7 Hz, 2H), 4.71 (d, *J* = 17.8 Hz, 2H), 4.65 (d, *J* = 17.8 Hz, 2H), 4.15 (s, 6H), 4.12 (d, 2H), 3.83 (d, 2H), 3.74 (s, 6H), 3.23 – 3.17 (m, 2H), 1.29 – 1.20 (m, 4H), 1.16 – 1.07 (m, 4H). HR-ESI-MS *m/z* for $C_{38}H_{42}{}^{69}GaN_4O_8$ $(M)^+$ calcd. (found): 751.2258 (751.2266) (1.1 PPM).

6.4.26 [Ga(*CHX*dedpa-*N,N'*-ee)][ClO_4], [Ga(6.15)][ClO_4]

^{1}H NMR (400 MHz, DMSO) δ 8.82 (t, *J* = 7.8 Hz, 2H), 8.50 (d, *J* = 7.6 Hz, 2H), 8.35 (d, *J* = 7.9 Hz, 2H), 5.14 (d, *J* = 18.2 Hz, 2H), 4.60 (d, *J* = 18.2 Hz, 2H), 3.64 – 3.37 (m, 8H), 3.19 (d, *J* = 8.2 Hz, 2H), 3.09 – 2.98 (m, 4H), 2.37 (d, *J* = 11.3 Hz, 2H), 1.89 (d, *J* = 7.0 Hz, 2H), 1.62 – 1.48 (m, 2H), 1.45 – 1.31 (m, 2H), 1.21 (t, *J* = 7.0 Hz, 6H). ^{13}C NMR (101 MHz, DMSO) δ 162.0, 151.9, 147.0, 144.0, 126.8, 123.6, 66.1, 65.9, 63.8, 57.6, 51.3, 48.8, 27.338, 23.9, 14.9. HR-ESI-MS *m/z* for $C_{28}H_{38}{}^{69}GaN_4O_6$ $(M)^+$ calcd. (found): 595.2047 (595.2048) (0.2 PPM).

6.4.27 [Ga(dedpa-*N,N'*-ee)][ClO_4], [Ga(6.16)][ClO_4]

^{1}H NMR (400 MHz, DMSO) δ 8.66 (t, *J* = 7.8 Hz, 2H), 8.35 (d, *J* = 7.6 Hz, 2H), 8.19 (d, *J* = 7.9 Hz, 2H), 4.71 (d, *J* = 17.6 Hz, 2H), 4.57 (d, *J* = 17.5 Hz, 2H), 3.65 (t, *J* = 4.8 Hz, 4H), 3.43 (q, *J* = 14.1, 7.1 Hz, 5H), 3.37 (d, *J* = 11.1 Hz, 2H), 2.93 (d, *J* = 11.1 Hz, 2H), 2.83 (t, *J* = 4.6 Hz, 4H), 1.11 (t, *J* = 7.0 Hz, 6H). ^{13}C NMR (101 MHz, DMSO) δ 162.2, 150.9, 146.4, 143.6, 128.2, 123.3, 65.8, 64.5, 56.3, 50.9, 48.5, 15.0. HR ESI-MS m/z for $C_{24}H_{32}{}^{69}GaN_4O_6$ (M^+) calcd. (found): 541.1584 (541.1578).

6.4.28 [Ga(*CHX*dedpa$_{OMe}$-*N,N'*-Bn$_{3OMe}$)][ClO_4], [Ga(6.19)][ClO_4]

^{1}H NMR (600 MHz, DMSO) δ 7.82 (s, 2H), 7.80 (s, 2H), 6.19 (s, 4H), 4.43 (dd, *J* = 17.8 Hz, 4H), 4.14 (s, 6H), 4.09 (d, *J* = 14.0 Hz, 2H), 3.76 (s, 12H), 3.69 (s, 6H), 3.29 (d, *J* = 14.5 Hz, 2H), 2.90 (d, *J* = 6.2 Hz, 2H), 1.49 – 1.38 (m, 4H), 1.16 – 1.05 (m, 2H), 0.88 – 0.78 (m, 2H).^{13}C NMR (151 MHz, DMSO) δ 173.4, 162.3, 162.0, 159.7, 153.1, 146.5, 111.8, 109.6, 101.4, 90.8, 65.4, 58.0, 56.0, 55.5, 50.9, 49.7, 29.5, 24.5. HR ESI-MS m/z for $C_{42}H_{50}{}^{69}GaN_4O_{12}$ (M^+) calcd. (found): 871.2681 (871.2684) (0.3 PPM).

6.4.29 ^{67}Ga Radiolabeling Studies

The ^{67}Ga radiolabeling protocol of all pro-ligands followed those previously described in Chapters 2 and 3.

6.4.30 Log *P* Determination

The log *P* of ^{67}Ga-complexes were measured experimentally following procedures outlined in Chapter 3.

6.4.31 Human *apo*-Transferrin Stability Studies

The *in vitro* kinetic inertness assays of ^{67}Ga-complexes against human *apo*-transferrin were performed according to the procedures outlined in Chapter 3.

Chapter 7: Hexadentate Acyclic Chelator H_3dpaa for Ga(III) Radiopharmaceuticals

This chapter is an adaptation of a manuscript in preparation, Ramogida, C. F.; Cawthray, J. F.; Weekes, D. M.; Patrick, B. O.; Adam, M. J.; Orvig, C., Acyclic hexadentate ligand H_3dpaa for Ga(III) radiopharmaceuticals. Expected submission date June **2015**.

7.1 Introduction

A new class of open-chain ligands with varying denticity based on the picolinic acid (pa) moiety have recently been developed by our group, which exhibit promising properties for an array of radiometals.[53,54,62,176] The hexadentate derivative H_2dedpa (N_4O_2) from this subsequently termed "pa" family of ligands, flaunts an exceptionally high thermodynamic stability constant with Ga(III) (log K_{ML} = 28.11(8)), is quantitatively radiolabelled with ^{68}Ga in 10 minutes at ambient temperature, yet, despite being acyclic, forms a kinetically inert Ga-complex.[54] In an effort to explore further the "pa" family and exploit the potential of these ligands in radiopharmaceutical elaboration, a modified hexadentate derivative H_3dpaa (*N,N'*-bis[(carboxypyridin-2-yl)methyl]glycine, N_3O_3) is investigated herein. H_3dpaa and its chelation properties with Lu(III) and Gd(III) as potential MRI contrast agents have been previously reported;[220] however, our interest with this ligand lies with its coordination potential with Ga(III) since $dpaa^{3-}$ would form a neutral charged metal complex with Ga^{3+}. It is often favourable for the ligand to form a metal-complex with overall neutral or near-neutral charge to facilitate clearance of the complex *in vivo* since highly-charged complexes are rapidly excreted through the kidney.

Ga(III) complexation properties, thermodynamic stability, radiolabeling studies with ^{67}Ga, and *in vitro* kinetic inertness were determined to assess the potential of H_3dpaa as a chelating ligand in radiopharmaceutical elaboration for PET imaging with ^{68}Ga.

7.2 Results and Discussion

7.2.1 Synthesis and Characterization

The ligand H_3dpaa (H_3dpaa = *N,N'*-bis[(carboxypyridin-2-yl)methyl]glycine) has been previously reported and its coordination properties with Gd(III) and Lu(III) were investigated as MRI contrast agents.[220] Herein, we were interested in the H_3dpaa ligand for its coordination capacity with Ga(III), as it has the potential to saturate the coordination sphere via the hexadentate N_3O_3 donor atoms and would form a neutral complex.

Scheme 7.1 Synthesis of **7.1**, and H_3dpaa.[a]

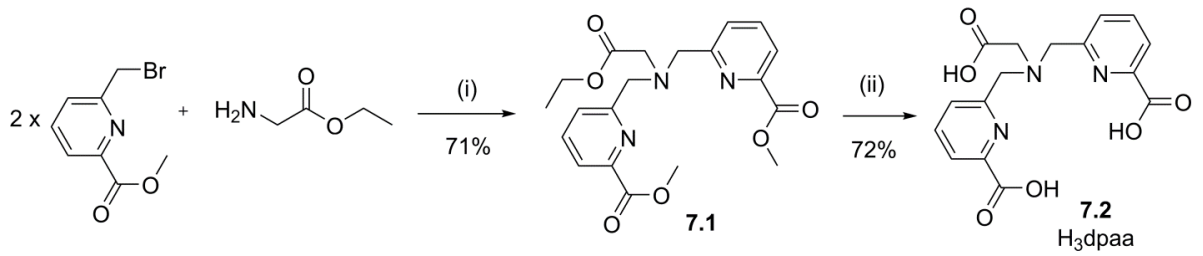

[a]Reagents and conditions: (i) CH_3CN, K_2CO_3, reflux, 18 h; (ii) HCl (6 M), reflux, 42 h.

The ligand H_3dpaa was prepared via a slightly modified synthesis from that previously reported (Scheme 7.1).[220] The synthesis began with bis-alkylation of glycine ethyl ester hydrochloride using methyl 6-(bromomethyl)picolinate under basic conditions (K_2CO_3) to yield

the ester protected ligand **7.1**, which was subsequently deprotected in refluxing HCl (6 M) to give H_3dpaa as an HCl salt (51% cumulative yield). X-ray quality crystals of H_3dpaa were isolated (Figure 7.1) which validated the solution ^{1}H and ^{13}C NMR spectra confirming that the ligand exhibits C_{2v} symmetry.

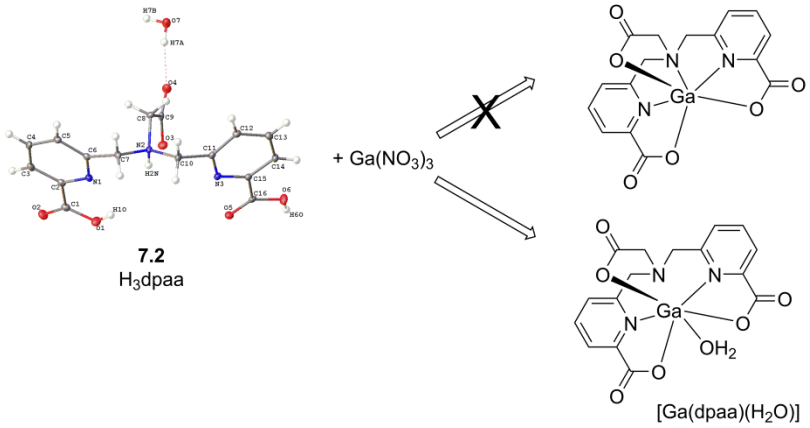

Figure 7.1 Solid-state structure of H_3dpaa·H_2O. Ellipsoids drawn with 50% probability. Projected binding of dpaa^{3-} with Ga(III).

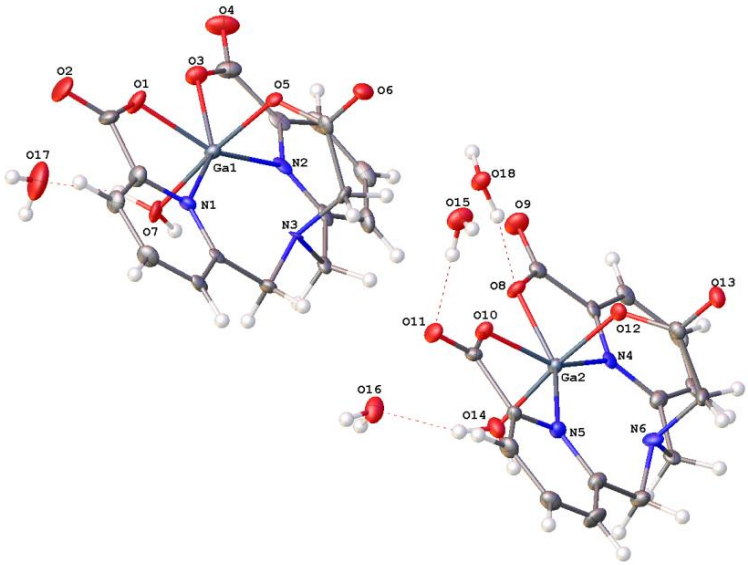

Figure 7.2 X-ray solid state structure of [Ga(dpaa)(H_2O)]. Ellipsoids drawn at 50% probability.

Table 7.1 Selected bond lengths (Å) of the two crystallographically independent units in solid-state structure of [Ga(dpaa)].

Bond	[Ga(dpaa)]1 Bond Length (Å)	[Ga(dpaa)]2 Bond Length (Å)
Ga-N(1)	2.219(4)	2.225(4)
Ga-N(2)	2.179(4)	2.183(4)
Ga-O(1)	2.022(4)	2.044(3)
Ga-O(3)	2.051(4)	2.007(3)
Ga-O(5)	1.932(4)	1.906(4)
Ga-O(7)	1.909(4)	1.916(4)

The Ga(III) complex was prepared via addition of one equiv. of $Ga(ClO_3)_4$ to a stirred solution of H_3dpaa at pH = 3. Solution NMR spectroscopy suggests that [Ga(dpaa)] preserves C_2 symmetry which is also evident in the free ligand, whilst diastereotopic splitting of the methylene hydrogens α to the pyridine arms was observed and used as a diagnostic handle to confirm successful metal coordination. The solid-state structure was also elucidated; the neutral [Ga(dpaa)] complex crystallizes with two crystallographically independent Ga-complexes in the asymmetric unit (Figure 7.2, Table 7.1), where both units exhibit a distorted octahedral structure (N_2O_4), formed by the two pyridine nitrogen atoms (2 x N_{pyr}) and three carboxylate oxygen donors (3 x O_{COO}) with the sixth site occupied by a water molecule (1 x O_{H2O}), and not the tertiary nitrogen atom of the ligand backbone, as expected. Although the solid-state structure shows that the central N atom is slightly puckered between the two picolinic acid arms and pointed fittingly towards the metal centre, this Ga-N_3 distance (2.509 and 2.485 Å, respectively, for each independent unit) is likely too long to be considered a bond, though the values are indeed shorter than the sum of the Van der Waals radii (3.42 Å for Ga-N). The two picolinic acid arms are in one plane, while the carboxylate arm acts as a claw capping the top of the plane with the water molecule capping the bottom of the plane. We predicted that the stability of this complex *in vitro* or *in vivo* would suffer because of this because the coordination site occupied by water would be an easy spot of 'attack' for endogenous ligands which could easily compete for Ga(III) transchelation from the chelate in vivo.

Table 7.2 Stepwise protonation constants (pK_as) of dpaa^{3-} compared with previously reported values.

	L = dpaa^{3-}	Previously reported[220]
$[H_4L]/[H_3L][H]$	1.99(7)	ND
$[H_3L]/[H_2L][H]$	2.65(15)	2.9(1)
$[H_2L]/[HL][H]$	3.59(15)	3.8(1)
$[HL]/[H][L]$	7.48(14)	7.33(3)

7.2.2 Thermodynamic Stability

Step-wise protonation constants (pK_a) of dpaa^{3-} in 0.15 M NaCl at 298 K were determined and compared to the previously reported values[220] which were undertaken at 0.1 M KCl. Good agreement was found between the two sets of values (Table 7.2). Determination of formation constants (log K_{ML}) of dpaa^{3-} with Ga(III) (1:1, metal/ligand) was attempted using potentiometric titration. Direct titration of equimolar amounts of Ga(III) and dpaa^{3-} were performed under a pH range of ~2 – 11. Preliminary fitting of the data yields a log K_{ML} > 20; therefore, meaningful values could not be obtained through direct titrations of ligand-metal and a ligand-ligand competition study with EDTA is required (such as what was done for the ligands dedpa^{2-} and *CHX*dedpa^{2-}). From these preliminary fittings, given a log K_{ML} of ~22, and presence of an MHL species (log K ~ 2) and possibly an ML(OH) species (log K ~13), then the pM would be ~23 (Table 7.3).

The system is further complicated by slow kinetics making it difficult to obtain equilibrium at a reasonable time (30 min) between additions of base, particularly in the pH range 5 – 8. This would be in the pH region where $[Ga(OH)]_3$ forms suggesting the presence of competing hydrolysis side reactions such as ligand to hydroxide exchange at the metal centre, or formation of ML(OH). Slow metal hydrolysis of Ga has also been observed in the literature,

where titrations must be performed in sealed containers and take several days to reach equilibrium.[221]

Table 7.3 Formation constants (log K_{ML}) and pM values of Ga(III) complexes of dpaa^{3-}, previously reported "pa" ligands and macrocyclic gold standard NOTA.

Ligand	Log K_{ML}	pM[a]
dpaa^{3-}	>20	~23
dedpa^{2-} [54]	28.11(8)	27.4
*CHX*dedpa^{2-} [176]	27.61(8)	26.7
*CHX*octapa^{4-} [176]	22.32(20)	21.4
NOTA[133]	30.98	27.9
transferrin[136] [b]	20.3	21.3

[a]Calculated for 1 μM total metal ion, 10 μM total ligand, pH 7.4 at 25 °C. [b]Stability constant for highest binding site in *apo*-transferrin.

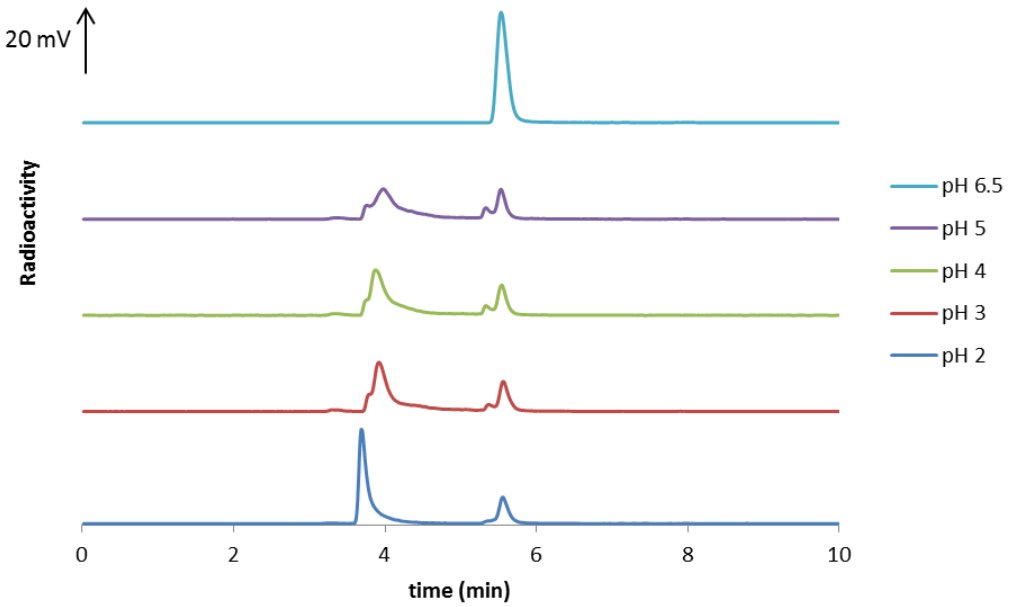

Figure 7.3 HPLC radio-traces of pH dependent labeling (pH = 2 – 6.5) of ^{67}Ga with dpaa^{3-}.

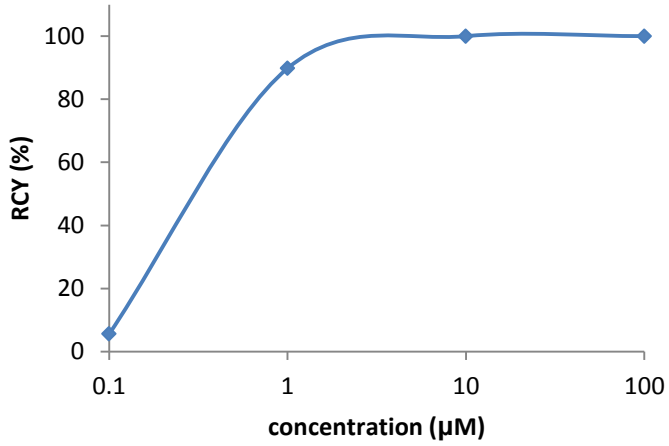

Figure 7.4 Radiochemical yields obtained from concentration dependent labeling (10^{-4} – 10^{-7} M ligand) of ^{67}Ga with $dpaa^{3-}$ at pH 6.5 in 10 minutes at RT.

7.2.3 Radiolabeling Experiments

The γ-emitter ^{67}Ga ($t_{1/2}$ = 3.26 days) was used as a model for ^{68}Ga in the labeling studies herein. Initial ^{67}Ga radiolabeling experiments with H_3dpaa were tested at a range of pHs (2 – 6.5) in NaOAc buffer (10 mM) or pure water. Quantitative labeling (RCY >99%, RCY = radiochemical yield) was achieved at initial ligand concentrations of 10^{-4} M at all pH values, in only 10 minutes at room temperature. However, the labeling behaviour of the ^{67}Ga-dpaa complex gradually changed as the pH was increased from pH 2 to 6.5 (Figure 7.3). Radiolabeling under the most acidic conditions (pH = 2, no buffer added), resulted in two distinct peaks in the HPLC radio-trace (t_R = 3.69 min, t_R = 5.56 min) with peak intensities of 77% and 23%, respectively. When radiolabeling at pH 3, broadening and definite shoulders appeared on each of the two distinct peaks, while the relative peak intensities remained roughly constant (74% and 26%, respectively) with a slight increase (3%) to the peak at later retention. This trend continued as the labeling pH was increased from 3 to 4 to 5; broadening and shoulders became more noticeable and a small increase in labeling yield towards the set of

peaks centred at t_R = 5.5 min was observed. At pH 6.5, one distinct peak in the HPLC radio-chromatogram was detected (t_R = 5.54, RCY >99%).

The appearance of multiple peaks in the HPLC radio-trace at varying pH may be indicative of multiple isomers in solution, which is typically disadvantageous in radiolabeling since different isomers may possess different stabilities *in vitro* and *in vivo*. The possibility of a 2:1 ligand/metal complex being formed in solution is high since there is always excess ligand present in the reaction mixture. Moreover, there is literature precedent of 2:1 $dpaa^{3-}$/Gd(III) complex formation,[220] which suggests the likelihood of such a 2:1 $dpaa^{3-}$/Ga(III) species being formed in solution as well.

Concentration dependent labeling of the [^{67}Ga(dpaa)] complex was performed at pH 6.5, since it resulted in the formation of one peak in the radio-trace (Figure 7.4). Quantitative ^{67}Ga labeling (RCY > 99%) in 10 minutes at room temperature was achieved at ligand concentrations of 10^{-5} M, radiochemical yields decreased to 90% and 6% at ligand concentrations of 10^{-6} and 10^{-7} M, respectively. Reaction conditions such as longer reaction times and increased temperatures were not tested to see whether the radiochemical yield could be improved at these lower ligand concentrations.

7.2.4 Human Serum Stability

In vivo kinetic inertness of the [^{67}Ga(dpaa)] complex was estimated by a 2 hour *in vitro* human serum competition assay and compared to the industry 'gold standards' in Ga chelation NOTA and DOTA (Table 7.4). Pre-formed ^{67}Ga-complex was incubated in excess human serum (37°C, pH 7.4), and aliquots of each reaction mixture were removed at 1 or 2 hour time points. Percent intact ^{67}Ga-complex was determined by size exclusion chromatography to separate any

^{67}Ga which may have transchelated with serum proteins. The macrocycle NOTA is well-known to form a Ga-complex of exceptional kinetic inertness, this fact is reflected in the results obtained by the serum stability assay; these suggest that only 2% of ^{67}Ga transchelated to serum proteins from the NOTA complex after 2 hours. Conversely, ^{67}Ga-dpaa remained approx. 58% intact, with 42% of the ^{67}Ga associated with serum proteins after 2 hours. Due to the modest stability of ^{67}Ga-dpaa in human serum, it is unlikely that dpaa^{3-} would make an appropriate ligand for use with ^{68}Ga *in vivo*.

Table 7.4 *In vitro* human serum stability (37 °C, 2 h) of ^{67}Ga(dpaa) and standards ^{67}Ga-NOTA, ^{67}Ga-DOTA (*n* = 3), with stability shown as the percentage of intact ^{67}Ga complex.

^{67}Ga-complex	1 h (%)	2 h (%)
[^{67}Ga(dpaa)]	60.4 ± 1.3	58.1 ± 3.4
[^{67}Ga(NOTA)]	97.5 ± 0.7	98.0 ± 0.6
[^{67}Ga(DOTA)]$^{-}$	80.1 ± 0.8	80.0 ± 1.9

7.3 Conclusions

The hexadentate bis-picolinic acid chelator H_3dpaa was investigated for its complexation properties with Ga(III). The solid-state X-ray structure of [Ga(dpaa)] revealed a 6-coordinate structure in distorted octahedral geometry with one site occupied by OH_2 instead of the predicted tertiary N of the ligand backbone. Radiolabeling of dpaa^{3-} with ^{67}Ga was accomplished at ambient temperature in 10 minutes; however, pH dependent labeling revealed the presence of multiple isomers in solution at labeling conditions of pH 2 to 5. One isomer was observed at pH 6.5, and quantitative labeling with ^{67}Ga was achieved at ligand concentrations as low as 10^{-5} M and decreased to 90% at 10^{-6} M ligand at this pH. Kinetic inertness of the ^{67}Ga-dpaa complex was assessed through a human serum stability assay and was found to be 58%

intact after 2 hours at 37°C, 22% less stable than ^{67}Ga-DOTA and 40% less stable than ^{67}Ga-NOTA.

It is likely that the presence of multiple isomers in the radiolabeling experiments are due to dimers forming (Ga/dpaa, 1:2), since such behaviour was also seen for the M/dpaa (M = Gd, Lu) complex previously reported.[220] Due to the modest stability of the Ga-dpaa complex *in vitro*, it is unlikely that H_3dpaa would be a suitable ligand for ^{68}Ga PET imaging agent elaboration.

7.4 Experimental

7.4.1 Materials and Methods

The general materials and methods for this chapter followed closely those described in Chapter 2. Compounds **7.1 - 7.2** were prepared from a modified version of a previously published protocol.[220]

7.4.2 Dimethyl 6,6'-(((2-ethoxy-2-oxoethyl)azanediyl)bis(methylene))dipicolinate (7.1)

To a solution of methyl-6-bromomethyl picolinate[138] (0.666 g, 2.90 mmol, 2 equiv) and glycine ethyl ester hydrochloride (0.202 g, 1.45 mmol) in acetonitrile (20 mL), potassium carbonate (1.20 g, 8.70 mmol, 6 equiv) was added and the suspension was stirred at reflux overnight. The mixture was cooled to ambient temperature and the salts were filtered out, and the filtrate was concentrated *in vacuo*. The crude oil was purified by column chromatography (CombiFlash R_f automated column system; 24 g HP silica; A: dichloromethane, B: methanol,

100% A to 20% B gradient) to yield **7.1** as a yellow solid (0.411 g, 71%). ^{1}H NMR (400 MHz, $CDCl_3$) δ 7.83 (dd, *J* = 7.5, 1.0 Hz, 2H), 7.73 (dd, *J* = 7.7, 1.0 Hz, 2H), 7.67 (t, *J* = 7.7 Hz, 2H), 4.00 (q, *J* = 7.1 Hz, 2H), 3.95 (s, 4H), 3.81 (s, 6H), 3.32 (s, 2H), 1.09 (t, *J* = 7.1 Hz, 3H). ^{13}C NMR (101 MHz, $CDCl_3$) δ 170.79, 165.48, 159.67, 147.10, 137.31, 126.10, 123.51, 60.34, 59.73, 55.06, 52.58, 13.98. MS (ES+) m/z = 424.3 $[M+Na]^+$.

7.4.3 H_3dpaa·HCl (7.2)

Compound **7.1** (0.411 g, 1.02 mmol) was dissolved in HCl (6 M, 5 mL) and stirred at reflux for 42 hours. Reaction progress was monitored by ES-MS until complete. The reaction mixture was concentrated *in vacuo* and the resultant white solid was resuspended in ethanol/acetone (1:1). The solid was isolated by vacuum filtration to afford **7.2** as a white solid (0.254 g, 72%). X-ray quality crystals were grown by slow evaporation from a water/methanol mixture. ^{1}H NMR (400 MHz, D_2O) δ 8.10 – 7.99 (m, 4H), 7.73 (dd, *J* = 7.2, 1.3 Hz, 2H), 4.74 (s, 4H), 4.26 (s, 2H). ^{13}C NMR (101 MHz, D_2O) δ 170.46, 166.14, 151.00, 146.21, 141.59, 128.57, 125.44, 58.63, 56.31. Elemental Anal. calcd. (found) for $C_{16}H_{15}N_3O_6$·HCl: C, 50.32 (50.15); H, 4.23 (4.22); N, 11.01 (10.86). HR-ESI-MS m/z for $C_{16}H_{16}N_3O_6$ ($M+H^+$) calcd. (found): 346.1039 (346.1033) (-1.7 PPM).

7.4.4 [Ga(dpaa)]

H_3dpaa•HCl (**7.2**) (29.9 mg, 0.078 mmol) was dissolved in methanol/water (1:1, 4 mL) with gentle heating. To this clear solution, $Ga(ClO_4)_3$•$6H_2O$ (82.0 mg, 0.173 mmol, 2.2 equiv) in water (500 μL) was added. The pH of this solution was adjusted to ~3 using NaOH (aq) (0.1 M), and stirred at 70°C for 1 hour. The mixture was cooled to room temperature at which time a

white precipitate formed, and the solid was isolated by centrifugation (4000 rpm, 10 min) to yield the product as a white solid (32.0 mg, >99%). X-ray quality crystals were grown by slow evaporation from a water/methanol mixture. ^{1}H NMR (400 MHz, DMSO) δ 8.08 (t, *J* = 7.4 Hz, 2H), 7.95 (d, *J* = 7.4 Hz, 2H), 7.61 (d, *J* = 7.5 Hz, 2H), 4.39 (d, *J* = 15.6 Hz, 2H), 4.29 (d, *J* = 15.4 Hz, 2H), 2.99 (s, *J* = 21.6 Hz, 2H). ^{13}C NMR (101 MHz, DMSO) δ 171.57, 157.37, 155.99, 141.74, 126.02, 122.26, 60.36, 60.33. HR-ESI-MS m/z for $C_{16}H_{13}N_3O_6{}^{69}Ga$ (Ga(L)+ H^+) calcd. (found): 412.0060 (412.0059) (-0.2 PPM).

7.4.5 ^{67}Ga Radiolabeling Studies

The chelator H_3dpaa was made up as stock solutions (1 mg/mL, ~10^{-3} M) in deionized water. A 100 µL aliquot of chelator stock solution was transferred to screw-cap mass spectrometry vials and diluted with pH 3 NaOAc (10 mM) buffer such that the final volume was 1 mL after the addition of $^{67}GaCl_3$, to a final chelator concentration of ~10^{-4} M for each sample. An aliquot of $^{67}GaCl_3$ (~1 mCi for labeling studies and ~3-6 mCi for serum competitions) was added to the vials containing the chelator and allowed to radiolabel at ambient temperature for 10 min, then analyzed by RP-HPLC to confirm radiolabeling and calculate yields. Areas under the peaks observed in the HPLC radiotrace were integrated to determine radiolabeling yields. Elution conditions used for RP-HPLC analysis were gradient: A: 0.1% trifluoroacetic acid (TFA) in H_2O, B: CH_3CN; 0 to 100% B linear gradient 20 min. (t_R = 3.3 min for free ^{67}Ga).

7.4.6 Human Serum Stability Data

The compound [^{67}Ga(dpaa)] was prepared with the radiolabeling protocol as described above. Human serum was removed from the freezer and allowed to thaw at ambient

temperature for 1 hour. In triplicate, solutions were prepared in vials with 750 μL of human serum, 500 μL of ^{67}Ga-complex, and 250 μL of phosphate buffered saline (PBS), and incubated at 37°C in a water bath. At time points 1 and 2 hours, 500 μL of the human serum competition mixture was removed from each vial, diluted to a total volume of 2.5 mL with PBS, and then counted in a Capintec CRC 15R well counter to obtain a value for the total activity to be loaded on the PD-10 column. The 2.5 mL of diluted human serum mixture was loaded onto a PD-10 column that had previously been conditioned via elution with 20 mL of PBS, and the empty vial was counted in a well counter to determine the residual activity left in the vial. The 2.5 mL of loading volume was allowed to elute into a waste container, and then the PD-10 column was eluted with 3.5 mL of PBS and collected into a separate vial. The eluent which contained ^{67}Ga bound/associated with serum proteins (size exclusion for MW < 5000 Da) was counted in a well counter and then compared to the total amount of activity that was loaded on the PD-10 column to obtain the percentage of ^{67}Ga that was bound to serum proteins and therefore no longer chelate-bound.

7.4.7 Solution Thermodynamics

The experimental procedures and details of the apparatus closely followed those of a previous study for H_2dedpa with Ga^{3+},[54] and those found in Chapter 2. Protonation constants of the pro-ligands and stability constants of Ga(III) were calculated using previously reported methods.[54]

7.4.8 X-ray Crystallography

X-ray crystallography was performed and solved by Dr. B. O. Patrick. A colourless prism crystal of $C_{16}H_{15}N_3O_6.H_2O$ (H_3dpaa·H_2O) having approximate dimensions of 0.15 x 0.24 x 0.35 mm was mounted on a glass fiber. All measurements were made on a Bruker APEX DUO diffractometer with graphite monochromated Mo-Kα radiation. The data were collected at a temperature of -183.0 ± 0.1°C to a maximum 2θ value of 60.1°. Data were collected in a series of ϕ and ω scans in 0.5° oscillations using 1.0-second exposures. The crystal-to-detector distance was 38.17 mm. Of the 21149 reflections that were collected, 4522 were unique (R_{int} = 0.026); equivalent reflections were merged. Data were collected and integrated using the Bruker SAINT[141] software package. The linear absorption coefficient, μ, for Mo-Kα radiation is 1.25 cm^{-1}. Data were corrected for absorption effects using the multi-scan technique (SADABS[142]), with minimum and maximum transmission coefficients of 0.900 and 0.981, respectively. The data were corrected for Lorentz and polarization effects. The structure was solved by direct methods.[146] The material crystallizes with two crystallographically independent molecules in the asymmetric unit. In one formula unit one phenyl ring is disordered in two orientations. The disorder is essentially a slight rotation about the N42—C81 bond. All non-hydrogen atoms were refined anisotropically. All NH hydrogen atoms were located in difference maps and refined isotropically. All other hydrogen atoms were placed in calculated positions. All refinements were performed using the SHELXL-2012[143] via the OLEX2[192] interface.

A colourless prism crystal of [Ga($C_{16}H_{12}N_3O_6$)]·$3H_2O$ ([Ga(dpaa)]) having approximate dimensions of 0.08 x 0.12 x 0.21 mm was mounted on a glass fiber. All measurements were made on a Bruker APEX DUO diffractometer with graphite monochromated Mo-Kα radiation. The data were collected at a temperature of -183.0 ± 0.1°C to a maximum 2θ value of 60.2°. Data were collected in a series of ϕ and ω scans in 0.5° oscillations using 10.0-second exposures.

The crystal-to-detector distance was 50.09 mm. The material crystallizes as a two-component 'split-crystal' with components one and two related by a 178° rotation about the (0 1 0) reciprocal axis. Data were integrated for both components, including both overlapped and non-overlapped reflections. In total 108372 reflections were integrated (50579 from component one only, 50288 from component two only, 7475 overlapped). Data were collected and integrated using the Bruker SAINT[1] software packages. The linear absorption coefficient, μ, for Mo-Kα radiation is 14.54 cm^{-1}. Data were collected and integrated using the Bruker SAINT[141] software packages. Data were corrected for absorption effects using the multi-scan technique (TWINABS[222]), with minimum and maximum transmission coefficients of 0.762 and 0.890, respectively. The data were corrected for Lorentz and polarization effects. The structure was solved by direct methods[146] using non-overlapped data from the major twin component. Subsequent refinements were carried out using an HKLF 4 format data set containing complete data from component one. The material crystallizes with two crystallographically independent Ga-complexes in the asymmetric unit. In addition, at least 6 water molecules are found in the asymmetric unit. Any residual electron density that could not be reasonably modeled was removed via the Olex2 solvent-mask function. All non-hydrogen atoms were refined anisotropically. All hydrogen atoms were placed in calculated positions, including water hydrogen atoms. All refinements were performed using the SHELXL-2013[143] via the OLEX2[192] interface.

Chapter 8: Conclusions and Future Work

8.1 Thesis Summary and Suggestions for Future Work

The studies throughout this thesis primarily focused on elaborating the hexadentate "pa" ligand H_2dedpa into a viable radiopharmaceutical for ^{68}Ga PET imaging. In addition to the β^+-emitter ^{68}Ga, some of the newly synthesized chelating systems were also studied for their coordination ability with copper and indium isotopes. A variety of modifications were made on the ligand backbone which required lengthy and sometimes challenging syntheses of polar amine-containing compounds. The result of much synthetic labour culminated in the preparation of three new chiral *CHX*-"pa" ligands in Chapter 2, nine nitroimidazole dedpa^{2-} and *CHX*dedpa^{2-} ligands in Chapter 3, two new bifunctional/"bi-modal" dedpa^{2-} ligands in Chapter 5, and six new lipophilic dedpa^{2-} and *CHX*dedpa^{2-} derivatives in Chapter 6. Through a combination of coordination chemistry, potentiometry, density functional theory, radiolabeling, *in vitro*, and *in vivo* studies the acyclic chelating ligands were evaluated as ligand systems in radiopharmaceutical design.

Chapter 2 studied the effect of changing the flexible ethylenediamine backbone in H_2dedpa and H_4octapa to the rigid chiral *trans*-cyclohexanediamine backbone. The newly termed *CHX*-"pa" ligands possess an augmented pre-organised set of donor atoms making them more 'macrocyclic-like' ligands. We hypothesized that H_2*CHX*dedpa and H_4*CHX*octapa would form metal complexes of high kinetic inertness and thermodynamic stability while retaining the ability to complex radioisotopes quickly, quantitatively, and at room temperature. Following the synthesis and evaluation of the *CHX*-"pa" ligands, the results of H_2*CHX*dedpa with Ga(III)/$^{67/68}$Ga and H_4*CHX*octapa with In(III)/^{111}In supported our hypothesis. These two chiral acyclic ligands can be added to the Orvig group's family of "pa" chelates for clinically relevant

and high impact radioisotopes. Although our preliminary studies were promising, further investigation with the *CHX*-"pa" ligands is required. The ultimate utility of these ligands will be dependent on two factors: 1. the biodistribution of their respective radiometal-complexes *in vivo*, and 2. The ability to synthesize bifunctional derivatives. Future work should entail biodistribution studies with $[^{68}Ga(\textit{CHX}dedpa)]^{+}$ and $[^{111}In(\textit{CHX}octapa)]^{-}$ and compared directly with previously studied $[^{68}Ga(dedpa)]^{+}$ and $[^{111}In(octapa)]^{-}$ in order to verify that the "bare" (non-targeted) radiometal-chelate complexes clear quickly from non-target tissue and are appropriately excreted. Secondly, the synthesis of bifunctional *CHX*-"pa" ligands will be necessary to attach targetting vectors of interest and move forward with testing *in vivo*; this will allow for the direct comparison of *CHX*-"pa" bioconjugates with the gold standards, such as *p*-SCN-benzyl derivatives of NOTA and DOTA. The same synthetic route employed to synthesize bifunctional H_2dedpa and H_4octapa, where bifunctionality was introduced via the ethylenediamine backbone to form H_2dedap-*p*-Bz-NCS[19,54] and H_2octapa-*p*-Bz-NCS,[59] is not available for H_2*CHX*dedpa and H_4*CHX*octapa which possess a cyclohexanediamine backbone. Development of a new synthetic strategy for functionalization of the cyclohexanediamine backbone would be of great interest in the future. Moreover, the synthetic strategy used to produce pyridyl-functionalized $dedpa^{2-}$ (H_2dedpa-$propyl_{pyr}$-NH_2) synthesized in Chapter 5 could be extended to make an equivalent bifunctional *CHX*$dedpa^{2-}$ or *CHX*$octapa^{4-}$ analogue. In addition, future work should also include evaluation of the octadentate ligand, H_4*CHX*octapa, with other radiometals such as ^{177}Lu, $^{86/90}$Y, and ^{44}Sc. Given the increase in stability observed for $[^{68}Ga(\textit{CHX}dedpa)]^{+}$ compared to $[^{68}Ga(dedpa)]^{+}$, substituting the rigid *CHX*-en onto some of the other higher denticity "pa" frameworks may result in ligands that form kinetically inert metal complexes, such as H_5decapa (N_5O_5) or H_3nonapa (N_6O_3) that originally displayed poor metal-complex stabilities.[61] Broadly speaking, the coordination chemistry of H_4*CHX*octapa with lanthanides may be interesting to study as potential MRI contrast agents.

In Chapter 3, nine nitroimidazole containing derivatives of the promising Ga(III) chelating ligands H_2dedpa and H_2*CHX*dedpa (N_4O_2) were synthesized, characterized and screened for their ability to bind Ga(III). Their feasibilities as PET imaging agents of hypoxia with ^{68}Ga were tested. These novel H_2(*CHX*)dedpa-*N,N'*-alkyl-nitroimidazole ligands were quantitatively radiolabelled with $^{67/68}$Ga (10 min, RT), exhibited exceptional *in vitro* stability, and showed promising preferential uptake in hypoxic cell lines. Preliminary *in vivo* dynamic PET and biodistribution results with one of the ^{68}Ga-radiotracers showed fast clearance of the tracer from non-target tissue and renal excretion. Unfortunately, all tumour xenografts were insufficient in size or non-existent resulting in no delineation of the tumour in the PET/CT images and marginal tumour uptake at 2 h p.i. in the biodistribution profile. Future *in vivo* studies should be performed with mice bearing larger tumours, and direct comparison between our novel ^{68}Ga-dedpa-NI tracers with clinical standard hypoxia agent ^{18}F-MISO should be made in order to give context to the results.

At the time of writing this thesis, copper isotopes could not be provided, consequently, much of the work in Chapter 4 focused on the non-radioactive Cu(II) coordination chemistry of pro-ligands synthesized in Chapters 2 and 3. Radioactive work should thus be completed in the future.

Chapter 5 presented the synthesis of a new bifunctional H_2dedpa derivative (H_2dedpa-propyl$_{pyr}$-NH_2); much of the synthetic protocol towards the preparation of this new BFC was developed by our group member Dr. Lisa Murphy. In Chapter 5, this BFC was utilized in a conjugation reaction for the first time with fluorophore FITC, making the first proof-of-principle "bi-modal" H_2dedpa agent for radio- and fluorescence imaging. The ramifications of attaching bulky fluorophores at the 4-position of the pyridyl system were such that ^{67}Ga radiolabeling was unsuccessful. These conclusions hammered home an important concept in ligand design:

the site of linker/biomolecule attachment on the chelate must not affect the metal complexation ability of the ligand. Nonetheless, H_2dedpa-propyl$_{pyr}$-NH_2 may be a candidate for bioconjugation to lighter molecular weight targeting vectors and future work should entail such studies. Moreover, the synthetic protocol used to synthesize this pyridyl functionalized H_2dedpa ligand can be extended for use with other higher denticity "pa" ligands, such as H_4(*CHX*)octapa, or H_5decapa, in order to produce new bifunctional "pa" ligands which can then be conjugated to clinically relevant biomolecules.

In Chapter 6, we hoped to exploit the mono-cationic [Ga(*CHX*dedpa)]$^+$ complex by synthesising a small library of lipophilic *CHX*dedpa^{2-} derivatives that would mimic properties associated with the commercially available ^{99m}Tc SPECT agents for myocardial perfusion imaging. Preliminary ^{67}Ga radiolabeling studies of the five newly synthesized lipophilic *CHX*dedpa^{2-} derivatives revealed some interesting radio-chromatograms which suggested ligand radiolysis of the *N,N'*-benzyl functionalized ligands was occurring. Future work should entail more in depth radiolabeling studies to test this hypothesis. The findings of Chapter 2, which revealed that *CHX*dedpa^{2-} forms exceptionally inert complexes with Ga(III), merits the study of other lipophilic *CHX*dedpa^{2-} analagoues in the future. Accordingly, the H_2*CHX*dedpa framework is a high priority target for incorporation into a MPI agent for ^{68}Ga PET. Moving forward, development of new synthetic strategies is necessary in order to incorporate different lipophilic appendages onto the ligand backbone which do not inhibit radiolabeling while forming a gallium complex that displays a fine balance between persistant heart uptake and low liver uptake. For example, H_2*CHX*dedpa analogues with integrated poly-ether linkages would be interesting synthetic targets.

The hexadentate N_3O_3 chelating ligand H_3dpaa studied in Chapter 7 displayed multiple isomers in ^{67}Ga radiolabeling reactions as well as only moderate stability of the resultant ^{67}Ga-

complex (~60% intact after 2 h in serum at 37°C). Due to the less than optimal properties for $^{67/68}Ga^{3+}$ chelation, this ligand should probably not be studied in the future. However, $dpaa^{3-}$ might be a ligand of interest for future study with radioisotopes of copper, scandium, or technetium.

8.2 Concluding Remarks and Outlook

Our group has extensively studied a class of acyclic chelating ligands which bear picolinic acid moieties, this "pa" family of ligands show great utility for labeling with a variety of clinically relevant radiometals.[53,54,59–63,131] The previous identification of lead ligand candidates H_2dedpa[19,54] and H_4octapa[53,59] for use in Ga(III) and In(III) radiopharmaceuticals, respectively, has sparked our interest in further developing these promising candidates for use *in vivo*. What is most remarkable about the acyclic "pa" ligands is that (in particular for H_2dedpa/H_2*CHX*dedpa with Ga^{3+} and H_4octapa/H_4*CHX*octapa with In^{3+}) they form kinetically inert radiometal complexes, while retaining the ability to quantitatively complex radiometals in 10 minutes at ambient temperature. This is in stark contrast to most commonly studied acyclic chelates (EDTA or DTPA) which fall victim to rapid decomplexation kinetics resulting in loss of the radiometal *in vivo*, or to macrocyclic chelates which often require radiolabeling at elevated temperatures and lengthy reaction times. Given their unique and attractive traits, H_2dedpa/H_2*CHX*dedpa and H_4octapa/ H_4*CHX*octapa warrant further investment.

In particular, H_2dedpa and H_2*CHX*dedpa should be further investigated with $^{68}Ga^{3+}$, some progress was made through the studies presented in this thesis, yet more development is needed to translate these ligand systems to the clinic. With the exception of one proof-of-principle bioconjugation of H_2dedpa-*p*-Bn-NCS with the cyclic peptide cRGDyk,[19] no other biomolecules have been affixed to either $dedpa^{2-}$ or *CHX*$dedpa^{2-}$. The attachment of these

ligands to new and emerging peptides or antibody fragments (particularly those which are heat sensitive and will not survive the labeling protocols imposed by macrocycles), and subsequent *in vivo* testing will undoubtedly add value to these hexadentate "pa" ligands.

Along with ^{68}Ga, many other promising β^+-emitting radiometals and therapeutic isotopes are gaining traction as viable alternatives to the standard radioisotopes used currently in nuclear medicine. The introduction of these radiometals in the clinic will strongly depend on research advances in chelate chemistry. For example, therapeutic nuclides such as ^{177}Lu, ^{212}Pb, ^{213}Bi, and ^{225}Ac (quite often) form unstable complexes with the current set of ligands available to the researcher or clinician. In this regard, the "pa" ligands have the potential to make an impact in radiopharmaceutical design. Some of the higher denticity "pa" ligands (CN = 8 or higher), such as H$_4$*CHX*octapa, H$_4$octapa, or H$_5$decapa, should be studied with these isotopes, as they may form stable complexes with some of these radiometals. Furthermore, their modular assembly will allow for the preparation of new "pa" ligands. By tuning the donor atom type, geometry, and denticity, the ligand properties can be matched appropriately to the unique coordination preferences of each radiometal. For example, swapping out the acetate arms in *CHX*octapa^{2-} for chelating arms that contain nitrogen donors would produce a softer donor set which could be more suitably matched for Pb(II) chelation.

Mild room temperature radiolabeling of the "pa" ligands will allow for conjugation to heat-sensitive biomolecules. Conjugation to new and relevant biomolecules, such as those discussed in Chapter 1, and testing *in vivo* should be the progression of future studies in order to bring H$_2$dedpa, H$_2$*CHX*dedpa, H$_4$octapa, or H$_4$*CHX*octapa to the next level and closer to use in a clinical setting.

Bibliography

(1) Cancer Fact Sheet No. 297. - World Health Organization, 2012. http://www.who.int/mediacentre/factsheets/fs297/en/ (accessed December 2012).

(2) Miller, P. W.; Long, N. J.; Vilar, R.; Gee, A. D. *Angew. Chem. Int. Ed. Engl.* **2008**, *47*, 8998–9033.

(3) Lilly, E. Cardinal Health - List of FDA approved radiopharmaceuticals http://www.cardinal.com/ (accessed March 2015).

(4) Bolzati, C.; Refosco, F.; Marchiani, A.; Ruzza, P. *Curr. Med. Chem.* **2010**, *17*, 2656–2683.

(5) Liu, S.; Chakraborty, S. *Dalton Trans.* **2011**, *40*, 6077–6086.

(6) Bhattacharyya, S.; Dixit, M. *Dalton Trans.* **2011**, *40*, 6112–6128.

(7) Holland, J. P.; Williamson, M. J.; Lewis, J. S. *Mol. Imaging* **2010**, *9*, 1–20.

(8) Wadas, T. J.; Wong, E. H.; Weisman, G. R.; Anderson, C. J. *Chem. Rev.* **2010**, *110*, 2858–2902.

(9) Smith, S. V. *J. Inorg. Biochem.* **2004**, *98*, 1874–1901.

(10) Gomes, C. M.; Abrunhosa, A. J.; Ramos, P.; Pauwels, E. K. J. *Adv. Drug Deliv. Rev.* **2011**, *63*, 547–554.

(11) Verel, I.; Visser, G. W. M.; van Dongen, G. A. *J. Nucl. Med.* **2005**, *46 Suppl 1*, 164S – 171S.

(12) Ganguly, B. N.; Mondal, N. N.; Nandy, M.; Roesch, F. *J. Radioanal. Nucl. Chem.* **2009**, *279*, 685–698.

(13) Zeglis, B. M.; Lewis, J. S. *Dalton Trans.* **2011**, *40*, 6168–6195.

(14) Volkert, W. A.; Goeckeler, W. F.; Ehrhardt, G. J.; Ketring, A. R. *J. Nucl. Med.* **1991**, *32*, 174–185.

(15) Boswell, C. A.; Brechbiel, M. W. *Nucl. Med. Biol.* **2007**, *34*, 757–778.

(16) Vaidyanathan, G.; Zalutsky, M. R. *Phys. Med. Biol.* **1996**, *41*, 1915–1931.

(17) O'Donoghue, J. A.; Wheldon, T. E. *Phys. Med. Biol.* **1996**, *41*, 1973–1992.

(18) Boswell, C. A.; Brechbiel, M. W. *J. Nucl. Med.* **2005**, *46*, 1946–1947.

(19) Boros, E.; Ferreira, C. L.; Yapp, D. T. T.; Gill, R. K.; Price, E. W.; Adam, M. J.; Orvig, C. *Nucl. Med. Biol.* **2012**, *39*, 785–794.

(20) Jurisson, S. S.; Lydon, J. D. *Chem. Rev.* **1999**, *99*, 2205–2218.

(21) Vāvere, A. L.; Lewis, J. S. *Dalton Trans.* **2007**, *0*, 4893–4902.

(22) Dearling, J. L. J.; Packard, A. B. *Nucl. Med. Biol.* **2010**, *37*, 237–243.

(23) Harris, W. R. *Struct. Bond.* **1998**, *92*, 121–162.

(24) Sun, H.; Cox, M. C.; Li, H.; Sadler, P. J. *Sruct. Bond.* **1997**, *88*, 72–102.

(25) Anderson, C. J.; Welch, M. J. *Chem. Rev.* **1999**, *99*, 2219–2234.

(26) Qaim, S. M. *Q. J. Nucl. Med Mol Imaging* **2008**, *52*, 111–120.

(27) Blower, P. J.; Lewis, J. S.; Zweit, J. *Nucl. Med. Biol.* **1996**, *23*, 957–980.

(28) Clinical Trials. http://www.clinicaltrials.gov/ (accessed February 2015).

(29) Shokeen, M.; Wadas, T. J. *Med. Chem.* **2011**, *7*, 413–429.

(30) Shannon, R. *Acta Crystallogr. Sect. A Cryst. Phys.* **1976**, *A32*, 751–767.

(31) Bartholomä, M. D. *Inorganica Chim. Acta* **2012**, *389*, 36–51.

(32) Fani, M.; Andre, J. P.; Maecke, H. R. *Contrast Media Mol. Imaging* **2008**, *3*, 53–63.

(33) Perk, L. R.; Visser, G. W. M.; Vosjan, M. J. W. D.; Walsum, M. S.; Tijink, B. M.; Rene, C.; Dongen, G. A. M. S. Van. *J. Nucl. Med.* **2005**, *46*, 1898–1906.

(34) Deri, M. A.; Zeglis, B. M.; Francesconi, L. C.; Lewis, J. S. *Nucl. Med. Biol.* **2013**, *40*, 3–14.

(35) Abou, D. S.; Ku, T.; Smith-Jones, P. M. *Nucl. Med. Biol.* **2011**, *38*, 675–681.

(36) Liu, S. *Adv. Drug Deliv. Rev.* **2008**, *60*, 1347–1370.

(37) Cutler, C. S.; Hennkens, H. M.; Sisay, N.; Huclier-Markai, S.; Jurisson, S. S. *Chem. Rev.* **2013**, *113*, 858–883.

(38) Milenic, D. E.; Brady, E. D.; Brechbiel, M. W. *Nat. Rev. Drug Discov.* **2004**, *3*, 488–499.

(39) Ma, D.; McDevitt, M. R.; Finn, R. D.; Scheinberg, D. A. *Appl. Radiat. Isot.* **2001**, *55*, 667–678.

(40) Donnelly, P. S. *Dalton Trans.* **2011**, *40*, 999–1010.

(41) Schötzig, U.; Schrader, H.; Schönfeld, E.; Günther, E.; Klein, R. *Appl. Radiat. Isot.* **2001**, *55*, 89–96.

(42) Yong, K.; Brechbiel, M. W. *Dalton Trans.* **2011**, *40*, 6068–6076.

(43) Bowen, M. L.; Orvig, C. *Chem. Commun.* **2008**, *41*, 5077–5091.

(44) Couturier, O.; Supiot, S.; Degraef-Mougin, M.; Faivre-Chauvet, A.; Carlier, T.; Chatal, J.-F.; Davodeau, F.; Cherel, M. *Eur. J. Nucl. Med. Mol. Imaging* **2005**, *32*, 601–614.

(45) Miederer, M.; Scheinberg, D. A.; McDevitt, M. R. *Adv. Drug Deliv. Rev.* **2008**, *60*, 1371–1382.

(46) McDevitt, M.; Ma, D.; Simon, J.; Frank, R. K.; Scheinberg, D. A. *Appl. Radiat. Isot.* **2002**, *57*, 841–847.

(47) Chappell, L. L.; Deal, K. A.; Dadachova, E.; Brechbiel, M. W. *Bioconjugate Chem.* **2000**, *11*, 510–519.

(48) Gustafsson, A. M. E.; Bäck, T.; Elgqvist, J.; Jacobsson, L.; Hultborn, R.; Albertsson, P.; Morgenstern, A.; Bruchertseifer, F.; Jensen, H.; Lindegren, S. *Nucl. Med. Biol.* **2012**, *39*, 15–22.

(49) Rosenblat, T. L.; McDevitt, M. R.; Mulford, D. a; Pandit-Taskar, N.; Divgi, C. R.; Panageas, K. S.; Heaney, M. L.; Chanel, S.; Morgenstern, A.; Sgouros, G.; Larson, S. M.; Scheinberg, D. a; Jurcic, J. G. *Clin. Cancer Res.* **2010**, *16*, 5303–5311.

(50) Hassfjell, S.; Brechbiel, M. W. *Chem. Rev.* **2001**, *101*, 2019–2036.

(51) Brechbiel, M. W.; Gansow, O. A.; Pippin, C. G.; Rogers, R. D.; Planalp, R. P. *Inorg. Chem.* **1996**, *35*, 6343–6348.

(52) Chappell, L. L.; Dadachova, E.; Milenic, D. E.; Garmestani, K.; Wu, C.; Brechbiel, M. W. *Nucl. Med. Biol.* **2000**, *27*, 93–100.

(53) Price, E. W.; Cawthray, J. F.; Bailey, G.; Ferreira, C. L.; Boros, E.; Adam, M. J.; Orvig, C. *J. Am. Chem. Soc.* **2012**, *134*, 8670–8683.

(54) Boros, E.; Ferreira, C. L.; Cawthray, J. F.; Price, E. W.; Patrick, B. O.; Wester, D. W.; Adam, M. J.; Orvig, C. *J. Am. Chem. Soc.* **2010**, *132*, 15726–15733.

(55) Chang, A. J.; Silva, R. A. De; Lapi, S. E. *Mol. Imaging* **2013**, *12*, 17–27.

(56) Ferreiros-Martinez, R.; Esteban-Gomez, D.; Platas-Iglesias, C.; de Blas, A.; Rodriguez-Blas, T. *Dalton Trans.* **2008**, *42*, 5754–5765.

(57) Platas-Iglesias, C.; Mato-Iglesias, M.; Djanashvili, K.; Muller, R. N.; Elst, L. Vander; Peters, J. A.; de Blas, A.; Rodriguez-Blas, T. *Chem. A Eur. J.* **2004**, *10*, 3579–3590.

(58) Ferreirós-Martínez, R.; Esteban-Gómez, D.; Platas-Iglesias, C.; De Blas, A.; Rodríguez-Blas, T. *Inorg. Chem.* **2009**, *48*, 10976–10987.

(59) Price, E.; Zeglis, B.; Cawthray, J. F.; Ramogida, C. F.; Ramos, N.; Lewis, J. S.; Adam, M. J.; Orvig, C. *J. Am. Chem. Soc.* **2013**, *135*, 12707–12721.

(60) Price, E. W.; Zeglis, B. M.; Cawthray, J. F.; Lewis, J. S.; Adam, M. J.; Orvig, C. *Inorg. Chem.* **2014**, *53*, 10412–10431.

(61) Price, E.; Ferreira, C.; Adam, M. J.; Orvig, C. *Can. J. Chem.* **2014**, *92*, 695–705.

(62) Bailey, G. A.; Price, E. W.; Zeglis, B. M.; Ferreira, C. L.; Boros, E.; Lacasse, M. J.; Patrick, B. O.; Lewis, J. S.; Adam, M. J.; Orvig, C. *Inorg. Chem.* **2012**, *51*, 12575–12589.

(63) Price, E. W.; Zeglis, B. M.; Lewis, J. S.; Adam, M. J.; Orvig, C. *Dalton Trans.* **2014**, *43*, 119–131.

(64) Correia, J. D. G.; Paulo, A.; Raposinho, P. D.; Santos, I. *Dalt. Trans.* **2011**, *40*, 6144–6167.

(65) Craig, A. S.; Parker, D.; Adams, H.; Bailey, N. A. *J. Chem. Soc., Chem. Commun.* **1989**, *1*, 1793–1794.

(66) Khan, I. U.; Beck-Sickinger, A. G. *Anticancer. Agents Med. Chem.* **2008**, *8*, 186–199.

(67) Tircsó, G.; Benyó, E. T.; Suh, E. H.; Jurek, P.; Kiefer, G. E.; Sherry, A. D.; Kovács, Z. *Bioconjug. Chem.* **2009**, *20*, 565–575.

(68) Notni, J.; Hermann, P.; Havlícková, J.; Kotek, J.; Kubíček, V.; Plutnar, J.; Loktionova, N.; Riss, P. J.; Rösch, F.; Lukeš, I. *Chem. A Eur. J.* **2010**, *16*, 7174–7185.

(69) Ferreira, C. L.; Lamsa, E.; Woods, M.; Duan, Y.; Fernando, P.; Bensimon, C.; Kordos, M.; Guenther, K.; Jurek, P.; Kiefer, G. E. *Bioconjugate Chem.* **2010**, *21*, 531–536.

(70) Ferreira, C. L.; Yapp, D. T.; Lamsa, E.; Gleave, M.; Bensimon, C.; Jurek, P.; Kiefer, G. E. *Nucl. Med. Biol.* **2008**, *35*, 875–882.

(71) Notni, J.; Šimeček, J.; Hermann, P.; Wester, H.-J. *Chem. A Eur. J.* **2011**, *17*, 14718–14722.

(72) Boswell, C. A.; Regino, C. A. S.; Baidoo, K. E.; Wong, K. J.; Bumb, A.; Xu, H.; Milenic, D. E.; Kelley, J. A.; Lai, C. C.; Brechbiel, M. W. *Bioconjugate Chem.* **2008**, *19*, 1476–1484.

(73) Maheshwari, V.; Dearling, J. L. J.; Treves, S. T.; Packard, A. B. *Inorg. Chim. Acta* **2012**, *393*, 318–323.

(74) Cooper, M. S.; Ma, M. T.; Sunassee, K.; Shaw, K. P.; Williams, J. D.; Paul, R. L.; Donnelly, P. S.; Blower, P. J. *Bioconjugate Chem.* **2012**, *23*, 1029–1039.

(75) Deal, K. A.; Davis, I. A.; Mirzadeh, S.; Kennel, S. J.; Brechbiel, M. W. *J. Med. Chem.* **1999**, *42*, 2988–2992.

(76) Wängler, C.; Schirrmacher, R.; Bartenstein, P.; Wängler, B. *Curr. Med. Chem.* **2010**, *17*, 1092–1116.

(77) Lebedev, A. Y.; Holland, J. P.; Lewis, J. S. *Chem. Commun.* **2010**, *46*, 1706–1708.

(78) Struthers, H.; Spingler, B.; Mindt, T. L.; Schibli, R. *Chem. A Eur. J.* **2008**, *14*, 6173–6183.

(79) Hanahan, D.; Weinberg, R. A. *Cell* **2000**, *100*, 57–70.

(80) Ciavarella, S.; Milano, A.; Dammacco, F.; Silvestris, F. *BioDrugs* **2010**, *24*, 77–88.

(81) Denoyer, D.; Perek, N.; Le Jeune, N.; Dubois, F. *Curr. Cancer Drug Targets* **2006**, *6*, 181–196.

(82) Ting, G.; Chang, C.; Wang, H. *Anticancer Res.* **2009**, *29*, 4107–4118.

(83) Hamoudeh, M.; Kamleh, M. A.; Diab, R.; Fessi, H. *Adv. Drug Deliv. Rev.* **2008**, *60*, 1329–1346.

(84) Dijkers, E. C. F.; Kosterink, J. G. W.; Rademaker, A. P.; Perk, L. R.; van Dongen, G. A. M. S.; Bart, J.; de Jong, J. R.; de Vries, E. G. E.; Lub-de Hooge, M. N. *J. Nucl. Med.* **2009**, *50*, 974–981.

(85) Ruzza, P.; Calderan, A. *Expert Opin. Med. Diagn.* **2011**, *5*, 411–424.

(86) De Graaf, A. J.; Kooijman, M.; Hennink, W. E.; Mastrobattista, E. *Bioconjugate Chem.* **2009**, *20*, 1281–1295.

(87) Langer, M.; Beck-Sickinger, A. G. *Curr. Med. Chem. Anticancer. Agents* **2001**, *1*, 71–93.

(88) Younes, C. K.; Boisgard, R.; Tavitian, B. *Curr. Pharm. Des.* **2002**, *8*, 1451–1466.

(89) Olafsen, T.; Wu, A. M. *Semin. Nucl. Med.* **2010**, *40*, 167–181.

(90) Knowles, S. M.; Wu, A. M. *J. Clin. Oncol.* **2012**, *30*, 3884–3892.

(91) Hoppmann, S.; Qi, S.; Miao, Z.; Liu, H.; Jiang, H.; Cutler, C. S.; Bao, A.; Cheng, Z. *J. Biol. Inorg. Chem.* **2012**, *17*, 709–718.

(92) Smith-Jones, P. M.; Solit, D. B.; Akhurst, T.; Afroze, F.; Rosen, N.; Larson, S. M. *Nat. Biotechnol.* **2004**, *22*, 701–706.

(93) Welch, M. J.; Hawker, C. J.; Wooley, K. L. *J. Nucl. Med.* **2009**, *50*, 1743–1746.

(94) Fani, M.; Maecke, H. R. *Eur. J. Nucl. Med. Mol. Imaging* **2012**, *39 Suppl 1*, S11–S30.

(95) Benedetti, E.; Morelli, G.; Accardo, A.; Mansi, R.; Tesauro, D.; Aloj, L. *BioDrugs* **2004**, *18*, 279–295.

(96) Koopmans, K. P.; Glaudemans, A. W. J. M. *Eur. J. Nucl. Med. Mol. Imaging* **2012**, *39 Suppl 1*, S4–S10.

(97) Maecke, H. R.; Hofmann, M.; Haberkorn, U. *J. Nucl. Med.* **2005**, *46*, 172–178.

(98) Gaertner, F. C.; Kessler, H.; Wester, H.-J.; Schwaiger, M.; Beer, A. J. *Eur. J. Nucl. Med. Mol. Imaging* **2012**, *39 Suppl 1*, S126–S138.

(99) Kim, J.-H.; Lim, J.-C.; Yun, K.-C.; Choi, S.-J.; Hong, Y.-D. *J. Label. Compd. Radiopharm.* **2012**, *55*, 10–17.

(100) Wadas, T. J.; Deng, H.; Sprague, J. E.; Zheleznyak, A.; Weilbaecher, K. N.; Anderson, C. J. *J. Nucl. Med.* **2009**, *50*, 1873–1880.

(101) Shi, J.; Kim, Y.-S.; Chakraborty, S.; Zhou, Y.; Wang, F.; Liu, S. *Amino Acids* **2011**, *41*, 1059–1070.

(102) Ma, M. T.; Neels, O. C.; Denoyer, D.; Roselt, P.; Karas, J. A.; Scanlon, D. B.; White, J. M.; Hicks, R. J.; Donnelly, P. S. *Bioconjugate Chem.* **2011**, *22*, 2093–2103.

(103) Liu, Z.; Shi, J.; Jia, B.; Yu, Z.; Liu, Y.; Zhao, H.; Li, F.; Tian, J.; Chen, X.; Liu, S.; Wang, F. *Mol. Pharmaceutics* **2011**, *8*, 591–599.

(104) Jiang, M.; Ferdani, R.; Shokeen, M.; Anderson, C. J. *Nucl. Med. Biol.* **2013**, *40*, 245–251.

(105) Shetty, D.; Lee, Y.-S.; Jeong, J. M. *Nucl. Med. Mol. Imaging (2010).* **2010**, *44*, 233–240.

(106) Wei, L.; Zhang, X.; Gallazzi, F.; Miao, Y.; Jin, X.; Brechbiel, M. W.; Xu, H.; Clifford, T.; Welch, M. J.; Lewis, J. S.; Quinn, T. P. *Nucl. Med. Biol.* **2009**, *36*, 345–354.

(107) Miao, Y.; Hoffman, T. J.; Quinn, T. P. *Nucl. Med. Biol.* **2005**, *32*, 485–493.

(108) Ma, M. T.; Donnelly, P. S. *Curr. Top. Med. Chem.* **2011**, *11*, 500–520.

(109) Mansi, R.; Wang, X.; Forrer, F.; Waser, B.; Cescato, R.; Graham, K.; Borkowski, S.; Reubi, J. C.; Maecke, H. R. *Eur. J. Nucl. Med. Mol. Imaging* **2011**, *38*, 97–107.

(110) Costantini, D. L.; Villani, D. F.; Vallis, K. a; Reilly, R. M. *J. Nucl. Med.* **2010**, *51*, 477–483.

(111) Rösch, F.; Baum, R. *Dalton Trans.* **2011**, *40*, 6104–6111.

(112) Bartholomä, M. D.; Louie, A. S.; Valliant, J. F.; Zubieta, J. *Chem. Rev.* **2010**, *110*, 2903–2920.

(113) Ramogida, C. F.; Orvig, C. *Chem. Commun.* **2013**, *49*, 4720–4739.

(114) Price, E. W.; Orvig, C. *Chem. Soc. Rev.* **2014**, *43*, 260–290.

(115) Ruser, G.; Ritter, W.; Maecke, H. R. *Bioconjugate Chem.* **1990**, *1*, 345–349.

(116) Andre P., J.; Maecke R., H.; Zehnder, M.; Macko, L.; Akyel G., K. *Chem. Commun.* **1998**, *12*, 1301–1302.

(117) Riesen, A.; Kaden, T. A.; Ritter, W.; Maecke, H. R. *J. Chem. Soc. Chem. Commun.* **1989**, 460–462.

(118) Brechbiel, M.; Gansow, O.; Atcher, R. W.; Schlom, J.; Esteban, J.; Simpson, D. E.; Colcher, D. *Inorg. Chem.* **1986**, *25*, 2772–2781.

(119) Wu, C.; Kobayashi, H.; Sun, B.; Yoo, T.; Paik, C. H.; Gansow, O. A.; Carrasquillo, J. A.; Pastan, I.; Brechbiel, M. W. *Bioorg. Med. Chem.* **1997**, *5*, 1925–1934.

(120) Camera, L.; Kinuya, S.; Garmestani, K.; Wu, C.; Brechbiel, M. W.; Pai, L. H.; McMurry, T. J.; Gansow, O. A.; Pastan, I.; Paik, C. H. *J. Nucl. Med.* **1994**, *35*, 882–889.

(121) Clifford, T.; Boswell, C. A.; Biddlecombe, G. B.; Lewis, J. S.; Brechbiel, M. W. *J. Med. Chem.* **2006**, *49*, 4297–4304.

(122) Milenic, D. E.; Garmestani, K.; Chappell, L. L.; Dadachova, E.; Yordanov, A.; Ma, D.; Schlom, J.; Brechbiel, M. W. *Nucl. Med. Biol.* **2002**, *29*, 431–442.

(123) Hens, M.; Vaidyanathan, G.; Zhao, X.-G.; Bigner, D. D.; Zalutsky, M. R. *Nucl. Med. Biol.* **2010**, *37*, 741–750.

(124) Burke, B. P.; Clemente, G. S.; Archibald, S. J. *J. Labelled Comp. Radiopharm.* **2014**, *57*, 239–243.

(125) Simeček, J.; Zemek, O.; Hermann, P.; Notni, J.; Wester, H.-J. *Mol. Pharmaceutics* **2014**, *11*, 3893–3903.

(126) Deri, M. A.; Ponnala, S.; Zeglis, B. M.; Pohl, G.; Dannenberg, J. J.; Lewis, J. S.; Francesconi, L. C. *J. Med. Chem.* **2014**, *57*, 4849–4860.

(127) Dale, A. V; Pandya, D. N.; Kim, J. Y.; Lee, H.; Ha, Y. S.; Bhatt, N.; Kim, J.; Seo, J. J.; Lee, W.; Kim, S. H.; Yoon, Y.-R.; An, G. Il; Yoo, J. *ACS Med. Chem. Lett.* **2013**, *4*, 927–931.

(128) Ma, M. T.; Cooper, M. S.; Paul, R. L.; Shaw, K. P.; Karas, J. A.; Scanlon, D.; White, J. M.; Blower, P. J.; Donnelly, P. S. *Inorg. Chem.* **2011**, *50*, 6701–6710.

(129) Boros, E.; Rybak-akimova, E.; Holland, J. P.; Rietz, T.; Rotile, N.; Blasi, F.; Day, H.; Lati, R.; Caravan, P. *Mol. Pharmaceutics* **2014**, *11*, 617–629.

(130) Boswell, C. A.; Sun, X.; Niu, W.; Weisman, G. R.; Wong, E. H.; Rheingold, A. L.; Anderson, C. J. *J. Med. Chem.* **2004**, *47*, 1465–1474.

(131) Boros, E.; Cawthray, J. F.; Ferreira, C. L.; Patrick, B. O.; Adam, M. J.; Orvig, C. *Inorg. Chem.* **2012**, *51*, 6279–6284.

(132) Boros, E.; Ferreira, C. L.; Patrick, B. O.; Adam, M. J.; Orvig, C. *Nucl. Med. Biol.* **2011**, *38*, 1165–1174.

(133) Clarke, E. T.; Martell, A. E. *Inorg. Chim. Acta* **1991**, *181*, 273–280.

(134) Clarke, E. T.; Martell, A. E. *Inorg. Chim. Acta* **1991**, *190*, 37–46.

(135) Geraldes, C. F. G. C.; Delgado, R.; Urbanof, A. M.; Costa, J.; Jasanadac, F.; Nepveu, F. *J. Chem. Soc. Dalton Trans.* **1995**, 327–335.

(136) Harris, W. R.; Pecoraro, V. L. *Biochemistry* **1983**, *22*, 292–299.

(137) Harris, W.; Chen, Y.; Wein, K. *Inorg. Chem.* **1994**, *33*, 4991–4998.

(138) Zeng, X.; Coquière, D.; Alenda, A.; Garrier, E.; Prangé, T.; Li, Y.; Reinaud, O.; Jabin, I. *Chem. A Eur. J.* **2006**, *12*, 6393–6402.

(139) Gans, P.; O'Sullivan, B. *Talanta* **2000**, *51*, 33–37.

(140) Gans, P.; Sabatini, A.; Vacca, A. *Talanta* **1996**, *43*, 1739–1753.

(141) *SAINT*, version 7.60A; Bruker AXS Inc.: Madison, WI, 1997–2010.

(142) *SADABS*, v2008/1; Bruker AXS Inc.: Madison, WI, 2008.

(143) Sheldrick, G. M. *Acta Crystallogr. A.* **2008**, *64*, 112–122.

(144) Farrugia, L. J. *J. Appl. Crystallogr.* **1999**, *32*, 837–838.

(145) Farrugia, L. J. *Appl. Crystallogr.* **2012**, *45*, 849–854.

(146) Altomare, A.; Burla, M. C.; Camalli, M.; Cascarano, G. L.; Giacovazzo, C.; Guagliardi, A.; Moliterni, A. G. G.; Polidori, G.; Spagna, R. *J. Appl. Crystallogr.* **1999**, *32*, 115–119.

(147) Parson, S.; Flack, H. D. *Acta Crystallogr.* **2004**, *A60*, s61.

(148) Frisch, M. J.; Trucks, G. W.; Schlegel, H. B.; Scuseria, G. E.; Robb, M. A.; Cheeseman, J. R.; Scalmani, G.; Barone, V.; Mennucci, B.; Petersson, G. A.; Nakatsuji, H.; Caricato, M.; Li, X.; Hratchian, H. P.; Izmaylov, A. F.; Bloino, J.; Zheng, G.; Sonnenberg, J. L.; Hada, M.; Ehara, M.; Toyota, K.; Fukuda, R.; Hasegawa, J.; Ishida, M.; Nakajima, T.; Honda, Y.; Kitao, O.; Nakai, H.; Vreven, T.; Montgomery, J. A.; Peralta, J. E.; Ogliaro, F.; Bearpark, M.; Heyd, J. J.;

Brothers, E.; Kudin, K. N.; Staroverov, V. N.; Kobayashi, R.; Normand, J.; Raghavachari, K.; Rendell, A.; Burant, J. C.; Iyengar, S. S.; Tomasi, J.; Cossi, M.; Rega, N.; Millam, J. M.; Klene, M.; Knox, J. E.; Cross, J. B.; Bakken, V.; Adamo, C.; Jaramillo, J.; Gomperts, R.; Stratmann, R. E.; Yazyev, O.; Austin, A. J.; Cammi, R.; Pomelli, C.; Ochterski, J. W.; Martin, R. L.; Morokuma, K.; Zakrzewski, V. G.; Voth, G. A.; Salvador, P.; Dannenberg, J. J.; Dapprich, S.; Daniels, A. D.; Farkas, Ö.; Foresman, J. B.; Ortiz, J. V.; Cioslowski, J.; Fox, D. J. *Gaussion 09*, Revision D.01; Gaussian Inc.: Wallingford, CT, 2009.

(149) Lee, C.; Yang, W.; Parr, R. *Phys. Rev. B* **1988**, *37*, 785–789.

(150) Becke, A. D. *J. Chem. Phys.* **1993**, *98*, 5648–5652.

(151) Krohn, K. A.; Link, J. M.; Mason, R. P. *J. Nucl. Med.* **2008**, *49*, 129S – 148S.

(152) Peitzsch, C.; Perrin, R.; Hill, R. P.; Dubrovska, A.; Kurth, I. *Int. J. Radiat. Biol.* **2014**, *90*, 636–652.

(153) Lucignani, G. *Eur. J. Nucl. Med. Mol. Imaging* **2008**, *35*, 838–842.

(154) Wilson, W. R.; Hay, M. P. *Nat. Rev. Cancer* **2011**, *11*, 393–410.

(155) Carlin, S.; Humm, J. L. *J. Nucl. Med.* **2012**, *53*, 1171–1174.

(156) Chitneni, S. K.; Palmer, G. M.; Zalutsky, M. R.; Dewhirst, M. W. *J. Nucl. Med.* **2011**, *52*, 165–168.

(157) Okuda, K.; Okabe, Y.; Kadonosono, T.; Ueno, T.; Youssif, B. G. M.; Kizaka-Kondoh, S.; Nagasawa, H. *Bioconjugate Chem.* **2012**, *23*, 324–329.

(158) Horsman, M. R.; Mortensen, L. S.; Petersen, J. B.; Busk, M.; Overgaard, J. *Nat. Rev. Clin. Oncol.* **2012**, *9*, 674–687.

(159) Nunn, A.; Linder, K.; Strauss, H. W. *Eur. J. Nucl. Med. Mol. Imaging* **1995**, *22*, 265–280.

(160) Padhani, A. R.; Krohn, K. A.; Lewis, J. S.; Alber, M. *Eur. J. Radiol.* **2007**, *17*, 861–872.

(161) Edwards, D. I. *J. Antimicrob. Chemother.* **1993**, *31*, 9–20.

(162) McClelland, R. A.; Panicucci, R.; Rauth, A. M. *J. Am. Chem. Soc.* **1987**, *109*, 4308–4314.

(163) Hicks, R. J.; Rischin, D.; Fisher, R.; Binns, D.; Scott, A. M.; Peters, L. J. *Eur. J. Nucl. Med. Mol. Imaging* **2005**, *32*, 1384–1391.

(164) Eschmann, S.; Paulsen, F.; Reimold, M.; Dittmann, H.; Welz, S.; Reischl, G.; Machulla, H.; Bares, R. *J. Nucl. Med.* **2005**, *46*, 253–260.

(165) Picchio, M.; Beck, R.; Haubner, R.; Seidl, S.; Machulla, H.-J.; Johnson, T. D.; Wester, H.-J.; Reischl, G.; Schwaiger, M.; Piert, M. *J. Nucl. Med.* **2008**, *49*, 597–605.

(166) Piert, M.; Machulla, H.; Picchio, M.; Reischl, G.; Ziegler, S.; Kumar, P.; Beck, R.; Mcewan, A. J. B.; Wiebe, L. I.; Schwaiger, M. *J. Nucl. Med.* **2005**, *46*, 106–113.

(167) Chitneni, S. K.; Bida, G. T.; Zalutsky, M. R.; Dewhirst, M. W. *J. Nucl. Med.* **2014**, *55*, 1192–1198.

(168) Komar, G.; Seppänen, M.; Eskola, O.; Lindholm, P.; Grönroos, T. J.; Forsback, S.; Sipilä, H.; Evans, S. M.; Solin, O.; Minn, H. *J. Nucl. Med.* **2008**, *49*, 1944–1951.

(169) Evans, S. M.; Kachur, A. V; Shiue, C. Y.; Hustinx, R.; Jenkins, W. T.; Shive, G. G.; Karp, J. S.; Alavi, A.; Lord, E. M.; Dolbier, W. R.; Koch, C. J. *J. Nucl. Med.* **2000**, *41*, 327–336.

(170) Brown, J. M.; Workman, P. *Radiat. Res.* **1980**, *82*, 171–190.

(171) Lopci, E.; Grassi, I.; Chiti, A.; Nanni, C. *Am. J. Nucl. Med. Mol. Imaging* **2014**, *4*, 365–384.

(172) Green, M. A.; Welch, M. J. *Int. J. Rad. Appl. Instrum. B.* **1989**, *16*, 435–448.

(173) Hoigebazar, L.; Jeong, J. M.; Choi, S. Y.; Choi, J. Y.; Shetty, D.; Lee, Y.-S.; Lee, D. S.; Chung, J.-K.; Lee, M. C.; Chung, Y. K. *J. Med. Chem.* **2010**, *53*, 6378–6385.

(174) Hoigebazar, L.; Jeong, J. M.; Hong, M. K.; Kim, Y. J.; Lee, J. Y.; Shetty, D.; Lee, Y.-S.; Lee, D. S.; Chung, J.-K.; Lee, M. C. *Bioorg. Med. Chem.* **2011**, *19*, 2176–2181.

(175) Fernández, S.; Dematteis, S.; Giglio, J.; Cerecetto, H.; Rey, A. *Nucl. Med. Biol.* **2013**, *40*, 273–279.

(176) Ramogida, C. F.; Cawthray, J. F.; Boros, E.; Ferreira, C. L.; Patrick, B. O.; Adam, M. J.; Orvig, C. *Inorg. Chem.* **2015**, *54*, 2017–2031.

(177) Long, A.; Parrick, J.; Hodgkiss, R. *Synthesis* **1991**, *9*, 709–713.

(178) Squella, J. A.; Núñez-Vergara, L. J.; Campero, A.; Maraver, J.; Jara-Ulloa, P.; Carbajo, J. *J. Electrochem. Soc.* **2007**, *154*, F77–F81.

(179) Valdez, C.; Tripp, J. *J. Med. Chem.* **2009**, *52*, 4038–4053.

(180) Wagh, N. K.; Zhou, Z.; Ogbomo, S. M.; Shi, W.; Brusnahan, S. K.; Garrison, J. C. *Bioconjugate Chem.* **2012**, *23*, 527–537.

(181) Huang, H.; Mei, L.; Chu, T. *Molecules* **2012**, *17*, 6808–6820.

(182) Bollo, S.; Jara-Ulloa, P.; Zapata-Torres, G.; Cutiño, E.; Sturm, J. C.; Núñez-Vergara, L. J.; Squella, J. A. *Electrochim. Acta* **2010**, *55*, 4558–4566.

(183) Malyshev, K. V.; Smirnov, V. V. *Radiokhimiya* **1975**, *17*, 137–140.

(184) Lin, K.-S.; Pan, J.; Amouroux, G.; Turashvili, G.; Mesak, F.; Hundal-Jabal, N.; Pourghiasian, M.; Lau, J.; Jenni, S.; Aparicio, S.; Benard, F. *Cancer Res.* **2015**, *75*, 387–393.

(185) Van der Sluis, P.; Spek, A. L. *Acta Crystallogr. Sect. A Found. Crystallogr.* **1990**, *46*, 194–201.

(186) Cai, Z.; Anderson, C. J. *J. Labelled Comp. Radiopharm.* **2014**, *57*, 224–230.

(187) Liu, S.; Li, D.; Huang, C.-W.; Yap, L.-P.; Park, R.; Shan, H.; Li, Z.; Conti, P. S. *Theranostics* **2012**, *2*, 589–596.

(188) Tan, K. V.; Pellegrini, P. a; Skelton, B. W.; Hogan, C. F.; Greguric, I.; Barnard, P. J. *Inorg. Chem.* **2014**, *53*, 468–477.

(189) Esteves, C. V; Lamosa, P.; Delgado, R.; Costa, J.; Désogère, P.; Rousselin, Y.; Goze, C.; Denat, F. *Inorg. Chem.* **2013**, *52*, 5138–5153.

(190) Woodin, K. S.; Heroux, K. J.; Boswell, C. A.; Wong, E. H.; Weisman, G. R.; Niu, W.; Tomellini, S. A.; Anderson, C. J.; Zakharov, L. N.; Rheingold, A. L. *Eur. J. Inorg. Chem.* **2005**, 4829–4833.

(191) Parsons, S.; Flack, H. *Acta Crystallogr. Sect. A Found. Crystallogr.* **2004**, *60*, s61–s61.

(192) Dolomanov, O. V.; Bourhis, L. J.; Gildea, R. J.; Howard, J. A. K.; Puschmann, H. *J. Appl. Crystallogr.* **2009**, *42*, 339–341.

(193) Thorp-Greenwood, F. L.; Coogan, M. P. *Dalton Trans.* **2011**, *40*, 6129–6143.

(194) Keereweer, S.; Kerrebijn, J. D. F.; Van Driel, P. B. a a; Xie, B.; Kaijzel, E. L.; Snoeks, T. J. A; Que, I.; Hutteman, M.; Van Der Vorst, J. R.; Mieog, J. S. D.; Vahrmeijer, A. L.; Van De Velde, C. J. H.; Baatenburg De Jong, R. J.; Löwik, C. W. G. M. *Mol. Imaging Biol.* **2011**, *13*, 199–207.

(195) Jennings, L. E.; Long, N. J. *Chem. Commun.* **2009**, 3511–3524.

(196) Emerson, D. K.; Limmer, K. K.; Hall, D. J.; Han, S.-H.; Eckelman, W. C.; Kane, C. J.; Wallace, a. M.; Vera, D. R. *Radiology* **2012**, *265*, 186–193.

(197) Bernhard, Y.; Winckler, P.; Perrier-Cornet, J.-M.; Decréau, R. A. *Dalton Trans.* **2015**, *44*, 3200–3208.

(198) Cui, L.; Zhong, Y.; Zhu, W.; Xu, Y.; Du, Q.; Wang, X.; Qian, X.; Xiao, Y. *Org. Lett.* **2011**, *13*, 928–931.

(199) Komatsu, H.; Harada, H.; Tanabe, K.; Hiraoka, M.; Nishimoto, S. *Med. Chem. Commun.* **2010**, *1*, 50–53.

(200) Nakata, E.; Yukimachi, Y.; Kariyazono, H.; Im, S.; Abe, C.; Uto, Y.; Maezawa, H.; Hashimoto, T.; Okamoto, Y.; Hori, H. *Bioorg. Med. Chem.* **2009**, *17*, 6952–6958.

(201) Tanabe, K.; Hirata, N.; Harada, H.; Hiraoka, M.; Nishimoto, S. I. *ChemBioChem* **2008**, *9*, 426–432.

(202) Sutherland, R.; Carlsson, J.; Durand, R.; Yuhas, J. *Cancer Res.* **1981**, *41*, 2980–2984.

(203) Zhang, J. Z.; Bryce, N. S.; Siegele, R.; Carter, E. A.; Paterson, D.; de Jonge, M. D.; Howard, D. L.; Ryan, C. G.; Hambley, T. W. *Integr. Biol.* **2012**, *4*, 1072–1080.

(204) Yamamoto, N.; Renfrew, A. K.; Kim, B. J.; Bryce, N. S.; Hambley, T. W. *J. Med. Chem.* **2012**, *55*, 11013–11021.

(205) Zhang, J. Z.; Bryce, N. S.; Lanzirotti, A.; Chen, C. K. J.; Paterson, D.; de Jonge, M. D.; Howard, D. L.; Hambley, T. W. *Metallomics* **2012**, *4*, 1209–1217.

(206) Kim, B. J.; Hambley, T. W.; Bryce, N. S. *Chem. Sci.* **2011**, *2*, 2135–2142.

(207) Pryor, K. E.; Shipps, G. W.; Skyler, D. a.; Rebek, J. *Tetrahedron* **1998**, *54*, 4107–4124.

(208) Bryce, N. S.; Zhang, J. Z.; Whan, R. M.; Yamamoto, N.; Hambley, T. W. *Chem. Commun.* **2009**, 2673–2675.

(209) American Heart Association http://www.heart.org/HEARTORG/HealthcareResearch/Healthcare-Research_UCM_001093_SubHomePage.jsp. (accessed March 2015)

(210) Hachamovitch, R.; Berman, D. S.; Shaw, L. J.; Kiat, H.; Cohen, I.; Cabico, J. A.; Friedman, J.; Diamond, G. A. *Circulation* **1998**, *97*, 535–543.

(211) Gibson, R. S.; Watson, D. D.; Craddock, G. B.; Crampton, R. S.; Kaiser, D. L.; Denny, M. J.; Beller, G. A. *Circulation* **1983**, *68*, 321–336.

(212) Liu, S. *Dalton Trans.* **2007**, 1183–1193.

(213) Maria, L.; Fernandes, C.; Garcia, R.; Gano, L.; Paulo, A.; Santos, I. C.; Santos, I. *Dalton Trans.* **2009**, 603–606.

(214) Yang, B. Y.; Jeong, J. M.; Kim, Y. J.; Choi, J. Y.; Lee, Y. S.; Lee, D. S.; Chung, J. K.; Lee, M. C. *Nucl. Med. Biol.* **2010**, *37*, 149–155.

(215) Tarkia, M.; Saraste, A.; Saanijoki, T.; Oikonen, V.; Vähäsilta, T.; Strandberg, M.; Stark, C.; Tolvanen, T.; Teräs, M.; Savunen, T.; Green, M. a.; Knuuti, J.; Roivainen, A. *Nucl. Med. Biol.* **2012**, *39*, 715–723.

(216) Tsang, B. W.; Mathias, C. J.; Fanwick, P. E.; Green, M. A. *J. Med. Chem.* **1994**, *37*, 4400–4406.

(217) Velikyan, I. *Med. Chem.* **2011**, *7*, 345–379.

(218) Hsiao, Y. M.; Mathias, C. J.; Wey, S. P.; Fanwick, P. E.; Green, M. A. *Nucl. Med. Biol.* **2009**, *36*, 39–45.

(219) Regueiro-Figueroa, M.; Bensenane, B.; Ruscsák, E.; Esteban-Gómez, D.; Charbonnière, L. J.; Tircsó, G.; Tóth, I.; De Blas, A.; Rodríguez-Blas, T.; Platas-Iglesias, C. *Inorg. Chem.* **2011**, *50*, 4125–4141.

(220) Nonat, A.; Fries, P. H.; Pecaut, J.; Mazzanti, M. *Chem. - A Eur. J.* **2007**, *13*, 8489–8506.

(221) Kubíček, V.; Havlíčková, J.; Kotek, J.; Tircsó, G.; Hermann, P.; Tóth, É.; Lukeš, I. *Inorg. Chem.* **2010**, *49*, 10960–10969.

(222) *TWINABS*, v2012/1; Bruker AXS Inc.: Madison, WI, 2012.

Appendix

Appendix A Supplementary Figures and Data

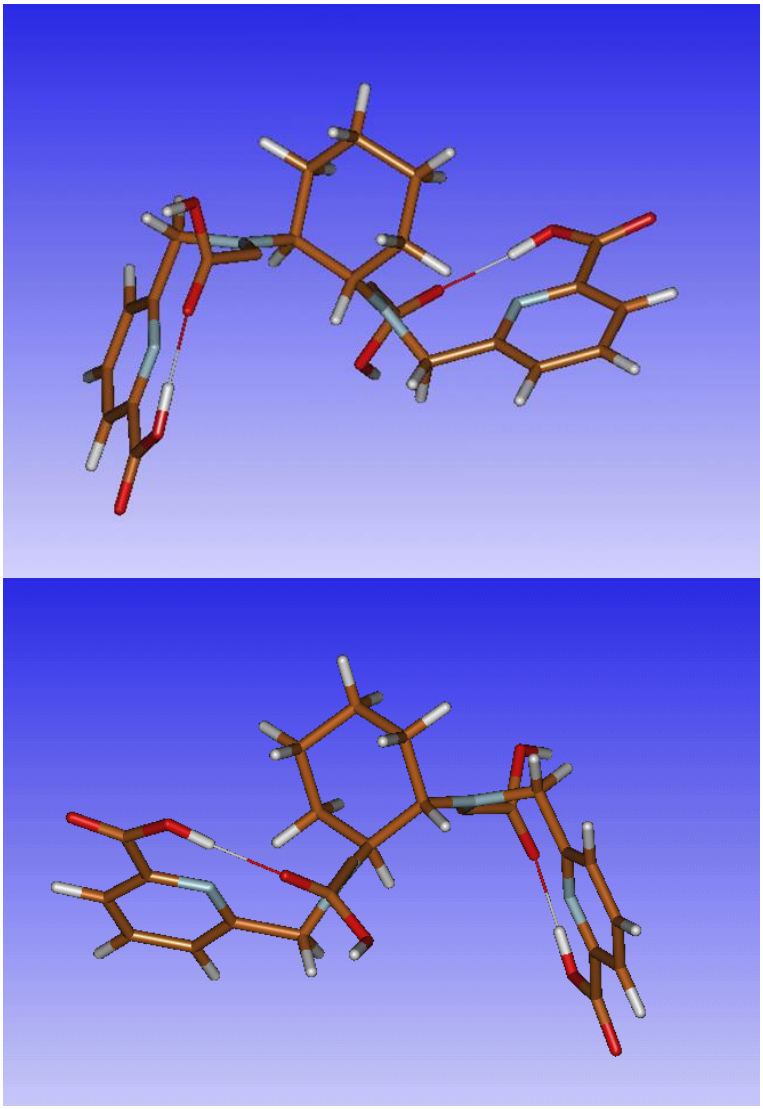

Figure A.1 DFT structure of H_4*CHX*octapa exhibiting intramolecular hydrogen bonding between hydrogen from pyridyl carboxylic acid ($H_{pyr\text{-}COOH}$) and oxygen from acetate carboxylic acid ($O_{Ac\text{-}COOH}$). O--H bond lengths are 1.955 Å and 1.869 Å, respectively, for each independent half of the ligand.

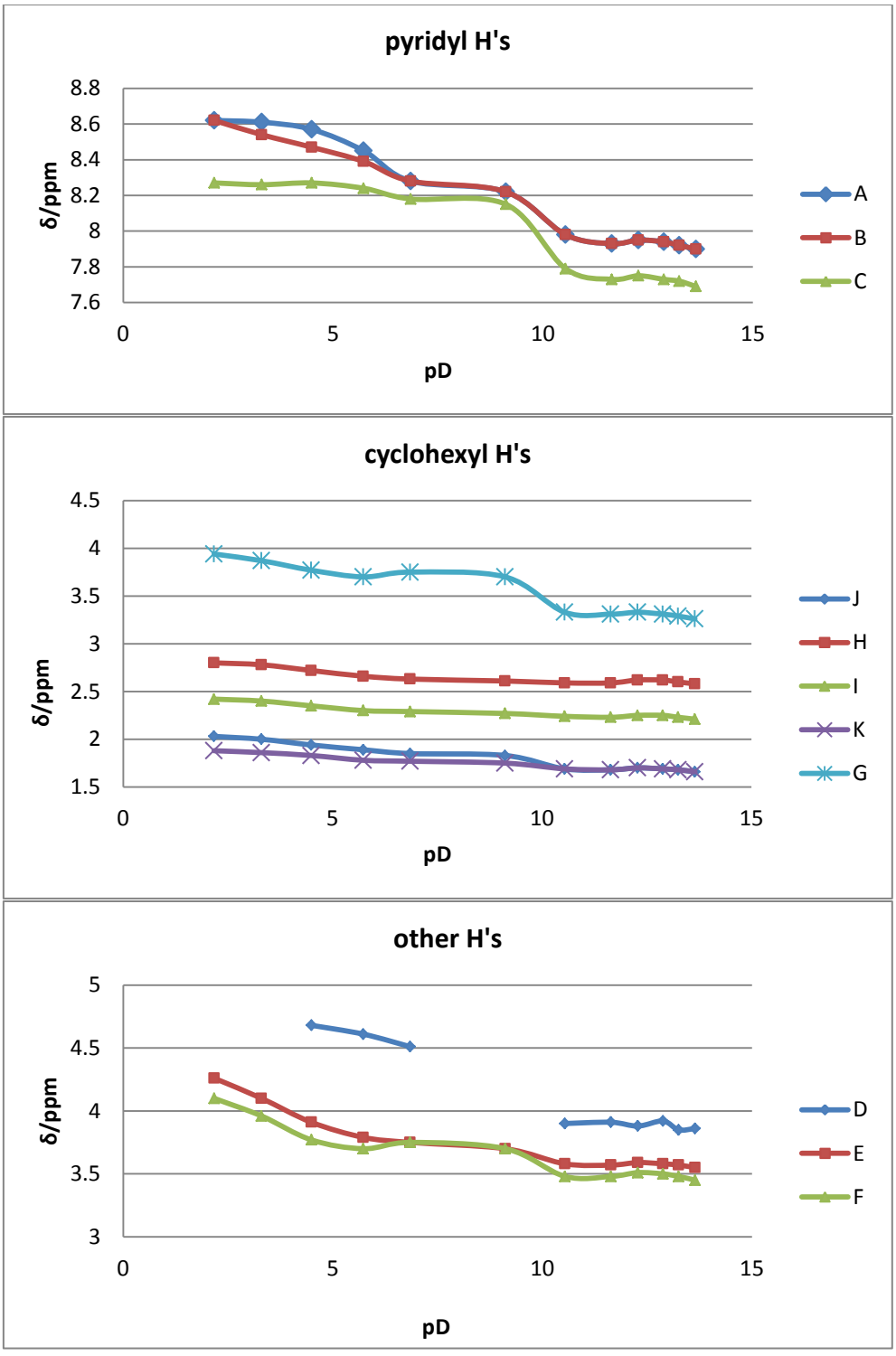

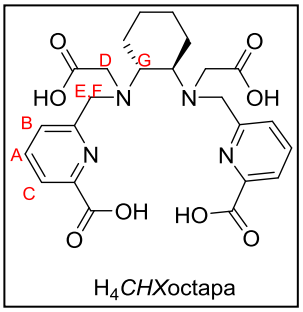

Figure A.2 ^{1}H NMR titration curves (400 MHz, D2O, 55 °C) of H_4CHXoctapa·2HCl. Initial pH of solution was acidic (~ 1.76), pH of solution was adjusted using NaOD (0.1 M in D_2O) and measured with a glass electrode. pH values were converted to pD values using the equation: pD = pH + 0.41.

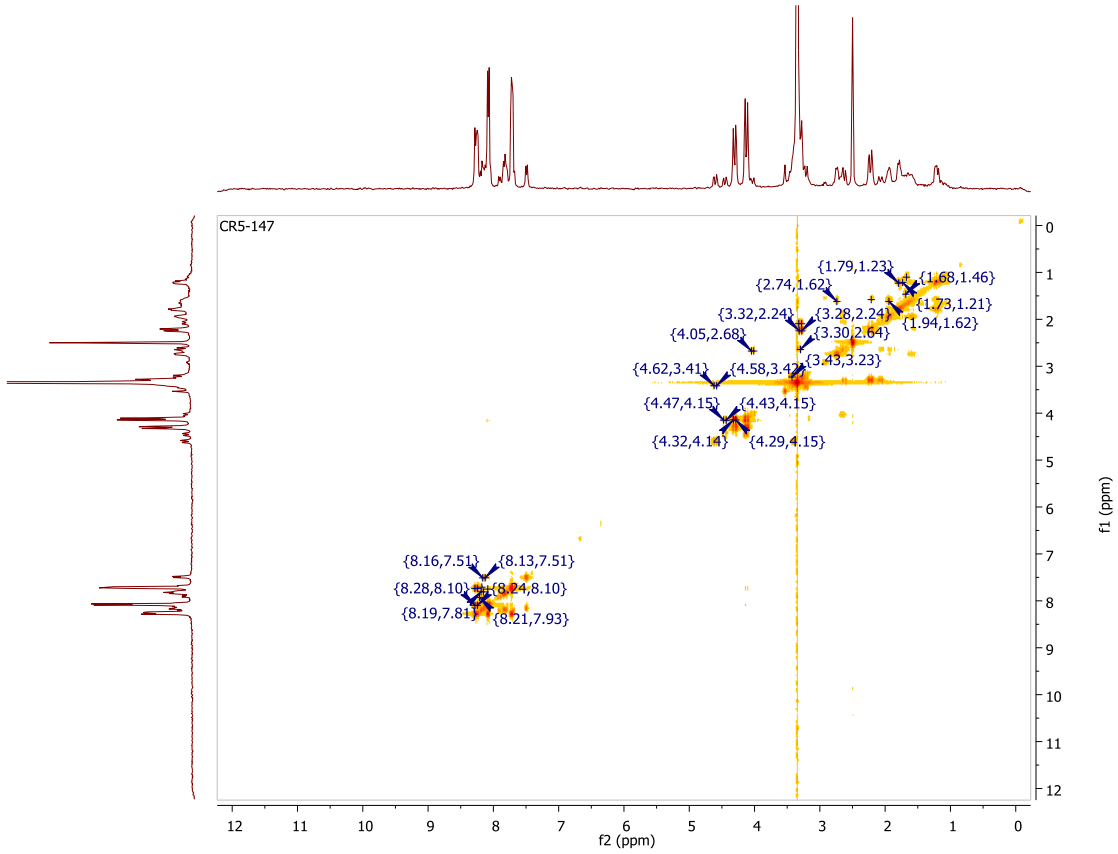

Figure A.3 ^{1}H-^{1}H COSY NMR spectrum of $[In(CHXoctapa)]^{-}$ (400 MHz, DMSO-d_6, 25°C).

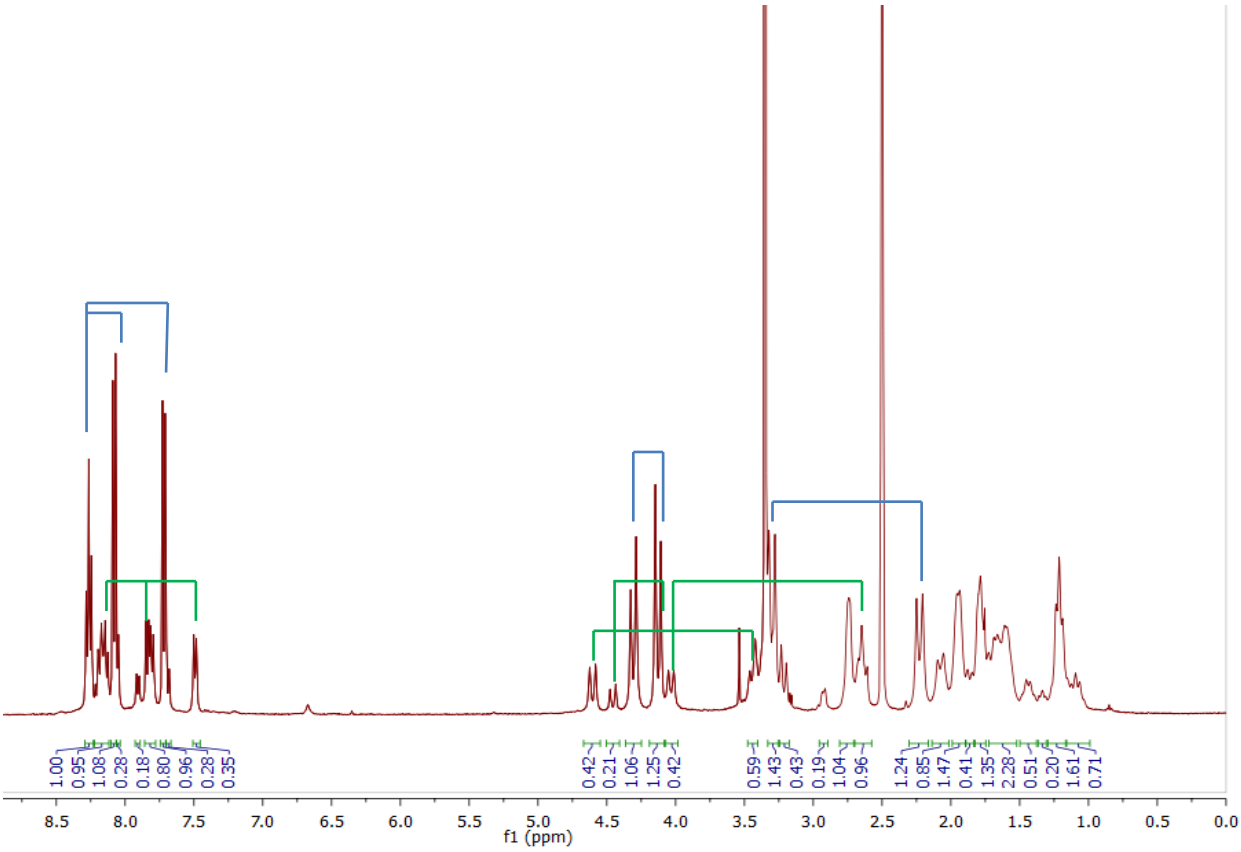

Figure A.4 ^{1}H NMR spectrum of **[In(*CHX*octapa)]**$^{-}$ (400 MHz, DMSO-d_6, 25°C), showing some ^{1}H-^{1}H correlations of the major symmetric isomer (blue) and minor asymmetric isomer(s) (green) obtained from 2D COSY NMR.

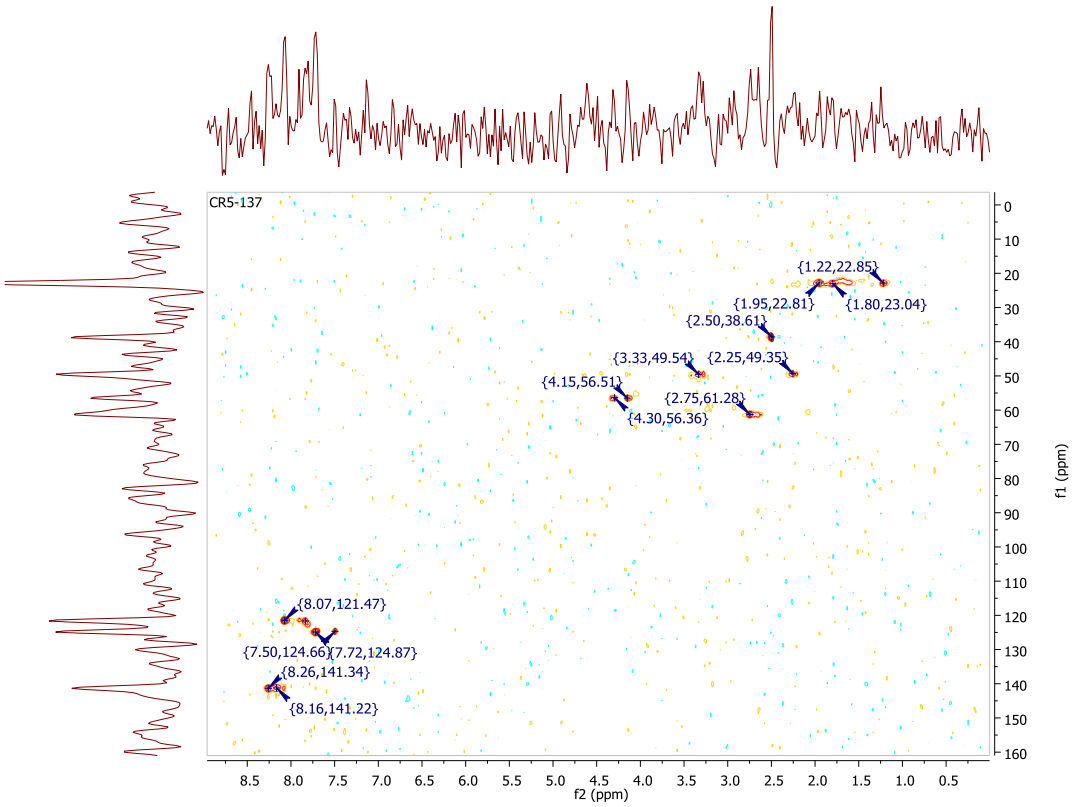

Figure A.5 ^{13}C HSQC NMR spectrum of $[In(CHXoctapa)]^-$ (101 MHz, 400MHz , DMSO-d_6, 25°C).

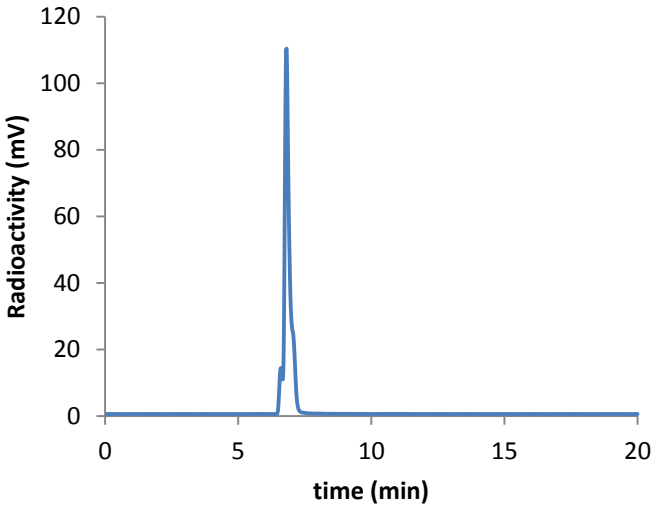

Figure A.6 HPLC radiotrace of $[^{67}Ga(CHXdedpa)]^+$ labelled at ambient temperature, 10 minutes reaction time and ligand concentration of 10^{-4} M.

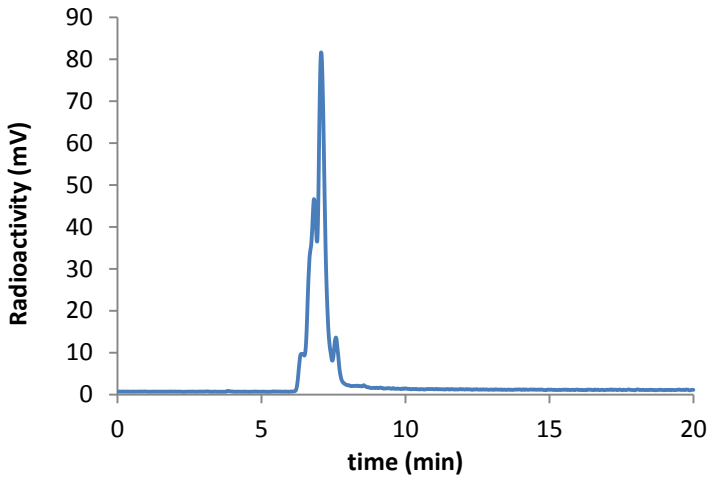

Figure A.7 HPLC radiotrace of [^{67}Ga(*CHX*octapa)]$^{-}$ labelled at ambient temperature, 10 minutes reaction time and ligand concentration of 10^{-4} M.

Table A.1 List of proton dissociation constants (pK_a) for *CHX*dedpa^{2-} and *CHX*octapa^{4-}, formation constants (log K_{ML}), and pM values for Ga^{3+} complexes of *CHX*dedpa^{2-} and *CHX*octapa^{4-} and In^{3+} complex of *CHX*octapa^{4-}; previously reported dedpa^{2-} and octapa^{4-} values listed for comparison. [(a)]Calculated for 1 μM total metal ion, 10 μM total ligand, pH 7.4 at 25°C.

Equilibrium quotient	Log *K*			
L =	dedpa^{2-}	*CHX*dedpa^{2-}	*CHX*octapa^{4-}	octapa^{4-}
$[H_6L]/[H_5L][H]$			1.91(8)	ND
$[H_5L]/[H_4L][H]$			1.82(6)	2.79(4)
$[H_4L]/[H_3L][H]$	2.59(6)	2.40(9)	3.34(2)	2.77(4)
$[H_3L]/[H_2L][H]$	3.06(6)	2.99(8)	3.94(2)	3.77(2)
$[H_2L]/[HL][H]$	6.30(5)	6.47(8)	5.40(2)	5.59(6)
[HL]/[L][H]	9.00(3)	9.23(5)	9.23(1)	8.59(4)
[GaL]/[Ga][L]	28.11(8)	27.61(8)	22.3(2)	
[GaLH]/[GaL][H]	3.9(2)	5.54(1)	4.60(4)	
[Ga(OH)L][H]/[GaL]	--	9.38(7)		
pM[(a)] M = Ga^{3+}	27.4	26.7	21.4	
[InL]/[In][L]			27.16(9)	26.76(14)
[InHL]/[InL][H]			--	2.89(23)
[In(OH)L][H]/[InL]			9.5(3)	--
pM[(a)] M = In^{3+}			26.3	26.5

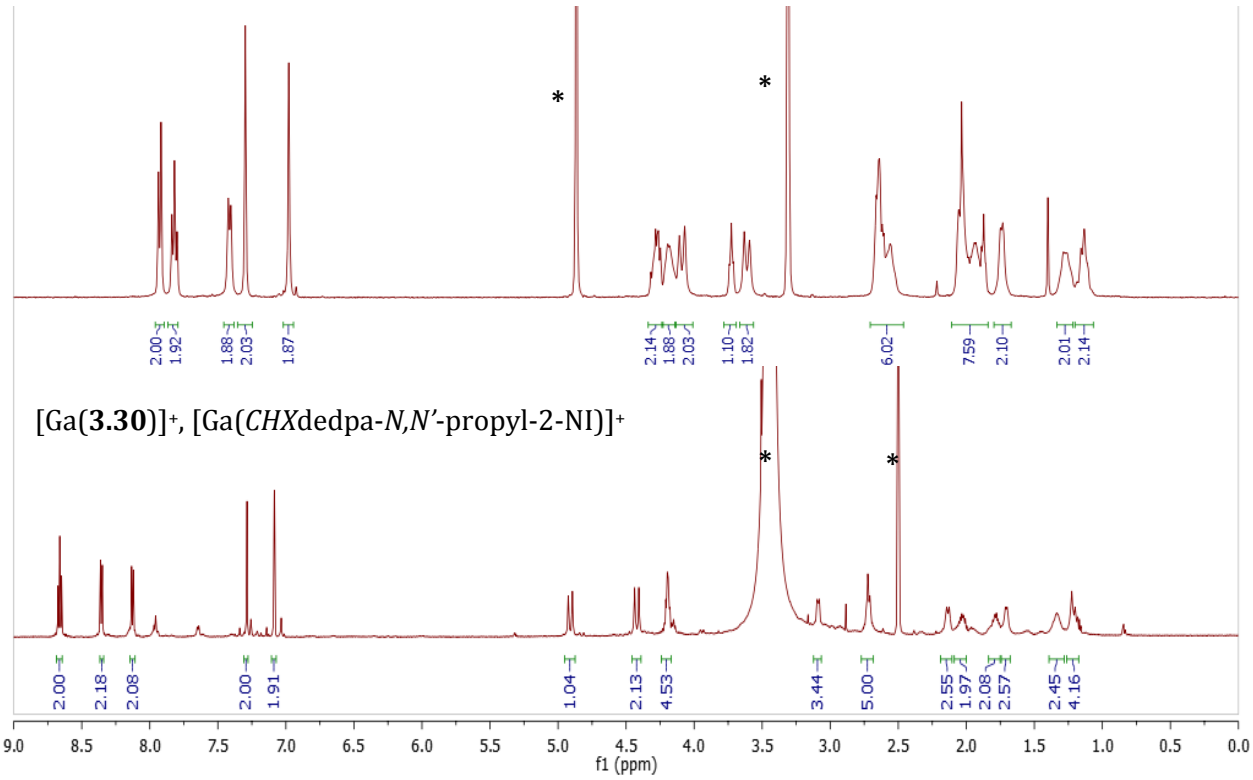

Figure A.8 ^{1}H NMR spectrum at 400 MHz and 25°C of (top) **3.30**, H_2*CHX*dedpa-*N,N'*-propyl-2-NI (MeOD-d_4) and (bottom) [Ga(**3.30**][ClO_4] (DMSO-d_6) highlighting resonance shifts upon gallium chelation. *Residual solvent peak.

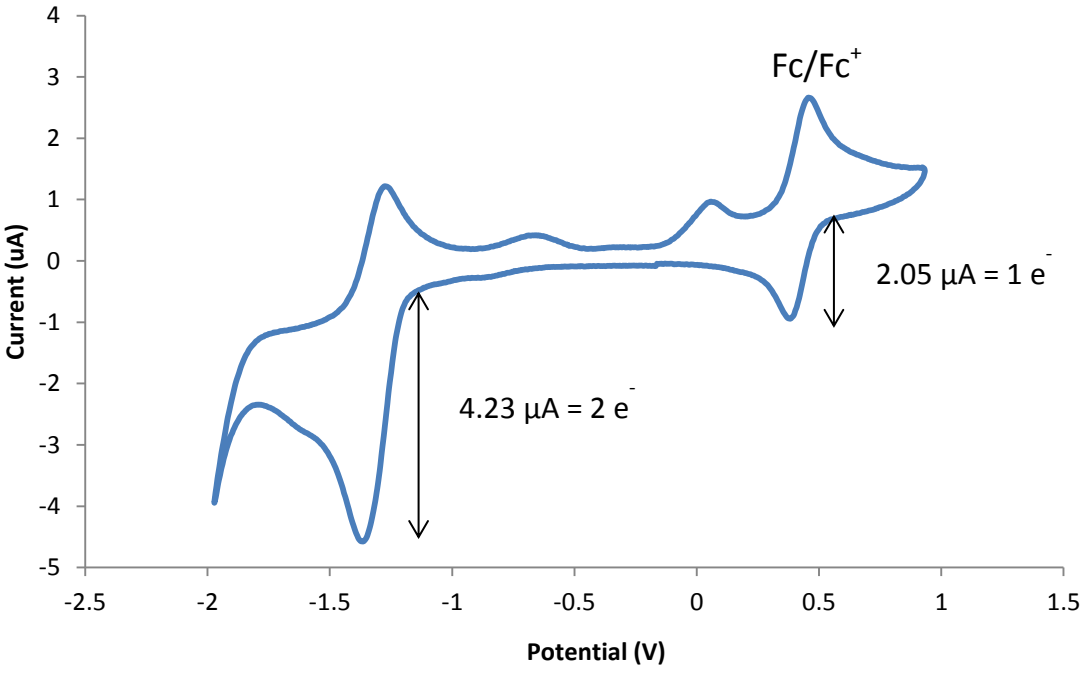

Figure A.9 Cyclic Voltammogram of [Ga(dedpa-*N,N'*-propyl-4-NI)]$^{+}$ with exactly one equiv. of ferrocene (Fc) added as an internal standard (DMSO, 0.1 M TBAP, 2 mM compound).

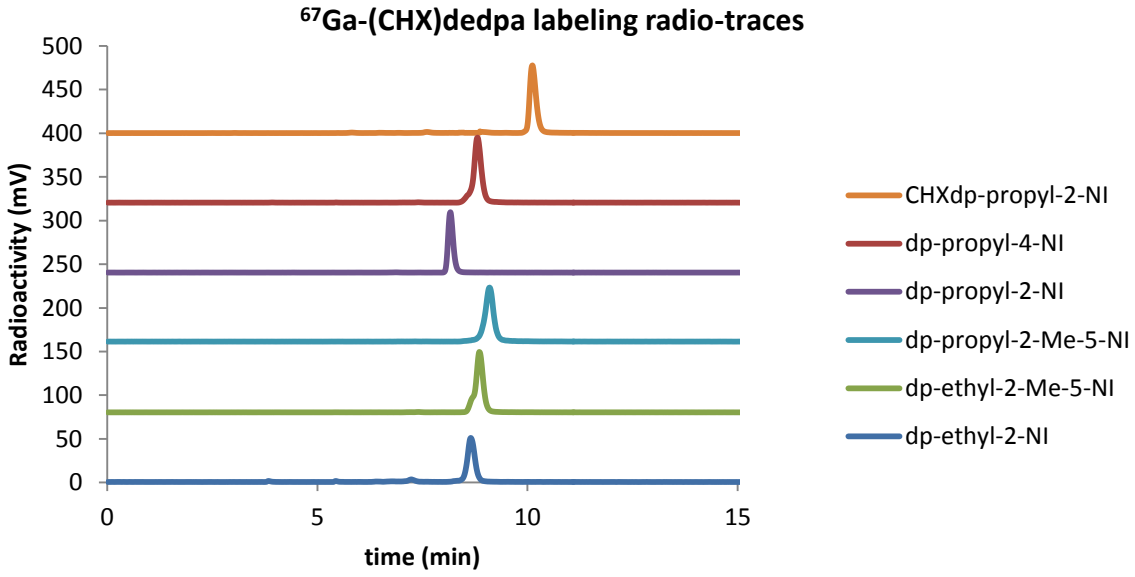

Figure A.10 Selected HPLC radio-traces of ^{67}Ga-labelled complexes in Chapter 3; all ligands labelled with ~1 mCi of ^{67}Ga at ambient temperature, 10 minutes reaction time and ligand concentration of 10^{-4} M.